

# **Progressive Collapse Assessment of Lightweight Ship Structures**

**Simon Benson**

**Submitted for the degree of Doctor of Philosophy**

November 2011

School of Marine Science and Technology  
Faculty of Science, Agriculture and Engineering  
Newcastle University  
Newcastle upon Tyne, UK

©2011 Simon Benson  
School of Marine Science and Technology  
Armstrong Building  
Newcastle University  
NE1 7RU  
United Kingdom

## Abstract

This thesis investigates the progressive collapse behaviour of lightweight ship hull girders including the effects of compartment level buckling modes. An extension to the progressive collapse methodology is proposed, which has capabilities to predict the compartment strength of a lightweight aluminium midship section. Nonlinear finite element analysis is used to validate both the progressive collapse methodology and the analytical approach proposed for determining the buckling capacity of orthogonally stiffened substructures within the hull girder compartment. The research has been undertaken due to the continued growth in the size of large lightweight craft in both commercial and naval vessels, combined with increasing operability requirements for these vessels. The development of large and lightweight marine structures, predominantly built from aluminium alloy, has raised important issues regarding the response of the hull girder under primary hull girder bending.

The main objective of the research is to examine the possible collapse modes of structure typical of a lightweight ship, focusing on the possibility of overall buckling modes affecting the entire compartment. The thesis presents an extended progressive collapse methodology, which has been developed to predict the strength behaviour of lightweight hull structures under primary bending moment and accounts for compartment level, gross panel buckling effects. The approach is based upon the principles of the conventional progressive collapse method, which has been shown as a capable measure of ultimate strength when applied to steel ships, where a fundamental premise is that buckling forms interframe. The proposed method extends the interframe progressive collapse method by including overall gross panel buckling effects in the determination of girder strength

The nonlinear finite element method (FEM) can also be utilised to predict hull girder progressive collapse and, provided computation time is acceptable, will predict collapse modes over an entire compartment. To formulate a realistic solution, the finite element model must include explicit characterisation of the material and geometric imperfections inherent in the structure. To validate the extended method, a series of analyses on an aluminium box girder structure with scantlings typical of a large lightweight vessel are completed. Case study analyses using the extended progressive collapse method are compared with nonlinear FEM and the conventional progressive collapse solutions and the influence of the various collapse modes observed in the structure are highlighted.

## Acknowledgements

First and foremost I would like to acknowledge my supervisor, Prof. Bob Dow, who has not only ably mentored me through the last four years but has also imparted an unrivalled array of experience and insight into ship structural analysis. This thesis extends upon the efforts of many esteemed academic researchers; and the most valuable has been that carried out by Prof. Dow himself and his colleagues at the Admiralty Research Establishment (to use one of the many names given to the Dunfermline institution). It has been an honour to work under his expert guidance.

I would like to thank Dr. Jonathan Downes, who has far exceeded the usual role of second supervisor. He has put up with me bouncing half ideas off him, sending him buggy programs to test and submitting half written papers to correct. Thanks for taking such an interest, not only in the project work but also my welfare.

My unofficial third supervisor does not escape a mention. Sincere thanks to John Garside who has provided ideas, insight and immensely valuable proof reading through his regular Tuesday visits. I have also had excellent support from numerous peers in the marine structures community. Particular thanks to Dr. Matthew Collette who wrote an excellent thesis from which my own is indebted. I also received welcome support from Dr. Paul Hess and colleagues from the Office of Naval Research, who sponsored this work.

The last four years study have been made most enjoyable by the company of fellow PhD students and researchers in the school of marine science and technology. In particular I would like to thank Konstantinos Misirlis and Umaru Ba, who have had me sat between them in room M1.22 for far longer than it feels. They have been excellent friends and compatriots; I couldn't have picked better office mates, even with Kostas' unique style of distraction. In addition I would like to wish good luck to fellow PhD students in MAST: Anuar Abu-Bakar, Achinike Ibekwe, David Trodden, Maryam Haroutunian, Musa Bashir, Kazeem Shittu, Mohammed Zoolfakar, Yassir Buraree, Amany Hassan and Stavros Karamperidis. Ben Wetenhall and Ignazio Maria Viola have provided excellent stress relief by letting me hit squash balls at them during my thesis write up.

Last but not least I would like to thank my family. My mum and dad have supported me throughout my lengthy student career and have always been there when I need them. I am lucky to have my sister Sally close at hand in Newcastle to help me out, provide good company and keep me well fed. Special thanks to Stella, who has kept me smiling through all the tough parts of writing up and has allowed my brain to escape ship structures and concentrate on the other fun parts of life too!

# Contents

<b>Abstract.....</b>	<b>iii</b>
<b>Acknowledgements.....</b>	<b>iv</b>
<b>Contents.....</b>	<b>v</b>
<b>List of Figures.....</b>	<b>x</b>
<b>List of Tables.....</b>	<b>xv</b>
<b>Nomenclature.....</b>	<b>xvii</b>
<b>1. Introduction .....</b>	<b>1</b>
<b>1.1. Research Context.....</b>	<b>1</b>
<b>1.2. Research Rationale .....</b>	<b>4</b>
<b>1.3. Research Objectives and Scope .....</b>	<b>6</b>
<b>1.4. Summary of Thesis Contribution .....</b>	<b>8</b>
<b>2. Background Material.....</b>	<b>9</b>
<b>2.1. Introduction .....</b>	<b>9</b>
<b>2.2. Applications of Lightweight Ship Structures .....</b>	<b>10</b>
<b>2.3. Hull Girder Structures .....</b>	<b>12</b>
2.3.1. The Longitudinal Framing System.....	12
2.3.2. Structural Components .....	14
2.3.3. Structural Arrangement of Lightweight Ships.....	15
<b>2.4. Marine Grade Aluminium.....</b>	<b>17</b>
2.4.1. Aluminium Stress-Strain Relationship.....	19
2.4.2. Heat Affected Zone .....	21
2.4.3. Residual Stress .....	25
<b>2.5. Typical Fabrications .....</b>	<b>28</b>
<b>2.6. Hull Girder Progressive Collapse Methods .....</b>	<b>32</b>
2.6.1. Limit State Design .....	32
2.6.2. Simple Beam Theory .....	33

2.6.3.	Stress Distribution Method.....	33
2.6.1.	The Progressive Collapse Method.....	34
2.6.2.	Nonlinear Finite Element Method .....	37
<b>2.7.</b>	<b>Summary.....</b>	<b>37</b>
<b>3.</b>	<b>Methods to Predict the Strength of Plates and Stiffened Panels .....</b>	<b>39</b>
<b>3.1.</b>	<b>Overview.....</b>	<b>39</b>
3.1.1.	Plate Strength .....	41
3.1.2.	Stiffener Strength.....	42
3.1.3.	Stiffened Panel Strength .....	43
<b>3.2.</b>	<b>Methods to Predict the In-Plane Strength of Unstiffened Plates .....</b>	<b>44</b>
3.2.1.	Experimental Data.....	44
3.2.2.	Elastic Buckling.....	46
3.2.3.	Elasto-Plastic Buckling.....	47
3.2.4.	Uniaxial Compression: Empirical Methods .....	48
3.2.5.	Uniaxial Compression: Load Shortening Behaviour.....	53
3.2.6.	Multiple Load Combinations.....	55
<b>3.3.</b>	<b>Analytical Methods to Predict the In-Plane Strength of Stiffened Panels.....</b>	<b>59</b>
3.3.1.	Overview .....	59
3.3.2.	Design Charts and Empirical Methods .....	61
3.3.3.	Beam-Column Methods .....	63
3.3.4.	Orthotropic Plate Methods.....	67
3.3.5.	Analytical Load Shortening Curves.....	74
<b>3.4.</b>	<b>Summary.....</b>	<b>75</b>
<b>4.</b>	<b>Finite Element Analysis of Unstiffened Aluminium Plates.....</b>	<b>77</b>
<b>4.1.</b>	<b>Introduction .....</b>	<b>77</b>
4.1.1.	General Parameters .....	78
4.1.2.	Reference Plates .....	80
<b>4.2.</b>	<b>Boundary Conditions.....</b>	<b>81</b>

4.2.1.	Out of Plane Constraints .....	82
4.2.2.	Rotational Restraints.....	82
4.2.3.	In-Plane Constraints .....	84
<b>4.3.</b>	<b>Aspect Ratio .....</b>	<b>86</b>
<b>4.4.</b>	<b>Geometric Imperfection .....</b>	<b>87</b>
4.4.1.	Causes of Geometric Imperfections.....	88
4.4.2.	Imperfection Patterns .....	90
4.4.3.	Single Mode Imperfection Shape.....	94
4.4.4.	Multiple Mode Longitudinal Imperfection Shape.....	95
4.4.5.	Summary .....	100
<b>4.5.</b>	<b>Heat Affected Zone .....</b>	<b>101</b>
4.5.1.	Longitudinal HAZ Location .....	102
4.5.2.	Effect of Transverse Edge HAZ .....	103
4.5.3.	Relative HAZ Width .....	106
<b>4.6.</b>	<b>Residual Stress.....</b>	<b>107</b>
<b>4.7.</b>	<b>Parametric Plate Load Shortening Curve Database.....</b>	<b>109</b>
<b>4.8.</b>	<b>Summary.....</b>	<b>115</b>
<b>5.</b>	<b>Finite Element Analysis of Orthogonally Stiffened Aluminium Panels .....</b>	<b>117</b>
<b>5.1.</b>	<b>Introduction .....</b>	<b>117</b>
<b>5.2.</b>	<b>Nonlinear FEM Modelling Techniques for Stiffened Panel Structures.....</b>	<b>118</b>
5.2.1.	Existing FEM Modelling Approaches.....	119
5.2.2.	The Building Block Approach .....	121
<b>5.3.</b>	<b>Model Extents and Boundary Conditions .....</b>	<b>123</b>
5.3.1.	Plate and Stiffener Models .....	124
5.3.2.	Plate-Stiffener Combination Models .....	126
5.3.3.	Orthogonal Stiffened Panel.....	129
<b>5.4.</b>	<b>Geometric Imperfections .....</b>	<b>131</b>
5.4.1.	Geometric Panel Imperfection Parameters .....	131

5.4.2.	Plate Imperfection .....	132
5.4.3.	Stiffener Imperfections .....	132
5.4.4.	Column Imperfection .....	133
5.4.5.	Imperfection Amplitude.....	134
5.4.6.	Implementation of Geometric Imperfections.....	135
5.4.7.	Eigenmode Superposition.....	136
5.4.8.	Direct Translation of Nodes .....	139
5.4.9.	Heat Affected Zone and Residual Stress Field .....	143
<b>5.5.</b>	<b>Analysis of Stiffener Elements .....</b>	<b>143</b>
5.5.1.	Tee Bar Stiffeners.....	144
5.5.2.	Flat Bar Stiffeners.....	153
<b>5.6.</b>	<b>Analysis of Plate Stiffener Combinations .....</b>	<b>155</b>
5.6.1.	Introduction .....	155
5.6.2.	Steel Panel Experiments.....	156
5.6.3.	ISSC2009 Benchmark Study .....	159
5.6.4.	SSC451 Aluminium Panels.....	161
5.6.5.	A.R.E. Steel Panel Column Collapse Curves.....	164
5.6.6.	Aluminium Panel Column Collapse Curves .....	168
<b>5.7.</b>	<b>Analysis of Orthogonal Panels .....</b>	<b>174</b>
<b>5.8.</b>	<b>Summary.....</b>	<b>186</b>
<b>6.</b>	<b>A Semi Analytical Panel Strength Methodology.....</b>	<b>188</b>
<b>6.1.</b>	<b>Introduction .....</b>	<b>188</b>
<b>6.2.</b>	<b>Rationale.....</b>	<b>190</b>
<b>6.3.</b>	<b>Calculation Methodology .....</b>	<b>192</b>
6.3.1.	Calculation Principles.....	192
6.3.2.	Calculation Procedure – Regular Stiffened Panel .....	197
6.3.3.	Plate and Stiffener Load Shortening Curves .....	201
6.3.4.	Interframe Panel Strength .....	202

6.3.5.	Overall Panel Properties .....	206
6.3.6.	Overall Panel Strength .....	209
6.3.7.	Panel Load Shortening Curve and Post Collapse Response .....	213
6.3.8.	Irregular Stiffened Panels.....	216
<b>6.4.</b>	<b>Case Studies – Multi Bay Stiffened Panels .....</b>	<b>219</b>
<b>6.5.</b>	<b>Summary .....</b>	<b>224</b>
<b>7.</b>	<b>Hull Girder Progressive Collapse Methods .....</b>	<b>225</b>
<b>7.1.</b>	<b>Introduction .....</b>	<b>225</b>
<b>7.2.</b>	<b>The Interframe Progressive Collapse Method.....</b>	<b>226</b>
<b>7.3.</b>	<b>The Extended Progressive Collapse Method.....</b>	<b>230</b>
<b>7.4.</b>	<b>FEM Methods .....</b>	<b>233</b>
<b>7.5.</b>	<b>Validation with Existing Physical and Numerical Experiments.....</b>	<b>239</b>
7.5.1.	IST Box Girders .....	240
7.5.2.	1/3 Scale Frigate.....	247
<b>7.6.</b>	<b>Box Girder Case Study .....</b>	<b>256</b>
<b>7.7.</b>	<b>Case Study – Aluminium Multihull .....</b>	<b>260</b>
<b>7.8.</b>	<b>Summary .....</b>	<b>268</b>
<b>8.</b>	<b>Conclusions and Recommendations for Future Work .....</b>	<b>269</b>
<b>8.1.</b>	<b>Conclusions .....</b>	<b>269</b>
<b>8.2.</b>	<b>Recommendations for Future Work.....</b>	<b>275</b>
<b>9.</b>	<b>References.....</b>	<b>279</b>
<b>10.</b>	<b>Appendix – ProColl User Manual .....</b>	<b>287</b>

## List of Figures

Figure 1 – The Prestige oil tanker, which sank off the Spanish coast in 2002 [2].....	2
Figure 2 – Example engineering stress-strain relationships for aluminium and steel [6] .....	6
Figure 3 – Isherwood longitudinal framing system for a cargo steamer (left) and oil steamer .....	13
Figure 4 – Example conventional longitudinal framed (left) and advanced double hull (right).....	14
Figure 5 –Midship section of the Pacificat multihull [16] .....	16
Figure 6 –Comparative 0.2% proof strengths of tensile test coupons .....	19
Figure 7 – Aluminium alloy 5083-H116 (left) and 6082-T6 (right) stress-strain relationship.....	20
Figure 8 - Effective HAZ breadth [25].....	22
Figure 9 – Through thickness HAZ formation [26].....	22
Figure 10 - Extent of HAZ for a range of plate thickness and specification codes.....	23
Figure 11 – Comparative HAZ material properties for 5083-H116 and 6082-T6 aluminium alloys .....	24
Figure 12 - Idealised residual stress distribution with weld along all four edges of the plate [37].....	26
Figure 13 – Measured residual stress distribution in an aluminium panel [22] .....	27
Figure 14 – Cross section geometry of a stiffened panel.....	28
Figure 15 – Stress distributions over ship cross section with a sagging bending moment .....	34
Figure 16 – Example panel load shortening curve.....	37
Figure 17 – Through thickness cross section for an aluminium plate. HAZ representation.....	51
Figure 18 – Comparison of empirical methods to predict aluminium plate strength .....	53
Figure 19 –Comparison of A.R.E. plate data with the Gordo method .....	55
Figure 20 – Ultimate strength interaction relationship for biaxial tension/compression .....	57
Figure 21 – Interaction diagram for plate in biaxial load.....	58
Figure 22 – Interaction curves for various slenderness ratio aluminium plates using Eq. 34. ....	59
Figure 23 - A.R.E. column collapse curves for average structural imperfections [76].....	62
Figure 24 – Initial column imperfection and boundary conditions .....	66
Figure 25 – Orthotropic plate geometry and coordinate system [96].....	68
Figure 26 – Comparison of results from Paik et al. [96] and the formulations in the present work. ...	74
Figure 27 – Plate coordinate system.....	79
Figure 28 – Plate imperfection patterns: alternating (left) and single direction (right).....	82
Figure 29 – USCGC Buttonwood in dry-dock. ....	83
Figure 30 – Comparison of simply supported and clamped boundary conditions.....	84
Figure 31 – Comparison of in-plane support conditions for Plate 1 and Plate 2.....	85
Figure 32 – Effect of plate aspect ratio.....	87

Figure 33 – Welding induced distortions [102].....	88
Figure 34 – Selected initial deflection shapes [103] .....	89
Figure 35 – Empirical methods to define initial deflection amplitude .....	91
Figure 36 – Relative frequency distribution of $w_{opt}$ for 78 plates analysed in SSC451 .....	92
Figure 37 – Comparison of multi mode imperfection shapes .....	93
Figure 38 – First linear eigenmode shape for Plate 1 in uniaxial compression .....	94
Figure 39 – Comparison of two mode imperfection shapes.....	97
Figure 40 – Comparison of two mode imperfection shapes – Plates 5 and 6. ....	97
Figure 41 – Profile view of Plate 1 in uniaxial compression.....	99
Figure 42 – Comparison of three mode vs. two mode .....	100
Figure 43 – Edge HAZ and Centre HAZ distributions .....	101
Figure 44 - Comparison of HAZ location. Plates 1 and 2 (left), Plates 5 and 6 (right) .....	102
Figure 45 – Ultimate strength curves, comparison of longitudinal HAZ location.....	103
Figure 46 – Plots of the post collapse deformed shape.....	104
Figure 47 - Comparison of transverse HAZ .....	105
Figure 48 - Comparison of Transverse HAZ.....	105
Figure 49 – Ultimate strength comparison of HAZ location. ....	106
Figure 50 - Comparison of HAZ ratio. 5083-H116 plates (1200x400), $\beta = 3.0$ . HAZ at all four edges. ....	107
Figure 51 – Residual stress modelling techniques .....	108
Figure 52 - Normalised stress-strain plates in uniaxial compression .....	111
Figure 53 - Normalised stress-strain plates in uniaxial compression .....	111
Figure 54 - Normalised stress-strain plates in uniaxial compression .....	111
Figure 55 - Normalised stress-strain plates in uniaxial compression .....	113
Figure 56 - Normalised stress-strain plates in uniaxial compression .....	113
Figure 57 - Normalised stress-strain plates in uniaxial compression .....	113
Figure 58 - Normalised stress-strain plates in uniaxial tension .....	115
Figure 59 – ISSC 2003 [109] (left) and 2007 [110] (right) benchmark models .....	120
Figure 60 – Graphical representation of the building block approach .....	122
Figure 61 - Stiffener rotational stiffness. ....	125
Figure 62 - Stiffener FEM model boundary conditions.....	125
Figure 63 - Modelling extent for plate stiffener combination models .....	126
Figure 64 – PSC boundary conditions .....	128
Figure 65 – Complete panel boundary conditions.....	129
Figure 66 – Half (left) and quarter (right) panel models.....	130

Figure 67 – Maximum plate imperfection amplitude.....	132
Figure 68 – Stiffener side imperfection .....	132
Figure 69 – Stiffener web imperfection .....	132
Figure 70 – Stiffener column deflection .....	133
Figure 71 – Example Eigenmode shapes.....	137
Figure 72 – Box girder Eigenmode buckling patterns.....	139
Figure 73 – Panel coordinate system.....	141
Figure 74 - Residual stress distribution.....	143
Figure 75 – Tee bar stiffener stress-strain curves.....	145
Figure 76 – Tee bar stiffener ultimate strengths vs. $\lambda$ , average imperfections, simply supported....	146
Figure 77 – Load shortening curves for $\lambda=0.4$ (left) and $\lambda=0.8$ (right).....	146
Figure 78 – Tee bar stiffener ultimate strengths vs. $\gamma$ , all datasets, zero rotational stiffness.....	148
Figure 79 – Tee bar stiffener ultimate strengths vs. $\gamma$ .....	148
Figure 80 – Comparative performance of regression lines.....	149
Figure 81 – Comparison of tee bar stiffener regression formulas.....	149
Figure 82 – Load shortening curves .....	150
Figure 83 – Load shortening curves .....	151
Figure 84 – Representative 5083-H116 load shortening curves.....	152
Figure 85 – Flat bar stiffener ultimate strengths vs. $\lambda$ (left) and $\gamma$ (right) .....	154
Figure 86 – Comparison of 5083-H116 flat bar stiffener regression formulas .....	154
Figure 87 – Representative 5083-H116 load shortening curves.....	155
Figure 88 – Comparison of ABAQUS PSC model .....	158
Figure 89 - Comparison of ABAQUS PSC model with experimental data .....	159
Figure 90 - Comparison of FABSTRAN with experimental data .....	159
Figure 91 – FEM load shortening curves for the ISSC 2009 benchmark panel. ....	161
Figure 92 – Comparison of ABAQUS PSC model with SSC451 experimental data.....	163
Figure 93 – Comparison of SSC451 ANSYS model (2 bay CIS) with SSC451 FEM analyses .....	163
Figure 94 – Comparison of ABAQUS PSC model with SSC451 experimental data.....	164
Figure 95 - Steel panel column collapse curves .....	165
Figure 96 – FEM of a short PSC panel (left) and long PSC panel (right).....	167
Figure 97 - Steel panel column collapse curves, comparison of FEM.....	168
Figure 98 – 5083 (left) and 6082 (right) column collapse curves, $A_s/A=0.2$ .....	169
Figure 99 – Percentage difference between average imperfection ultimate strength.....	170
Figure 100 – A6082-T6 PSC model, $\lambda=0.3$ , $\beta=2.0$ , post collapse .....	171

Figure 101 – Comparison of 5083-H116, 6082-T6 and steel column collapse curves,.....	172
Figure 102 – Load shortening curves for PSCs with different stiffener cross sections.....	173
Figure 103 – Load shortening curves for PSCs with different stiffener cross sections.....	174
Figure 104 – Panel M1 3 bay models.....	177
Figure 105 – Panel M1 7 bay models.....	178
Figure 106 – Panel M1 20 longitudinal models.....	179
Figure 107 – Panel M1, comparison of transverse frame size.....	181
Figure 108 – Panel M2, comparison of transverse frame size.....	181
Figure 109 – Panel M3, comparison of transverse frame size.....	182
Figure 110 – Panel M4, comparison of transverse frame size.....	182
Figure 111 – Panel M1 displacement plots.....	183
Figure 112 – Panel M3 displacement plots.....	183
Figure 113 – Comparison of panels M1, M5 and M6.....	184
Figure 114 – Comparison of panels M1, M7 and M8.....	184
Figure 115 – Steel Panels S1-S4 compared to 5083 panels M1-M4. 20x7 panel size.....	185
Figure 116 – Aluminium multihull top deck.....	192
Figure 117 – Deck A load shortening curves.....	194
Figure 118 – Variant deck load shortening curves.....	195
Figure 119 – Variant deck mesh plots.....	195
Figure 120 –Semi analytical method calculation flow chart.....	200
Figure 121 – Example measurement of component resistance and tangent modulus.....	202
Figure 122 – Column curves for steel PSCs.....	204
Figure 123 - PSC load shortening curves.....	206
Figure 124 – Orthotropic plate calculation flow chart.....	212
Figure 125 – Example PSC and overall panel strength curves.....	214
Figure 126 – Post collapse region curve prediction methods.....	216
Figure 127 – Irregular panel calculation method.....	217
Figure 128 – PSC load shortening curve predicted by the semi analytical method.....	218
Figure 129 – Panel load shortening curves.....	219
Figure 130 – Comparison between FEM and semi analytical ultimate strength.....	221
Figure 131 - Panel load shortening curves.....	222
Figure 132 - Panel load shortening curves.....	223
Figure 133 - Panel load shortening curves.....	223
Figure 134 - Panel load shortening curves.....	224

Figure 135 – Element subdivision in the progressive collapse method.....	228
Figure 136 - Example element load shortening curve. ....	230
Figure 137 – Example ProColl element stiffness plot for the 1/3 scale frigate (see section 7.5.2) ....	232
Figure 138 – FEM extents for hull girder models.....	234
Figure 139 – Neutral axis position across multiple frame spaces.....	235
Figure 140 – Example of a compartment level hull girder model .....	237
Figure 141 – Hull girder boundary conditions (half model shown) .....	238
Figure 142 – Lisbon box girder test experimental setup .....	241
Figure 143 – Complete FEM model extents.....	241
Figure 144 – IST box girder experiments comparison with FEM models .....	242
Figure 145 – FEM mesh plots for F200 test .....	242
Figure 146 – Load points for four point bending [121].....	243
Figure 147 –Representation of the spring boundary conditions .....	244
Figure 148 – Comparative results showing the effect of spring .....	244
Figure 149 – Comparison of implicit and explicit FEM solvers .....	246
Figure 150 – Profile of frigate test section, taken from [120] .....	248
Figure 151 – Structural arrangement in the central compartment of the 1/3 scale frigate .....	248
Figure 152 – 1/3 scale frigate scantlings.....	249
Figure 153 – Geometric imperfection in the ½+1+1/2 bay frigate model .....	250
Figure 154 – Load shortening curves for the 1/3 scale frigate .....	251
Figure 155 – Interframe bending moment – curvature plot .....	252
Figure 156 – ProColl element stiffness contour plots.....	252
Figure 157 – Example of an unsuccessful FEM analysis on a half model of the 1/3 scale frigate .....	254
Figure 158 – Compartment level progressive collapse curves .....	255
Figure 159 – Compartment level FEM deformed mesh plots. Magnification x10.....	255
Figure 160 - Progressive collapse under vertical bending of the four box girder models.....	259
Figure 161 – Deformed mesh plots of box girder M1.....	259
Figure 162 – Deformed mesh plots of box girder M3.....	260
Figure 163 – Aluminium multihull scantlings.....	262
Figure 164 – Aluminium multihull PSC curves .....	263
Figure 165 – Interframe bending moment – curvature of the aluminium multihull.....	265
Figure 166 – Overall bending moment – curvature of the aluminium multihull.....	267

## List of Tables

Table 1 - DNV Minimum Material Properties [18].....	18
Table 2 - ABS Minimum Material Properties [18].....	18
Table 3 - Knee Factors for Ramberg Osgood relationship – comparison of literature values.....	20
Table 4 - HAZ Properties .....	24
Table 5 – Alcan T-Bar Extrusions.....	30
Table 6 – Alcan Bulb Extrusions .....	30
Table 7 – Admiralty Long Stalk Tees .....	31
Table 8 – Pacificat Deck Extrusions.....	31
Table 9 – Plate properties - case study database .....	80
Table 10 – Plate Boundary Conditions: 0 = Free, 1 = Constrained.....	81
Table 11 – Fourier Coefficients for Paik Imperfection Patterns, from [103] .....	93
Table 12 – Ultimate strength of Plate 1 and Plate 2.....	95
Table 13 – Ultimate strength of test plates with two mode imperfection.....	96
Table 14 – Curve Dataset – 5083-H116, Slight Imperfection Amplitude.....	112
Table 15 – Curve Dataset – 5083-H116, Average Imperfection Amplitude.....	112
Table 16 – Curve Dataset – 5083-H116, Severe Imperfection Amplitude.....	112
Table 17 – Curve Dataset – 6082-T6, Slight Imperfection Amplitude .....	114
Table 18 – Curve Dataset – 6082-T6, Average Imperfection Amplitude .....	114
Table 19 – Curve Dataset – 6082-T6, Severe Imperfection Amplitude .....	114
Table 20 – Curve Dataset – Uniaxial Tension - 5083-H116 and 6082-T6.....	115
Table 21 – Formulae to describe fabrication induced initial imperfections.....	135
Table 22 – Imperfection Properties for Steel and Aluminium Plates .....	135
Table 23 – Summary of Tee Bar Stiffener Datasets .....	144
Table 24 – Coefficients for Eq. 95 for stiffeners with simple supports at the web – plate joint.....	147
Table 25 – Summary of Flat Bar Stiffener Datasets .....	153
Table 26 – Coefficients for Eq. 95 for flat bar stiffeners.....	154
Table 27 – Test Panel, FABSTRAN and PSC Experiment Results .....	157
Table 28 – ISSC2009 Benchmark Panel Dimensions .....	160
Table 29 – ISSC Panel ultimate strength under uniaxial compression.....	160
Table 30 – Comparison of methods to predict SSC451 panel strength .....	162
Table 31 – Multi bay panel test dataset .....	175
Table 32 – Multi Bay Panel Transverse Frame Dataset .....	175

Table 33 – Ultimate Strength Results – 5083-H116 Panels .....	180
Table 34 – Ultimate Strength Results – 245MPa Steel Panels.....	186
Table 35 – Ultimate Strength Results – 5083-H116 panels .....	220
Table 36 – Ultimate Strength Results 6082-T6 panels.....	221
Table 37 – Ultimate Strength Results – Steel panels .....	221
Table 38 - Box Girder Ultimate Strength Results .....	257
Table 39 – Box Girder Panel Dimensions .....	258
Table 40 – Aluminium Multihull Panels .....	261

## Nomenclature

$A$	Cross Section Area
$A_x$	Longitudinal Cross Section Area of Stiffened Panel
$A_y$	Transverse Cross Section Area of Stiffened Panel
$A_{sx}$	Longitudinal Stiffener Area, $A_{sx}=h_{wx} \cdot t_{wx}+b_{fx} \cdot t_{fx}$
$A_{sy}$	Transverse Stiffener Area, $A_{sy}=h_{wy} \cdot t_{wy}+b_{fy} \cdot t_{fy}$
$D$	Plate Flexural Rigidity
$D_H$	Horizontal cross section tangent rigidity
$D_V$	Vertical cross section tangent rigidity
$D_x$	Orthotropic plate flexural rigidity in longitudinal direction
$D_y$	Orthotropic plate flexural rigidity in transverse direction
$E$	Young's Modulus
$E_T$	Tangent modulus of the material stress-strain curve
$E_{T,p}$	Tangent modulus of the plate load shortening curve
$E_{T,s}$	Tangent modulus of the stiffener load shortening curve
$E_x$	Orthotropic plate elastic modulus in longitudinal direction
$E_y$	Orthotropic plate elastic modulus in transverse direction
$HR_L$	Longitudinal HAZ ratio
$I_x$	Second moment of area of the plate-stiffener cross section
$K_{\square}$	Distributed rotational stiffness on stiffener
$L$	Total panel length, $L=a \cdot (n_{sy}+1)$
$M_H$	Horizontal bending moment
$M_V$	Vertical bending moment
$a$	Interframe Panel Length
$b_p$	Plate width / Spacing between adjacent longitudinal stiffeners
$b_{fx}$	Longitudinal stiffener flange width
$b_{fy}$	Transverse stiffener flange width
$b_{HAZ}$	Heat affected zone width
$b_t$	Tensile residual stress width
$b_e$	Effective plate width
$h_{wx}$	Longitudinal stiffener web height
$h_{wy}$	Transverse stiffener web height
$n_{sx}$	Number of longitudinal stiffeners in an orthogonally stiffened panel
$n_{sy}$	Number of transverse frames in an orthogonally stiffened panel
$t_p$	Plate thickness
$t_{wx}$	Longitudinal stiffener web thickness
$t_{fx}$	Longitudinal stiffener flange thickness
$t_{wy}$	Transverse stiffener web thickness
$t_{fy}$	Transverse stiffener flange thickness
$v_{os}$	Maximum side imperfection amplitude in stiffener
$w_{opl}$	Maximum out of plane imperfection amplitude in plate
$w_{oc}$	Maximum column imperfection amplitude in panel
$\alpha / AR$	Plate Aspect Ratio
$\beta$	Plate slenderness ratio
$\varepsilon$	Material strain
$\varepsilon_0$	Material yield strain (steel) / 0.2% proof strain (aluminium)*
$\varepsilon_{0.2}$	0.2% proof strain (aluminium)*

$\varepsilon_0$	Yield strain (steel)*
$\gamma$	Stiffener cross section non dimensional parameter
$\lambda$	Column slenderness ratio
$\sigma_0$	Material yield stress (steel) / 0.2% proof stress (aluminium)*
$\sigma_{0.2}$	0.2% proof stress (aluminium)*
$\sigma_Y$	Yield stress (steel)*
$\sigma$	Material stress
$\sigma_U$	Ultimate strength of a structural element
$\sigma_{ave}$	Average edge stress on a plate or stiffened panel
$\sigma_{cr}$	Critical Elastic Buckling Stress
$\sigma_{u,x}$	Ultimate strength in longitudinal direction
$\sigma_{u,y}$	Ultimate strength in transverse direction
$\sigma_{0HAZ}$	Reduced proof stress in the heat affected zone (HAZ)
$\sigma_{rcx}$	Compressive residual stress magnitude in longitudinal direction
$\sigma_{rcy}$	Compressive residual stress magnitude in longitudinal direction
$\sigma_{rtx}$	Compressive residual stress magnitude in longitudinal direction
$\sigma_{rty}$	Compressive residual stress magnitude in longitudinal direction
$\phi_H$	Horizontal curvature
$\phi_V$	Vertical curvature
$\nu$	Poisson Ratio

### **Abbreviations**

<i>A.R.E.</i>	Admiralty Research Establishment
<i>HAZ</i>	Heat Affected Zone
<i>FEM</i>	Finite Element Method
<i>ProColl</i>	Compartment Level Progressive Collapse Program
<i>PSC</i>	Plate Stiffener Combination representation (single stiffener with attached plating – interframe)

\* Use of yield/proof stress and yield/proof strain for steel and aluminium: Where equations/graphs are proposed specific to steel the yield stress/strain is denoted with the subscript “Y”. Where equations/graphs are proposed specific to aluminium the proof stress/strain is denoted with the subscript “0.2”. Where equations are interchangeable (i.e. the equation is valid if used with the steel yield stress/strain or aluminium proof stress/strain) the generic subscript “0” is used to denote the yield/proof stress/strain.

*“The history of engineering is really the history of breakages, and of learning from those breakages”,*  
C.A. Claremont, Spanning Space [1]

# Chapter 1

## Introduction

### 1.1. Research Context

Structural engineering is fundamentally concerned with ensuring that a load bearing system has sufficient strength and robustness to perform satisfactorily under a wide range of load scenarios. Successful applications of this maxim, some dating back many thousands of years, are evident throughout our civil infrastructure; buildings, bridges and monuments continue to fulfil, and in certain cases exceed, their original purpose. However, the success of such buildings can be contrasted with others which are either judged to be too weak to remain standing safely or, worse still, collapse unexpectedly due to unforeseen load conditions.

A similar comparison can be made about ship structures. Most fulfil their role throughout their intended service life but occasionally ships fail catastrophically, with severe consequences for both the vessel itself and the surrounding environment. An accidental collapse of a structure is almost

always due to the failure of its skeleton structure. Such a failure flows from a large number of different causes, but the fundamental effect is that the ultimate capacity of the structure is exceeded.

Unlike most land based structures, a ship operates in a dynamic and ever changing ocean environment. A ship structure must therefore be designed to perform satisfactorily under a probabilistic range of environmental load conditions. For the most part these loads are much less than the structural capacity of the ship's skeleton – the hull girder. However, the ship must not only be capable of withstanding normal loads, but also with extreme scenarios that, whilst probabilistically rare, must be adequately accounted for in the structural design. Thus the ultimate capacity of the ship is a critically important measure. If the vessel experiences a primary load scenario over this critical point, known as the ultimate strength, the hull structure may fail, which sometimes results in a complete catastrophic loss of the ship (see Figure 1).



**Figure 1 – The Prestige oil tanker, which sank off the Spanish coast in 2002 [2]**

Within the broad context laid out above, this thesis explores this behaviour of lightweight ship structures when loaded up to and beyond their ultimate capacity. A ship experiences many types of loads, which are usually divided into specific categories [3]. The two most important in terms of the overall hull girder strength are the static (calm water) loads together with the low frequency dynamic loads from the action of ocean waves. These produce a distribution of longitudinal bending moments which are resisted by the longitudinally effective structure. Longitudinal bending moment is critical for large ships (normally taken to be vessels over approximately 70 metres in length) because the girder is long enough to act as a simple beam. Should the bending moment exceed the ultimate capacity of the girder, the ship can fail due to buckling and progressive collapse of the compressed portion of the structure.

There are numerous examples of hull girder failures due to insufficient structural strength, which have led to major damage or complete loss of a ship. A brief review of two cases is now presented.

A well-documented hull girder failure is that of the crude oil carrier *Energy Concentration*, which was loaded beyond her ultimate capacity whilst in Rotterdam harbour in 1980 [4]. The accident was caused by the cargo unloading procedure, causing a high hogging still water bending moment which surpassed the midship cross section capacity and broke the ship's back. The accident shows an example of how a structure can fail when loaded in an unusual and unintended scenario, placing the hull girder under excessive bending moment.

The *Prestige* disaster is another noteworthy example of primary structural failure with catastrophic consequences. *Prestige* was a 240m oil tanker, which sank off the Galician coast in Northwest Spain in 2002, spilling most of the fuel oil on board into the sea and subsequently causing a massive environmental disaster. The *Prestige* sank because the hull girder was first damaged, which caused severe flooding, and was subsequently overstressed by the flooded load condition and dynamic wave loads. This produced a sagging bending moment which exceeded the ultimate capacity of the girder, which had potentially been reduced through poor quality repairs to the hull.

The failure of the *Prestige* was due in the first instance to damage, but the final structural collapse occurred because of the addition of primary wave bending moment to an already overstressed girder. This is a graphic example of a progressive collapse type of failure. The ship broke its back in the midship region, which meant that the deck buckled under the excessive compressive loading caused by the wave induced bending moments together with the reduced effective cross section due to the damage. The deck failure effectively reduced its effectiveness to resist the applied bending moment, thus transferring load into the remaining parts of the structure. The structural failure thus progressed through the entire cross section and caused overall collapse of the cross section. The ship split into two parts and sank.

The *Prestige* disaster also highlights how the ultimate capacity of a ship can change, sometimes dramatically, if the hull girder is damaged. Damage removes or reduces the effectiveness of the longitudinal structure and thus the ultimate capacity of the vessel is compromised. Damage is difficult to quantify at the design stage, as typical accident scenarios can only be postulated. Damage is also a wide ranging criteria, including corrosion, small scale damage, repair, collision, grounding and, for naval combatants, shock and blast. These areas are all subject to much research, and the prediction of the residual hull girder strength is important to quantify. Although damage is not

researched explicitly in this thesis, the methods developed for the intact condition have potential for expansion to damaged cases.

To minimise the probability of catastrophic failures, ships are designed to ensure that the ultimate hull girder strength never exceeds the maximum expected wave induced bending moment. Limit state approaches have become an accepted methodology for first principles based design, and are especially suited to weight critical and novel ship types. Limit state design is a philosophy in which the capacity (ultimate strength) of a structure is evaluated directly and compared to the demand (extreme load) applied to the structure. Partial safety factors are employed to account for uncertainties in the capacity and demand. Unlike allowable stress design the limit state method is based on explicit quantification of the ultimate strength of the structure under specific conditions – thus the structure needs to be evaluated up to and beyond failure. Limit state design is conducted at several levels: ultimate limit states concerns the overall maximum strength of the intact system; damage limit states assess the residual capacity of the system after sustaining structural damage; and service limit states concern non catastrophic and usually localised failures in parts of the structure which limit or prevent the system from fulfilling its intended purpose.

Limit states have application both for the initial design of a vessel and also for analysing scenarios for existing ships. If the ship is analysed using a limit state approach, the ultimate strength of the hull girder is quantified and checked against a maximum load criteria which takes into account the expected “worst case” loading conditions experienced during the vessel life span. The quantification of ultimate strength is not a trivial matter, and thus a good deal of research and experiments have been undertaken to improve the understanding of primary bending moments and their effect on the progressive collapse of the hull girder.

## **1.2. Research Rationale**

Within the context of ultimate strength assessment, this thesis investigates the progressive collapse characteristics of lightweight ship structures. There has been continued growth in the size of large lightweight craft for both commercial and naval applications, exemplified by the recently completed littoral combat ship commissioned for the US Navy. This is combined with increased operability requirements for these vessels, including exposure to open ocean environments. The development of such vessels has raised important issues regarding the response of critical structure under primary hull girder bending. There is wide scope for improvement of the methodologies to predict the ultimate strength of a hull girder taking into account the specific complexities of lightweight arrangements.

Because of its favourable strength to weight ratio compared to steel, marine grade aluminium has now become a standard hull structure material for conventional high speed vessels. The size of these vessels is increasing, with a number of aluminium ships operating in the high speed ferry market now surpassing 100 metres in length. The US Navy has also reconsidered the value of using aluminium for high speed applications and has recently commissioned a 127 metre aluminium trimaran, the Littoral Combat Ship (LCS). Primary hull girder bending becomes an increasingly important strength criterion for these larger class vessels.

Maximum longitudinal hull girder bending usually occurs in the midbody region of a vessel, and imparts in-plane forces on the panel elements making up the hull girder. The response of these panels to uni axial compressive or tensile loading is important both in order to assess the local strength of the element and also its contribution to the overall strength of the girder. In particular, the response of the panels to compressive forces, which cause collapse due to buckling instabilities, is an important aspect to address. Overall hull girder strength assessment methodologies, such as the progressive collapse method, have been developed for steel vessel structures and require explicit characterisation of the load shortening behaviour of beam-column type elements making up the hull girder.

The progressive collapse method makes a number of assumptions about the hull girder, in particular the assumption that transverse stiffeners are much stronger than longitudinals and that the longitudinally oriented beam-column units fail in an interframe manner. Failure modes involving overall collapse of the panel are not accounted for; either interframe panel failure, where a number of beam-columns fail as one unit, or in overall panel failure, where the entire cross structure buckles between supporting transverse bulkheads, for example. This has been seen as a valid assumption for steel vessels, where overall buckling is unlikely to occur except in lightly stiffened panels such as superstructure decks, which do not contribute to the strength of the hull girder (Smith 1991). However, the lighter scantlings expected in the deck and bottom structure of high speed vessels needs to be assessed for the possibility of overall collapse modes before an appropriate progressive collapse type analysis can be developed.

The ultimate strength of a hull girder can be affected by the post-ultimate strength of the components. The stress of a stiffened panel element in compression will decrease in the post collapse region, and an adequate representation of the large strain response of a panel beyond the ultimate strength is thus important to quantify.

With significant commercial and military interest in large aluminium ships, it is clear that a rigorous structural design methodology is needed to design a large aluminium ship. In marine structural design, aluminium is often treated simply as steel with reduced stiffness - a simplification which masks many of the important response characteristics of aluminium structures. Additionally, current aluminium marine structural design methods are largely simple modifications of steel methods that do not account for all of the differences between aluminium and steel [5].

The strength characteristics of aluminium differ with steel in terms of its stress-strain relationship. Figure 2 shows a comparison between the typical engineering stress-strain curve for steel and aluminium. It can be seen that unlike steel, aluminium does not exhibit a clear yielding point. Aluminium also has round shaped stress-strain curve when it passes the elastic range. The ultimate elongation and also ultimate strength to yield strength ratio is lower than that of steel.

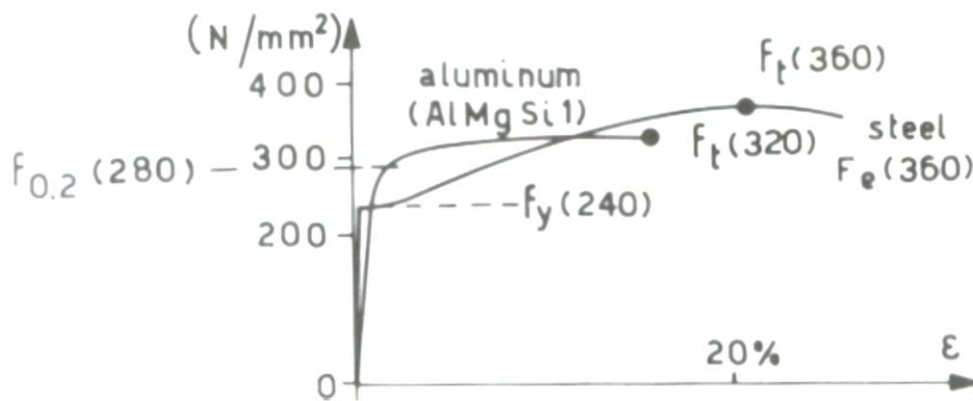


Figure 2 – Example engineering stress-strain relationships for aluminium and steel [6]

Another feature of aluminium is the significant effect that welding has on the strength of the material in the heat affected zone (HAZ). This process causes a strength reduction in the parent metal in the HAZ. Understanding this effect is important due to welding being the primary jointing process used in the fabrication of marine vessels.

### 1.3. Research Objectives and Scope

The main objective of this thesis is to examine the possible collapse modes of structure typical of a lightweight hull girder and, using this knowledge, to propose an extension to the Smith progressive collapse method [7], which is a well-known approach to calculate the ultimate capacity of a hull girder under combinations of primary bending moment.

Chapter 2 provides relevant background material for the research. The use of aluminium in the shipbuilding industry is reviewed in the context of the development of lightweight ship structures.

The hull girder ultimate strength problem, and how it fits within the context of assessing the structural performance of a lightweight ship, is introduced. Various methods to predict the progressive collapse of a hull girder are discussed. The limitations in the application of the progressive collapse method to a lightweight aluminium ship are highlighted.

Chapter 3 discusses analytical approaches to predict the strength of a stiffened panel including design charts, empirical approaches, a beam column method and an orthotropic plate method. The approaches are compared and their suitability to assess interframe and overall collapse modes within an orthogonally stiffened structure is discussed.

Chapter 4 describes detailed FEM analysis of plate elements, which are the fundamental building blocks of a ship cross section. Existing research and its relevance to the present work is reviewed. A series of initial studies using nonlinear FEM are then described. The influence of material and geometric parameters on the strength of steel and marine grade aluminium plates are highlighted. From the findings of the initial studies a rigorous FEM methodology is developed to model ship type plates in a realistic and representative manner. A set of parametric curve data sets are developed using the FEM methodology.

The FEM methodology is extended in Chapter 5 to model interframe and orthogonal stiffened panels. The findings of the plate study are used to develop further rigorous modelling techniques to include geometric imperfections, residual stresses and heat affected zones.

A semi analytical method to predict local and global buckling modes of an orthogonal stiffened panel is developed in Chapter 6. The approach utilises the results from the component FEM studies together with an extension of the orthotropic plate approach. The method is validated using FEM to demonstrate how it can predict overall buckling modes over multiple frame spaces.

Chapter 7 implements the semi analytical method from the previous Chapter in an extended progressive collapse methodology. The methodology is validated using a variety of box girder and hull girder examples. The extended method is compared to numerical analyses using a nonlinear FEM approach which encompasses the rigorous modelling methods developed in previous Chapters.

Chapter 8 provides overall conclusions to the research and recommends areas for future research efforts.

## **1.4. Summary of Thesis Contribution**

The research contained in this thesis contains several contributions in the research fields of progressive collapse analysis and hull girder ultimate strength prediction. The following provides a brief overview of the main research efforts.

Detailed stiffened panel analyses using a robust nonlinear FEM approach show that buckling over several frame spaces is a potential and realistic collapse mode for stiffened panels typical of a lightweight structure. These findings demonstrate the need to account for compartment level collapse modes in the progressive collapse method.

An extension of the simplified progressive collapse methodology is thus proposed and validated. The methodology is encapsulated in a usable computer program which first predicts the load shortening characteristics of a multi-stiffened panel using a semi-analytical calculation method and then uses this information to carry out a compartment level progressive collapse analysis with an extension of the Smith method.

Validations of the simplified analytical methodology are carried out with detailed numerical analysis utilising the nonlinear FEM approach. Several important insights into the numerical procedure have been gathered to propose a robust modelling approach for nonlinear FEM analyses of stiffened panels and entire ship cross sections. This robust procedure yields improved reliability in the solution of panel and girder analyses with nonlinear FEM.

*“At a very early period after the introduction of iron ships, Mr. Brunel perceived the great advantages attaching to longitudinal framing”, W.H. White, A Manual of Naval Architecture [8].*

# Chapter 2

## Background Material

### 2.1. Introduction

This Chapter provides background information to support the main body of research within this thesis. The Chapter is divided into two main sections. Firstly, a brief review of lightweight ships and the use of marine grade aluminium alloy sets out the context and timeliness of the research in this thesis. The evolution of the longitudinal framing system is then described, which provides the foundation for understanding how hull girder strength is designed into a modern ship structure. This leads to a definition of scantlings typical of a modern lightweight vessel. The material properties of marine grade aluminium alloys are then discussed. An adequate definition of the aluminium stress-strain relationship, and an understanding of the differences between different alloys and steel, is of crucial importance for correctly analysing structure using numerical methods.

The second part of the Chapter explores the existing tools available to predict the progressive collapse behaviour of a ship structure under primary longitudinal bending moment. The limit state

design approach is summarised to explain why progressive collapse tools are an important part of ship design and analysis. Analysis tools are then described, including the Smith progressive collapse method and the nonlinear finite element method.

## **2.2. Applications of Lightweight Ship Structures**

A broad definition of a lightweight ship is one where the hull structural weight is minimised through the use of unconventional materials or specialist structural arrangement to provide a specific benefit to the ship's operational capability. The resulting structural weight is significantly less than an equivalently sized vessel built from normal marine grade steel. The three predominant materials used for lightweight applications are aluminium, high tensile steel and composites such as fibre reinforced plastic (FRP). Lightweight ships are commonly designed for high speed applications, where the benefits of reducing the hull structural weight outweigh the additional costs of materials and design work.

High strength steel has been used in many shipbuilding applications where strength to weight ratio is a critical factor. High strength steel grades were first introduced into classification guidelines in the 1960s and some of its first uses were in high stress areas of VLCCs and other cargo vessels. High strength steels have been used as the primary structural material in some fast ferries, specialist naval vessels and large pleasure yachts.

FRP composites have been used in specialist applications, most notably for low signature corvettes and mine countermeasure craft for various navies. The UK developed the Hunt and Sandown class, the former was the largest warship built from glass reinforced plastic when introduced in the 1980s. The Visby class corvettes built for the Swedish Navy are amongst the largest composite craft currently afloat at 73 metres LOA. Composites are used extensively in the small craft industry, and have recently been applied to mega yacht designs such as the Mirabella-V, which is the largest sloop rigged sailing yacht in the world at 75 metres LOA.

Marine grade aluminium alloy has a typical strength to weight ratio over 2.5 times higher than normal grade shipbuilding steel. This beneficial quality combined with acceptable construction methods and operational performance has meant that, over the past two decades, aluminium has become a proven alternative structural material for high speed ships such as ferries and naval vessels.

The historical use of aluminium in shipbuilding stretches back over 100 years. The first notable marine vessel constructed from aluminium was a sloop rigged 17 metre racing yacht called

Vendenesse, launched in 1893 from Loire shipbuilders in France. In the 19<sup>th</sup> century aluminium was still a novel and new material, the metal having first been produced in its impure form in 1825. Even by the 1850s, bars of aluminium were more expensive than gold. The Vendenesse was therefore certainly a luxury yacht by any standards, and received sizeable press attention on launch [9]. The aluminium structure was riveted, and was used to reduce the structural weight, with 5mm plating used in the deck.

Vendenesse heralded a brief surge in the use of aluminium for shipbuilding during the 1890s, mostly in the superstructures of various small naval vessels built by the French, British and US Navies. She also influenced the US America's Cup challenger of 1894, Defender, which used aluminium in the deck for weight reduction and to lower the centre of gravity, thus improving the stability. However, corrosion problems were reported in the Vendenesse, and were probably also evident in the aluminium of the naval vessels. Although this may have had as much to do with the galvanic reaction caused by copper rivets used in construction, the poor performance of the metal in seawater is a likely reason why aluminium quickly dropped out of vogue and was not used as a hull structural material of ocean going ships for another 40 years.

However, the material properties of aluminium alloys make them a highly valuable engineering material and therefore the metal could not be ignored completely. The primary advantage of aluminium recognised by the designers of Vendenesse was its high strength to weight ratio. The New York Times reported that "...even twenty five persons could stand on the deck, which is made of aluminium and only 5 millimetres thick, without producing the slightest depression" [9]. It is this property, which surpasses the qualities of normal shipbuilding steel, which has driven the increasing use of aluminium as a structural material for weight critical ships throughout the 20<sup>th</sup> and into the 21<sup>st</sup> century.

In the 1930s aluminium began to be used in the superstructures of destroyers, where lightweight topsides were becoming increasingly important [10]. The use of aluminium steadily grew as the technology proved successful. After a temporary halt in the production of aluminium alloy during World War Two, due to shortages in the base material, the use of aluminium in deck houses became commonplace in the post war period. Welded construction replaced riveting, bringing the technology in line with equivalent steel production. In addition to Naval applications, aluminium was also used in the superstructures of cruise liners, including the SS United States, which also benefited from the weight benefits of using the material [11].

The modern use of aluminium alloys as a primary hull girder material has grown from the high speed ferry industry, which grew rapidly in the early 1990s. Australian shipbuilders InCat can claim to be the pioneers of modern aluminium ship construction, specifically in the fast ferry market. The company recognised the advantages of aluminium during the 1970s for light weight applications and expanded their facilities to manage aluminium construction. To meet demands for high speed sea transport, InCat developed the wave piercing catamaran concept and in 1990 they marked a watershed in the use of aluminium with the delivery of a 74 metre wave piercer to the British company Hoverspeed. Its success and the subsequent expansion of the fast ferry market saw a significant uptake in the use of aluminium alloys for a new generation of light weight, high speed vessels operating regular short sea shipping routes. A number of shipbuilders developed specialisation in aluminium construction techniques. In recent years larger aluminium high-speed vessels have been built, including some notable innovations on the original wave piercing concept.

Whilst the fast ferry market continues to be economically turbulent, with questions over the viability of fast short sea shipping routes, its overall expansion has meant that aluminium is now an established material choice to the shipping industry as a whole. In particular, the use of high speed designs for future naval applications is continuing to be explored by several Navies, in particular the USA. Lightweight and fast methods of transporting troops and heavy equipment at a lower cost than airlift are of great interest. The recognition of the potential of the commercial technology in a Naval role was tested by the temporary acquisition of various aluminium ferries for consideration by both the U.S Navy and the U.S Army. The progression of the U.S. Navy's Littoral Combat Ship program included the construction of a 127 metre aluminium trimaran (USS Independence), which will be tested alongside an equivalent steel monohull vessel (USS Freedom). Independence has been built by Austal USA and is outwardly similar to the Benchijigua Express.

## **2.3. Hull Girder Structures**

### **2.3.1. The Longitudinal Framing System**

The stiffening layout in the mid-section of a modern ship usually comprises relatively close spaced, continuous longitudinal members intersected by more widely spaced transverse framing. This arrangement has evolved from steady development over the past 150 years.

Early iron and steel vessels were built with transverse framing, replicating the well established system used in wooden ship building. The method of placing closely spaced frames, radiating from

the keel up to the decks and intersecting with transverse deck beams, was the only practical way to construct a wooden hull.

Isambard Kingdom Brunel, together with his project partner Scott Russell, pioneered the longitudinal framing arrangement [8]. Their design of the Great Eastern, which was 5 times larger than any other vessel afloat at the time, adopted a longitudinal system. Brunel recognised that, given the size of the vessel, the longitudinal bending moment and thus the longitudinal strength of the hull was critical. However the concept was slow to gain wider acceptance. Substantial vessels such as Great Eastern were uncommon (she remained the world's largest ship until 1901), so longitudinal strength was generally not considered a priority at the design stage. Furthermore, the structural arrangement required deep transverse frames to support the longitudinals, causing interference with stowage.

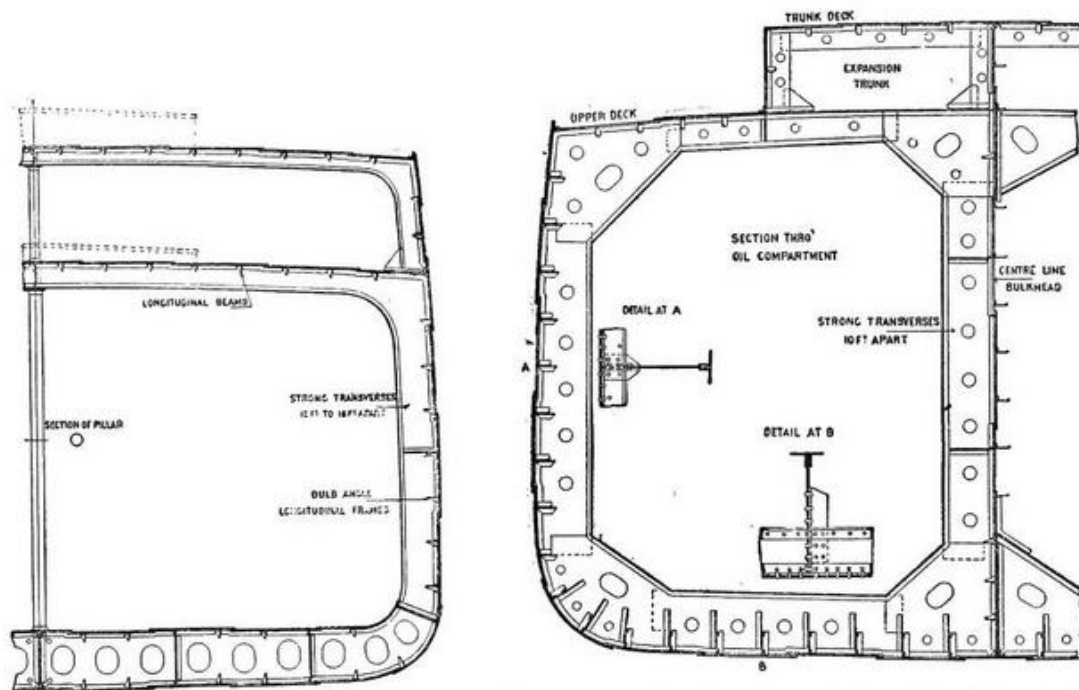


Figure 3 – Isherwood longitudinal framing system for a cargo steamer (left) and oil steamer (right) [12]

In 1906 Joseph Isherwood developed and patented a combined framing system that found particular favour for oil tankers, and subsequently led acceptance amongst the industry at large. The system combines widely spaced deep transverse frames with relatively closely spaced longitudinals stiffening decks, side shell and bottom. The arrangement was typically applied to double bottomed ships, with the side shell remaining single skin. The main advantage was claimed to be greater strength with reduced scantling weight. The system was also applicable to larger vessels. Example cross sections are shown in Figure 3, reproduced from Nicol's *Ship Construction and Calculations* published in 1909 [12].

The restriction on cargo space was a particular problem for dry cargo ships and for several decades the Isherwood system was rarely used. However, primary bending moment becomes a dominating load for seagoing ships surpassing about 70 metres in length. The increasing size of cargo and Naval vessels through the 20<sup>th</sup> century therefore led to the general acceptance of combined longitudinal-deep frame scantlings. A cross section of a typical longitudinal stiffening system is shown in Figure 4. The longitudinals are relatively small and closely spaced, the spacing is regular, and the number of stiffeners are rationalised to meet local and global load requirements. Deep longitudinal girders are located at widely spaced intervals across the panel. The transverse web frames and floors run orthogonally to the longitudinals and are usually deeper but more widely spaced.

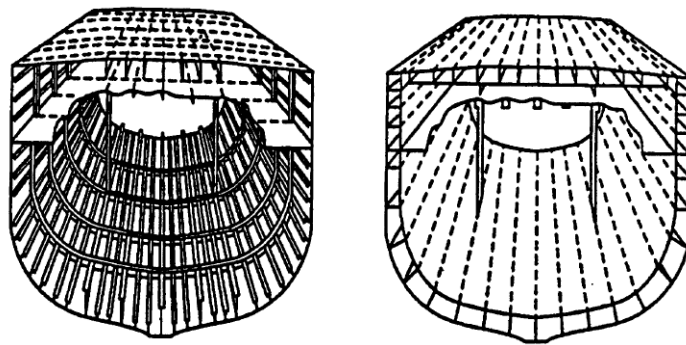


Figure 4 – Example conventional longitudinal framed (left) and advanced double hull (right) midship section arrangements [13]

A number of alternatives to the conventional framing system have been proposed. For example, the Advanced Double Hull concept was developed by the US Office of Naval Research to combine the global bending strength and weight saving benefits of longitudinal framing with a cellular structure to improve local strength [14]. A similar uni directional girder system was developed by Hitachi-Zosen [15]. The system, as shown in Figure 4, consists of an inner and outer hull connected by longitudinal girders running between transverse bulkheads. There is no intermediate transverse structure between bulkheads and the concept claims benefits in weight and production costs whilst maintaining structural strength.

### 2.3.2. Structural Components

Use of predominantly longitudinal scantlings produces an “interframe” structure comprising long plates bounded by relatively small stiffeners along the long edges and deeper transverse frames along the short edges. The plates and stiffeners perform a multiplicity of functions.

The plating is important in maintaining the integrity of the local hull structure but also as an important contributor to global hull strength. At the local level, an individual plate will likely serve

multiple functions. This may include being part of the watertight shell, providing internal compartments and/or supporting cargo. For example the plates on the main car deck on a high speed ferry would typically be required to support wheel loads.

Stiffeners also fulfil local and global strength functions. At the local level, the stringers and frames are effective in maintaining the stiffness, and hence the integrity, of the shell structure under localised lateral and in-plane loads. For example, a deck must be sufficiently stiff to prevent excessive deflection from maximum cargo loads. The side shell must not deform under hydrostatic and hydrodynamic pressure loads. Adding regularly spaced stiffeners is an effective way of improving the panel strength economically, by increasing the second moment of area of the cross section using a minimum of additional structural weight.

In addition to local functions, the stiffened structure is also critical in contributing to the primary bending capacity of the hull girder. The longitudinal stiffeners, together with attached plating, provide the effective structure to resist primary longitudinal bending. Thus the longitudinals are spaced such that the slenderness ratio of the adjacent plating is not excessive, giving the plate adequate strength to resist compressive in-plane forces. The stiffener dimensions are also important to provide sufficient resistance to compressive forces. The transverse structure contributes to the stiffness of the panel and also provides intermediate support to the longitudinals, effectively acting as nodal supports to shorten the column length and increase the buckling strength. Transverse structure also provides a significant contribution to the resistance of lateral load, which is particularly important for a multihull. The transverse structure is usually, but not always, characterised by relatively deep frames. Frames are typically spaced between 2 and 5 times the distance between the longitudinals.

### **2.3.3. Structural Arrangement of Lightweight Ships**

In order to better define the stiffener geometry for the purposes of strength assessment, this section considers typical arrangements of structural members for a large, lightweight, high speed aluminium vessel. Typical examples are the multihulls produced by Austal and InCat. These reach speeds of up to 50 knots and the designs are almost certainly driven by a need to reduce scantling weight in order to minimise fuel costs and maximise vehicle carrying capacity.

There is very little open source information regarding the structural arrangement of these types of vessel, partly because of the commercial interests of the builders. However, there are various sources of information which can give a better idea of how the structure is arranged. An excellent and highly useful open literature example of a high speed ship framing system is provided in an SSC

report by Kramer et al. [16], which investigated the conversion of a 122 metre INCAT catamaran to support a military payload. A midship cross section is reproduced in Figure 5. The report includes structural details of several deck extrusions and some general comments about the arrangement can be made.

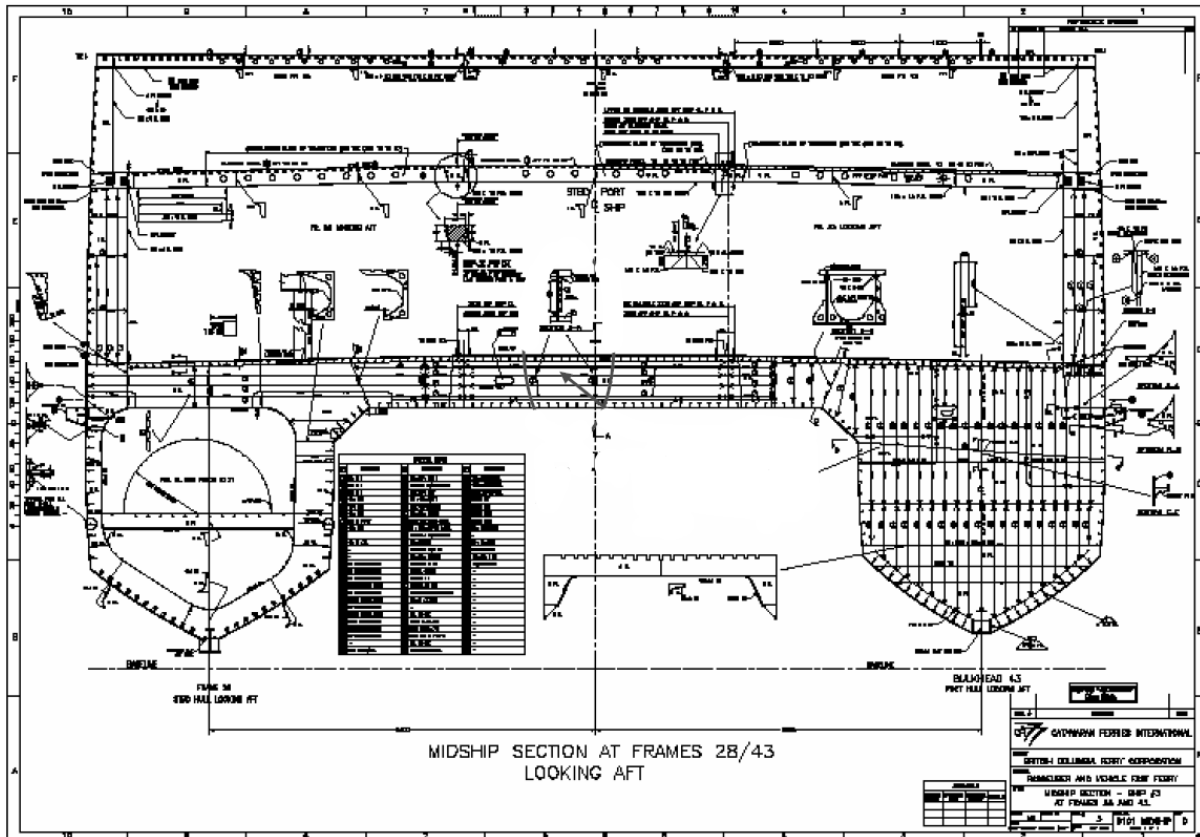


Figure 5 –Midship section of the Pacificat multihull [16]

The ship is longitudinally stiffened with transverse frames spaced at 1200mm intervals. Typical longitudinal spacing is 200-300mm. This creates a very detailed cross section with over 100 longitudinals situated across the main deck spans. The structure is almost more akin to an airframe than a conventional cargo ship cross section. The close stiffening is enabled because stiffened panels are extruded, reducing the welding requirements. A simplified version of the vessel is analysed in Chapter 7 of this thesis.

Further information on typical stiffener sizes can be found from aluminium manufacturer product lists. For example, Alcan produce standard profiles specifically for marine applications [17]. These are reviewed in the next section.

## 2.4. Marine Grade Aluminium

Aluminium is obtained in fused form from the mineral bauxite, and an electrolysis process is used to separate the element from the compound. The base material is then usually alloyed with small quantities of a number of elements, including magnesium, silicon, manganese, zinc, copper and titanium. The alloying process increases the strength of aluminium and can also increase corrosion resistance, reduce the melting point and change the ductility of the metal.

The grades of aluminium alloys typically used in the marine industry are the 5xxx and 6xxx series. These both include magnesium as an alloying element, which increases the resistance of the material to corrosion from seawater. Other alloys, including the 2000 and 7000 series, have been used in the past for marine construction, including high performance naval craft, and are more commonly found in aerospace applications. However, these alloys are highly susceptible to corrosion in a salt water environment; even with specifically designed coatings craft suffered from severe corrosion and fatigue problems [10].

5000 series aluminium has Magnesium (Mg) as the main alloying element and may also comprise a significant amount of manganese. 5000 series alloys are strengthened by work hardening. Alloys of this series are the most commonly used material in aluminium ship construction. They are weldable, formable, highly corrosion resistant, have high weld zone ductility and high strength. Various variations in strength values exist between alloys in the 5000 series.

Aluminium alloys of the 6000 series use Magnesium and Silicon as the main alloying elements. These agents form magnesium silicide and the alloy is therefore heat treatable and can be extruded into complex shapes. 6000 series alloys are mainly used in shipbuilding to form extruded parts. They are mainly used in shipbuilding to form parts that are extruded such as beams, stiffeners and bars but are also used in sheet or plate form. In general, the 6000 series alloys have less fracture toughness compared to the 5000 series. These alloys also have variations in strength between the various tempers.

Due to variations in the composition of the various alloys of aluminium, the modulus of elasticity varies, but in general it can be taken as 70GPa. This is approximately one third of the stiffness of steel, which has an elastic modulus of around 210GPa. As can be seen in Figure 1, there is no clear yielding point for aluminium. As a result of this, the yield point is usually assumed to be the stress corresponding to when the plastic component of strain is 0.2%. This point is otherwise known as the 0.2% proof stress.

A complete list of alloys certified for use in a marine environment is given by classification authorities including DNV and ABS, and are summarised by Sielski (2007). The most common alloys currently used in high speed craft are 5083-H116, 5383-H116, 6061-T6 and 6082-T6.

Probably the most commonly used alloy in recent aluminium ship construction is 5083-H116. The H116 temper designation indicates that the alloy is strain hardened to specific tensile property limits. The characteristics of 5083-H116 are seen to be a good combination of strength, formability, corrosion resistance and weldability. Of the 6000 series alloys 6061 and 6082 are commonly used for extruded stiffeners and beams as well as for plate stiffener extrusions in some vessels. Both alloys have a temper designation T6 indicating that they are solution heat treated and then artificially aged to improve the mechanical properties of the material. A number of alloys have been specifically developed for marine applications including 5059, 5383 and 7108. Perhaps the most widely researched of these materials is 5383, which comes in a number of temper designations but most commonly H116. 5383 has similar chemical composition and material properties to 5083.

Classification societies specify nominal material properties for different aluminium alloys and tempers. Table 1 and Table 2 present DNV and ABS material properties, which are very similar for the alloys considered in this study.

**Table 1 - DNV Minimum Material Properties [18]**

	<i>Ultimate Strength</i>	<i>0.2% Proof Strength</i>	<i>Elongation (%)</i>	<i>Remark</i>	<i>Notes</i>
5083-H116	305	215	10	Rolled	$t_p < 50$
5383-H116	305	220	10	Rolled	$t_p < 50$
6061-T6	260	240	10	Extruded	$t_p < 50$
6082-T6	310	260	10	Extruded	$5 < t_p < 50$

**Table 2 - ABS Minimum Material Properties [18]**

	<i>Ultimate Strength</i>	<i>0.2% Proof Strength</i>	<i>Elongation (%)</i>	<i>Remark</i>	<i>Notes</i>
5083-H116	303	214	10	Rolled	$1.6 < t_p < 38$
5383-H116	300	216	10	Rolled	$3 < t_p < 50$
6061-T6	262	241	10	Extruded	$t_p > 6.6$
6082-T6	310	262	10	Extruded	$t_p < 12.5$

Similar nominal values are repeated in a number of recent papers concerning aluminium plates and panels [19]. However, coupon test data from a number of experimental programmes carried out by the Admiralty Research Establishment (A.R.E.) [20], Trondheim University [21] and Pusan University

[22] amongst others shows considerable scatter and uncertainty in defining the material properties of 5000 and 6000 series alloys. Figure 6 below presents an example of coupon test data for 5083-H116 samples of different thickness as given in the studies.

The coupon tests generally give higher yield and ultimate strengths than the code values given in Table 1 and Table 2. However there are exceptions (such as the results from A.R.E.). Tests usually show consistent results for coupons from the same plate but a wide scatter can be found between plates.

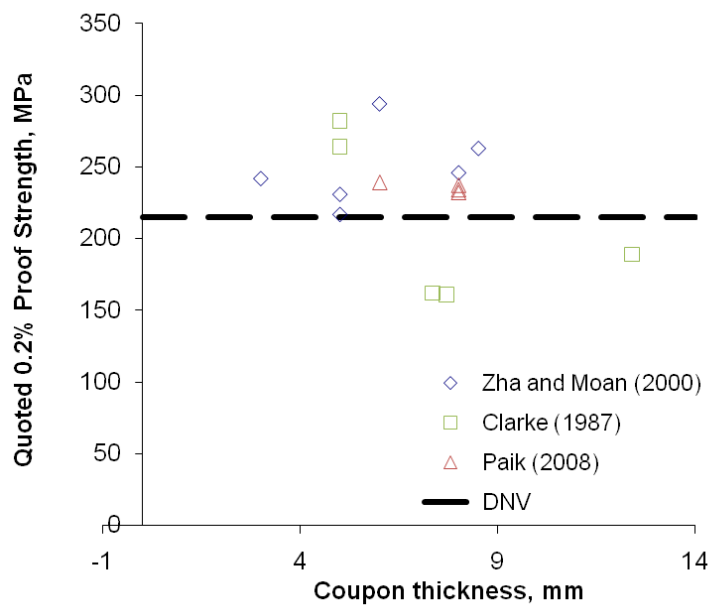


Figure 6 –Comparative 0.2% proof strengths of tensile test coupons

5000 series alloys are often significantly stronger in tension than compression. The aluminium association specifies a lower compression 0.2% proof stress for A5083-H116 of 180MPa [23]. This suggests that the compression properties of 5383 alloy will also be different. 6061-T6 is listed with the same 0.2% proof stress in tension and compression by the Aluminium Association.

#### 2.4.1. Aluminium Stress-Strain Relationship

As has been shown in Figure 2, the true stress-strain curve of an aluminium alloy is rounded and does not have a well-defined yield point or plastic region after yield. This is significantly different to the relationship found for steel. It is possible to represent this relationship using a simple elastic perfectly plastic model, an elastic-plastic bilinear model which takes into account the strain hardening or a more complete nonlinear relationship.

The Ramberg-Osgood equation [24] has been found to give a close approximation to actual alloy stress-strain curves. It is defined as:

$$\varepsilon = \frac{\sigma}{E} + 0.002 \left( \frac{\sigma}{\sigma_{0.2}} \right)^n \tag{1}$$

where  $n$  is an exponent or “knee factor” defined either by physical tests or using established approximation techniques [6]. As the value of the exponent rises the stress-strain curve flattens out and more closely represents the elastic perfectly plastic approximation.

Values of the exponent for the alloys considered in this study from recent literature are presented below. There is significant uncertainty in the values.

**Table 3 - Knee Factors for Ramberg Osgood relationship – comparison of literature values**

	Mazzolani (Zunaidi)	Mazzolani	Collette (2005)	Paik (2005)	Zha (2001)*	US DOD (1998)
A5083-H116	24	27	12	15	14-21	
A5383-H116		23		15		
A6061-T6	43	45				21
A6082-T6		47	30	15	30-46	

\* Increasing exponent for increasing plate thickness

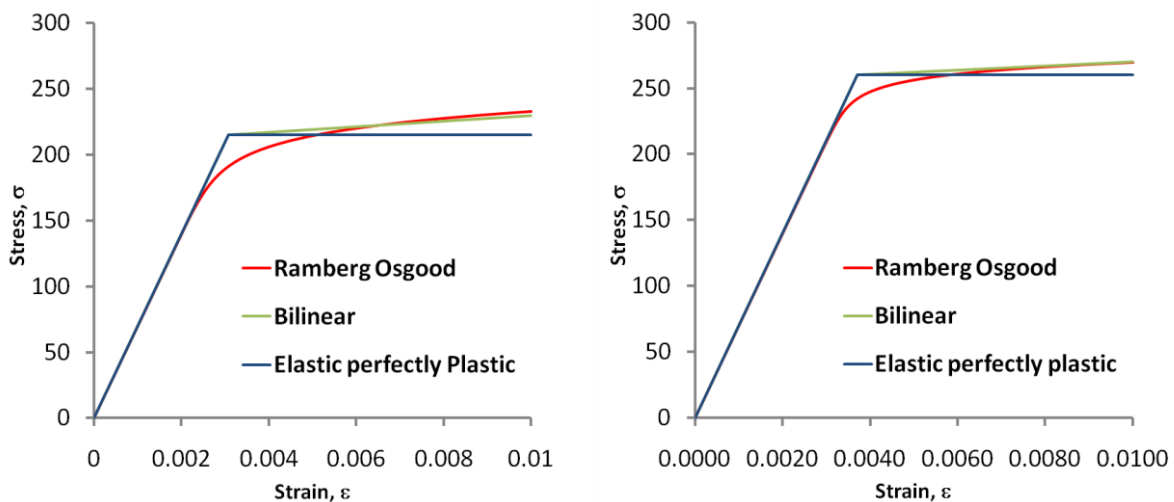


**Figure 7 – Aluminium alloy 5083-H116 (left) and 6082-T6 (right) stress-strain relationship**

Example stress-strain relationships are shown in Figure 7 for 5083 series and 6082 series alloys. It can be seen from these two figures that the 5000 series alloys depart noticeably from the linear elastic response at about 70% of the yield stress. The 6000 series alloys have a stress-strain curve more closely approximating the elastic perfectly plastic approximation. The bilinear approximation

provides a better correlation at high strain levels but cannot replicate the rounded portion of the curve before the 0.2% offset proof stress point.

#### **2.4.2. Heat Affected Zone**

The material properties of a welded aluminium alloy plate are affected by two significant phenomena associated with the welding process. Welding inputs heat non-uniformly across the plate during panel fabrication; the heat softens the material adjacent to the weld, causing a heat affected zone, and also imparts internal residual stresses over the plate area. These material imperfections have separate physical causes, but both are caused by welding. The idealised heat affected zone used for design purposes is described here whilst the residual stress pattern is detailed in the next section.

The heat affected zone (HAZ) describes the area of plate weakened by the welding process. HAZ occurs at the edges of plates adjacent to fillet welds for stiffeners (rolled plate) or butt welds for adjacent plating (extruded plate with stiffeners). The formation of HAZ is due to different metallurgical processes for 5000 and 6000 series alloys.

5000 series alloys are strengthened by work hardened in the milling process. Subsequently, the high heat of fusion welding raises the temperature of material that is close to the weld above the recrystallisation temperature, removing the work hardening and leaving the material in the weaker annealed (O) state.

6000 series alloys are heat treated to increase their strength. The heat generated during welding causes the magnesium silicide precipitates, which provide extra strength in the alloy, to turn back into solution in the weld itself. Further away from the weld the precipitates grow in size, which reduces the local alloy strength by nearly half.

The mechanical strength properties of an aluminium plate gradually decrease close to a welded connection, reaching a minimum at the centre of the weld. Because the temperature during welding decreases with increased distance from the weld, the material properties in the HAZ region also change with distance from the weld. It is difficult to accurately model the correct material property throughout the weakened zone in numerical analyses. Usually the HAZ is assumed to have constant representative material properties over a defined breadth of plating to approximate the actual material properties. Figure 8 shows an example sketch from Hill et al. [25] of the design approach to represent the HAZ breadth. For a stocky plate the properties may also be different through the plate thickness (Figure 9).

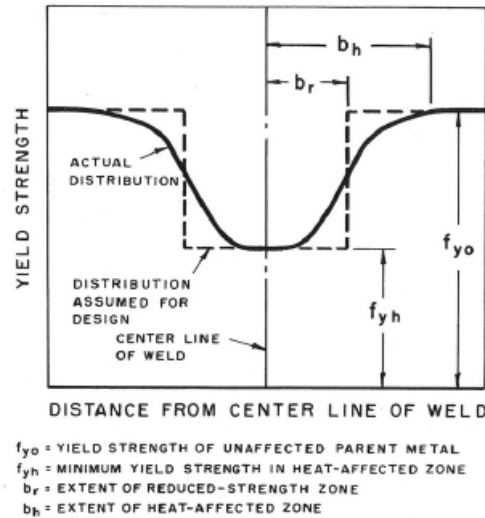


Figure 8 - Effective HAZ breadth [25]

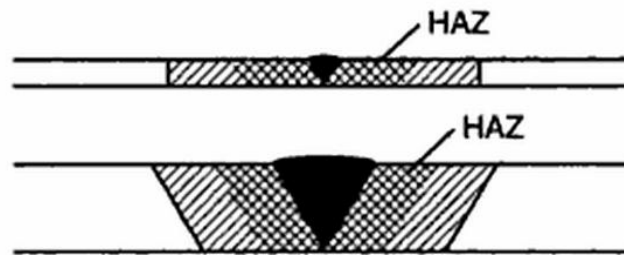


Figure 9 – Through thickness HAZ formation [26]

The HAZ width can be established by testing the hardness of the area close to the boundaries of welded plates. Some early experiments of 6000 series plates were carried out by Hill et al [25]. Normally, a simplification of the HAZ distribution is made by assuming a constant reduced elastic limit zone. The size of this representative zone is less than the actual affected area, as shown in Figure 8. Mazzolani [6] suggests a 25mm representative HAZ, based on experiments. Zha & Moan [27] and Paik [19] also propose a 25mm HAZ breadth. In addition, Zha & Moan tested HAZ breadths of 12.5mm. Both 25mm and 12.5mm HAZ breadths are used by Collette [5] in numerical analyses of aluminium box sections.

BS8118 [28] and Eurocode 9 [29] include explicit formulas to estimate the HAZ width. Both codes give HAZ breadth as a function of the plate/stiffener thickness to include the effect of the temperature distribution in different thickness material. The following formulas given are valid for fillet welds applied to 5000 or 6000 series alloys.

BS8118 defines the HAZ breadth as:

$$z = \alpha\eta z_0 \quad 2$$

where  $\alpha$  and  $\eta$  are modifying factors to account for the material being at an elevated temperature and increased heat build up during the welding process. Both values can be taken as 1.0 for the purposes of this study, consistent with the approach of Kristensen and Moan [30].  $Z_0$  is defined as:

$$z_0 = \min\left(20 + \frac{t_A}{t_B}, \frac{3t_B^2}{t_A}\right) \quad 3$$

where  $t_B$  and  $t_C$  are the thickness of the thickest and thinnest element respectively and  $t_A$  is the lesser of  $0.5(t_B+t_C)$  and  $1.5t_B$ .

Eurocode 9 gives HAZ breadths for ranges of the average material thickness as follows:

$$\begin{aligned} 0\text{mm} < t_p \leq 6\text{mm} : & \quad b_{HAZ} = 20\text{mm} \\ 6\text{mm} < t_p \leq 12\text{mm} : & \quad b_{HAZ} = 30\text{mm} \\ 12\text{mm} < t_p \leq 25\text{mm} : & \quad b_{HAZ} = 35\text{mm} \\ 25\text{mm} < t_p : & \quad b_{HAZ} = 40\text{mm} \end{aligned} \quad 4$$

The code values are shown in Figure 10 for a range of plate thicknesses. The plate is assumed to be of equal thickness to the attached stiffener/plating. It can be seen in Figure 10 that Eurocode 9 predicts a larger HAZ breadth than BS8118 for all usual plate thicknesses. For the range of plate thicknesses considered in this study the codes give HAZ breadths in the region of 25mm.

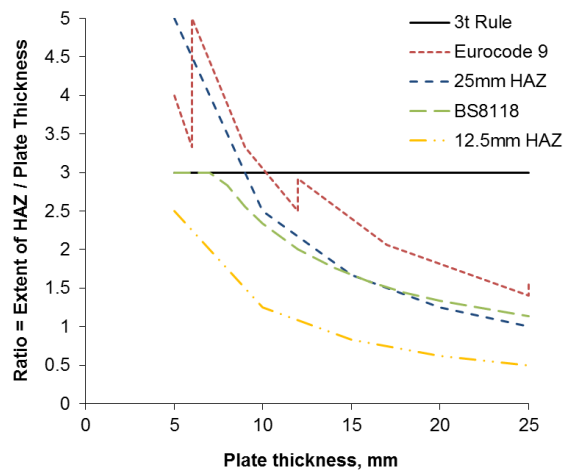


Figure 10 - Extent of HAZ for a range of plate thickness and specification codes

The reduced proof strength in the HAZ can be approximated by a knock down factor. Factors are specified by classification societies. Knock down factors are also presented in a number of recent papers.

Material properties in the HAZ are usually determined by testing. Specimens from a standard butt weld are cut, normally either 50mm or 250mm in length. Most data has been collected with 250mm specimens and this has led to anomalous results because the HAZ constitutes a smaller percentage of material in these larger test pieces. Data from numerous sources is presented in Table 4, partly reproduced from SSC-452 [10].

The assumed heat affected stress strain curves for 5083-H116 and 6082-T6 as used in this study are shown in Table 4. The curves are based on strength reductions of 67% for 5083-H116 and 53% for 6082-T6 [29]. The knock down factor can also be applied to the Ramberg-Osgood exponent [5, 27].

**Table 4 - HAZ Properties**

		<i>Collette</i> [5]	<i>Paik</i> [19]	<i>Zunaidi</i> [31]	<i>Zha</i> [27]a	<i>DNV</i> [18]	<i>Alcan</i> [17]	<i>Kissell</i> [23]	<i>ABS</i> [32]b
A5083	$\sigma_{0HAZ}$	144	144	145	144	125	125	115	165
	$\sigma_{0HAZ}/\sigma_{0.2}$	0.67	0.67	0.67	0.67	0.58	0.58	0.53	0.77
A5383	$\sigma_{0HAZ}$	-	154	-	-	145	145	-	165
	$\sigma_{0HAZ}/\sigma_{0.2}$	-	0.7	-	-	0.67	0.67	-	0.77
A6061	$\sigma_{0HAZ}$	-	-	104	-	115	-	105	103-138c
	$\sigma_{0HAZ}/\sigma_{0.2}$	-	-	0.43	-	0.48	-	0.40	0.40-0.53
A6082	$\sigma_{0HAZ}$	138	138	-	138	115	-	-	-
	$\sigma_{0HAZ}/\sigma_{0.2}$	0.53	0.53	-	0.53	0.44	-	-	-

a:Based on DNV data, b:Values for butt welded alloys, c:Lower value for material under 9.5mm thickness

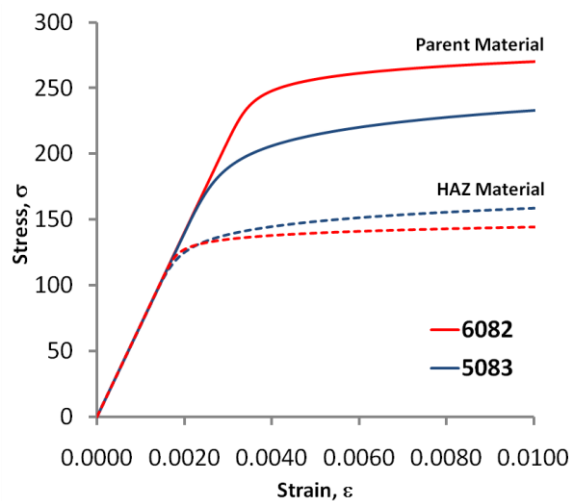


**Figure 11 – Comparative HAZ material properties for 5083-H116 and 6082-T6 aluminium alloys**

The knock down factor can also be applied to the Ramberg-Osgood exponent [5, 27]. Based on the typical values given in Table 4, a knockdown factor of 0.67 and 0.53 were applied to the 5083-H116 and 6082-T6 material models respectively. The resulting stress-strain curves are shown in Figure 11.

### **2.4.3. Residual Stress**

Residual stress is the term used to describe the self-equilibrated internal stresses present in otherwise unloaded structural elements. Internal localised stress patterns are created when some or all areas of a structural member undergoes physical or thermal induced deformation, and is subsequently prevented from returning to its previous non deformed state. This creates a permanent, inhomogeneous deformation field in the structural member.

Residual stress fields are generated in most metal structures and manufactured parts during construction [33]. For ship structure the most significant cause of residual stress is the welding process during fabrication [10]. As it cools following a weld pass, the liquid weld bead at the joint is resisted from contracting by the bulk of the parent material. This causes tensile residual stresses to form within and near to the weld, and equilibrating compressive stress fields in the unheated plate region away from the weld joint.

The intensity of the heat input from welding is a function of a number of variables, including: the type of weld procedure used; the pass size; and the depth of penetration [6]. Recent studies have found that the heat input and associated mechanical properties of the material at high temperatures is the significant contributor to residual stresses for both molten state (arc) and solid state (friction stir) welding [34, 35]. This suggests that the quantity of heat introduced during welding is the primary contributor to residual stress rather than the specific levels of plastic deformation caused by the weld method. Therefore there is a possible advantage in using less heat intense weld methods, such as friction stir, if the residual stresses have a significant detrimental effect on the structural strength.

For the purposes of numerical analysis, the residual stress field can be idealised into stress blocks with an abrupt discontinuity between the tensile and compressive zones. Measurement of residual stress by Paik et al [36], using a hole drilling procedure, shows that this idealisation matches reasonably to actual stress distributions (Figure 13). The residual stress pattern is two dimensional; with the longitudinal weld causing tensile stress in the x-direction and the transverse weld causing corresponding tensile stress in the y-direction.

The tensile zone distribution is similar to the HAZ distribution as discussed previously. Thus the position of the tensile zone in the longitudinal direction depends on the construction method (rolled or extruded panels), with weld usually either at the edge or down the middle of the plate. The idealised residual stress pattern for weld about the plate edges are illustrated in Figure 12.

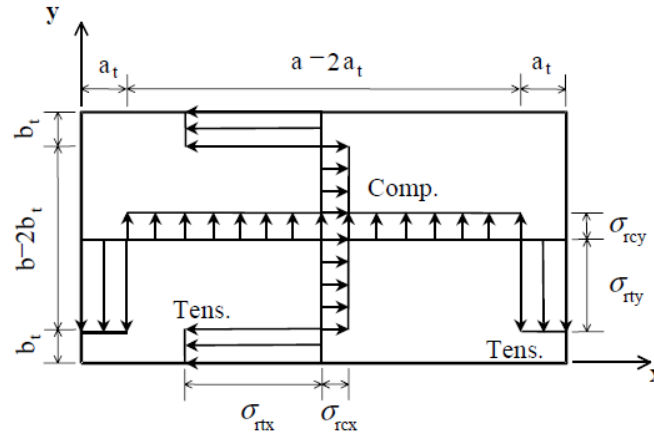


Figure 12 - Idealised residual stress distribution with weld along all four edges of the plate [37].

To ensure equilibrium over any plate cross section a relationship between the residual stress and the width of the tensile stress field is:

$$b_t = \frac{\sigma_{rcx}}{2(\sigma_{rcx} - \sigma_{rtx})} b \quad 5$$

For a steel plate the tensile residual stress zone should usually be considered to be equal to or just less than the material yield stress. However, due to the heat induced softening produced near welded aluminium joints, the corresponding tensile residual stress for aluminium is closer to the HAZ proof stress. This assumption has been validated by residual stress measurements taken in a recently conducted aluminium panel experimental programme [22], which indicate tensile residual stresses well below the parent metal strength and closer to the assumed HAZ strength.

The width of the tensile zone depends on the level of heat input during welding. An empirical approach to estimate the compressive residual stress of steel plates is given by Smith et al. [38], which can then be used in combination with Eq. 5 to calculate the tensile residual stress zone[38]:

$$\frac{\sigma_{rcx}}{\sigma_Y} = \frac{\sigma_{rcy}}{\sigma_Y} = \begin{cases} -0.05 & \text{slight} \\ -0.15 & \text{average} \\ -0.30 & \text{severe} \end{cases} \quad 6$$

This expression is based on survey data from predominantly steel test pieces.

When applied to typical aluminium geometry, Eq. 6 can result in specifying quite large tensile zones, much greater than the corresponding HAZ width. The discussion regarding HAZ width has concluded that the heat input during welding usually conducts a certain distance from the weld joint. Because residual stress is also formed by heat input, this suggests that the tensile residual stress zone and HAZ can be assumed to cover the same width.

A recent SSC study [22] provides some evidence to validate the assumption of equal HAZ and tensile residual stress zone width. The study measured residual stresses in aluminium panels using a hole drilling procedure, with carefully positioned gauges to capture the strain released at the test points [22]. Some limited results from the tests for a 5083 panel are given, which are reproduced in Figure 13. The tensile stress region is of similar magnitude to the expected HAZ breadth.

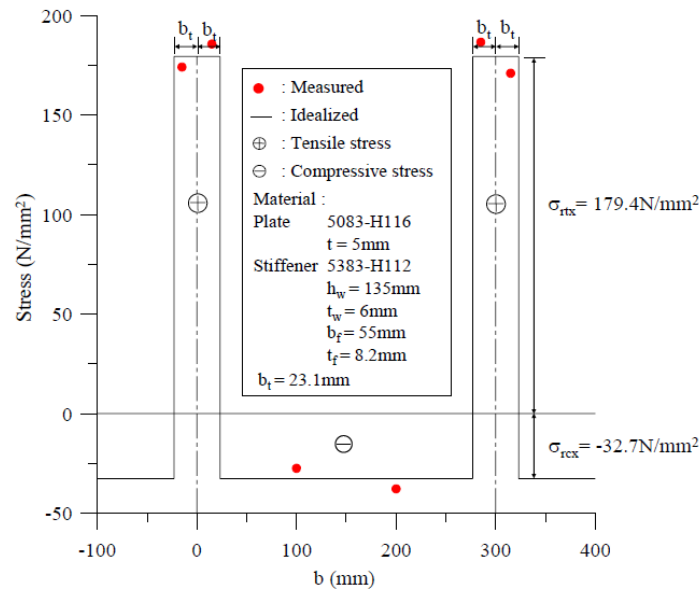


Figure 13 – Measured residual stress distribution in an aluminium panel [22]

Throughout this study, the residual stress field in steel and aluminium plates are derived using different approaches based on the discussion above:

- **Aluminium:** The tensile residual stress zone for an aluminium plate or stiffener is assumed to extend the same distance away from the weld joint as the HAZ. The tensile residual stress is assumed to be slightly less than the material proof stress and Eq. 5 is used to define the compressive stress.
- **Steel:** The residual stress field for steel plates and stiffeners is calculated using the equations of Smith et al. [38], where the compressive residual stress zone is as defined in Eq. 6 and then the tensile width is calculated with Eq. 5

## 2.5. Typical Fabrications

Panel geometry for an orthogonal stiffened hull girder structure is typically described by the spacing between longitudinal stiffeners, the spacing between transverse frames, the thickness of the shell plating and the profile of the stiffening members. This section summarises the variety of forms in which aluminium is supplied and gives some indicative data for typical geometry definitions. The dimensions of a stiffened panel are as shown in Figure 14 and defined in the nomenclature.

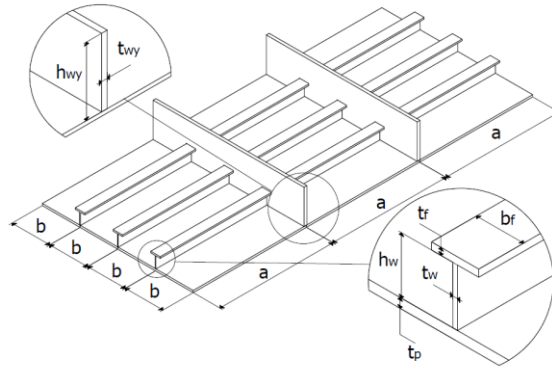


Figure 14 – Cross section geometry of a stiffened panel

A panel is defined by two non dimensional quantities, which together can quantify the relative slenderness. The plating is defined by the plate slenderness ratio ( $\beta$ ):

$$\beta = \frac{b}{t} \sqrt{\frac{\sigma_0}{E}} \quad 7$$

The plate-stiffener combination is defined by a column slenderness ratio ( $\lambda$ ):

$$\lambda = \frac{a}{\pi r} \sqrt{\frac{\sigma_0}{E}} \quad 8$$

where the radius of gyration is:

$$r = \sqrt{\frac{I_x}{A}} \quad 9$$

$I_x$  is the second moment of area of the plate-stiffener cross section:

$$I_x = b_p t_p^3 + b_p t_p \left( z_0 - \frac{t_p}{2} \right)^2 + t_w h_w^3 + t_w h_w \left( z_0 - t_p - \frac{h_w}{2} \right)^2 + b_f t_f^3 + b_f t_f \left( z_0 - t_p - h_w - \frac{t_f}{2} \right)^2 \quad 10$$

These equations are equally valid when applied to a steel panel (using the material yield stress) and aluminium alloy panel (using the 0.2% proof stress).

Aluminium is procured in three forms: sheet, plate and extruded profiles. A flat rolled panel with thickness less than 6mm is known as sheet, otherwise it is plate. To avoid confusion in this report the term plate will be used to describe rolled aluminium alloy of any thickness. Plate is usually rolled into a large rectangle of uniform thickness and then cut to size either using mechanical means or with numerically controlled plasma arc cutting machines. A less commonly used computer numerical control (CNC) method is fluid jet cutting, which has the advantage of leaving no heat affected zone close to the cut edge [10]. CNC cutting is usually the most accurate and efficient method to employ; it produces a weld ready edge and can be used to produce intricate shapes and cutouts. Even relatively small boatyards may prefer to have plate cut and prepared using CNC off site rather than using mechanical saws or shears on site [10].

Aluminium stiffeners are fabricated by extruding the stiffener cross section or building the section from rolled plate. Similarly, stiffeners can either be attached by fillet welds to the plate or entire plate-stiffener extrusions can be formed, including a number of stiffeners and associated plating in one extrusion and then butt welding adjacent panels to form the complete panel.

Extrusions are formed by pressing heated (solid but malleable) billets through a steel die. The process is relatively simple and can be used to produce a wide variety of profile shapes. For marine purposes typical extrusions are commonly standard stiffener profiles, often in standard flat, tee, angle and bulb shapes. The extrusions are usually fillet welded directly to plate to form a stiffened panel. Alternatively a stiffener-plate combination can be extruded, whereby a complete profile including either a single or multiple stiffeners with associated plating is formed. The extrusions are then butt welded together, usually at the plate mid span, to form the complete panel.

It is difficult to extrude most 5000 series alloys and therefore it is usual to assume that panels constructed from 5083 or similar are built up from rolled plate. Alloy 5383-H116 can be extruded, and Alcan Marine produce standard tee and bulb extrusions in their proprietary alloy brand Sealium.

6000 series alloy is more adaptable, its composition allowing a greater choice of construction methods depending on the preferences of the shipyard. This enables the exploitation of potential benefits associated with an extruded panel, including less plate area exposed to high heat input from welding with the associated lowering of strength in the heat affected zone.

A wide range of standard extrusion shapes are available. Alcan Marine produce standard tee and bulb extrusions in their proprietary alloy Sealium (5383-H116). This range of profiles is listed in Tables 1 and 2. SNAME T&R Bulletin 207 details a set of stiffener extrusions developed in the 1960s for the topsides of Naval vessels. These extrusions are still used as a standard in aluminium shipbuilding [10] and are listed as “off the shelf” shapes by some suppliers.

Perhaps not so applicable to extruded aluminium are the Admiralty Long Stalk Tees used in British warship designs and also employed for the aluminium panel tests conducted at the A.R.E. [20]. Standard dimensions are as listed in Table 4. Long stalk dimension ratios, as defined in Figure 3, are also used to construct the stiffener geometry in the steel stiffened panel parametric studies by Smith [39]. A ratio of stiffener area to total cross section area is defined and using this, the thickness of the stiffener web and hence the complete stiffener geometry can be defined.

**Table 5 – Alcan T-Bar Extrusions**

Ref.	$h_{wx}$ (mm)	$t_{wx}$ (mm)	$b_{fx}$ (mm)	$t_{fx}$ (mm)	$A_{sx}$ (mm <sup>2</sup> )	$I_x$ (mm <sup>4</sup> )
T50	50	3	30	4.5	299.4	84661
T60	60	3.5	35	5.1	402.5	162062
T70	70	4	40	6.1	536.3	287199
T80	80	4.5	45	6.2	650.6	459593
T100	100	5	50	6.4	830.3	927951
T120	120	5.5	55	7.7	1091.9	1735149
T140	140	6	60	8.7	1367.9	2942592
T170	170	6.5	65	10.3	1777.5	5598533

**Table 6 – Alcan Bulb Extrusions**

Ref.	$h_{wx}$ (mm)	$t_{wx}$ (mm)	$b_{fx}$ (mm)	$t_{fx}$ (mm)	$A_{sx}$ (mm <sup>2</sup> )	$I_x$ (mm <sup>4</sup> )
P50	50	3	10	-	218.1	56879
P60	60	3.3	12	-	284.9	107491
P70	70	3.5	14.5	-	360.1	185623
P80	80	3.7	16.6	-	436.8	294579
P100	100	4.2	21	-	620.8	655095
P120	120	4.6	26	-	833.8	1262306
P140	140	5.1	30.5	-	1106.4	2249169
P170	170	5.8	37.5	-	1580.4	4673733

**Table 7 – Admiralty Long Stalk Tees**

Ref.	$h_{wx}$ (mm)	$t_{wx}$ (mm)	$b_{fx}$ (mm)	$t_{fx}$ (mm)	$A_{sx}$ (mm <sup>2</sup> )	$I_x$ (mm <sup>4</sup> )
ALS1	69.8	4.4	25.4	6.4	469.7	279548
ALS2	104.8	5.1	44.5	9.5	957.2	1263323
ALS3	113.6	6.65	63.5	13.4	1606.3	2438715
ALS4	138.2	7.15	76.2	14.2	2070.2	4589788
ALS5	162.6	7.65	88.9	15.2	2595.2	7885356
ALS6	186.9	8.15	101.6	16.3	3179.3	12661097
ALS7	235.7	9.15	127.0	18.3	4480.8	28091475

Standard profiles are useful for defining typical ranges of stiffening used in aluminium craft. However, the relatively minimal costs of producing steel die for the extrusion process allows shipbuilders to develop their own profiles to meet their design requirements more exactly than with standard shapes. Furthermore, the designer is not restricted to extruding the stiffener only.

An example use of extruded panel construction is detailed in a ship structure committee project completed in 2005 by John J. McMullen Associates [16], who investigated the conversion of a generic HSV to transport military vehicles in unrestricted, open service. The study uses the Canadian built Pacificat ferry owned by BC Ferries and designed by INCAT. The vessel is a 122m LOA catamaran with an operating speed of 35 knots. Various structural details of the Pacificat are presented, giving some insight into likely stiffened panel dimensions used in a HSV built from extruded panels.

The structural and material properties of the main vehicle deck are as shown in Table 8. The deck plating / stiffener combination is extruded 6061-T6 or 6082-T6. The extrusions are 1200mm in length and include 1 stiffener. The extrusions are welded to transverse floors at the ends of the panel bay. The report gives detailed drawings of the welding arrangement. Two extrusions are used in the vehicle deck, a heavy extrusion near the centreline and a light extrusion further outboard. Structural details of the extrusions are given below.

**Table 8 – Pacificat Deck Extrusions**

Ref.	$h_{wx}$ (mm)	$t_{wx}$ (mm)	$b_{fx}$ (mm)	$t_{fx}$ (mm)	$A_{sx}$ (mm <sup>2</sup> )	$I_x$ (mm <sup>4</sup> )
Heavy	127.8	7	50	9.6	1374.6	2695672
Light	95	4.3	50	8.7	843.5	876331

Some general comments can be made about typical stiffener dimensions based on this data. The ratio of stiffener height to stiffener web thickness ranges between 15 and 30. The ratio generally increases as the stiffener height increases. The ratio of stiffener height to flange breadth ranges between 1 and 2.5, again with the ratio increasing as stiffener height increases. The ratio of flange thickness to web thickness ranges around 1.1 to 2 but most commonly the ratio is about 1.5. The admiralty long stalk tee dimensions are therefore suitably sized for aluminium type structure.

## **2.6. Hull Girder Progressive Collapse Methods**

### **2.6.1. Limit State Design**

Ultimate limit state design is a philosophy in which the “capacity” (ultimate strength) of a structure is evaluated directly and compared to the “demand” (load) applied to the structure. Partial safety factors are employed to account for uncertainties in the capacity and demand. Unlike allowable stress design the ultimate limit state method is based on explicit quantification of the ultimate strength of the structure under specific conditions – thus the structure needs to be evaluated up to and beyond failure.

As discussed in the introduction to this thesis, primary hull girder bending is resisted by the continuous longitudinal structure running through the main body of a ship. This normally comprises the longitudinal stiffeners and plating making up the side shell and decks of the hull and is known as the hull girder. Overall bending imparts in-plane forces on the longitudinal structure. The structure may also be subjected to transverse in-plane loads and local bending arising from pressure loads.

An advantage of limit state design, as applied to a ship, is to ensure adequate performance of the primary structure whilst minimising the lightship mass, thus increasing the payload capacity and also keeping material costs to a minimum. Usually a ship structure designed using limit states is assessed to the ultimate limit state criteria; that is the strength of the hull girder is compared to the expected maximum global loading throughout the intended service life. Damage limit states may also be assessed, for example by considering the residual strength of the structure after a collision or grounding accident. The classification of damage can also include corrosion, fatigue cracks and other in service phenomenon, which may also be important to consider. Fatigue is sometimes classed separately as a fatigue limit state. Service limit states also need to be considered, for example to check that the out of plane deformations of a load bearing cargo deck are within tolerable limits.

As part of a limit state design process, accurate numerical tools are required to predict the strength of the hull girder and to assess the forces at which service, damage and ultimate limits are reached.

These tools are also used to assess the strength of a structure after entering service, with specific considerations of damage or age related effects. A number of ultimate strength analysis methods continue to be developed. They range in complexity from simple empirical formulae assessing the strength of individual structural elements to fully nonlinear analyses of the entire midship region of a hull girder. The following sections summarise a range of methods.

### **2.6.2. Simple Beam Theory**

A fundamental premise of hull structural design is that the girder acts as a simple beam under a distributed load. An easy way of solving the ultimate strength problem is to use simple beam theory, which can give a first failure estimate for the girder. The approach uses the standard beam bending moment equation to calculate the stress at the outermost fibre of the cross section under an applied bending moment.

Simple beam theory and plastic beam theory is not adequate for hull girder strength assessment because it does not take into account the effect of buckling in the compressed portion of the girder. However, it is useful as a precursor to more advanced approaches because the premise of the hull girder acting as a simple beam bending about a neutral axis is the foundation of most methods. The limitations of the simple beam theory approach are that the structure is assumed to act elastically in compression (neglecting buckling effects) and that the instantaneous neutral axis remains at the elastic position. These two premises are re-evaluated in the simplified approaches described below.

### **2.6.3. Stress Distribution Method**

Caldwell [40] developed a more rigorous approach, based on the foundation of simple beam theory. The approach has subsequently been called the stress distribution method and various enhancements have been developed [2]. The stress distribution method is only capable of calculating the ultimate strength of the girder; it does not consider the progressive collapse relationship between bending moment and curvature.

The method accounts for the reduced strength of the compressed portion of the hull cross section. A typical bending stress distribution over the cross section is shown in Figure 15a. The compressed portion buckles and thus the strength is reduced whilst the tension region ultimate strength is the yield strength of the material. The neutral axis is calculated at the centroid of the bending stress distribution.

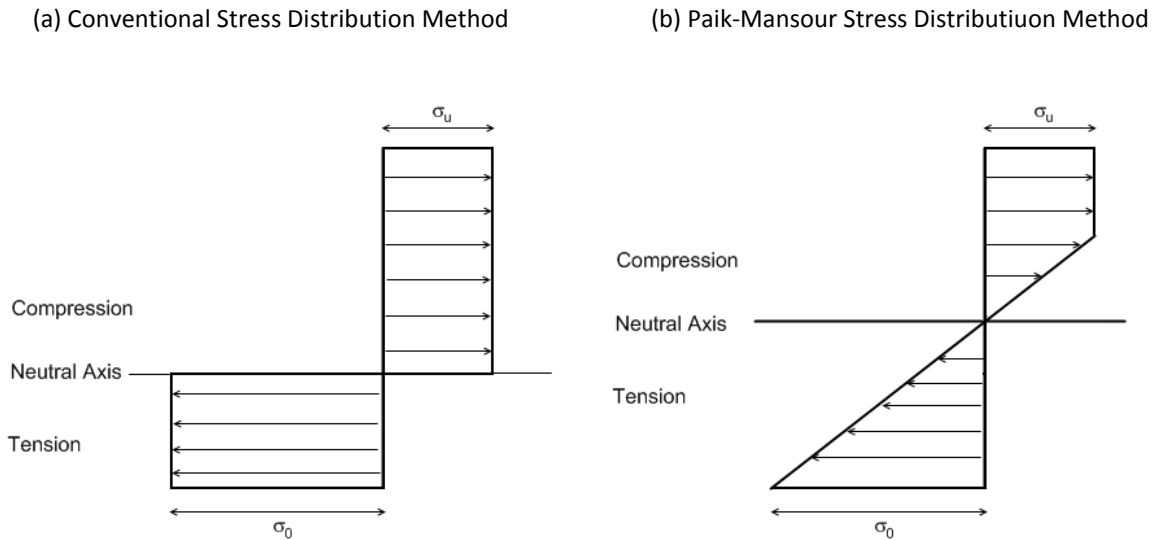


**Figure 15 – Stress distributions over ship cross section with a sagging bending moment**

The method will overestimate the ultimate strength of most modern ship structures because the girder usually collapses before buckling and tensile yield spreads over the entire cross section. Usually the ultimate strength is governed by the collapse of the outermost compressed flange (the top deck for a sagging bending moment). This causes a neutral axis shift towards the tensioned flange, which has the effect of delaying yielding in the tension region and thus allows further increases in bending moment. However, the hull will fail well before the structure yields over the entire tension region. Therefore, various modifications to the approach have been proposed, most recently by Paik and Mansour [41] who suggested a bending stress distribution as shown in Figure 15b. This provides a more realistic stress distribution at the ultimate strength whilst keeping the calculation method closed form.

The stress distribution method requires an estimation of the in-plane buckling strength of the compressed portion of the hull girder. It demonstrates the need to assess the buckling characteristics of the plate and stiffener structural elements which make up the continuous structure. In the diagrams below, the compressive ultimate strength is considered uniform over the entire section. More rigorous methods are needed to take into account the behaviour of individual elements.

### 2.6.1. The Progressive Collapse Method

Perhaps the most well known simplified approach to estimate the hull girder ultimate strength is the Smith progressive collapse method, which has early origins in the design of aircraft [42] and the work of Caldwell [40] as described above. The method was developed into a rigorous approach for

the analysis of ship structures by Smith [7] and thus the methodology is associated with his name. Progressive collapse analysis has been used in numerous ultimate strength analyses of steel hulled ships [43] and different forms of the method are coded as research tools. It is also found as built in features of some commercial ship structural analysis software, such as *Paramarine*.

Two similar methodologies came to prominence: the Smith progressive collapse method [7] and the idealised structural unit method (ISUM) [44]. Both use a similar conceptual approach in predicting hull girder strength. This study refers to the Smith progressive collapse method but the general approach is also valid for adaptation to the ISUM approach.

For a progressive collapse type analysis the hull girder is usually divided into plate-stiffener combination (PSC) elements; each element comprises a single longitudinal stiffener with attached plating located between adjacent transverse frames. Failure of the hull girder in overall bending occurs by interframe failure of these elements; thus the transverse frames are assumed to be sufficiently strong to act as boundary supports.

The progressive collapse method evaluates the strength of longitudinally effective structure between adjacent frames, usually located at or near to amidships, which is also generally the region of maximum bending moment. A complete description of the method can be found in many papers relating to the subject [4, 7, 43, 45]. A conventional cargo ship typically has a parallel middle body and thus an evaluation of the midship section only is often sufficient for an ultimate strength analysis. For a lightweight, high speed ship without parallel middle body the strength of sections away from amidships may also need to be evaluated. This is normal practice for a warship design.

The Smith method follows a relatively straightforward incremental procedure:

1. A cross section of the girder is selected. For a ship this is usually at or near amidships where the maximum bending moments usually occur. Only longitudinally effective structure is included in the cross section;
2. The cross section is divided into small elements;
3. Each element is assigned a “load shortening” curve, describing the behaviour of the element under incremental compression/tension. The load shortening curve may implicitly include other load effects;
4. The initial position of the cross section neutral axis is calculated;

5. Incremental vertical curvature is applied about the instantaneous neutral axis. At each increment of curvature:
  - a. The incremental strain of each element is calculated assuming the cross section remains plane;
  - b. Element incremental stresses are derived from the slope of the load shortening curve;
  - c. Stresses are integrated over the cross section to obtain bending moment increments;
  - d. The position of the neutral axis is adjusted to account for the loss of stiffness over areas of the hull exhibiting high compressive strains.
6. Incremental moments and curvatures are summed to obtain total cumulative values.

The fundamental assumptions of the progressive collapse method are:

- Plane sections remain plane;
- Elements act independently;
- Buckling and collapse of the section is interframe.

The governing equations of the progressive collapse method are detailed in Chapter 7.

The load shortening curves assigned to each element are the fundamental inputs which control the resulting progressive collapse behaviour of the cross section. It is therefore crucial to define representative curves for all elements in the cross section. An example load shortening curve is shown in Figure 16. Strictly speaking, the graph is not a force-displacement plot but actually shows a normalised relationship between average stress across the panel cross section and the strain in the longitudinal direction. However, to keep with current conventions and to clearly differentiate from descriptions of material properties, the plots are referred to as load shortening curves throughout this thesis.

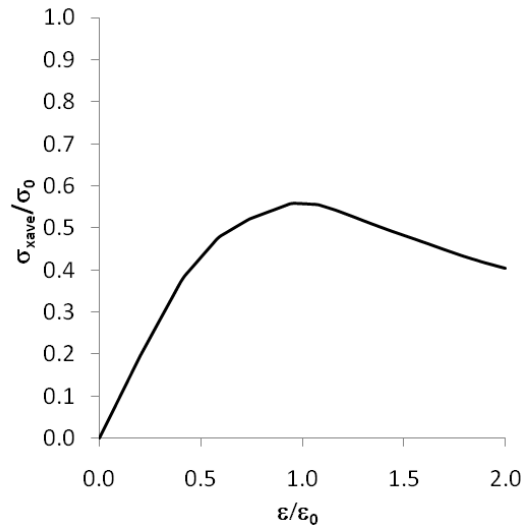


Figure 16 – Example panel load shortening curve

The progressive collapse method has proved robust in the analysis of steel vessels with relatively stocky transverse frames which ensure interframe collapse. However the progressive collapse method in its present form does not account for the possibility of failure modes over a number of frame spaces. An extension of the progressive collapse method, incorporating an evaluation of overall collapse modes, is a key objective of this thesis and is proposed in Chapter 7.

### 2.6.2. Nonlinear Finite Element Method

Nonlinear FEM is now a viable option for hull girder strength assessment. However, from a design perspective, FEM requires detailed knowledge of the geometry, imperfections and residual stresses in the structure whilst in service, which are not well understood even at the final design stage. Furthermore, from an analysis perspective, FEM requires considerable computer time both in setting up and solving the discrete model. Elements must be sized sufficiently small to represent the local structure including stiffeners and plating adequately. For aluminium panels this also includes the heat affected zone adjacent to welded joints. The element mesh for an entire hull girder is therefore large.

## 2.7. Summary

This Chapter first summarises the evolution of modern lightweight vessels constructed from aluminium, exemplified by the current state-of-art multihulls developed for the fast ferry and defence markets. These vessels are longitudinally stiffened and are predominantly built from either 5083-H116 or 6082-T6 aluminium alloys. The properties of these alloys are important in the context of determining their strength characteristics. The stress-strain relationship is nonlinear and can be

approximated using the Ramberg Osgood relationship. Various coefficients proposed by class societies and researchers are synthesised into a set of representative used in this study to define the stress-strain curve for the two different aluminium alloys. An important emphasis is placed on established knowledge concerning the heat affected zone and residual stress distributions which are created close to welded aluminium joints. Current knowledge is encapsulated in aluminium design guides, but in some respects a more nuanced understanding of the welded properties are required for the purposes of detailed nonlinear analysis of the strength of aluminium structures. Therefore, the chapter summarises some of the latest research findings which are important to the analyses carried out in subsequent Chapters.

In the final part of the Chapter the established progressive collapse methodologies currently available for hull girder ultimate strength analyses are summarised. This review demonstrates the continued reliance on variations of the simplified Smith progressive collapse method. The description of this approach highlights both its continued applicability and also its limitations in respect to analysing aluminium hull girder structures. In particular, the simplified progressive collapse method is a wholly interframe approach, with the assumption that buckling occurs between adjacent transverse frames. Challenging this assumption forms a fundamental thrust of this research effort.

*“[I am] opposed to the laying down of rules or conditions to be observed in the construction of bridges, lest the progress of improvement tomorrow might be embarrassed or shackled by recording or registering as law the prejudices or errors of today.”*, Isambard Kingdom Brunel speaking to the 1847 commission investigating the River Dee Bridge.

# Chapter 3

## Methods to Predict the Strength of Plates and Stiffened Panels

### 3.1. Overview

The progressive collapse method utilises load shortening curves describing the strength behaviour of stiffened panel elements, which usually, but not exclusively, comprise a single stiffener with associated plating. There are a variety of methods available to produce suitable load shortening curves, which are themselves sometimes derived from the strength assessment of component stiffeners and plating.

It is useful to categorise the various methodologies that are important for assessing a ship structure in primary bending. The categories form a “structural hierarchy”, ranging from component level sub structures such as individual plate elements through to an entire hull girder midship section. The categories are:

- Level 1 – Plates and stiffeners
- Level 2 – Interframe panels
- Level 3 – Orthogonally stiffened panels
- Level 4 – Hull girder

An assessment of hull girder strength using simplified methods normally follows a progression through these analysis levels. For example, the prediction of PSC element strength (Level 2) often requires information about the strength behaviour of the individual components (Level 1). The strength characteristics of PSC elements are then used in a progressive collapse method to predict the strength of the hull girder (Level 4).

Investigating the requirements and methodologies for the inclusion of Level 3, which for example may assess the overall buckling strength of an entire deck, is a key objective of this thesis. As previously discussed, the progressive collapse method assumes that panels fail interframe, and this means that the analysis excludes orthogonal panel representations by assuming that the cross section is adequately represented by interframe elements. A more rigorous approach is to evaluate the strength of the interframe (Level 2) and orthogonal (Level 3) panel and to include both in an extended hull girder (Level 4) methodology.

An assessment of hull girder strength using the finite element method (FEM) can also be related to the structural hierarchy. Whereas simplified methods typically use information directly from sub analyses of components to predict the strength of the global structure, an FEM approach must include all component and global structural details in the same analysis model.

It is therefore useful to view FEM analysis methods using the proposed hierarchical structure. An FEM model of an orthogonally stiffened structure must include an adequate representation of the geometric and material properties of the components. For example, a nonlinear FEM model of an entire hull girder must include structural details up to and including plate/stiffener imperfections (level 1), as well as global imperfection characteristics in the strength decks (levels 2 and 3). The relevance of this construct to the FEM modelling of components and stiffened panels is discussed in Chapters 4 and 5.

### 3.1.1. Plate Strength

For the purposes of structural analysis, plates are usually categorised into individual unstiffened elements, bounded by stiffeners on all four edges. Each plate element must adequately fulfil a number of roles within the ship structure. These can be broadly split into local and global functions. Local functions are usually considered to fulfil service limit states, such as withstanding local hydro pressure loads, whilst the global function of the plate as an integral part of the continuous hull girder is of primary importance for ultimate limit state analysis. However, the influence of local effects on the global effectiveness of the plate is important to account for.

It is important to quantify the strength of a plate element in a ship or civil structure in isolation before investigating its function as part of a stiffened structure. A brief summary of noteworthy literature concerning flat plate stability is presented in the following paragraphs whilst a discussion of the key formulas which are important for analytical plate strength methods are given in Section 3.2.

Theories to predict the strength of a flat plate under various load combinations have been studied extensively for over 120 years, with the first theoretical examination of the plate buckling problem by Bryan in 1891 [46]. Since then the instability of plate elements under a wide variety of loading conditions has been extensively studied using numerous different experimental, theoretical and numerical approaches.

A historical perspective of this research provides the foundations for modern design guidance and analysis methods. Following Bryan, who presented a method to determine the elastic capacity of a plate [46], von Karman derived equations to describe the post buckling behaviour [47]. Subsequent theory extended on von Karman's governing equations, which describe compatibility of displacements and equilibrium of forces. Maguerre [48] modified the equations to take into account the presence of initial imperfections. Energy methods were first postulated by Cox [49] and solved rigorously by Maguerre [48], who assumed an approximate deflected form for the plate and employed the principle of minimum potential energy, rather than the equilibrium equation, to find a solution [50].

This fundamental research into plate strength and stability has driven the development of modern design guidance, which usually aims to minimise the weight of a structure whilst maintaining sufficient local and global strength under prescribed load criteria. Well established design methods, such as the Johnson-Ostenfeld parabola [37], adapted theoretical work into empirical equations suitable for allowable stress methods. Extensive physical and numerical tests have complemented

theory, developing a better understanding of real plate behaviour and thus improving practical design guidance.

More recent plate strength research has been undertaken to develop limit state design approaches, which requires a more thorough consideration of the ultimate capacity of the plate under specific load scenarios. Modern statutory guidelines, such as the steel and aluminium Eurocodes [29, 51], have extended design formulas to encapsulate numerical and physical test data and present a more rational approach to design. They derive the plate strength as a limit state criteria, where the strength is judged directly against the load at the ultimate, accidental, fatigue and serviceability level [37].

### **3.1.2. Stiffener Strength**

Interframe stiffened panels buckle in three different ways: plate or stiffener local buckling, stiffener web buckling or lateral-torsional buckling (tripping) of the stiffener. Each of these modes are considered in turn.

If the plating buckles between relatively strong stiffeners, the load in the plate is shed into the stiffeners which usually cause panel failure. In beam column type failures the plate and stiffeners buckle together and subsequent collapse is due to the loss of stability and stiffness over the whole cross section. Alternatively, if the stiffener has insufficient rigidity or stability, it can buckle prematurely. This usually precipitates failure of the panel because the stiffeners shed load into the attached plating. The support along the bounding edges of the plate is also compromised, effectively reducing the strength capacity. Thus overall buckling of the plate and stiffener usually follows immediately.

A stiffener has several potential failure modes. The stiffener web can buckle, especially if the height to thickness ratio is relatively high. Alternatively, a stiffener may exhibit lateral-torsional instability, which is often called stiffener tripping. This causes buckling by the stiffener twisting about the line of attachment to the plating. Local buckling of the stiffener is highly undesirable. It often occurs elastically, and is then usually accompanied by a sudden loss of panel strength.

To some extent, for the purposes of analysing tripping, a stiffener can be treated as a special type of column. Timoshenko and Gere [52] present the governing equations for the torsional buckling of an axially loaded column with an enforced line of rotation. Hughes [53] simplifies the formulation for a ship type stiffener, by assuming the shear centre is located at the rotation line and that the warping constant is zero. The equation also takes into account the rotational restraint which the plating

exerts on the stiffener. Web buckling can be determined by treating the stiffener as an equivalent plate with support at the plate joint and at the flange intersection.

### 3.1.3. Stiffened Panel Strength

For the purposes of analysing a complete stiffened panel a rigorous classification of panel collapse modes is provided by Paik and Thayamballi [37]. Interframe collapse modes involving component buckling have already been discussed. Further modes, concerning overall collapse, extend the possible buckling phenomena which must be accounted for in a stiffened panel analysis. The categories provide a useful way of separating the different buckling and yielding mechanisms that can occur in a panel under in-plane combinations of compressive load.

The complete classification as given by Paik and Thayamballi [37] is as follows:

- Mode 1: Overall collapse:
  - Mode1-1: Uniaxial stiffened panels (single frame space)
  - Mode1-2: Cross stiffened panels (multiple frame spaces)
- Mode 2: Biaxial collapse
- Mode 3: Beam-column collapse
- Mode 4: Local buckling of the stiffener web
- Mode 5: Lateral-torsional buckling (tripping) of the stiffener
- Mode 6: Gross yielding
- Mode 7: Local plate buckling

The categories do not necessarily occur in isolation; some can interact to create complex collapse modes. In other cases collapse in one mode can initiate additional collapse modes. For example, a beam-column collapse, caused by yielding in the plate stiffener combination at mid span, can initiate an overall collapse pattern over a single frame space.

Elastic buckling analysis techniques are useful to determine likely buckling modes and provide a first estimate for panel strength. Hughes [53] provides a thorough treatment of the elastic buckling problem. However, most stiffened panels typical of a ship structure are proportioned such that

buckling is inelastic. Therefore methods in which the complex inelastic compressive collapse of the panel is accounted for are of more relevance to the ultimate strength problem.

The ultimate strength of stiffened panels can be evaluated using numerous different methods, ranging in complexity and including design charts, empirical approaches, analytical methods, nonlinear FEM and experimental tests. Key methodologies are presented in section 3.3.

## **3.2. Methods to Predict the In-Plane Strength of Unstiffened Plates**

Methods to predict the ultimate strength of unstiffened plates can be broadly divided into classical theory of elasto-plastic buckling and empirical formulae based on experimental results. Empirical formulae usually extend classical theory to fit experimental and numerical test data. Therefore, an understanding of the important theoretical equations governing plate buckling and ultimate strength provide a background to design equations.

Most classical theory assumes material is isotropic, with a simple elastic region defined by the material Young's modulus. Plasticity is modelled using an elastic-perfectly plastic stress-strain relationship with a clearly defined yield point. These assumptions are typical for steel plate.

Aluminium can also be approximated to the elastic perfectly plastic model, using the 0.2% offset proof strength in place of yield. However, the nonlinearity of the material stress-strain curve together with inhomogeneous material properties through near welds are more complicated to approximate. Methods, such as the Eurocode9 formulation, have been developed to account specifically for aluminium plate properties. Aluminium methods are thus presented appropriately in the following text.

### **3.2.1. Experimental Data**

#### **3.2.1.1. Steel Plates**

A large pool of information has been collected relating to the instability characteristics of steel plate. A substantial amount of experimental work was carried out from the 1960s to the 1990s, particularly at Cambridge University, UCL and UK Naval research agencies (under various guises – principally the A.R.E.). This complemented work from Europe and Japan including experimental tests of long plates under uniaxial compression [54-56] and biaxial compression [57].

Theoretical investigations have used various special purpose finite difference and finite element codes to develop strength data for steel plates in uniaxial compression [54, 58-61], biaxial compression [62] and biaxial compression with lateral pressure [60, 63, 64].

Smith [38] brought together the extensive numerical and experimental test data available at the time to plot effective load shortening curves for long plates in uniaxial compression. The family of curves are given for plates of varying slenderness.

The numerical and experimental analyses from which the curves are defined consider steel plating only. The significant effect of initial geometric imperfection amplitude is taken into account by defining three characteristic curve sets for slight, average and severe imperfection levels. The imperfection magnitudes are based on surveys of actual ship plating. Slight and severe levels relate to 3 percentile and 97 percentile values of the data distribution. The peak strength of the plate curves fall close to the current British Standard of the time and the empirical expression presented by Faulkner [65].

Further work detailed by Smith et al [38] describe the strength of long plates under transverse load, square plates under uniaxial compression (which must be considered separately to long plates due to the different effects of imperfection on the buckling mode) and long plates in biaxial compression.

The hull girder progressive collapse program NS94, developed by the A.R.E., utilises Smith's plate load shortening curves in the special purpose beam-column finite element code, FABSTRAN, which develops the load shortening curve for a given plate-stiffener cross section [39].

#### **3.2.1.2. Aluminium Plates**

Parametric steel plate design curves cannot be applied directly to equivalent aluminium plates. The load shortening behaviour of aluminium structural elements has been shown to differ considerably from steel in numerical analyses [66, 67]. In particular, the nonlinear material stress-strain curve of aluminium can affect the shape of the load shortening curve. The material properties are further affected in areas close to welded joints, where the high heat input during the weld process causes localised softening.

Research specific to ship type aluminium alloy plates can be found dating back many years, with pioneering work being carried out by Muckle [11] and Snaith [68] amongst others. However, the continuing improvements in marine grade alloys means that much of this early work, whilst useful, is difficult to apply directly for modern aluminium ships.

Some significant efforts to analyse the ultimate strength characteristics of ship type aluminium structures were initiated in the 1980s. Little [69] carried out numerical analysis on a range of rectangular plates including different alloys and initial imperfections, but neglecting the heat affected zone (HAZ). Mofflin and Dwight carried out laboratory tests on 76 aluminium plates taking

into account the initial distortions and heat affected zones [70]. The results published by Mofflin, Dwight and Little were used extensively in the development of Eurocode 9 [29] and have also been re analysed numerically in more recent work [71]. Hopperstad [72] has also investigated the strength of outstand (supported on three sides only) aluminium plates.

More recent research into aluminium plate strength has been undertaken numerically, using nonlinear finite element analysis. Kristensen [67] undertook extensive finite element analysis, predominantly on 6082-T6 alloy plates, and investigated the effects of many parameters including initial imperfections, residual stress and HAZ location. Paik and Duran [19] carried out a series of nonlinear analyses for 5383-H116 plate and used the data to derive a design formula to predict aluminium plate ultimate strength, taking into account the size of the heat affected zone. Recent work at Newcastle by Zunaidi [31] has further demonstrated the effects of various parameters on the non dimensional load shortening curves of aluminium plates, including the imperfection magnitude, imperfection shape, heat affected zone and alloy type.

### 3.2.2. Elastic Buckling

The elastic buckling stress,  $\sigma_{cr}$ , is defined according to the solution of the Euler differential equations governing the buckled shape of a plate, originally proposed by Bryan [46]. For long flat rectangular plates with simply supported edges the critical elastic buckling stress can be approximated to:

$$\sigma_{cr} = k_c \frac{\pi^2 D}{b^2 t} \quad 11$$

The coefficient  $k_c$  is a function of the boundary support, aspect ratio and the buckling shape of the plate. For a long, simply supported plate with a square or approximately square buckling mode shape,  $k_c$  approximates to 4.

The flexural rigidity of the plate,  $D$ , is defined as:

$$D = \frac{Et^3}{12(1-\nu^2)} \quad 12$$

For a typical steel plate, with  $\nu = 0.3$  (Poisson's Ratio), substitution reduces Eq. 11 to:

$$\frac{\sigma_{cr}}{\sigma_Y} = \frac{3.62}{\beta^2} \quad 13$$

### 3.2.3. Elasto-Plastic Buckling

The critical elastic buckling stress cannot be used directly as a measure of ultimate strength. The mechanism of plate collapse is complex and does not usually occur at the theoretical elastic buckling stress. Collapse of a relatively stocky plate occurs before the critical elastic buckling stress is reached due to elasto-plastic yielding. Conversely, a relatively slender plate does not collapse at the critical buckling stress and has additional strength in the post buckled region.

For a slender plate ( $\beta > 2.5$ ) the elastic buckling stress lies significantly below the material yield stress. Collapse does not occur when the elastic buckling load is reached, meaning that the plate exhibits stable postbuckling behaviour. This is due in part to the boundary conditions imposed at the unloaded edges, which prevent the portions of the plate close to the boundary from deflecting. Only the centre region of the plate deflects and therefore partially escapes the compressive load. Thus the outer portions of the plate provide additional strength in the postbuckling region. As the load continues to increase the maximum stress in the plate sides eventually reach the material yield stress and collapse occurs.

The theoretical elastic buckling stress for intermediate plates ( $1 < \beta < 2.4$ ) is similar in magnitude to the yield stress of the material and the mechanism of collapse is therefore somewhat different. Buckling and collapse is significantly influenced by initial imperfections in the plate. The initial deflections in the plate magnify as the applied load increases, causing a loss of stiffness and some local yielding, which in turn causes non-uniform stress redistribution. Rather than shirking the applied load, stresses in the central regions of the plate may reach the yield stress, meaning no more additional load can be supported in these regions. As for slender plates, the load is supported by the outer portions of the plate and collapse occurs when the average equivalent stress along the sides of the plate (given by the von Mises failure criterion) reaches the yield stress.

One of the first to thoroughly consider inelastic collapse was von Karman [47]. He developed the effective width concept, which encompasses the effects of slenderness ratio and the different mechanism of collapse for slender and stocky plates. The method proposes that the ultimate collapse load is taken by two yielding strips of plating adjacent to the supported unloaded edges, as is the case for slender plates. The collapse stress can be calculated using the width of these strips along with the plate thickness and material properties. The effective width becomes equal to the actual width for stocky plates and the ratio of effective width to actual width reduces as the slenderness of the plate increases.

The effective width concept is particularly appropriate for steel, which has a well-defined yield point and can be assumed to have an elastic perfectly plastic stress-strain curve. If the critical elastic buckling stress in Eq. 11 is replaced by the material yield stress, the equation can be rearranged to calculate an effective width,  $b_e$ :

$$\begin{aligned}
 b_e &= \pi \sqrt{\frac{E}{3(1-\nu^2)\sigma_Y}} && \text{when } b_e < b \\
 b_e &= b && \text{when } b_e \geq b
 \end{aligned}
 \tag{14}$$

For a plate with  $\nu = 0.3$ , the formula reduces to:

$$\frac{b_e}{b} = \frac{\sigma_u}{\sigma_Y} = \frac{1.9}{\beta} \quad \text{when } b_e < b
 \tag{15}$$

The effective width theory as presented does not adequately account for all the mechanisms of collapse in a simply supported plate of arbitrary dimensions. Furthermore, it does not reflect the general nonlinear stress-strain relationship of aluminium alloys. However, although not useful for direct application in ultimate limit state design, the equations do provide the theoretical context from which more suitable empirical formulae and theory are derived [65].

### 3.2.4. Uniaxial Compression: Empirical Methods

The effective width concept does not take into account the geometric imperfections and residual stresses inherent in a typical welded and fabricated plate. Numerous experimental and numerical tests have found that the concept over predicts the plate strength, particularly for plates of intermediate slenderness.

Therefore empirical methods have been proposed to take into account the departure from classical theory due to the effects of imperfections and the post buckled strength of slender plates. Faulkner [65] provides a useful history of the development of methods up to 1975. Since Faulkner's paper much work has been continued by a number of authors to develop ultimate strength design formulas suitable for plates with various aspect ratios, boundary conditions and loading scenarios.

Four relevant plate ultimate strength formulations are presented here to give a broad overview of the different ways the plate collapse problem has been tackled. This is by no means an exhaustive review; the methods have been chosen as those likely to be used in current design practice. The Faulkner [65] and Johnson-Ostenfeld [37] formulas are well known and are repeated in many classification guides. They were originally developed for steel plates. Eurocode 9 [73] provides a

code formulation that has been developed specifically for aluminium structures and includes reduction factors to take into account the reduced HAZ strength. A regression formula from extensive FEM testing of marine grade aluminium plate is presented, which also attempts to include the effects of the HAZ.

#### 3.2.4.1. Faulkner Formula

Possibly the most commonly quoted [74] empirical formula used in the marine industry to estimate the strength of simply supported steel plates under longitudinal compression was proposed by Faulkner [65]. This defines the non dimensional ultimate plate strength,  $\phi_{xu}$ , as a function of the slenderness ratio:

$$\frac{\sigma_u}{\sigma_0} = 1.0 \quad \text{when } \beta < 1$$

$$\frac{\sigma_u}{\sigma_0} = \frac{2}{\beta} - \frac{1}{\beta^2} \quad \text{when } \beta \geq 1 \quad 16$$

This equation is written using the generic symbol for yield/proof stress ( $\sigma_0$ ) because the formula is assessed for its adequacy in predicting steel and aluminium plate strength.

The two term approach had been developed well before Faulkner's postulation (e.g. Frankland [65]) and various researchers have suggested slightly different values for the numerators in Eq. 16, but Faulkner's simple and elegant formula has proved adequately representative for a simply supported long plate. The two term formula incorporates parts equivalent to the effective width approach and critical elastic buckling stress approach. For high slenderness ratios the formula approximates to the effective width formula whilst at lower slenderness ratios the increased influence of the  $1 / \beta^2$  term reduces the overall collapse load significantly.

Faulkner's formula has been found to correlate well with test data from various steel and aluminium plate experiments [38]. The formula includes the effects of residual stress and distortion implicitly, providing a good fit through test data derived from plates constructed under normal manufacturing conditions.

#### 3.2.4.2. Johnson-Ostenfeld Parabola

The Johnson-Ostenfeld parabola formula is used by classification societies including ABS [75] and DNV [18]. The method is a correction of the theoretical linear elastic buckling formula. It disregards the margin between buckling and collapse for slender plates, assuming that if the elastic buckling stress is less than half the yield stress, the critical stress equals the former. For stockier plates an empirical correction based on the same principles as the effective width concept is employed.

The full formula is defined as:

$$\begin{aligned} \sigma_u &= \sigma_{cr} && \text{for } \sigma_{cr} \leq 0.5\sigma_0 \\ \frac{\sigma_u}{\sigma_0} &= 1 - \frac{\sigma_0}{4\sigma_{cr}} && \text{for } \sigma_{cr} > 0.5\sigma_0 \end{aligned} \quad 17$$

where  $\sigma_{cr}$  is as defined in Eq. 13.

The formula is conservative for slender plates, preferring to define the elastic buckling strength effectively as the ultimate strength, which perhaps gives more of a serviceability limit than an ultimate limit. However, this is considered an acceptable conservatism to impose for classification requirements and where other stress based criteria may also be imposed.

### 3.2.4.3. Eurocode 9

Eurocode9 [73] was originally developed for the design of buildings and civil engineering works made from wrought and cast aluminium alloys, but is equally applicable to marine grade aluminium plates. The code is extensive and supersedes BS8118 [28]. It defines an empirical formula for ultimate plate strength in a similar form to Faulkner's method but with explicit corrections for the softening in the HAZ. The code defines the ultimate strength of a plate under uniform uniaxial in-plane compression in the form of a limit state:

$$\frac{N_{ED}}{N_{Rd}} \leq 1.0 \quad 18$$

$N_{ED}$  is the design value of the compression force and  $N_{Rd}$  is the design resistance to normal forces, otherwise known as the collapse load. For the purposes of comparison with the other empirical formulas  $N_{ED}$  can be considered to equal  $N_{Rd}$ .

Assuming a simply supported homogenous rectangular flat plate,  $N_{Rd}$  is defined in terms of an effective cross section area of the plate ( $A_{eff}$ ):

$$N_{Rd} = \frac{A_{eff}\sigma_0}{\gamma_{M1}} \quad 19$$

The  $\gamma_{M1}$  term is a partial safety factor to account for design uncertainties. Eurocode 9 recommends a factor of 1.1, but for the purposes of comparison with the other ultimate strength formulas and the test data conducted in this study  $\gamma_{M1}$  is given a value of unity.

The definition of effective cross section depends on the slenderness of the plate. For the representative slenderness ratios for a typical ship plate all cross sections are defined as “class 4” and the same formulations apply. The effective cross section is obtained by taking a reduced thickness to allow for buckling and HAZ softening. Reduction factors are applied separately to the cross section area of the unheated area and the area within the HAZ. The reduction factor for the main cross section is defined in a form similar to the Faulkner formula:

$$\rho_c = \frac{C_1}{\left(\frac{\beta}{\varepsilon}\right)} - \frac{C_2}{\left(\frac{\beta}{\varepsilon}\right)^2} \quad 20$$

where  $\beta = b/t$ , rather than the usual defined slenderness parameter and  $\varepsilon = \sqrt{250/\sigma_0}$ . The factors  $C_1$  and  $C_2$  depend on the material grade/alloy classification. For the marine grade aluminium alloys considered here the two factors are given as 29 and 198 respectively.

The reduction factor for the area in the HAZ is simply the ratio of the proof stress in the HAZ to the proof stress of the parent metal:

$$\rho_{0HAZ} = \frac{\sigma_{0HAZ}}{\sigma_0} \quad 21$$

Using the geometric dimensions shown in Figure 17, the overall effective area is defined as:

$$A_{eff} = 2b_{HAZ}\rho_{0HAZ}t + (b - 2b_{HAZ})\rho_c t \quad 22$$

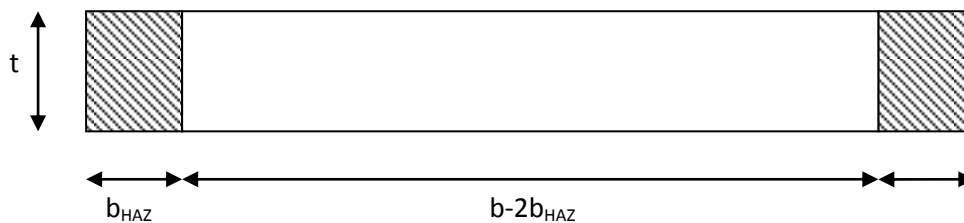


Figure 17 – Through thickness cross section for an aluminium plate. HAZ representation.

#### 3.2.4.4. Paik and Duran Empirical Formula

Paik and Duran [19] developed a regression formula method to define the ultimate strength of flat rectangular unstiffened aluminium plates including the effects of the HAZ. The formulation is based on FEM studies of plates with material properties equivalent to 5083-H116, 5383-H116 and 6082-T6 aluminium alloys. An account is made for average geometric imperfections. The effects of the HAZ are taken into account by defining a revised slenderness ratio:

$$\beta' = \frac{b}{t} \sqrt{\frac{\sigma_{0eq}}{E}} \quad 23$$

$$\sigma_{0eq} = \frac{P_p}{ab} \quad 24$$

$$P_p = (a - 2b_{HAZ})(b - 2b_{HAZ})\sigma_0 + 2[ab_{HAZ} + (b - 2b_{HAZ})b_{HAZ}]\sigma_{0,HAZ} \quad 25$$

The regression formula is then defined as:

$$\begin{aligned} \frac{\sigma_u}{\sigma_0} &= 1.0 && \text{when } \beta' \leq 0.46 \\ \frac{\sigma_u}{\sigma_0} &= -0.215\beta' + 1.1 && \text{when } \beta' \leq 0.46 \\ \frac{\sigma_u}{\sigma_0} &= -0.083\beta' + 0.81 && \text{when } \beta' \leq 0.46 \end{aligned} \quad 26$$

#### 3.2.4.5. Comparison of Methods

The four empirical methods are compared in Figure 18 alongside relevant test data from plate tests carried out by Mofflin [5]. The Eurocode 9 and Paik regression formula plots are for a typical 5083-H116 aluminium alloy plate of breadth 400mm, length 1200mm and with a HAZ breadth,  $b_{HAZ}$ , of 25mm.

Most ship structures tend to fall within the intermediate slenderness region as highlighted in Figure 18. The plot shows that the general relationship between strength and slenderness are universal across methods. In the intermediate slenderness region there is a spread between results. Paik and Duran's formula forms the lower bound whilst Eurocode9 gives an upper bound. This is interesting as these are the two aluminium specific methods compared. Paik's method is generally closer to the experimental data. In the high slenderness region the Johnson Ostenfeld parabola does not take into account post buckling behaviour and thus gives a highly conservative solution. The other methods correlate closely, demonstrating that, for very thin plates, collapse behaviour is dictated by geometry rather than material properties.

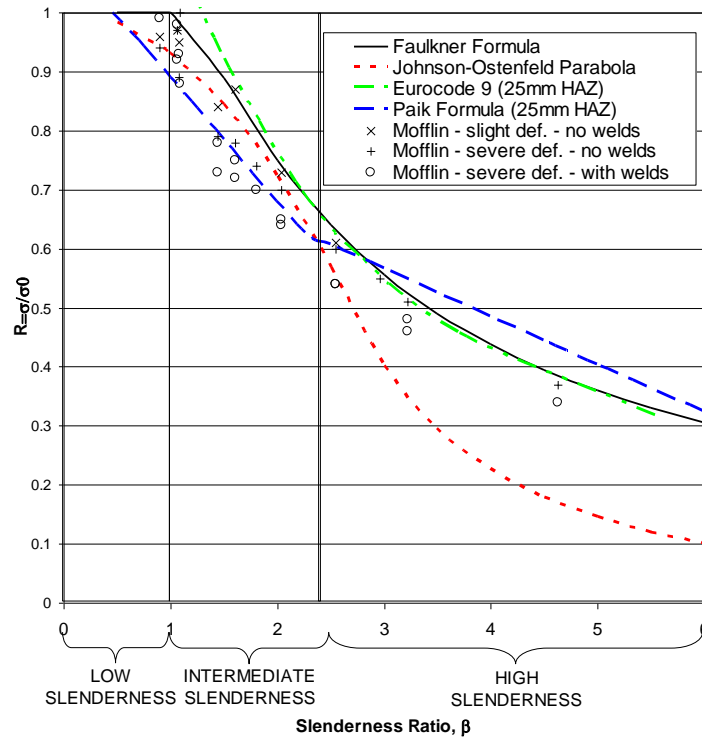


Figure 18 – Comparison of empirical methods to predict aluminium plate strength

### 3.2.5. Uniaxial Compression: Load Shortening Behaviour

The formulations presented thus far have been exclusively concerned with the ultimate strength of the plate. However, for use in a progressive collapse analysis, the behaviour of the plate over the entire strain scale is required. As discussed previously, the A.R.E. produced a parametric series of steel plate curves, using a combination of nonlinear FEM and test data [76]. These can be implemented directly as datasets in a higher level analysis methodology. An example is shown in Figure 19.

An alternative approach to numerical analysis is to develop a closed form method to determine the plate strength at a given strain. A proposed method for steel plates by Gordo and Guedes Soares [77] is shown here, which derives a simple approximation of plate behaviour using the Faulkner formula and effective width concept. The approach assumes an elastic-perfectly-plastic material, meaning it is suitable for steel. Collette [78] further develops the methodology using Stowell's unified buckling theory [79].

According to the effective width concept, the plate is supported by two longitudinal strips of plating adjacent to the plate edges, and the plate collapses when these strips reach yield. The width of these

strips can be calculated using the Faulkner formula (Eq. 16). Gordo extends this concept by calculating the edge stress for a given strain level,  $\varepsilon$ :

$$\begin{aligned} \sigma_e &= \varepsilon E \text{ if } \sigma_e < \sigma_Y \\ \text{else } \sigma_e &= \sigma_Y \end{aligned} \quad 27$$

A revised slenderness ratio is defined as:

$$\beta_e = \frac{b}{t} \sqrt{\frac{\varepsilon}{\varepsilon_Y}} \quad 28$$

The instantaneous effective width is calculated by substituting Eq. 28 into Eq. 7, replacing  $\beta$  with  $\beta_e$ :

$$\frac{b_e}{b} = \frac{2}{\beta_e} - \frac{1}{\beta_e^2} \quad 29$$

The average stress across the plate cross section is the product of the edge stress and the effective width:

$$\sigma_a = \sigma_e \frac{b_e}{b} \quad 30$$

The above formulation can be used incrementally to produce a complete load shortening curve for a plate. The original formulations also include correction factors to take into account different residual stress, initial imperfections and their interaction. However, because the method uses Faulkner's formula, the basic equations as presented can be assumed to represent average imperfections and residual stresses.

The closed form method is compared with Smith's curve database in Figure 19. The calculations assume a plate with a breadth of 300mm. The comparison shows some limitations of the closed form method. The peak strength value is reasonably well predicted as compared to the A.R.E. data, which is unsurprising because A.R.E. curves compare well to the Faulkner formula. However, using the closed form approach, the peak strength will always occur when the normalised strain is 1.0. The peak strengths as given by the A.R.E. data always occur much further along the strain scale.

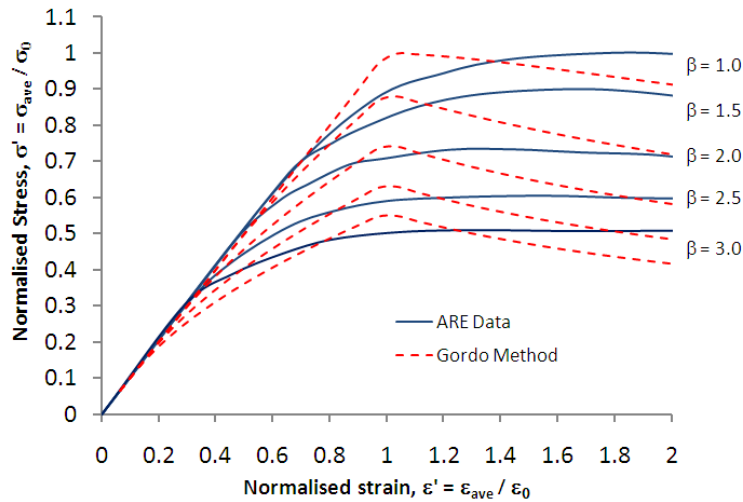


Figure 19 –Comparison of A.R.E. plate data with the Gordo method, assuming average levels of imperfection

### 3.2.6. Multiple Load Combinations

Design equations, such as Faulkner's formula, are concerned with the uniaxial in-plane strength of a plate in the longitudinal direction. However plate elements in ship structures will normally be subjected to combined force components including in-plane transverse loads, lateral load and biaxial in-plane bending. Because a ship structure is large compared to the plate size, in-plane bending effects may be negligible [80]. Therefore the following section reviews methods to predict the plate strength under biaxial in-plane loads and lateral pressure only.

The combined loads can be particularly significant in a large HSV due to the unconventional hull form, usually a multihull, and high speed operation. A HSV is therefore likely to encounter significant transverse loads and moments as well as torsional loads along the longitudinal and transverse rotation axes. In catamarans the transverse component of the load may even dominate over the longitudinal component. In some cases transverse stiffening is employed in the hull structure, effectively turning the problem back into the uniaxial compression scenario discussed earlier. However, this will certainly not always be the case and therefore research has been carried out to determine the strength of plating under combined loading scenarios.

#### 3.2.6.1. Transverse In-Plane Load

A plate under transverse loading is also known as a wide plate, where the plate length in the direction of loading is shorter than the plate breadth. The prediction of transverse plate strength is important both when considering the strength of the plate in biaxial compression.

A design formula for transverse steel plate strength is proposed by Valsgard [62]. The formula applies a correction to Faulkner's longitudinal formula as follows:

$$\frac{\sigma_{uy}}{\sigma_Y} = \frac{\sigma_u}{\alpha\sigma_Y} + 0.008 \left( 1 + \frac{l}{\beta^2} \right)^2 \left( 1 - \frac{l}{\alpha} \right) \quad 31$$

The transverse ultimate strength is used for the interaction diagrams of plates under biaxial compression.

### 3.2.6.2. Biaxial Load

The effect of combined in-plane loading on plate strength has received a good deal of research attention in recent years. Significant biaxial loads are likely to occur on plate elements in a stiffened panel of a multi hull HSV due to the significant transverse load components. Therefore, the interaction between longitudinal and transverse edge loads is important to quantify.

The majority of research into the biaxial strength of plates has been carried out for steel structures [60, 63, 81]. Biaxial plate strength is usually presented on interaction diagrams which combine the ultimate strength of the plate in the longitudinal direction with the corresponding load applied in the transverse direction. The applied longitudinal and transverse stresses are usually presented on the interaction diagram as non dimensional ratios by dividing by respective uni axial compressive stress of the plate in the same load direction, for example by using the empirical formulae given by Faulkner [65] and Valsgard [62]. Thus:

$$R_x = \frac{\sigma_{ave,x}}{\sigma_u} \quad R_y = \frac{\sigma_{ave,y}}{\sigma_{uy}} \quad 32$$

Various formulae are presented in literature to predict the interaction of biaxial compression loads. The formulas generally take a similar form to the von Mises yield criterion [37] with coefficients replacing the power terms. Neglecting the effects of edge shear and lateral pressure, the expression takes the form:

$$\left( R_x \right)^{c1} + \gamma R_x R_y + \left( R_y \right)^{c2} = 1 \quad 33$$

The equation can equate to the von Mises formula by setting  $c1 = c2 = 2$  and  $\gamma = 1$ . For plates in biaxial tension it is assumed the stress field is constant over the plane of the plate and therefore failure occurs when the resulting stresses from the combined load equates to the von Mises yield

criterion. Therefore the interaction diagram is equivalent to von Mises ellipse in the wholly tension region.

For situations when one load direction is in tension and the other is in compression it can be assumed that the stress field continues to be constant over the plane of the plate and the coefficients can continue to be equivalent to the von Mises criteria. However, this assumption may not be valid if the compressive load component is dominant and the plate fails by buckling rather than tensile yield. Results presented by Paik [80] and reproduced in Figure 20 show complete interaction diagrams for plates in biaxial tension/compression with a reduced curve in the tension-compression sectors.

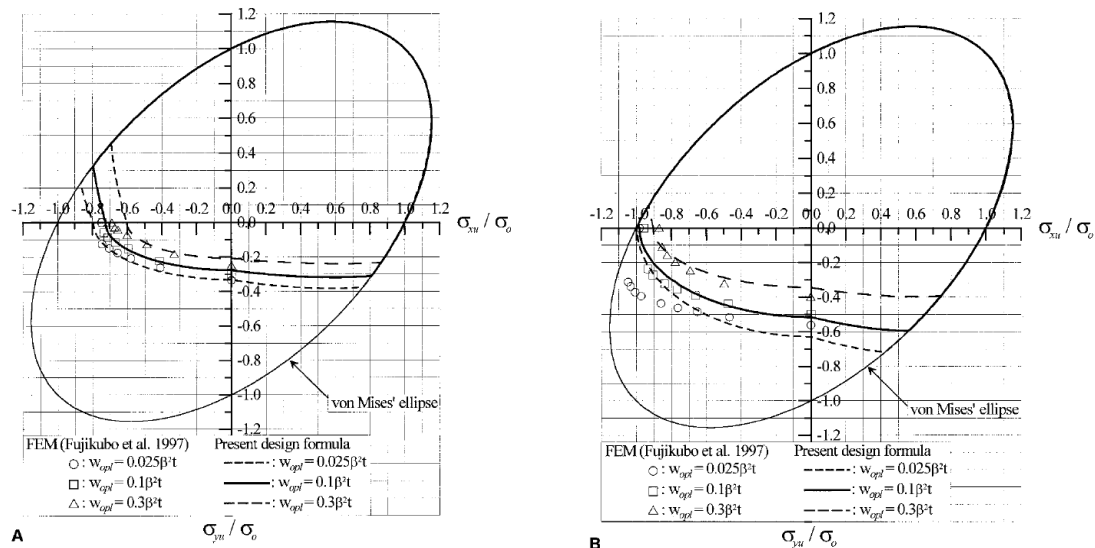
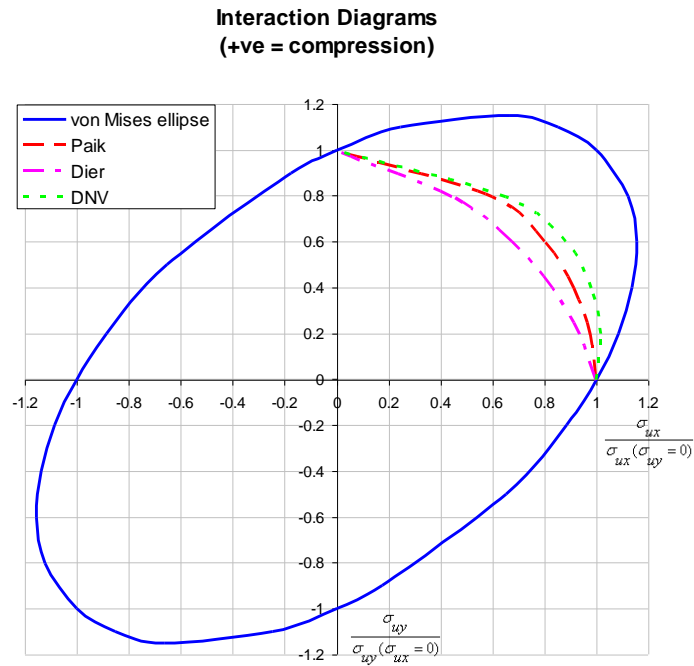


Figure 20 – Ultimate strength interaction relationship for biaxial tension/compression for a thin plate (left) and thick plate (right) – reproduced from [80]

With both load directions in compression a number of different coefficients are suggested to predict the interaction curve, some of which are summarised by Paik [37]. Generally the  $\gamma$  term in Eq. 33 is modified to reduce the curve in the compression-compression sector of the interaction diagram. For example, Paik [80] suggests  $c_1 = c_2 = 2$  and  $\gamma = 0$  when both load components are compressive. Dier [37] gives coefficients of  $c_1 = c_2 = 2$  and  $\gamma = 0.45$ . DNV HSLC rules [18] contains an interaction formula for aluminium plates which, for the slenderness ratios considered in this study, can be approximated to Eq. 33 with the coefficients  $c_1 = 1$ ,  $c_2 = 1.2$  and  $\gamma = -0.8$ . These interaction curves are as shown in Figure 21.



**Figure 21 – Interaction diagram for plate in biaxial load**

An interaction curve formula specific to aluminium plates is given in a numerical study by Kristensen and Moan [30]. The authors carried out biaxial compression experiments on 6082-T6 plates using FEM. The results showed that the biaxial compressive interaction relationship was dependent on the plate slenderness ratio. A regression analysis was then used to derive a relationship as follows in Eq. 34, which is plotted for various slenderness ratios in Figure 22.

$$R_x = \min \begin{cases} 1 + cR_y \\ \frac{1 - R_y^2}{1 - \eta R_y} \end{cases}$$

$$\eta = 0.213 - 0.275(\beta - 3)$$

$$c = 0.05 - 0.1\beta$$

34

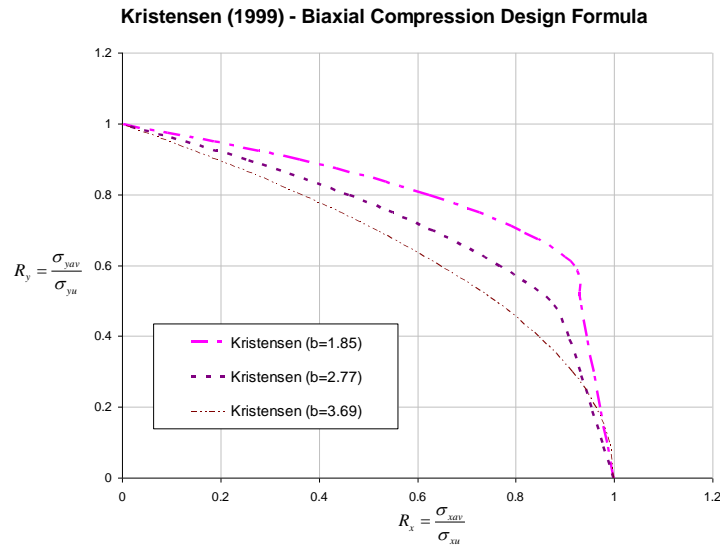


Figure 22 – Interaction curves for various slenderness ratio aluminium plates using Eq. 34.

### 3.3. Analytical Methods to Predict the In-Plane Strength of Stiffened Panels

#### 3.3.1. Overview

Relevant methods available to predict the strength of stiffened panels, taking into account elastic buckling and plastic collapse phenomena, are broadly categorised as follows:

- Empirical and closed form expressions
- Beam-column methods
- Isotropic / orthotropic large deflection plate theory
- Nonlinear FEM

Other approaches, listed by Mansour [82] but not discussed here, are the intersecting beam method and energy methods. To some extent, elements of these methods have been incorporated into the other analytical approaches. For example, Chen [83] develops a beam column method incorporating some principles of intersecting beam theory.

Simple analysis methods, such as empirical expressions, are often only able to predict the ultimate strength value of the panel in compression, with no indication of the strain at collapse or the preceding and subsequent behaviour of the panel. More advanced approaches can be used explicitly to determine the complete load-end shortening behaviour of the panel. However, the increased

complexity inherent in these methods requires more detailed information about the characteristics of the panel, which can be difficult to quantify.

A stiffened panel can fail due to different collapse mechanisms, including overall failure of the plate and stiffeners as a unit, lateral-torsional buckling (tripping) of the stiffeners and localised plate buckling. Theoretical approaches may neglect certain collapse modes and therefore care must be taken in selecting an appropriate methodology to use depending on the type of panel and the resulting use of the solution.

Recently the application of FEM has dominated much research effort and numerous studies have successfully applied the method for buckling analysis of plates, single bay stiffened panels and multi bay stiffened panels made from steel [22] and aluminium [19, 84-88]. Linear FEM can be used to predict the bifurcation strength of a structure using an Eigenvalue solution. For an imperfect structure, nonlinear FEM will readily predict the complete load shortening using an incremental solution procedure. To ensure the analysis can continue for large end displacements a suitable equilibrium search method needs to be used. For example, the Riks arc length method is available in the ABAQUS FEM software package. Arc length methods can find equilibrium in highly nonlinear systems. For a stiffened panel under compression the method can solve the negative stiffness behaviour of the panel in post collapse.

However, FEM requires explicit characterisation of all the geometric and material imperfection patterns in the panel. Different imperfection patterns in the panel will affect the collapse characteristics and can significantly alter the shape of the load shortening curve. Furthermore, the boundary conditions and extents of the FEM domain must be set very carefully to ensure all the relevant collapse modes can be represented. Differences of between 15-20% have been reported from a world-wide FEM benchmark study analysing a standard specified stiffened panel [89]. Most of the variation is thought to be caused by inexperience of some investigators in specifying the boundary conditions and model extents to adequately represent the panel.

Therefore, whilst nonlinear FEM is now feasible for a large scale stiffened panel model, simplified methods are also highly relevant to provide an efficient prediction of element strength behaviour for use in a design environment.

### 3.3.2. Design Charts and Empirical Methods

Simple closed form methods to predict PSC collapse behaviour are the most easily applied in a design situation. They have been derived by [19, 77, 90]. Methods generally use empirically based equations to calculate the panel ultimate strength and thus cannot compute load shortening behaviour.

There are several established empirical corrections to the Euler buckling formula that are used to predict the ultimate strength of a beam column. The two common formulations used by classification rules and design guidelines are the Johnson-Ostenfeld and Perry-Robertson formulae. An alternative and equally simple approach is to apply a direct empirical formulation, such as are described in the next sections. Alternatively, recourse can be made to analytical or numerical methods.

The Johnson-Ostenfeld approach as detailed previously for plates can also be used to predict the strength of a stiffened panel. The formulation is as given in Eq. 17. The Perry-Robertson approach is an extension of the Euler buckling formula, where the plate stiffener combination is treated as a column. The ultimate strength of the column is described as follows:

$$\frac{\sigma_u}{\sigma_0} = \frac{1}{2} \left( 1 + \frac{1+\eta}{\lambda^2} \right) - \left[ \frac{1}{4} \left( 1 + \frac{1+\eta}{\lambda^2} \right)^2 - \frac{1}{\lambda^2} \right]^{0.5} \quad 35$$

where  $\lambda$  is the column slenderness ratio and  $\eta = A\delta_0 z/l$ .  $\delta_0$  is the total deflection in the column, meaning that the formulation is able to account for initial geometric imperfections, which are important in nonlinear numerical approaches. The Perry-Robertson approach is more complex than Johnson-Ostenfeld, but results are comparable as shown by Paik and Thayamballi [37].

#### 3.3.2.1. Steel Panel Design Charts

Steel panel column collapse curves are published by Chalmers [76]. They are based on a combination of numerical analysis [39] and experimental data [69, 91]. The numerical approach uses a finite element beam-column method called FABSTRAN. The FABSTRAN program models the stiffener element in the beam-column using a finite element mesh. The attached plating is represented implicitly with a plate load shortening curve, derived from a combination of FEA and physical model tests [38]. These curves have approximately the same peak strength as defined by the Faulkner formula [65].

The column collapse curves allow quick and easy synthesis of a grillage to meet design criteria. The curves are presented in two forms: as a function of plate slenderness and column slenderness. An example curve set for average imperfection levels is reproduced in Figure 23.

The curves have been derived predominantly using Admiralty long stalk tee bar #2 (104.8x5.1x44.5x9.5 – see Table 7). Figure 23 applies to cross sections where  $A_s/A = 0.2$ . Separate charts are given in [39] for different area ratios from 0.1 – 0.4.

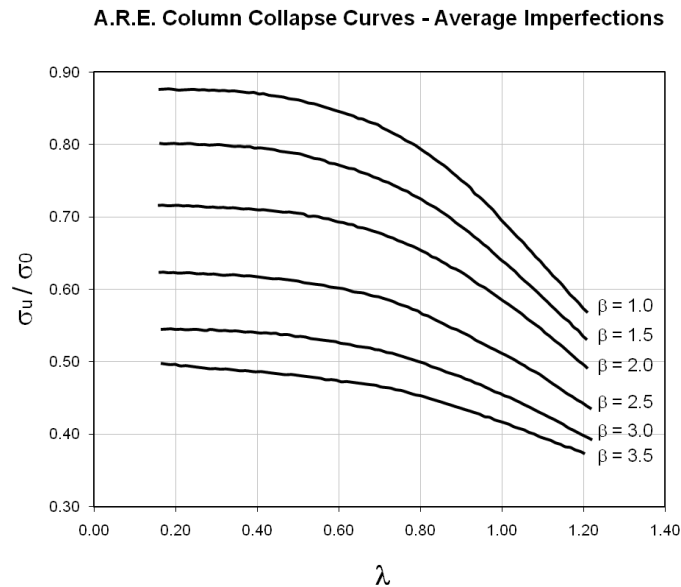


Figure 23 - A.R.E. column collapse curves for average structural imperfections [76]

The A.R.E. curves are revisited in Chapter 5, where they are compared against equivalent nonlinear FEM analyses of PSC models.

### 3.3.2.2. Empirical Formulae

A regression formula to describe the ultimate strength of a steel stiffened panel is presented by Paik and Thayamballi [37]. The formula is based on existing mechanical collapse test data with ‘average’ imperfection levels and defines strength based on the plate slenderness and column slenderness of the panel:

$$\sigma_u = \frac{\sigma_Y}{\sqrt{0.995 + 0.936\lambda^2 + 0.170\beta^2 + 0.188\lambda^2\beta^2 - 0.067\lambda^4}} \leq \frac{I}{\lambda^2} \quad 36$$

Paik and Duran develop a modified formula specific to aluminium panels, which is based on FEM of 50 5083-H116 panels with a range of column slenderness between 0.23 and 2.24:

$$\sigma_u = \frac{\sigma_{0.2}}{\sqrt{1.148 + 1.180\lambda^2 + 0.096\beta^2 + 0.052\lambda^2\beta^2 - 1.651\lambda^4}} \leq \frac{1}{\lambda^2} \quad 37$$

These empirical formulae are highly useful because they are easy to apply. However, they are limited by their datasets (either numerically or experimentally produced), and should only be applied for panels which fall within the range analysed.

### 3.3.3. Beam-Column Methods

A beam-column model assumes that a single stiffener, together with attached plating, can adequately represent the response of a complete panel. The beam is subjected to an axial compressive load and, if relevant, a lateral load. The capacity of the beam is calculated under the specified load conditions.

Beam-column methods are attractive from a design point of view because they are usually simple and follow either a closed form or efficient numerical approach [82]. As a representation of the complete stiffened panel, the beam-column is assumed to act independently. This means no account is made for interaction with adjacent longitudinals or the edge boundary conditions of the panel. Thus the beam-column method cannot predict overall collapse modes and is most suited to geometry where the stiffeners dominate over the plating.

The column ends are usually assumed to be pinned or clamped, although the method of Chen, discussed in detail below, accounts for interaction between adjacent frame spaces. Failure is assumed to occur when a plastic hinge is formed, usually at the centre of the span. The hinge forms when the compressed portion of the cross section becomes fully plastic, or the entire section loses its flexural stiffness. Potential for local web buckling, stiffener tripping and plate buckling must be checked using separate procedures.

#### 3.3.3.1. Perfect Geometry Solutions

If the material is assumed to follow an elastic-perfectly-plastic response, and the beam is initially geometrically perfect, relatively simple closed form solutions can be derived to calculate the plastic capacity, as defined by Paik and Thayamballi [37]. The basic equations governing the plastic capacity are as follows.

Under an axial load only, the plastic capacity,  $P_p$ , is:

$$P_p = A_p \sigma_{Y,P} + A_s \sigma_{Y,S} \quad 38$$

Under combined bending moment and axial load, the capacity depends on the position of the plastic neutral axis, which may lie on the plating or the stiffener web. It is not considered to lie on the stiffener flange, which is assumed to be relatively small.

If  $A_p \sigma_{Y,P} > A_s \sigma_{Y,S}$ :

$$z_p = \frac{A_p \sigma_{Y,P} + A_s \sigma_{Y,S}}{2b \sigma_{Y,P}} \quad 39$$

If  $A_p \sigma_{Y,P} < A_s \sigma_{Y,S}$ :

$$z_p = \frac{-A_p \sigma_{Y,P} + A_s \sigma_{Y,S}}{2t_w \sigma_{Y,W}} + t \quad 40$$

Assuming the yield strength of the cross section is represented by an equivalent yield stress,  $\sigma_{Yeq}$ , the plastic bending formula simplifies to:

$$M_p = \pm Z_p \sigma_{Yeq} \quad 41$$

Where  $Z_p = C_1 + C_2/bn + C_3$ .  $C_1 = \frac{1}{2}(b_e t^2 + t_w h_w^2 + b_f t_f^2)$ ,  $C_2 = -(b_e t - t_w h_w - b_f t_f)^2/4$  and  $C_3 = h_w b_f t_f$ .  $bn = b$  if the plastic neutral axis lies on the plating.  $bn = t_w$  if the plastic neutral axis lies on the stiffener web.

Because the PSC is unsymmetrical about the neutral axis, the plastic capacity interaction relationship between the bending moment,  $M$ , and the axial load,  $P$ , depends on the direction of each load component and the position of the plastic neutral axis. For a positive (compressive)  $P$ , Paik proposes using the expression for a rectangular beam in the interests of simplicity:

$$\left| \frac{M}{M_p} \right| + \left( \frac{P}{P_p} \right)^2 = 1 \quad 42$$

Approximations to account for material plasticity can be applied to some extent, by replacing elastic modulus with tangent modulus [92].

Recourse can also be made to solving the Eigenvalue of the differential equations describing the deflection of a beam-column under various load combinations, including axial load, bending moment, normal load and shear [52].

### **3.3.3.2. Numerical Approaches to Account for Geometric Imperfections**

Simple closed form approaches normally assume that a member is geometrically perfect and failure is by bifurcation buckling. It is well known that geometric imperfections cause a reduction in compressive strength in thin plated structure, and that the amplitude and shape of imperfections influences the actual collapse strength. An imperfect beam-column will deflect laterally as soon as load is applied. Therefore, if geometric imperfection is to be included in a mathematical model, recourse to numerical solution techniques must be made. This will trace the complete load-deflection response of the member up to a critical load. Common techniques used in stability analyses employ either the energy method or a numerical method.

Energy methods include Galerkin and Rayleigh-Ritz [93]. These solution techniques assume the structure is elastic and will buckle conservatively. They are therefore limited to calculating the elastic buckling load of a beam-column. Therefore, for an inelastic beam-column, a numerical method is more appropriate. This is because the beam is divided into segments, with displacements calculated at each division point, rather than the assumption of the energy method that displacement is a continuous function.

FEM is probably the most well known numerical method. Smith [39] describes an FEM beam column-approach as developed in the FABSTRAN computer program. Simpler approaches using beam-column theory can also be applied as described by Chen and Lui [92], including Newmark's method [94] and other step by step approaches. An approach derived by Chen [83], using a numerical step by step method, is summarised below.

### **3.3.3.3. Chen Beam-Column Model**

Beam-column methods typically only consider a single span with pinned or clamped supports. The influence of adjacent structure (intersecting beams) is often neglected, although end effects can be included. A recent application of the beam-column approach is derived by Chen [83], based on a step-by-step formulation, which can model the effects of three adjacent frame spaces. The method is validated using 107 panel tests and compared to ABAQUS and an orthotropic plate theory.

The initial imperfection and boundary conditions are shown in Figure 24. The model assumes, with justification, that the initial deflection shape in the column follows an up-down-up half sine wave

pattern in adjacent bays. Because the cross section of the column is usually non-symmetric, the added deflection of the centre bay will usually be different from the end bays under a given load. However, the slope of the deflection can be assumed to be continuous as it crosses the intermediate supports. Therefore, a reactionary bending moment is created at the mid supports, meaning that the centre bay no longer has a pinned support due to the end effects from the adjacent bays.

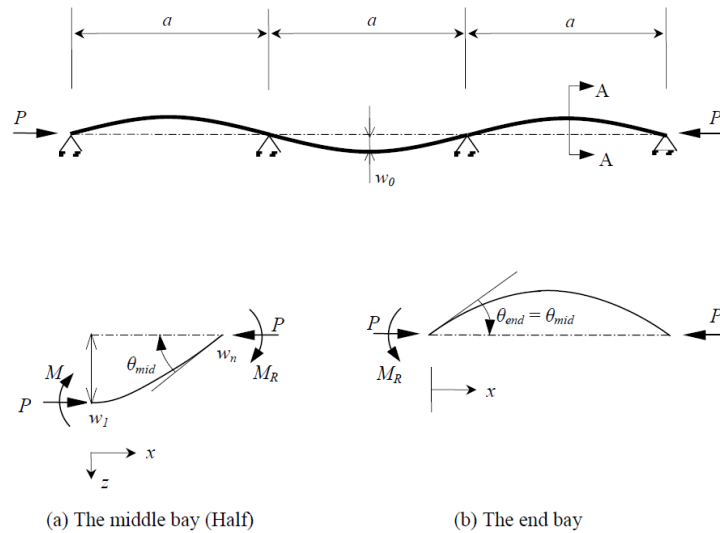


Figure 24 – Initial column imperfection and boundary conditions for a 3 bay beam-column model [83]

A modified step-by-step procedure, based on the formulation given by Chen and Lui [92], is developed to estimate both the maximum deflection of the beam at mid span and the unknown bending moment at the intermediate supports. Using a trial and error loop, the method estimates the axial load and reaction moment for a given deflection,  $w_0$ , at the centre of the beam.

In the first iteration,  $M_R$  and  $P$  are estimated. The step by step procedure is then employed to estimate the beam deflection at any point along the length. To do this, the beam is divided into segments and the deflection at each division point is calculated in series, starting from the centre.

The calculations are repeated iteratively, adjusting values of  $P$  and  $M_R$  until the boundary conditions of zero deflection and continuity of slope at the intermediate support are satisfied:

$$\begin{aligned}
 w &= 0 & \text{at } x &= \frac{a}{2} \\
 w' &= \theta_{end} & \text{at } x &= \frac{a}{2}
 \end{aligned}
 \tag{43}$$

The calculations are repeated incrementally for a progressively increasing centre displacement until the peak load is surpassed.

The analytical load-deflection equation for a three bay beam-column under axial load, P, and end bending moment,  $M_R$ , is:

$$w(x) = \frac{M_R}{k^2 EI_x} \left( \cos(kx) - \frac{\sin(kx)}{\tan(ka)} + \frac{x}{a} - 1 \right) + \left( \frac{I}{I - \frac{P}{P_E}} \right) w_0 \sin \frac{\pi x}{a} \quad 44$$

$$k = \sqrt{\frac{P}{EI_x}} \quad 45$$

The first derivative of Eq. 44 gives the slope,  $\theta$ , at the connection between the end bay and the middle bay.

Chen's beam-column method is demonstrated to give a closer approximation to the strength of a panel than the orthotropic plate method encapsulated in the ULSAP computer program, as compared to equivalent FEM using ABAQUS.

### 3.3.4. Orthotropic Plate Methods

Classical theory, founded on the large deflection plate theory of von Karman and Maguerre [95], can be implemented to calculate the local buckling of a stiffened panel assuming an orthotropic plate model.

#### 3.3.4.1. Development of Orthotropic Plate Theory

Orthotropic methods treat the plating and stiffeners as an equivalent plate with different elastic properties in the two orthogonal directions. The elastic constants in each direction are calculated assuming the stiffeners are "smeared" into the plating. Solutions to the orthotropic plate problem are presented by Mansour [82], Hughes [53] and Paik et al. [96]. DNV have also developed a stiffened panel buckling program, PULS, which uses an orthotropic type modelling approach [97].

The orthotropic plate theory has usually been considered more suitable for a panel with a large number of relatively small, closely spaced stiffeners running in both directions. For example, the A.R.E. [98] found that orthotropic plate theory was valid for simply supported panels with multiple stiffeners in both directions, but less accurate for panels with different edge boundary conditions or with less than three stiffeners in each direction.

However, a recent study by Paik et al. [96] found that a large deflection orthotropic plate method shows good correlation to finite element results for buckling problems between adjacent frames as

well as for overall panel buckling of multiple framed panels. Paik’s approach is incorporated into the ULSAP computer program [37].

For these reasons an extension to the large deflection orthotropic plate method is conducted as part of the present work. This section

### 3.3.4.2. Large Deflection Orthotropic Plate Approach

The orthotropic method, as derived fully by Paik et al. [96], is now summarised. The method assumes material is isotropic with a well-defined yield stress, Young’s modulus and Poisson ratio. The coordinate system and geometry definition is as shown in Figure 25. The longitudinal stiffeners are assumed to lie in the x direction and the transverse frames in the y direction. The thickness of the plate is constant and the stiffeners are regularly sized and spaced. The number of longitudinal and transverse stiffeners is  $n_{sx}$  and  $n_{sy}$  respectively. The stiffener and plate areas are as defined in Chapter 2.

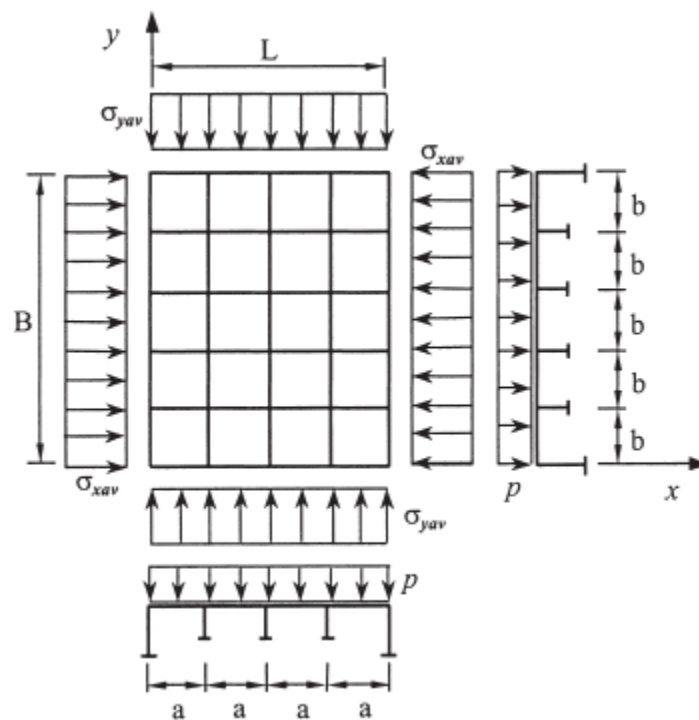


Figure 25 – Orthotropic plate geometry and coordinate system [96]

If the plate and stiffeners have different material properties an equivalent material yield stress for the entire stiffened panel can be approximated as:

The panel edge boundary conditions are conservatively assumed to be simply supported. The edges are kept straight with zero rotational restraint along the edge axis. Out of plane edge deflection is

constrained. The panel is subject to combined in-plane ( $\sigma_{ave,x}$ ,  $\sigma_{ave,y}$ ), shear ( $\tau_{xy}$ ) and lateral pressure (p) loads. The pressure load is assumed to be constant and applied first. The ultimate strength of the panel under a prescribed combination of in-plane loads is then assessed.

### **Governing Equations**

The governing nonlinear equations of large deflection orthotropic plate theory are extended from von Karman's original equilibrium and compatibility equations. The form of the governing equations depends on the orthotropic plate method, which range from small deflection linear theory to large deflection nonlinear theory. The large deflection equilibrium and compatibility equations were originally derived by Rostovstev [99]:

$$D_x \frac{\partial^4 w}{\partial x^4} + 2H \frac{\partial^4 w}{\partial x^2 \partial y^2} + D_y \frac{\partial^4 w}{\partial y^4} - t \left[ \frac{\partial^2 F}{\partial y^2} \frac{\partial^2 (w + w_0)}{\partial x^2} - 2 \frac{\partial^2 F}{\partial x \partial y} \frac{\partial^2 (w + w_0)}{\partial x \partial y} + \frac{\partial^2 F}{\partial x^2} \frac{\partial^2 (w + w_0)}{\partial y^2} + \frac{p}{t} \right] = 0 \quad 46$$

$$\frac{1}{E_y} \frac{\partial^4 F}{\partial x^4} + \left( \frac{1}{G_{xy}} - 2 \frac{\nu_x}{E_x} \right) \frac{\partial^4 F}{\partial x^2 \partial y^2} + \frac{1}{E_x} \frac{\partial^4 F}{\partial y^4} - \left[ \begin{aligned} & \left( \frac{\partial^2 w}{\partial x \partial y} \right)^2 - \frac{\partial^2 w}{\partial x^2} \frac{\partial^2 w}{\partial y^2} + 2 \frac{\partial^2 w_0}{\partial x \partial y} \frac{\partial^2 w}{\partial x \partial y} \\ & - \frac{\partial^2 w_0}{\partial x^2} \frac{\partial^2 w}{\partial y^2} - \frac{\partial^2 w_0}{\partial y^2} \frac{\partial^2 w}{\partial x^2} \end{aligned} \right] = 0 \quad 47$$

The components of Eq. 46 and Eq. 47 are now defined.

### **Orthotropic Plate Deflection**

The nonlinear governing equations are a function of the out of plane deflection of the panel, which comprise initial as fabricated imperfection ( $w_0$ ) and added deflection ( $w$ ) due to buckling. The distribution of deflection across the plate is usually expressed by a Fourier series. The initial deflection is thus defined as:

$$\frac{w_0}{w_{opl}} = \sum \sum B_{oij} \sin \frac{i\pi x}{L} \sin \frac{j\pi y}{B} \quad 48$$

where  $B_{oij}$  is the initial imperfection amplitude. Because the initial post welding initial deflections of a plate are also important variables in nonlinear finite element analysis a full definition of initial imperfection is not provided here. Section 4.4 provides a more complete description of the statistical formulations used to define Fourier series functions and initial imperfection amplitudes.

If a half wave deflection term associated with the panel buckling shape in each direction is assumed dominant, the initial deflection formula can be simplified to include only one buckling mode in x and y. The general case under biaxial in-plane load is:

$$w_0 = A_0 \sin \frac{m\pi x}{L} \sin \frac{n\pi y}{B} \quad 49$$

where m and n are the half wave modes in the longitudinal and transverse direction respectively. The buckling mode shape, and hence the value of m and n, depends on the structural orthotropy. If the panel is only loaded in one direction, the half wave mode in the unloaded direction is assumed to be 1. The initial imperfection amplitude,  $A_0$ , can be defined using typical statistical representations of panel imperfection (see section 5.4).

The added deflection can also be defined by a Fourier series with buckling modes as for the initial imperfection. For an arbitrarily loaded panel the added deflection is:

$$w = A_m \sin \frac{m\pi x}{L} \sin \frac{n\pi y}{B} \quad 50$$

Where  $A_m$  is the added deflection amplitude. To analytically solve the governing equations the maximum amplitude of the added deflection function ( $A_m$ ) must be obtained.

### **Solutions of Airy Stress Function**

Substituting the equations for initial and added deflection into the compatibility equation results in:

$$\frac{1}{E_y} \frac{\partial^4 F}{\partial x^4} + \left( \frac{1}{G_{xy}} - 2 \frac{\nu_x}{E_x} \right) \frac{\partial^4 F}{\partial x^2 \partial y^2} + \frac{1}{E_x} \frac{\partial^4 F}{\partial y^4} = \frac{m^2 \pi^4}{2L^2 B^2} A_m (A_m + 2A_0) \left( \cos \frac{2m\pi x}{L} + \cos \frac{2n\pi y}{B} \right) \quad 51$$

F is the Airy stress function, which describes the non-uniform distribution of stress across the plate. The particular solution of the stress function under combined load, obtained by solving Eq. 51, is:

$$F_P = \frac{A_m (A_m + 2A_0)}{32} \left( E_y \frac{n^2 L^2}{m^2 B^2} \cos \frac{2m\pi x}{L} + E_x \frac{m^2 B^2}{n^2 L^2} \cos \frac{2n\pi y}{B} \right) \quad 52$$

If uniaxial load in the longitudinal direction is considered, the homogeneous solution which satisfies the loading condition is:

$$F_H = \sigma_{xav} \frac{y^2}{2} \quad 53$$

Similarly, under uniaxial load in the transverse direction, the homogenous solution is:

$$F_H = \sigma_{yav} \frac{x^2}{2} \quad 54$$

The total stress function F is the sum of the particular and homogeneous solution.

$$F = F_P + F_H \quad 55$$

### **Discrete Solution**

By substituting the stress function and deflection equations into the equilibrium equation (Eq 46) and applying the Galerkin method, the continuous problem is converted into a discrete third order equation with respect to the unknown amplitude of the added deflection,  $A_m$ . The solution for  $A_m$  is presented fully in section 0.

### **Evaluation of Buckling Stress**

The use of large deflection equations means that the stress distribution over the panel is non uniform. The panel is assumed to act equivalent to a simply supported plate and thus, as described previously, the central region of the plate sheds load into the edge regions as the load, and corresponding out of plane deflection, increases. The maximum applied stress at collapse can thus be assumed to occur at the plate corners (e.g.  $x=0, y=0$ ) whilst the minimum stress is at the centre of the plate edges (e.g.  $x=0, y=L/2$  or  $x=B/2, y=0$ ).

The Airy stress function, which is defined previously, must satisfy the following conditions at the panel boundaries:

$$\sigma_x = \frac{\partial^2 F}{\partial y^2}, \sigma_y = \frac{\partial^2 F}{\partial x^2}, \tau = \frac{\partial^2 F}{\partial x \partial y} \quad 56$$

Thus the stress anywhere along the plate boundary is found by twice differentiating Eq. 52 appropriately. The maximum and minimum stress can then be formulated. Ultimate strength is

assumed to be when stress in the plate edges reaches yield. Yielding can be assessed using the von Mises stress criterion.

### **Elastic Constants**

The method requires calculation of the orthotropic geometric properties, which are functions of the various elastic constants of the orthotropic plate. The elastic constants in an isotropic plate comprise the Young's modulus,  $E$ , and the Poisson ratio,  $\nu$ . For an orthotropic plate, separate constants in the  $x$  and  $y$  directions must be defined, to take into account the anisotropy arising from the different geometry. These are the elastic moduli ( $E_x$  and  $E_y$ ), Poisson ratios ( $\nu_x$  and  $\nu_y$ ), flexural rigidity ( $D_x$  and  $D_y$ ), torsional rigidity ( $H$ ) and elastic shear modulus ( $G_{xy}$ ).

It is important to define these constants adequately as the subsequent accuracy of the orthotropic approach depends almost entirely on them. The definitions as given by Paik et al are described in this section. The extension to the orthotropic method, described fully in Chapter 6, re-examines these equations to derive nonlinear constants which change as the incremental application of in-plane loads cause deformation and plasticity in the plate.

Assuming that the material itself is isotropic, and that the panel comprises equally spaced, identical stiffening, the elastic moduli can be approximated to:

$$E_x = E \left( 1 + \frac{n_{sx} A_{sx}}{Bt} \right) \quad 57$$

$$E_y = E \left( 1 + \frac{n_{sy} A_{sy}}{Lt} \right) \quad 58$$

The revised elastic modulus is thus a function of the stiffener area relative to the plate area only, and is independent of the geometry distribution. The definition of the stiffener areas is consistent with previous formulations in this thesis.

The flexural and torsional rigidities are approximately expressed as:

$$D_x = \frac{Et^3}{12(1-\nu_{xy}^2)} + \frac{Etz_{0x}^2}{1-\nu_{xy}^2} + \frac{EI_x}{b} \quad 59$$

$$D_y = \frac{Et^3}{12(1-\nu_{xy}^2)} + \frac{Etz_{0y}^2}{1-\nu_{xy}^2} + \frac{EI_y}{a} \quad 60$$

$$H = \frac{1}{2} \left( \nu_y D_x + \nu_x D_y + G_{xy} \frac{t^3}{3} \right) \quad 61$$

where  $I_x$  and  $I_y$  are the second moment of areas of the orthogonal stiffeners, using consistent nomenclature as used in the previous Chapter. The revised Poisson's ratio,  $\nu_{xy}$ , is defined as:

$$\nu_{xy} = \sqrt{\nu_x \nu_y} \quad 62$$

To determine the orthotropic Poisson's ratios,  $\nu_x$  and  $\nu_y$ , the reciprocity theorem by Betti can be used. This states that the work done by a set P through the displacement produced by Q is equal to the work done by Q through the displacement produced by P. This can be applied to the plate problem by considering the behaviour in the y direction when applying a small displacement in x. Assuming the plate behaviour is linear, the Poisson's ratio causes a corresponding force in the y direction. The force is also proportional to the elastic moduli and flexural rigidities. Thus:

$$\nu_x E_y = \nu_y E_x \quad 63$$

$$\nu_x D_y = \nu_y D_x \quad 64$$

Substituting the elastic constant equations into the above produces:

$$\left[ \frac{EI_x}{b} \left( \frac{E_y}{E_x} \right)^2 - \frac{EI_y}{a} \left( \frac{E_y}{E_x} \right) \right] \nu_x^3 - \left[ \frac{E_y}{E_x} \left( \frac{Et^3}{12} + Etz_{0x}^2 + \frac{EI_x}{b} \right) - \frac{Et^3}{12} - Etz_{0y}^2 + \frac{EI_y}{a} \right] \nu_x = 0 \quad 65$$

This equation is rearranged and Betti's reciprocity is reapplied to yield equations for the orthotropic Poisson's ratios:

$$\nu_x = c \left[ \frac{\frac{E_y}{E_x} \left( \frac{Et^3}{12} + Etz_{0x}^2 + \frac{EI_x}{b} \right) - \frac{Et^3}{12} - Etz_{0y}^2 - \frac{EI_y}{a}}{\frac{EI_x}{b} \left( \frac{E_y}{E_x} \right)^2 - \frac{EI_y}{a} \left( \frac{E_y}{E_x} \right)} \right]^{0.5} \quad 66$$

$$\nu_y = \frac{E_y}{E_x} \nu_x \quad 67$$

The correction factor  $c$  is added to correlate the derived Poisson ratio with that for an isotropic plate, and is approximated as  $c = \nu / 0.86$ .

### **Implementation**

The formulations are checked by repeating the illustrative example in [96], which uses the orthotropic plate method built into the ULSAP computer program. The example uses a single bay stiffened panel with an overall length of 2640mm, breadth of 3600mm and with a plate thickness of 21mm. Three flat bar stiffeners with thickness 12mm run longitudinally. Material is steel with  $\sigma_0 = 252\text{MPa}$  and  $E = 210\text{GPa}$ . Average imperfections using Smith's criteria [39] are used.

The figure shows good correlation with the ULSAP results as reported by Paik et al. [96]. The two curves slightly separate as the stiffener height is increased. The ULSAP results show a transition point at  $h_{wx}/t_{wx} = 12$ , suggesting that a different buckling mode, probably tripping as the panel is flat bar stiffened, may also be accounted for. The formulations developed in this study only evaluate the overall buckling mode and hence the resulting strength prediction is higher. The full formulation as presented in Chapter 6 accounts for all buckling modes.

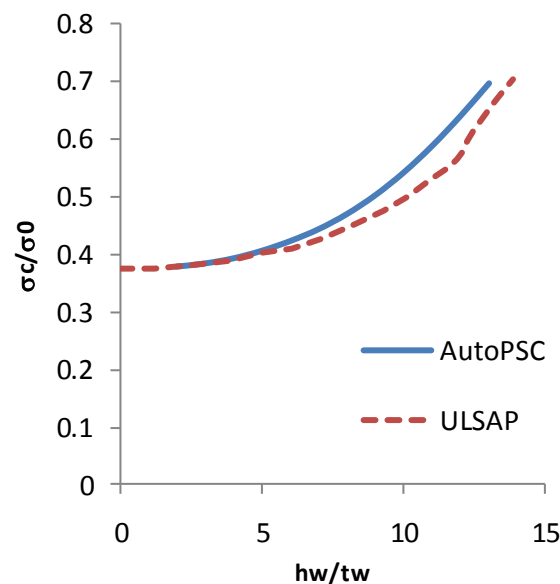


Figure 26 – Comparison of results from Paik et al. [96] and the formulations in the present work.

### **3.3.5. Analytical Load Shortening Curves**

Although the beam-column and orthotropic plate methodologies have been proved to adequately predict panel strength in certain circumstances, neither directly map the load shortening curve. Although the beam-column method traces the out of plane deflection of the panel as load is

increased, this is not readily useful to estimate the in-plane displacement. Similarly, the orthotropic plate approach only derives the ultimate strength of the panel.

Therefore, an incremental method is needed to predict the pre-collapse stiffness and enable a complete load shortening curve to be traced. Paik and Thayamballi [37] provide such a method, as incorporated into the ULSAP computer program.

The stress is calculated incrementally using the following formula:

$$\Delta\sigma_x = \frac{L}{A} k_E \varepsilon_x \quad 68$$

where

$$k_E = \left[ \frac{L}{EA} + \frac{\pi^2 (\delta_0 + w_{qmax})^2}{2LP_E (1 - P/P_E)^3} \right]^{-1} \quad 69$$

The formula allows an evaluation of the load shortening curve up to and beyond the collapse strength of the panel.

### 3.4. Summary

This Chapter has reviewed several established analytical methods, with varying complexity, which can be employed to predict the strength of plates and stiffened panels. Methods are broadly divided into those used for unstiffened plates and those for stiffened panels.

There are numerous approaches available to predict the ultimate strength of a plate under a variety of load combinations. However, for the purposes of progressive collapse analysis, the ultimate strength is not a sufficient measure to describe the entire load shortening behaviour of the plate. Although there are analytical approaches available to predict the entire load shortening curve, they are not necessarily of sufficient accuracy to give enough fidelity to describe the curve shape and the post collapse characteristics adequately when compared to equivalent results generated using nonlinear FEM.

A similar conclusion is reached in the review of methods to predict stiffened panel analysis. Most established analytical approaches are able to predict the ultimate strength only and cannot describe the load shortening relationship. Furthermore, most methodologies are by definition interframe. The orthotropic plate method is an exception in that it can be used to predict orthogonally stiffened

panel strength. Although it has traditionally been reserved for studying very lightly stiffened panels only, recent applications of the large deflection orthotropic plate approach have shown it to be valid for structure more typical of normal ship scantlings. Therefore, in this respect, the orthotropic plate method holds a significant advantage over comparable beam column approaches. The formulation is also easily adaptable to account for the specific properties of aluminium and, as will be shown in Chapter 6, can be extended to deal with the nonlinear response of the plate and stiffener components within an orthogonally stiffened panel.

*“Engineering problems are under defined; there are many solutions, good, bad and indifferent. The art is to arrive at a good solution”, Ove Arup [100]*

# Chapter 4

## Finite Element Analysis of Unstiffened Aluminium Plates

### 4.1. Introduction

This Chapter presents comprehensive numerical experiments, using the nonlinear finite element method, investigating aluminium and steel plates typical of ship shell structure. Nonlinear FEM is a well-known numerical approach to efficiently model simple structural elements and assess the influence of various material and geometric parameters. This Chapter presents comprehensive numerical experiments, using ABAQUS nonlinear FEM [101], to investigate strength and stability characteristics aluminium and steel plates typical of ship shell structure.

FEM is also increasingly used for assessing the ultimate strength of more complex ship type structures ranging from stiffened panels through to the entire hull girder. The general modelling

approach for plates as described in this Chapter is extended to panels and girders in Chapters 5 and 7 respectively.

A rigorous modelling approach is developed which includes the influence of geometric and material nonlinearities and provides adequate recognition of factors which affect the plate strength, including:

- Edge boundary conditions;
- Initial geometric imperfections;
- Material properties;
- The heat affected zone (HAZ);
- Weld induced residual stresses.

A key objective is to reduce the uncertainties inherent in appropriately modelling these factors; discounting those which make a relatively minimal difference to the plate behaviour whilst ensuring the methods properly take into account those that do influence strength significantly.

The findings of the plate study, as detailed in the latter part of this Chapter, are important to consider when modelling more complex geometry. Furthermore, the techniques used to model the imperfection, residual stresses and heat affected zone in a simple plate are also important to replicate in a more complex stiffened panel model. Therefore the studies detailed below not only generate raw data to quantify the strength of plates but also provide a case study for the causes of the various imperfections within a welded aluminium structure and how these are represented within an FEM analysis.

#### 4.1.1. General Parameters

Load shortening curves are normalised with respect to the 0.2% proof stress (aluminium) or yield stress (steel) of the material (which throughout this Chapter is denoted by the generic symbol  $\sigma_0$ ) and the material strain at the yield/proof stress (which throughout this Chapter is denoted by the generic symbol  $\varepsilon_0$ ). For a plate in uniaxial longitudinal compression, the normalising expressions are:

$$\sigma' = \frac{\sigma_{x,ave}}{\sigma_0}$$

70

$$\varepsilon' = \frac{\varepsilon_{x,ave}}{\varepsilon_0}$$

71

where  $\sigma_{x,ave}$  is the average stress on the loaded edge, assuming the plate cross section area is unchanged, and  $\varepsilon_{x,ave}$  is the non-dimensional displacement of one plate end relative to the opposite end ( $\varepsilon_{x,ave} = u_x/a$ ). The same principle is used to non dimensionalise stress and strain in the transverse direction ( $\sigma_{y,ave}, \varepsilon_{y,ave}$ ). The plate coordinate system is shown in Figure 27.

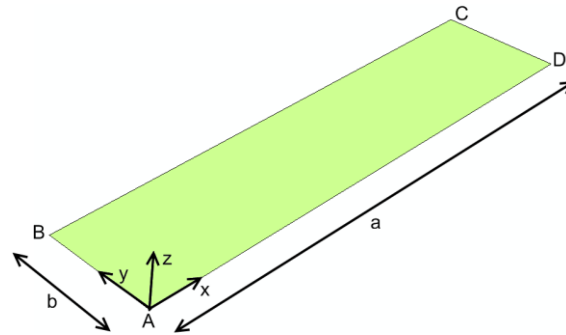


**Figure 27 – Plate coordinate system**

All analyses completed in this thesis use the ABAQUS 6.9 FEM code [101]. The ABAQUS solver has rigorous nonlinear capabilities and has been shown to provide good comparative results to physical test data of plates in compressive instability [27].

An arc length convergence method is used to handle the nonlinear response typical of plate collapse. In ABAQUS the Riks approach is employed [93]. The incremental form of the Rik's analysis enables production of complete load shortening curves in the post processing module. All analyses use sufficiently small increments to enable an accurate track of the plate response over a displacement range up to twice the yield/proof strain.

Quadrilateral shell elements with reduced integration (S4R) are used for all plates modelled in the parametric study. An initial check on result convergence for different mesh densities was carried out and based on these results the mesh for all plates is specified so that at least one element, and more usually two, span the HAZ region. Element type and mesh size are consistent with previous studies [27].

Initial imperfection is introduced by applying an out-of-plane Fourier series translation to each node in the mesh using an external script to directly edit the node coordinate input file. The imperfection of plates forms part of the development of large scale stiffened panel models and therefore the details of the methods used to handle the introduction of imperfection are described in Chapter 5.

Residual stress is introduced using the \*INITIAL CONDITIONS feature of ABAQUS, which allows elements to be prescribed an initial stress field prior to any displacement of the model. A detailed discussion of these features follows.

Complete plate geometry with supports along all four edges was used for the FE model. There are only small computational benefits to be gained by reducing the mesh size to a ½ or ¼ size model with symmetry boundary conditions. Furthermore, the use of complete plate geometry has the added advantage that unsymmetrical parameters, such as a complex geometric imperfection pattern, can be adequately modelled.

#### 4.1.2. Reference Plates

A case study database of plates typical of aluminium ship structures is used to highlight the influence of the various material and geometric parameters listed previously. The properties are given in Table 1. The dimensions have been derived so as to give integer  $\beta$  values and a range of plate aspect ratios (both integer and non-integer).

Table 9 – Plate properties - case study database

	$a$	$b$	$t$	$AR$	$Beta$	$HAZ$	$Material$	$\sigma_0$
	mm	mm	mm			mm		MPa
Plate 1	1200	400	11.1	3	2	25	5083	215
Plate 2	1200	400	7.4	3	3	25	5083	215
Plate 3	1000	400	11.1	2.5	2	25	5083	215
Plate 4	1000	400	7.4	2.5	3	25	5083	215
Plate 5	2100	400	11.1	5.25	2	25	5083	215
Plate 6	2100	400	7.4	5.25	3	25	5083	215
Plate 7	1200	400	12.2	3	2	25	6082	260
Plate 8	1200	400	12.2	3	2	25	6082	260

Throughout this Chapter, analyses are compared to reference results, which use boundary conditions and imperfection parameters typical of an “average” plate. The methods used to develop these parameters are discussed in corresponding sections and are summarised as follows:

- Boundary Conditions – Simply supported on all 4 sides (Eq.72). For uniaxial load cases the unloaded edge is free to move in-plane but constrained to remain straight (Eq.74). In biaxial cases load is applied on all four edges with displacement controls.

- Geometric Imperfection – Three mode longitudinal imperfection pattern (Eq.81). Average imperfection amplitude (Eq. 77).
- Heat Affected Zone – Located on all four edges with width of 25mm (Table 9). HAZ material proof stress as defined by a Ramberg Osgood approximation as shown in section 2.4.2.
- Residual Stress – Longitudinal and transverse residual stress pattern with tensile zone width equal to the HAZ width and equilibrating compressive stress (Eq. 5). Tensile residual stress of 130MPa.

## 4.2. Boundary Conditions

An unstiffened plate in a longitudinally stiffened ship structure is usually bounded by longitudinal stiffeners along the longer plate edges and frames along the shorter edges. Primary longitudinal bending of the hull girder can be assumed to impart uniaxial in-plane forces on the short edges of the plate. Transverse bending, which is particularly relevant in regions of a multi hull structure, imparts in-plane forces on the longer plate edges. Other common global load scenarios including shear, torsion and lateral hydrostatic pressure add further forces to the plate both in-plane and normal to the surface.

To represent a plate as part of an integrated part of a ship structure, the boundary conditions of the FEM model needs to adequately reflect the local support and load scenarios. The plate element local coordinate system is defined in Figure 27. Position is defined in  $x$ ,  $y$  and  $z$  with associated displacement in  $u$ ,  $v$  and  $w$ .

**Table 10 – Plate Boundary Conditions: 0 = Free, 1 = Constrained**

	Simple Support		Clamped	
	AB and CD	BC and AD	AB and CD	BC and AD
Displacement $x$ ( $u$ )	1*	0	1*	0
Displacement $y$ ( $v$ )	0	1 <sup>#</sup>	0	1 <sup>#</sup>
Displacement $z$ ( $w$ )	1	1	1	1
Rotation $x$ ( $\theta_x$ )	1	0	1	1
Rotation $y$ ( $\theta_y$ )	0	1	1	1
Rotation $z$ ( $\theta_z$ )	1	1	1	1

\* AB is displacement controlled in  $X$ , <sup>#</sup> BC and DA constrained to move bodily in  $y$  but remain straight

### 4.2.1. Out of Plane Constraints

The longitudinal and transverse stiffeners bounding the plate edges are assumed to prevent out of plane displacement:

$$w=0 \text{ at } x=0,a \text{ and } y=0,b$$

72

The boundary conditions set out above assume that the bounding stiffeners do not buckle, thus preventing out of plane displacement, and also keep the plate boundary straight. To allow this assumption, the structure must be designed such that the plates buckle well before the stiffeners. If the stiffeners buckle before or soon after the plate then the assumption of straight edges no longer holds.

### 4.2.2. Rotational Restraints

For a plate considered as part of an orthogonally stiffened panel, the boundary condition on the plate edges is affected by the rotational restraint of the adjacent structure and the prescribed loading conditions on the plate. The rotational boundary condition is partly a function of the out of plane imperfection pattern in the plating.

A conservative, and typical, approach is to assume that the rotational restraint at the boundary is minimal and thus the plate is simply supported along its edges. This is considered adequate if the plating imperfections, and subsequent buckling patterns, alternate between adjacent spaces, as is shown in Figure 28a. If the stiffener is assumed to be a knife edge and the buckling pattern is asymmetric across the boundary then the restraint about the edge axis is zero. In reality, buckling may predominate in one plate producing some rotational restraint, but for design purposes this effect can be neglected.

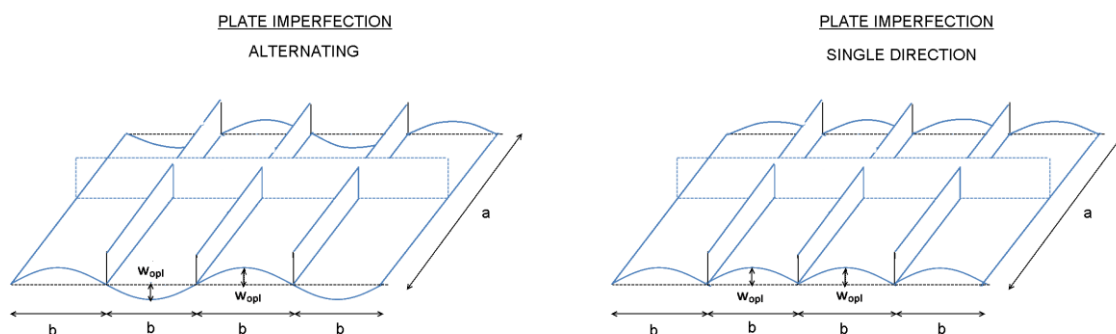


Figure 28 – Plate imperfection patterns: alternating (left) and single direction (right)

Alternatively, plate imperfections can be predominantly patterned in a single direction (Figure 28b). This is often termed a “hungry horse” imperfection pattern and is perhaps more common on light side/bottom structure where weld wrap up and subsequent lateral pressure loads both contribute to producing imperfections into the hull (Figure 29). This type of imperfection pattern also implies simultaneously occurring pressure forces and axial compression.



**Figure 29 – USCGC Buttonwood in dry-dock. Evidence of hungry horse imperfections in the side shell plating.**

With a single direction imperfection pattern the action of the adjacent plate elements may have a more significant effect on the rotational restraint. If it is assumed the plate material is continuous over the stiffener, which forms a knife edge, and buckling occurs in adjacent plates, with deformation in the same direction, then the plate rotation at the stiffener edge will be reduced. If the rotation is assumed to be zero this is equivalent to a clamped boundary condition. Mathematically, the clamped boundary condition is expressed:

$$\frac{dw}{dx} = 0 \quad \text{at } x = 0, a$$

$$\frac{dw}{dy} = 0 \quad \text{at } y = 0, b$$

73

Figure 30 shows a comparison of fixed and simply supported boundary conditions for Reference plates 1 and 2 (Table 9). As would be expected, the clamped support provides additional strength to the plate. The ultimate strength of Plate 1 increases by 18% and Plate 2 by 22%.

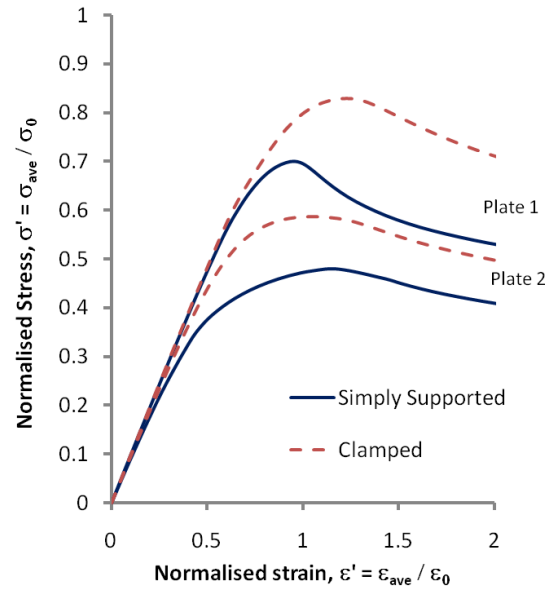


**Figure 30 – Comparison of simply supported and clamped boundary conditions for Plate 1 and Plate 2. Plate imperfections as specified in section 4.1.2.**

In reality, the boundary support will often be intermediate between simply supported and clamped. The stiffeners provide an amount of rotational restraint along the axis of the plate edge [53]. Furthermore, the behaviour of adjacent plate elements will also influence the rotational and displacement boundary support conditions and in some instances this may need to be considered. The effects of rotational restraint are considered in combination with the stiffener strength in Chapter 5.

#### 4.2.3. In-Plane Constraints

For a long plate, the shorter plate edges will displace due to the applied load. Therefore, under uniaxial longitudinal load, the short plate edges will move inwards but remain straight. In an FEM analysis, compressive load is applied on the plate using displacement control on the boundary nodes.

The in-plane restraint of the unloaded edge is less simple to define. In tests of plates under uniaxial compression, a common assumption for the unloaded edges is to constrain the edge to remain straight but free to move bodily in-plane. Test data usually refers to plates with this type of constraint, which prevents an artificial transverse in-plane load on the long edges due to Poisson effects. In mathematical terms the boundary condition is:

$$\int_0^a F_y dx = 0, \quad \frac{dv}{dx} = 0 \quad \text{at } y=0, b$$

74

It is questionable whether Eq. 74 adequately represents the actual boundary condition in a ship structure. With such a condition in place and under uniaxial compression, the unloaded edge will usually move outwards before the plate buckles, due to Poisson effects, and then reverse to move inwards subsequent to plate buckling. However, if considered as part of a panel, the long plate edge should remain constrained from in-plane movement in  $y$ , as adjacent plates will also be under similar load conditions. This would lead to a zero displacement edge constraint:

$$v = 0 \quad \text{at } y=0, b$$

75

However, the problem is not necessarily a significant one for the purposes of load shortening curve generation. Figure 31 presents the results from analyses of two plates in uniaxial compression, with properties described in Table 9 and average geometric imperfections. The curves show that there is minimal difference in the load shortening behaviour comparing the boundary condition set using Eq. 74 or Eq. 75. The zero displacement boundary condition (Eq. 75) shows slightly higher stiffness before collapse and slightly reduced overall strength. Post collapse characteristics are very closely matched.

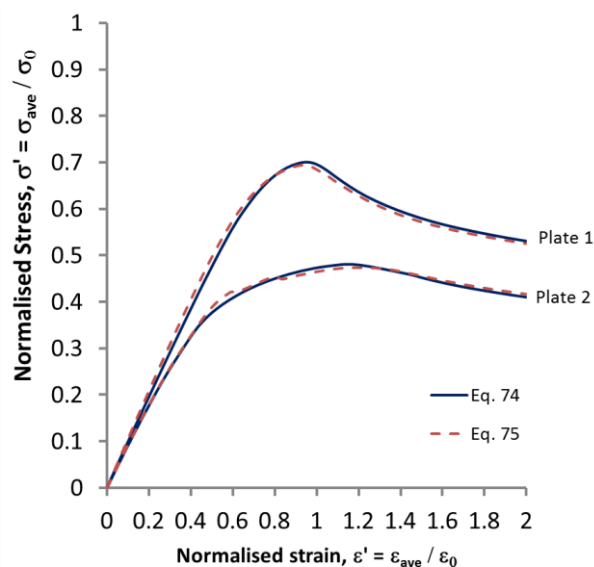


Figure 31 – Comparison of in-plane support conditions for Plate 1 and Plate 2.

### 4.3. Aspect Ratio

Plates in a longitudinally stiffened ship are usually bounded by relatively closely spaced longitudinals and widely spaced frames, giving plate aspect ratios typically in the range 2-6 [61]. Steel plate strength equations such as the Faulkner formula [65] and load shortening curve data (e.g. by Smith et al [38]) are applicable to long plates. Curves are given in terms of the plate slenderness ratio only, thus assuming that the strength of long plates is independent of aspect ratio. They do not apply to wide (plate length less than width) or square (length equal to width) plates.

However, it is reasonable to assume that the collapse behaviour of a square plate with an appropriate initial imperfection shape represents the nucleated collapse region of a longer plate. This means that when a long plate fails in compression the end shortening localises to a single, approximately square, collapse region. The rest of the plate exhibits no further strain and can even unload elastically.

Therefore, an approach was suggested by Smith [7] to adapt a square plate curve to represent a long plate, with a correction factor on the unloading part of the strain scale to take into account the nucleation of the collapse. However, the components of the imperfection shape are significantly different for long plates as compared to square plates, and this can significantly affect the performance of the respective plates in compression. In a long plate the buckling mode imperfection amplitude is typically much less than the single half wave shape. In a square plate the overall distortion is entirely comprised of the buckling mode shape. For this reason a square plate is usually much weaker in compression than an equivalent long plate.

It is therefore proposed that load shortening curves for long plates should be derived directly from long plate FEM models. To demonstrate this, and also to study the effect of increasing the aspect ratio, a series of FEM models, using as a base case Plates 1 and 2 from Table 9, are tested in uniaxial compression. Derivatives of the base case have differing plate length only. All other parameters are as given in section 4.1.2. All plates have the same width to minimise the relative HAZ width effect as described in section 4.5.3.

The resulting load shortening curves, presented in Figure 32, are presented in three groups. The blue curves show relatively short plates ( $AR < 3$ ), the red curves are intermediately long ( $3 < AR < 4$ ) and the green curves show longer plates ( $AR > 4$ ).

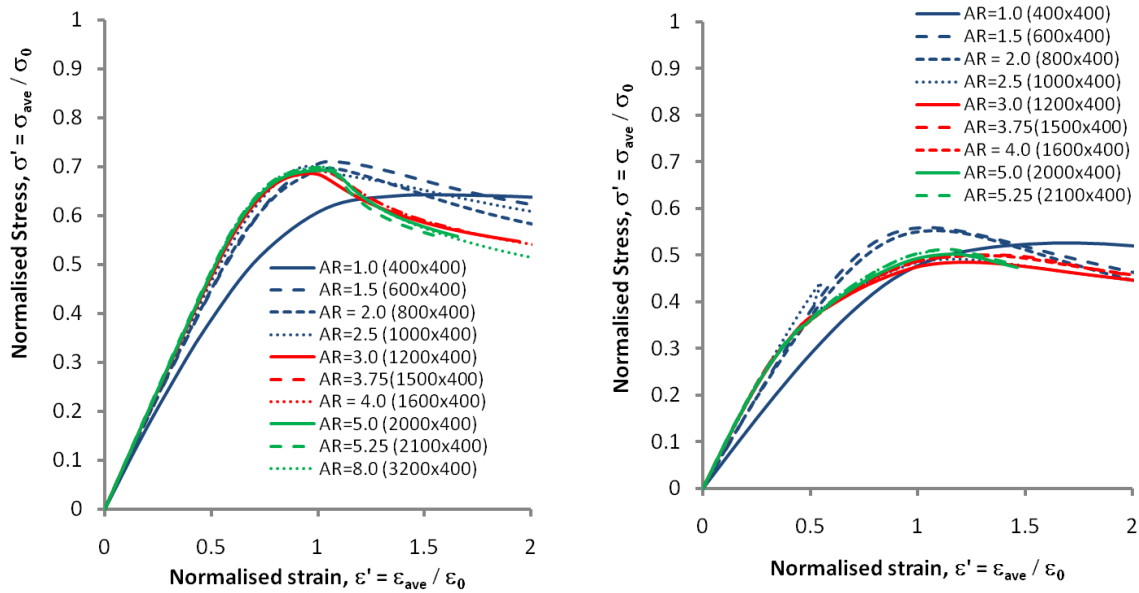


Figure 32 – Effect of plate aspect ratio – Plate 1 and derivatives (left), Plate 2 and derivatives (right)

The results show that a square or nearly square plate does not adequately represent the peak load or general shortening characteristics of a long plate. The short plates show significantly less stiffness in the pre-collapse region and significant variation in the prediction of the peak collapse load. This is probably due to the shape of the initial imperfection. As the aspect ratio increases (aspect ratio of 3.0 and above), the plate load shortening curves converge towards a representative shape, showing close agreement in the pre collapse region and at the peak load.

For the longer plate results, there is a small effect on the strain scale in the post collapse region. As the plate length is increased, the unloading part of the curve generally becomes steeper. The results for the more slender plate are less distinct, but still show the same general trend. These results confirm that nucleation of collapse has some effect on the strain scale in the post collapse region. However, for the range of aspect ratios considered typical of a ship structure, the effect is not considered significant.

#### 4.4. Geometric Imperfection

As already mentioned, the magnitude and pattern of geometric imperfections are a critical parameter affecting the buckling characteristics of structure under compressive load. This section discusses the causes of geometric imperfections in a welded plate structure and then summarises the equations which describe the geometric imperfections in the plate when treated as an isolated case.

The following description focuses on the cause of geometric imperfections in plating, but is equally valid for stiffened panel structures. The imperfection is implemented in the FEM using direct node translation methods, which are discussed in more detail as part of the stiffened panel analyses covered in Chapter 5.

#### 4.4.1. Causes of Geometric Imperfections

Geometric out of straightness in an aluminium plate is initially introduced during the rolling and extrusion process. Usually close tolerances are employed during milling to ensure geometric imperfection is minimised. Further geometric imperfections in a plate are normally introduced or amplified during the construction process with the most significant effects usually caused by welding. Misalignment and forcing together of panel elements will also result in initial out of straightness. Imperfections may then be exacerbated or introduced when a vessel is in service.

Welding induced distortion can include transverse and longitudinal shrinkage of the plate close to the weld, angular rotation of the plating around the weld bead axis, longitudinal bending of the plate-stiffener combination, rotational distortion and buckling distortion, as shown in Figure 33. In practice, angular change (wrap up) and longitudinal bending have been found to be the significant contributors to weld induced plate distortion [37].

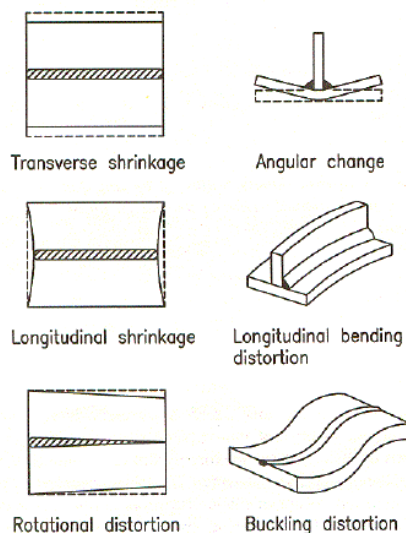


**Figure 33 – Welding induced distortions [102]**

Imperfection of a welded rectangular plate usually has the form of a single half sine wave shape along the plate length with localised distortions superimposed. A single half sine wave shape is also observed in the short direction. Observations of vessels with relatively slender plating, such as warships, clearly show a “hungry horse” or barrel shaped type of plate distortion with a single half

wave shape. The amplitude of the dished plating is often exacerbated by lateral pressure loads and slamming during service. Localised imperfections due to fabrication errors, dents and out of balance residual stress distribution are also superimposed onto this dished shape.

Localised deflections have been found to vary significantly for plates with different slenderness ratios, with slender plates exhibiting much larger local imperfections. Smith et al. [38] gives two reasons for this; the uneven residual stress distribution tends to amplify initial distortion to a greater extent for slender plate and slender plating is much more susceptible to dents caused by localised impacts during and after construction.

Some selected initial deflection patterns for steel plate caused by welding are shown in Figure 34. These example plots show how the imperfection shape can vary greatly between otherwise similarly fabricated plates.

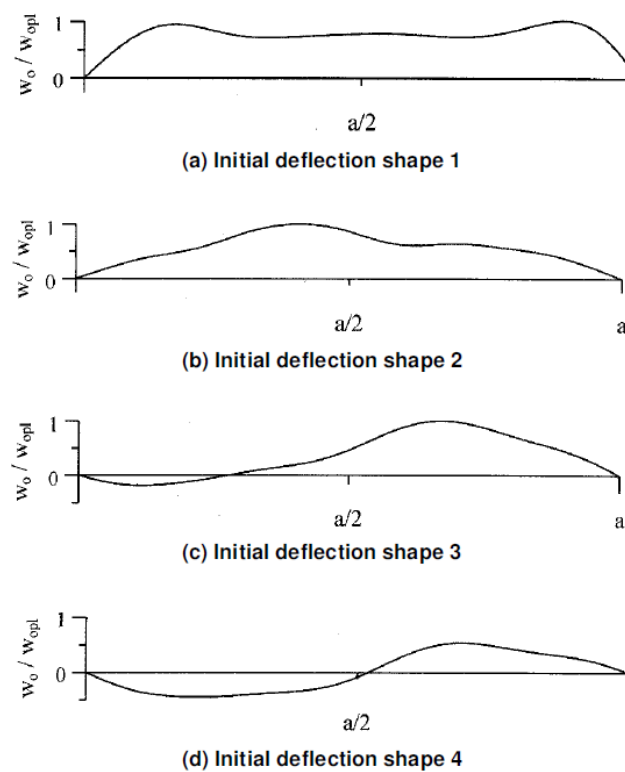


**Figure 34 – Selected initial deflection shapes [103]**

The elastic buckling mode of a simply supported plate under uniaxial compression normally forms an approximate pattern of square sinusoidal half waves [38]. However, inelastic buckling and collapse usually localises into a single half wave with a length less than or equal to the aspect ratio  $a/b$ . It is well recognised that the shape of the initial deflection can significantly affect the formation of these collapse mode shapes in a uniaxially loaded plate.

#### 4.4.2. Imperfection Patterns

Theoretical and experimental studies have shown that the shape and amplitude of the initial imperfection in a long plate will have a large effect on the response characteristics under a load which induces buckling [61, 103, 104]. The choice of imperfection shape therefore adds considerable complication in the analysis of a plate using FEM, compared to standard code formulations in which imperfection is accounted for implicitly.

Theoretically, if the exact imperfection shape of a plate is known, an equivalent FEM model can be constructed and analysed to predict that particular plate strength. However, in most instances, the actual imperfection shape of a plate is not known. Instead, the imperfection must be defined by other means, with the aim of giving a representative shape and amplitude.

Previous studies have often idealised the distortion typical of ship plating in a stiffened hull panel to a single half sine wave shape across the plate breadth and the sum of a number of half sine wave shapes superimposed along the plate length. The equation to define the idealised imperfection pattern is a Fourier series where the deflection amplitude,  $w$ , at any point on the plate surface is defined as:

$$\frac{w}{w_{0pl}} = \left( \sum_{i=1}^M B_i \sin \frac{i\pi x}{a} \right) \sin \frac{\pi y}{b} \quad 76$$

The maximum imperfection,  $w_{0pl}$ , can be defined either from actual plate measurements or using a statistical representative value. Smith [39] uses extensive measurement data to determine slight, average and severe characteristic levels of imperfection typical of steel plate, corresponding to 3 percentile, mean and 97 percentile values of  $w_{0pl}$ .

$$w_{0pl} = \begin{cases} 0.025\beta^2 t & (\text{slight}) \\ 0.1\beta^2 t & (\text{average}) \\ 0.3\beta^2 t & (\text{severe}) \end{cases} \quad 77$$

Smith's measurements are representative only. The actual magnitude of deflection in a plate depends on many factors that are difficult to quantify numerically, including the quality of the fabrication process and how the plate has been treated in service.

Alternatively, Paik and Duran [19] use a formula in a numerical analysis of aluminium panels based on limited data from numerous sources including [27] as follows:

$$w_{opl} = 0.009b$$

78

Figure 35 demonstrates that Smith’s average formula gives deflections of similar magnitude to Paik’s for the usual range of slenderness ratios and plate breadths, although as slenderness increases the values diverge. This would suggest that the use of either formula is valid when modelling average imperfection magnitudes.

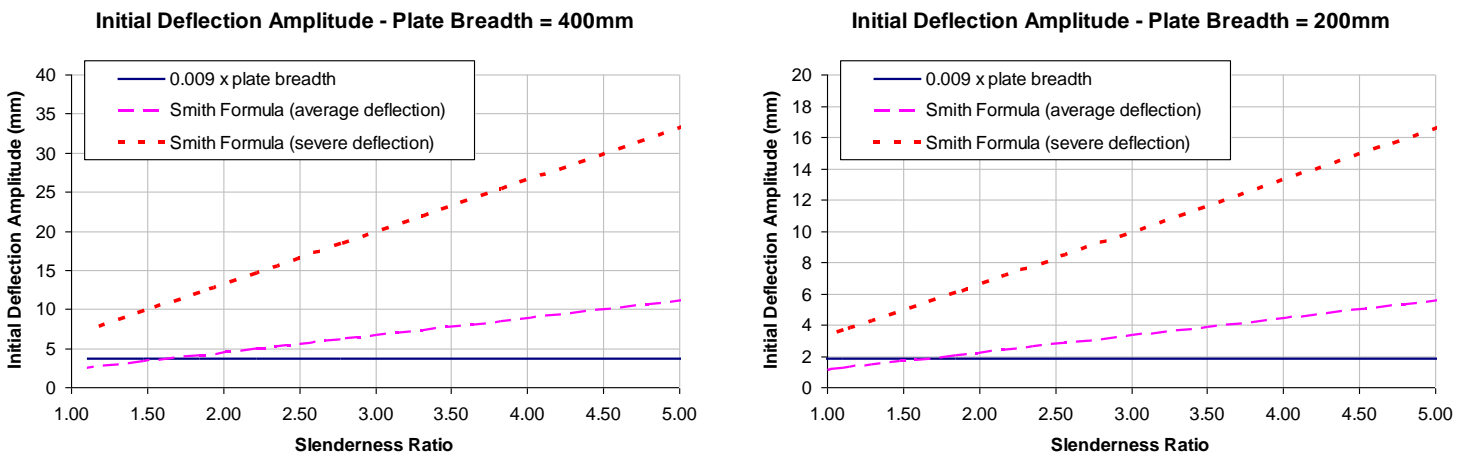


Figure 35 – Empirical methods to define initial deflection amplitude

Design formulas have been proposed in a very recent study sponsored by the Ship Structure Committee [22]. As part of the study the imperfections in 78 aluminium panels typical of a high speed vessel, constructed using normal practices at a Korean shipyard, were measured. All stiffeners were located at 300mm intervals and three plate thicknesses (5, 6 and 8mm) were used to construct the panels. Statistical analysis of the imperfection measurements were then used to produce similar design formulations. For the maximum imperfection, one half wave deflection, localised deflection and buckling mode deflection of the plating between stiffeners. The equation for the maximum initial deflection is:

$$\frac{w_{opl}}{t} = \begin{cases} 0.018\beta^2 & \text{for slight level} \\ 0.096\beta^2 & \text{for average level} \\ 0.252\beta^2 & \text{for severe level} \end{cases}$$

79

where the slight and severe levels consider the lowest 5% and highest 95% of the data respectively.

Figure 36 shows a plot of the relative frequency of occurrence of the maximum imperfection from the 252 data readings presented in the SSC report. The data is divided by  $\beta^2 t$  and a Weibull distribution is fitted to derive the coefficients in Eq. 79.

Referring to the plates in the SSC reports, this gives a maximum deflection amplitude,  $w_{opl} = 2.7$  mm, which sits approximately in the middle of the distribution of Figure 36. This is in contrast to the calculated deflection using Eq. 79 for the three plate thicknesses used in the SSC study. These give values of deflection well above the majority of the data, especially for the thinner 5mm plating (see Figure 36).

Apart from the results of the SSC study presented here there is relatively limited data in open literature pertaining to the deflection amplitude of aluminium plating. The formulas defined by the SSC report are very similar to those originally proposed in Eq. 77 and, coupled with the disparity of the data to the average imperfection equation, it is difficult to justify their use in the current study without further verification testing. The data presented here does suggest that deflection amplitude is independent of the slenderness ratio and the plate thickness.

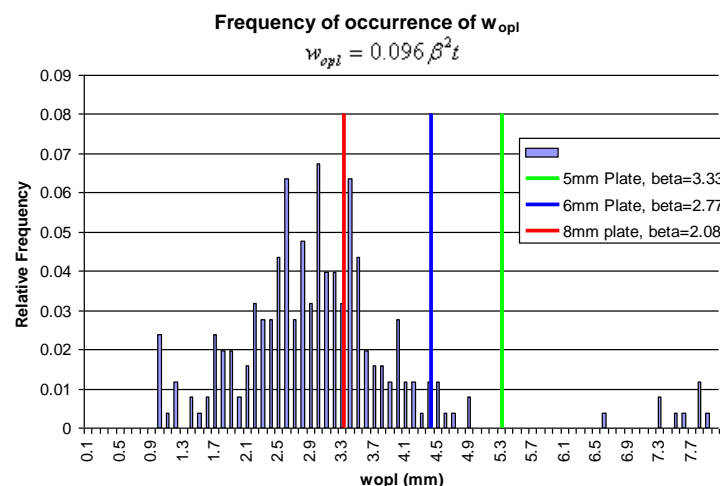


**Figure 36 – Relative frequency distribution of  $w_{opl}$  for 78 plates analysed in SSC451**

It is difficult to predict accurately, in advance, the likely imperfection shape of a plate. Initial deformation is typically barrel shaped, on which are superimposed local dents due to point loads and accidental impacts occurring during fabrication and service.

In some cases, for example when FEM is used to validate a physical test, the plate geometry is surveyed and thus the exact imperfection shape can be determined. A number of research studies have undertaken detailed measurement of the deflection in merchant ship plating. If analysing these particular plates, the actual imperfection shape can be idealised by an expanded Fourier series and

used to modify the FEM mesh. For example, Paik et al. [103] have calculated Fourier series coefficients for selected imperfection patterns as measured by Ueda and Yao [105]. The patterns are used to construct imperfect geometries for FEM analysis and the resulting load shortening curves in [103] demonstrate the significant effect the initial deflection shape has on the ultimate strength.

The deflection shapes, with Fourier coefficients as defined in Table 11, are applied to Plates 1 and 2 from Table 9. The resulting load shortening curves are plotted in Figure 37. The plates are modelled with an average residual stress field and HAZ at all four edges. Imperfection amplitude is average as given by Eq. 77.

Table 11 – Fourier Coefficients for Paik Imperfection Patterns, from [103]

	Mode Shape, $m$										
	1	2	3	4	5	6	7	8	9	10	11
11Mode-1	1	-0.02	0.38	-0.03	0.21	-0.04	0.05	-0.02	0.00	-0.01	0.00
11Mode-2	0.88	0.06	0.03	-0.11	0.02	0.05	0.02	-0.01	0.01	0.00	-0.01
11Mode-3	0.55	-0.50	0.00	0.02	-0.06	-0.04	0.02	-0.01	0.00	-0.01	0.00
11Mode-4	0.00	-0.50	0.00	0.02	-0.06	-0.04	0.02	-0.01	0.00	-0.01	0.00
3Mode	0.80	-	-	0.20	0.01	-	-	-	-	-	-

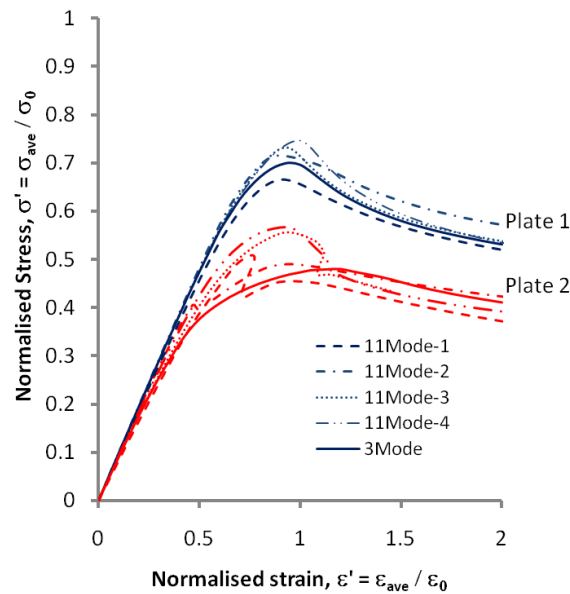


Figure 37 – Comparison of multi mode imperfection shapes – Plate 1 and Plate 2: average imperfection amplitude, HAZ at all four edges.

The load shortening curves show a similar pattern to the steel plate curves originally analysed by Paik. They show that imperfection shape is an important parameter and can affect the strength

characteristics of a plate considerably. The more slender Plate 2 shows a larger sensitivity to imperfection shape than Plate 1.

#### 4.4.3. Single Mode Imperfection Shape

It is well known that elastic buckling of a simply supported plate under uniaxial compression forms a pattern of approximately square sinusoidal half waves along the plate length [38]. Thus the first eigenmode of a long flat plate in uniaxial compression, analysed using linear FEM, will form a shape whereby the length of the longitudinal half waves is approximately equal to the width of the plate.

An example first eigenmode shape for Plate 1 is shown in Figure 38. The number of half waves equals the aspect ratio of the plate. If the aspect ratio of the plate is non integer then the half wave length is usually somewhat shorter than the plate width, resulting in an imperfection shape that is still approximately square. The eigenmode corresponds to classical theory, which shows that inelastic buckling tends to nucleate into a single half wave with a length equal to or less than the plate width.

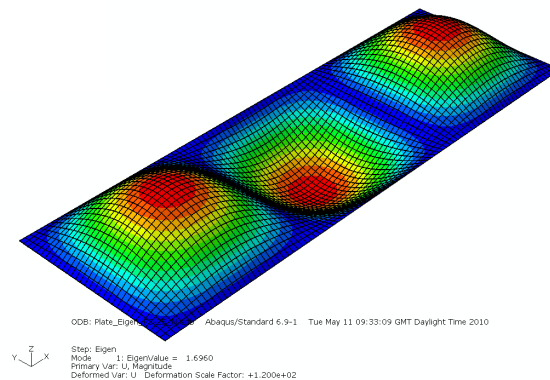


**Figure 38 – First linear eigenmode shape for Plate 1 in uniaxial compression**

However it has been shown that, for thin steel plates, the preferred mode can change as the plate begins to buckle and reach its ultimate strength, switching from a linear type shape before buckling to a shorter wave pattern in the post buckling range [106]. Thus the plate can snap into a different mode shape during an incremental analysis. Furthermore the influence of the softened HAZ in an aluminium plate may also shift the preferred mode shape as local yielding within the zone may change the effective length of the plate, also changing the preferred buckling mode shape.

To study the effect of increasing the number of half waves over the plate length, a series of analyses were undertaken on two simply supported long plates in uniaxial compression. Both plates have

aspect ratio of 3 and complete details are as given in Table 9. Each plate is analysed several times using a single mode imperfection shape with an increasing number of half sine waves in the longitudinal direction.

Table 12 compares the calculated ultimate strength of each plate with increasing half wave mode initial imperfection. The results show that the first eigenmode imperfection shape (3 half waves) does not give a lower bound solution. For plate 1 the conservative result is with 5 half waves. Plate 2 continues to reduce in strength as the number of half waves increase. For both plates, the ultimate strength converges towards a lower bound solution as the number of half waves increase.

The results suggest that a more conservative buckling mode shape is induced with an initial imperfection with shorter half wave length than the plate width. A “square” initial imperfection shape may give a non-conservative result. Therefore the choice of the initial shape cannot be based solely on a linear analysis.

**Table 12 – Ultimate strength of Plate 1 and Plate 2 analysed with different single mode imperfection shapes**

	Number of half waves along plate length						
	1	2	3	4	5	6	7
Plate 1 (1200x400, $\beta=2.0$ )	0.802	0.751	0.641	0.579	<b>0.563</b>	<b>0.563</b>	0.569
Plate 2 (1200x400, $\beta=3.0$ )	0.584	0.563	0.490	0.399	0.364	0.349	<b>0.343</b>

#### 4.4.4. Multiple Mode Longitudinal Imperfection Shape

The use of a single mode sinusoidal imperfection shape, approximating the linear buckling pattern, is an overly conservative representation of an actual, as built, ship type plate. It is very unlikely for a plate to be distorted in an exact sinusoidal pattern. However, it is also impossible to predict in advance the actual imperfection shape of an arbitrary dimensioned plate and approximate this using an expanded Fourier series with multiple mode shapes, such as has been done with the plate measurements in Table 11.

Instead a compromise must be made, using an appropriate imperfection to represent a “real” plate whilst ensuring that the plate buckling will nucleate into an appropriate pattern. Appropriate equations should thus be defined for use with plates of any dimension. These can then be used with confidence to model plate imperfection in any nonlinear FEM analyses of plated structure, such as an orthogonally stiffened panel. For this reason extensive analyses have been undertaken in this study to provide suitable guidelines in determining the proportion of each mode shape and an appropriate number of mode shapes to include.

A common approach is to superimpose two or more imperfection mode shapes along the plate length using a limited Fourier series equation. A single half wave is generally considered sufficient across the plate width. This approach has been taken by a number of studies of welded steel and aluminium plates [61, 67, 88]. However, there are, at present, no conclusive guidelines for defining an appropriate imperfection shape for a plate of arbitrary dimensions.

If two imperfection modes are combined, the general form of the Fourier series expansion simplifies to:

$$\frac{w}{w_{0pl}} = \left( B_1 \sin \frac{\pi x}{a} + B_m \sin \frac{m \cdot \pi \cdot x}{a} \right) \cdot \sin \frac{\pi y}{b} \quad 80$$

where m denotes the number of half waves for the higher mode imperfection shape

A suitable ratio of the coefficients, as used in British Naval design, is  $B_1/B_m = 4$  [66]. The values of the coefficients depend on the value of m. For this study they have been calculated to ensure that the maximum imperfection,  $w_{0pl}$ , in Eq. 80 is as given by Eq. 77, taking into account that the maximum is not necessarily in the middle of the plate. The calculated coefficients for different values of m are given in Table 13. Both coefficients are always positive in this paper; a negative value of  $B_m$  will introduce a different overall imperfection shape into the plate.

**Table 13 – Ultimate strength of test plates with two mode imperfection , lower bound solutions are underlined.**

Plate Dimensions	High mode imperfection shape					
	m=3	m=4	m=5	m=6	m=7	m=8
	$B_1=1.12$ $B_3=0.28$	$B_1=0.84$ $B_4=0.21$	$B_1 = 0.8$ $B_5 = 0.2$	$B_1=0.82$ $B_6=0.21$	$B_1=1.12$ $B_7=0.28$	$B_1=0.8$ $B_8=0.2$
Plate 1 (1200x400, $\beta=2.0$ )	0.713	<b>0.684</b>	0.704	0.711	-	-
Plate 2 (1200x400, $\beta=3.0$ )	0.582	0.485	0.480	<b>0.478</b>	-	-
Plate 3 (1000x400, $\beta=2.0$ )	0.700	<b>0.687</b>	0.715	0.726	-	-
Plate 4 (1000x400, $\beta=3.0$ )	0.570	<b>0.475</b>	0.494	0.500	-	-
Plate 5 (2100x400, $\beta=2.0$ )	-	-	0.735	0.699	0.691	<b>0.691</b>
Plate 6 (2100x400, $\beta=3.0$ )	-	-	0.538	0.513	0.493	<b>0.485</b>

The results from a series of analyses on six plates, in which the high mode imperfection shape is progressively increased, are presented above. The peak strength results in Table 13 and load shortening curves in Figure 39 and Figure 40 show that varying the high mode imperfection shape has a significant effect on the strength characteristics of the plate. In terms of ultimate strength, the

lower bound results, underlined in Table 13, occur for high mode patterns where the half wave length is less than the plate width. The results suggest that with  $m > a/b$  the resulting ultimate strength will be at or near to the lower bound.

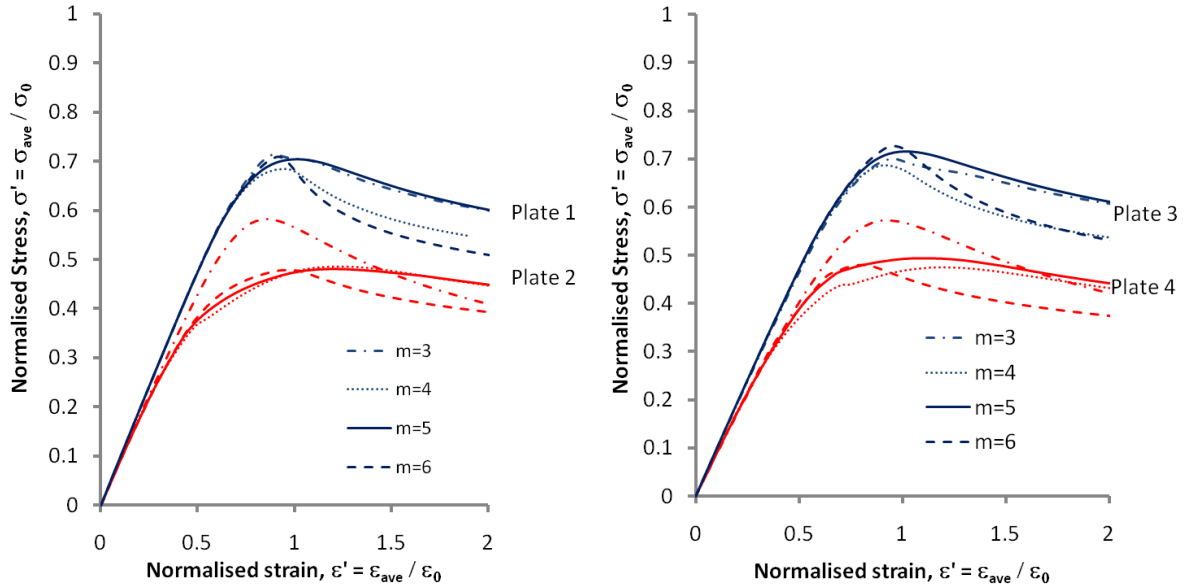


Figure 39 – Comparison of two mode imperfection shapes – Plates 1 and 2 (left), Plates 3 and 4 (right)

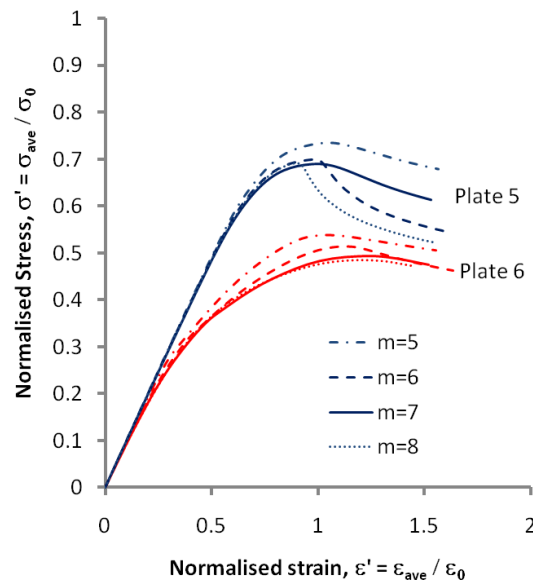


Figure 40 – Comparison of two mode imperfection shapes – Plates 5 and 6.

However, the load shortening curves show a more complex variation in the response of the plate as m is progressively increased. With different high mode imperfection shape, the post collapse response can be significantly affected. Whilst the ultimate strength may be similar, the curve peak

occurs at different positions on the normalised strain scale depending on the value of  $m$ . Also some curves demonstrate much steeper unloading than others.

The differences in the load shortening curves can be attributed to how the mode shape affects the post collapse strain. Figure 41 shows the development of the buckling and collapse shape at different stages of the FEM analysis for Plate 1. The plots demonstrate that the plate buckling and post buckling shape normally retains the number of half waves as initially set by the high mode imperfection coefficient. The buckling normally nucleates into a single lobe in the post collapse region with a half wave length less than the plate width.

However, where an odd number of half waves are used for the higher mode imperfection shape, the FEM model is asymmetrical along its length. Because initial imperfection lobes are identical in two or more spaces, buckling may also nucleate in two or more spaces at once to satisfy the equilibrium conditions in the FEM solver.

An example of this phenomenon occurs for Plate 1 when  $m=5$ , as shown in Figure 41. Nucleation occurs identically in both end lobes of the plate. This causes an increased strain rate in the post collapse region of the load shortening curve, meaning that the unloading gradient is shallower than for plates where collapse occurs in one area only. The effect is unrealistic, as a real plate would have a more random distribution of initial imperfection and it would be highly unlikely for two areas of the plate to collapse identically. The strain rate in the unloading region is affected significantly. This collapse scenario, due to the asymmetry of the plate, should be avoided in numerical analysis of plates.

Therefore, to prevent the possibility of nucleation in two or more regions, a three mode initial imperfection shape can be used. The first two modes are specified as before and contribute most of the initial imperfection. The third mode ensures the imperfection distribution is unsymmetrical by superimposing an additional high mode half wave shape. The coefficient for the third mode ( $B_{m+1}$ ) should have a low magnitude so that it does not affect the overall imperfection amplitude significantly, but provides enough additional imperfection to ensure nucleation of the collapse into one area of the plate only. For this study it was found that  $B_{m+1} = 0.01$  was sufficient.

The three mode Fourier series imperfection equation is written:

$$\frac{w}{w_{0pl}} = \left( B_1 \sin \frac{\pi x}{a} + B_m \sin \frac{m \cdot x \cdot \pi}{a} + B_{m+1} \sin \frac{(m+1) \pi \cdot x}{a} \right) \cdot \sin \frac{\pi y}{b} \quad 81$$

Where  $m$  is the lowest integer value such that:

$$m > \frac{a}{b}$$

82

Note that if  $a$  is a multiple of  $b$  (i.e. the aspect ratio is an integer) then  $m$  should be equal to the aspect ratio plus one. As an example, for a plate with aspect ratio 3,  $m=4$ .

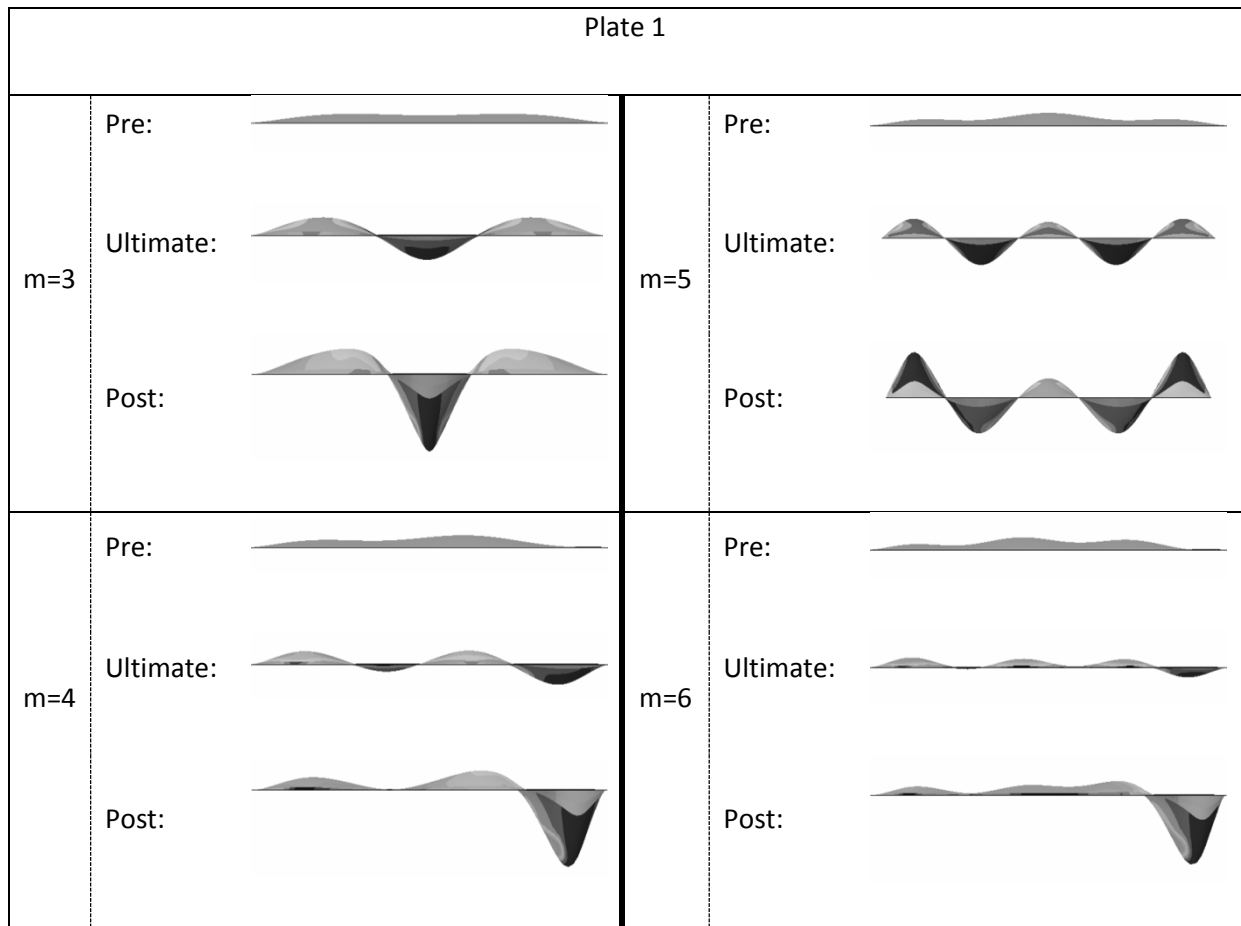
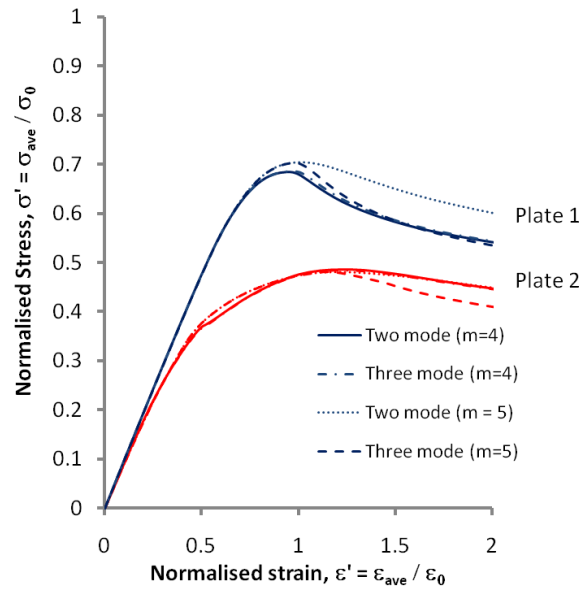


Figure 41 – Profile view of Plate 1 in uniaxial compression with mode imperfection parameter  $m$  progressively increased.

The differences in using Eq. 80 or Eq. 81 are compared in Figure 42. The two mode imperfection shape with  $m=5$  shows a shallower unloading due to nucleation at both ends of the plate. The addition of a third half wave pattern using Eq. 81 has minimal effect prior to collapse, but causes nucleation in only one area of the plate, producing a steeper unloading curve.

Therefore Eq. 81 gives a more conservative solution and is considered most suitable for representing plate imperfection for design purposes.



**Figure 42 – Comparison of three mode vs. two mode – Plate 1 and Plate 2, average imperfection amplitude, HAZ at all four edges.**

The imperfection amplitude has a significant effect on the overall plate strength and thus has a bearing on the entire load shortening curve shape [66]. Separate load shortening curve data sets are produced in section 4.7 to describe the response of a plate with each of the three levels of imperfection amplitude as defined in Eq. 77.

#### 4.4.5. Summary

The analyses presented here demonstrate clearly the significant influence of imperfection shape on the strength of a simply supported long plate. The continuing problem for the analyst is selecting an appropriate shape for adequately representing the plate imperfection without requiring multiple analyses each time to check the solution is adequately conservative.

This study suggests that a three mode Fourier series pattern (Eq. 81) is appropriate for representing the longitudinal imperfection. The first mode creates a barrel type shape whilst the high mode allows the plate buckling to nucleate into a short wave pattern. The introduction of a third imperfection mode with small amplitude ensures that collapse nucleates in one area of the plate only. The results have also shown that superimposing the first linear eigenmode for the higher mode shape will not necessarily give a lower bound solution. Instead, the results indicate that the higher imperfection mode,  $m$ , needs to be set to give a half wave length shorter than the plate breadth. Although this does not guarantee the most conservative solution it has been shown here to consistently predict an ultimate strength near to the lower bound.

#### 4.5. Heat Affected Zone

The causes of a heat affected zone in aluminium plates are discussed in section 2.4.2. The effects of the HAZ on the strength of a flat plate are now investigated. The location of the HAZ depends on the build method for the panel. A standard approach in construction of orthogonally stiffened panels is to use large sheets of rolled plate, with stiffeners fillet welded at appropriate intervals. This is common when using 5000 series plate, which is normally supplied as flat plate, with either 5000 or 6000 series stiffeners. Welding such a panel usually produces a HAZ pattern as shown in Figure 43a.

Alternatively a panel extrusion method is used, where the plate-stiffener section over one or more stiffener spaces is extruded in its entirety. Panels are then butt welded together, usually but not always at mid plate width. The extrusion is usually only one frame spacing in length, and transverse frames are therefore welded to the plate edges. The resulting HAZ pattern is sketched in Figure 43b. Equivalent HAZ distributions on the longitudinal edges only are shown in Figure 43c and Figure 43d.

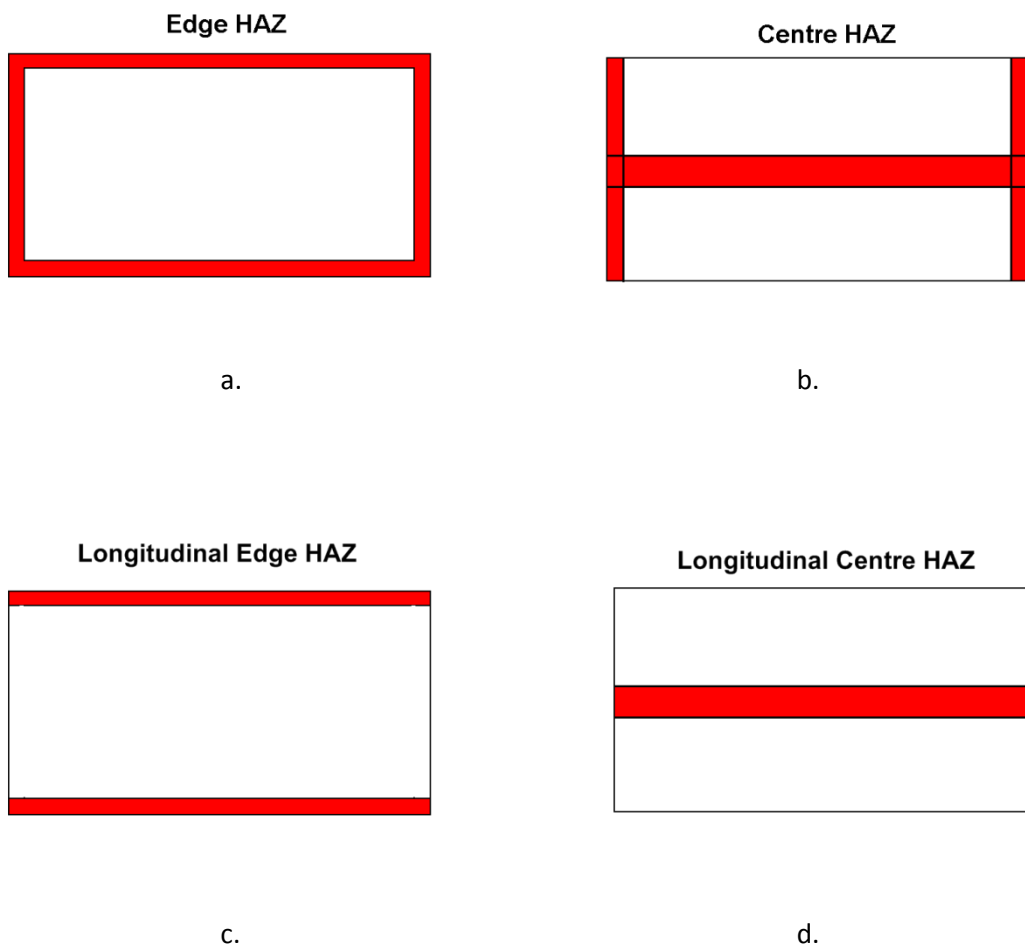


Figure 43 – Edge HAZ and Centre HAZ distributions

#### 4.5.1. Longitudinal HAZ Location

A comparison of the effects of edge or centre HAZ location (a and b in Figure 43) is shown in Figure 44 for Plates 1, 2, 5 and 6. All the plates are 5083-H116 with varying aspect ratio. Note that the models also include tensile residual stress zones in the HAZ and equilibrating compressive residual stress elsewhere. Analyses of an un-welded plate with no HAZ or residual stress are also shown.

The load shortening curves show that for these cases welded aluminium plates are weaker than equivalent un-welded plates but that the location of the longitudinal HAZ has a significant effect. The centre HAZ plates show increased stiffness compared to the edge HAZ plates prior to reaching the peak load. The peak strength is therefore higher. This phenomenon corresponds to the effective width concept whereby, as compressive load increases, the centre of the plate buckles and shirks loading, causing an increasing proportion of the load to be supported by the edge regions of the plate. Thus the strength of the longitudinal edges has a greater influence on the overall strength of the plate.

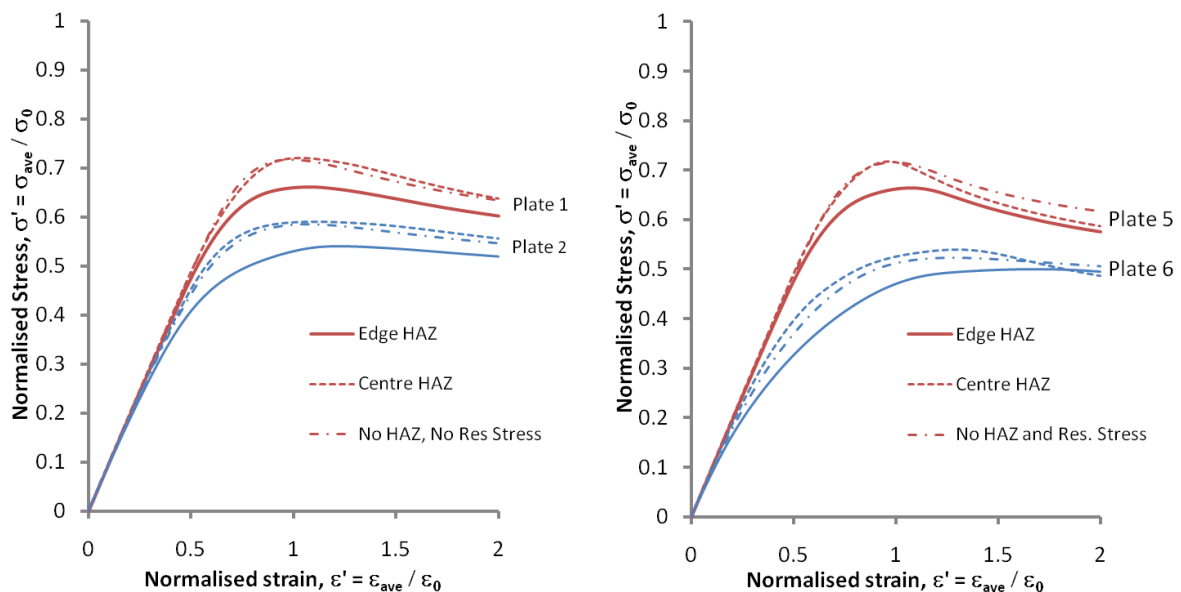


Figure 44 - Comparison of HAZ location. Plates 1 and 2 (left), Plates 5 and 6 (right)

The ultimate strength curves for the 5083-H116 plates in Figure 45 shows that the location of the HAZ at the plate centre results in a higher overall strength over the complete range of plate slenderness ratios tested. The zero HAZ/residual stress curve is also plotted, and shows an interesting comparison with the centre HAZ results. At low to medium slenderness the zero HAZ plates are stronger, but the curves intersect at about  $\beta=3$ , and above this the welded zone actually increases the plate strength. However, this is probably more due to the effect of residual stress.

The 6082-T6 results in Figure 45 show a similar pattern to 5083-H116. A substantial difference between the zero HAZ results occurs at lower slenderness. However, this is due to the HAZ on the loaded edges of the plate rather than the location of the longitudinal HAZ, as is shown in the next section.

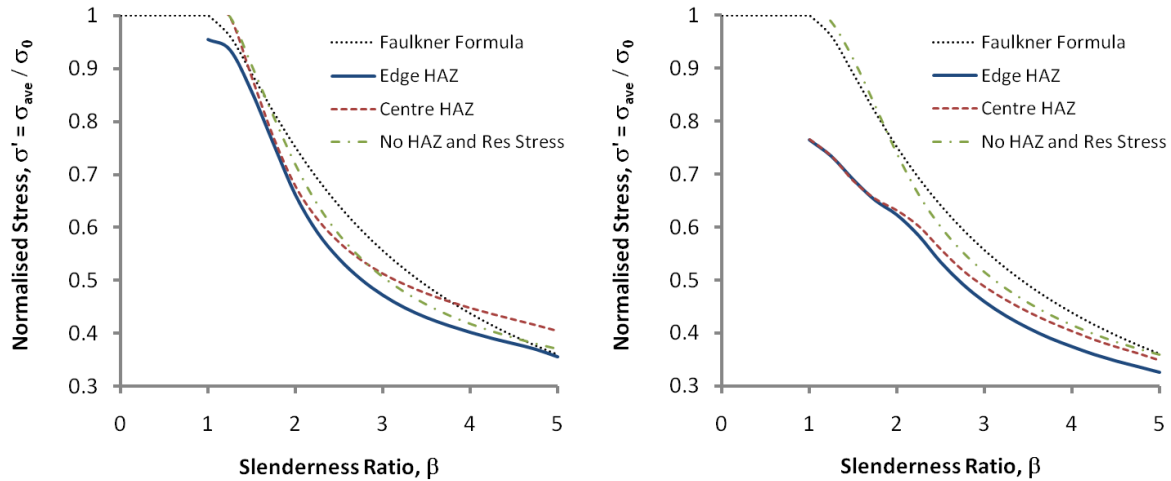


Figure 45 – Ultimate strength curves, comparison of longitudinal HAZ location, 5083 (left) and 6082 (right), average imperfections

#### 4.5.2. Effect of Transverse Edge HAZ

The transverse HAZ, located on the short edges of the plate is caused by the weld joint connecting the plate to the transverse frames. As has already been shown in Figure 45, this can have a significant effect on the uniaxial strength and the collapse mode of the plate [19, 67]. If the average compressive stress on the plate edge surpasses the reduced proof stress of the HAZ material, the end region can deform plastically and cause premature localised plate buckling.

The effect of transverse edge HAZ is clearly shown by comparative load shortening curves of plates modelled with and without HAZ at the short edges. Comparative tests on long 6082-T6 plates with varying slenderness show significant loss of both compressive and tensile strength due to the presence of the transverse HAZ region (Figure 47). The compressive test results show the most pronounced differences for low slenderness plates. For these cases the average compressive stress surpasses the proof stress of the HAZ material, causing localised plasticity to develop in the ends of the plate. An example plot of the post collapse deformation shape for a plate with slenderness of 2.0 clearly shows localised failure in the end HAZ region (Figure 46).

A significant strength reduction is also observed with the 6082-T6 plates under tensile in plane load. This again demonstrates that as the applied average stress exceeds the proof stress of the HAZ the

end region fails plastically, resulting in an overall loss of capacity for the entire plate. However, the tensile load shortening curve for the plate with edge HAZ included does not track the material stress-strain relationship of the HAZ material (see Figure 11). The curve diverges from the elastic linear relationship at about  $0.7\sigma_0$ , which is somewhat higher than the HAZ proof stress ( $0.53\sigma_0$ ). This means the plate does not behave as it would if the entire plate material was softened to HAZ stress-strain properties. This suggests that the influence of the boundary, which is immediately adjacent to the softened zone, and the parent material in the central part of the plate, have some beneficial effect in maintaining strength.

The effect seen in the 6082-T6 plates is not observed in equivalent 5083-H116 comparative results (Figure 48). This is because the softened proof stress for 5083-H116 is a higher proportion of the parent metal strength. Therefore, the comparative results only show a slight negative strength effect at very low plate slenderness.

The effect of the transverse HAZ on the compressive ultimate strength is also observable in strength curves, which are presented in Figure 49. For slender plates the strength curve follows the same pattern as given by Faulkner's classic two term formula developed for steel plate [65]. With only longitudinal HAZ, both aluminium strength curves remain close to the Faulkner curve. However if the ultimate strength, given as a normalised stress ratio, is greater than the proof stress of the HAZ, the plate strength for cases with HAZ on all four edges is significantly affected, and the strength curve deviates away from Faulkner's line. The effect on 6082-T6 plate is much greater than for 5083-H116.

The findings of this study have important implications when assessing the strength of welded aluminium structure, particularly if using 6000 series alloy. If a weld line on a stocky plate is parallel to the loaded edge then that region may yield prior to buckling and result in a lower ultimate strength prediction for the plate.

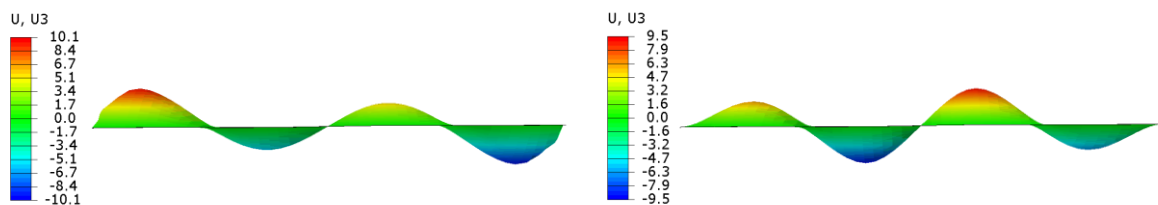


Figure 46 – Plots of the post collapse deformed shape(magnification x20) for Plate 7 with transverse HAZ (left), without transverse HAZ (right). Position on load shortening curve marked in Figure 47.

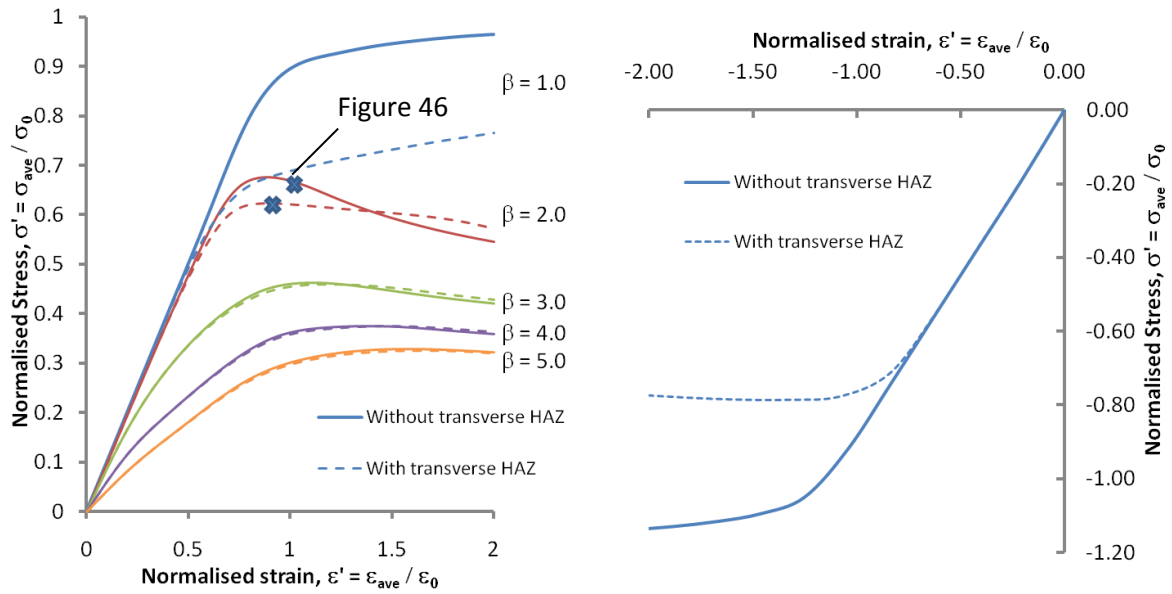


Figure 47 - Comparison of transverse HAZ – 6082-T6 plates (1200x400). Edge HAZ pattern (Figure 43a and Figure 43c).

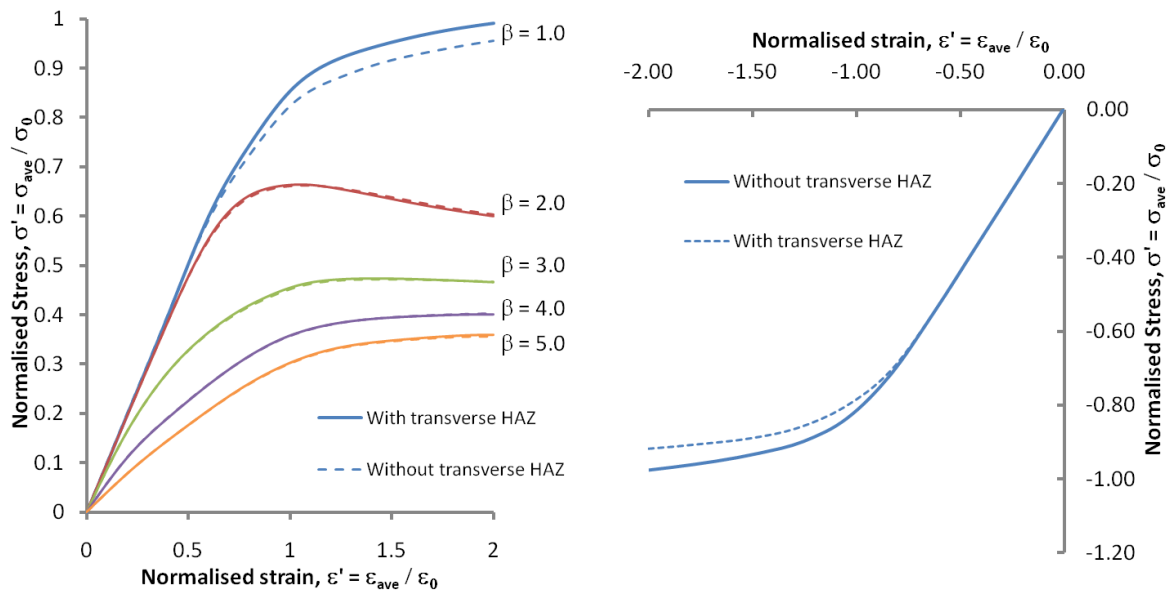


Figure 48 - Comparison of Transverse HAZ – 5083-H116 plates (1200x400). Edge HAZ pattern (Figure 43a and Figure 43c).

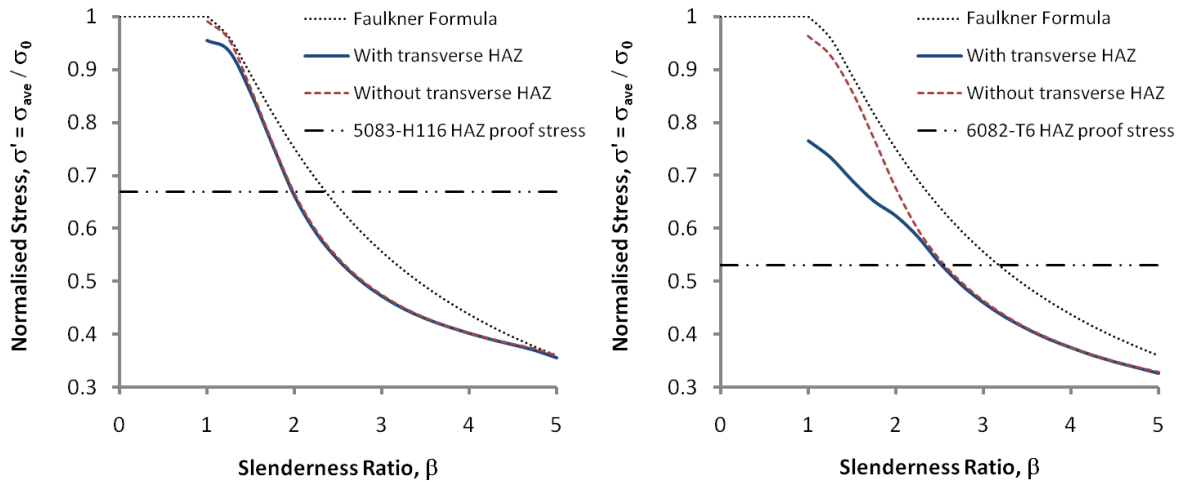


Figure 49 – Ultimate strength comparison of HAZ location. 5083 (left) and 6082 (right). Average imperfection amplitude.

### 4.5.3. Relative HAZ Width

The magnitude of the HAZ width is independent of the total dimensions of the plate. Therefore, the relative width of the HAZ compared to the relevant plate dimension also plays an important role influencing the ultimate strength and load shortening relationship of an aluminium plate. Assuming that the HAZ width is equal on all plate edges, a longitudinal HAZ ratio is defined as:

$$HR_L = \frac{2 \cdot b_{HAZ} \cdot L}{b}$$

83

A load shortening curve plot comparing plates all of width 400mm but with varying length (Figure 32) and with a 25mm width HAZ demonstrates that the aspect ratio for plates with equal width, and hence also equal transverse HAZ ratio, is not a significant factor of influence for long plates.

However, the longitudinal HAZ ratio does have an influence on the non dimensional strength characteristics, which is shown by comparing plates of differing width but with the same length and plate slenderness ratio (Figure 50). This shows that an increased HAZ ratio, usually due to increased plate width, has a beneficial effect on the normalised plate strength. This requires explicit definition in the design database. Note that for all analyses a residual stress pattern as shown in Figure 12 and with  $b_t = b_{HAZ}$  is included. Therefore the plot in Figure 50 accounts for the influence of HAZ and residual stress combined.

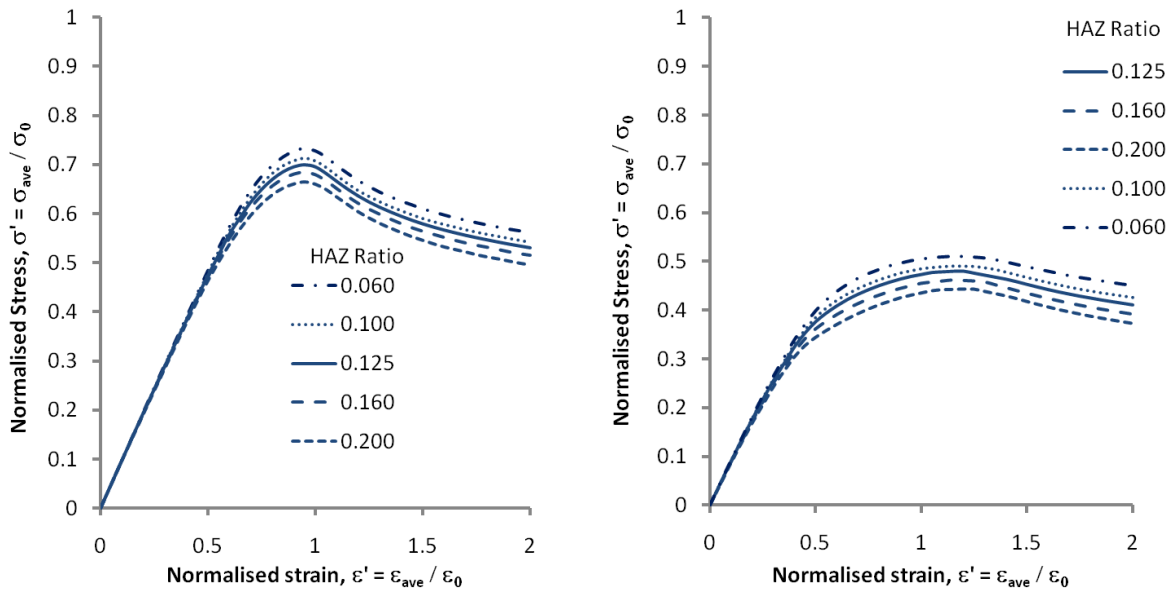


Figure 50 - Comparison of HAZ ratio. 5083-H116 plates (1200x400),  $\beta = 3.0$ . HAZ at all four edges.

#### 4.6. Residual Stress

The causes of residual stress in welded metal structures are summarised in section 2.4.3. The effects of the residual stress on the strength of a flat plate are now investigated. There are a number of ways to model residual stress in a plate, ranging in complexity and including:

- Specifying initial stress vectors at integration points;
- Applying line loads;
- Modelling the thermal stress distribution from a simulated weld pass.

The latter method has been successfully applied in a number of studies [107], but the numerical requirements are far too intensive for consideration in this study. Therefore, the current study employs a simple approach utilising the \*INITIAL CONDITIONS feature of ABAQUS to apply uniform stress components equally over all integration points in an element. The elements within residual stress zones are grouped into assembly sets and the initial conditions are specified for all elements within a particular set.

Residual stress is an internal material property, and should not exert any external displacement or resultant force on the boundaries. If the geometric imperfection is zero, the initial conditions will equilibrate exactly and this condition is satisfied. Unfortunately, the introduction of geometric imperfection complicates the force system and will usually cause an imbalance because elements no longer act in the same plane.

The force imbalance can affect the resulting load shortening relationship as predicted by nonlinear FEM. To demonstrate this, two alternative modelling techniques are compared in Figure 51. The first modelling approach consists of a single step analysis, where the boundary conditions are set as detailed previously and a Riks load step is carried out with displacement control at one end of the plate. Hence, the attainment of load equilibrium is solved through the first increment of the Riks load step. The second model includes a two step approach. The first step uses a standard Newton Raphson solver. No end displacement is specified, and one end of the plate is left free to move bodily in-plane, but remain straight. The opposite end is constrained to prevent rigid body movement. A load imbalance will cause a displacement of the free end to achieve equilibrium. A second load step, using the Riks method, is then initiated using displacement control.

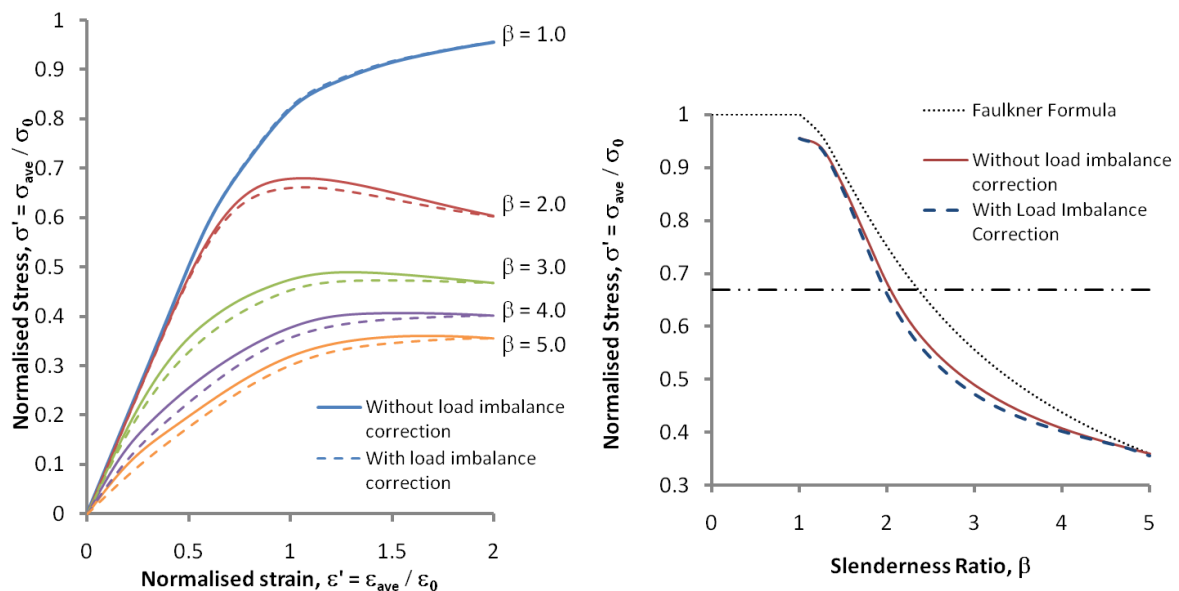


Figure 51 – Residual stress modelling techniques

The second modelling method allows the plate forces to balance through displacement of nodes both in and out of plane. The intermediate load step allows changes in imperfection shape, the distance between the two plate ends and the residual stress distribution. Because the initial geometric imperfection is usually small in relation to the plate dimensions, the load imbalance is usually also small. Thus the effects on the plate imperfections are relatively minor. The first modelling approach means that the plate begins with the imperfection and residual stress as initially specified. However, the load imbalance can have a significant effect on the ultimate strength and plate collapse behaviour, as is shown in Figure 51. The imbalance correction results in a more conservative solution and is considered a more rigorous approach to modelling the residual stress distribution.

#### 4.7. Parametric Plate Load Shortening Curve Database

A set of parametric design curves for aluminium plates are presented, together with coordinate data to enable reproduction of the curves. The curves can be closely reproduced by fitting a cubic spline to the data points (cubic spline functions are typically used to generate smooth curves in commercial graph packages).

The geometric and material properties of the plates have been chosen to give a representative description of an actual as built plate as defined in the previous part of this paper, consisting of:

- Separate curves for 6082-T6 and 5083-H116 plates;
- Plate dimensions 1200x400 (Aspect Ratio = 3);
- Slenderness ratio between 1.0 (very stocky) and 5.0 (very slender);
- Three mode imperfection shape as given in section 4.4.4;
- HAZ at all four plate edges - assuming a conservative position for the longitudinal HAZ;
- HAZ width of 25mm - correction factors derived for different HAZ ratios;
- Biaxial residual stress pattern;
- Three levels of imperfection as defined by Eq. 7.

The models have been developed to provide a conservative representation of an as built plate; they are thus suitable for use in reliability and ultimate limit state design calculations. The curves are not lower bound solutions; if the plate characteristics are changed the ultimate strength and response characteristics are subject to a degree of variability.

Uniaxial compression curves are presented in Figure 52 - Figure 57. Curves for slight, average and severe levels of imperfection amplitude and for 5083-H116 and 6082-T6 alloy plates are presented. Equivalent datasets are also given in Table 14 - Table 20. The data sets are not given for a complete range of curves but sufficient data is presented so that a load shortening curve for a plate of any slenderness ratio within the range 1.0 to 5.0 can be estimated using appropriate interpolation and curve fitting techniques.

Multiplication factors for different HAZ ratios are given for the average imperfection case only. Equivalent factors for the severe and slight imperfection curves have not been derived because the curves relate to “extreme” levels of imperfection, and thus the uncertainty inherent in the imperfection is deemed to significantly outweigh the influence of HAZ ratio.

The response of the plates in tension was found to be independent of plate slenderness and imperfection amplitude. The HAZ ratio only has a minimal effect on the strength and is also discounted. However, the difference between the two alloys is significant with the 6082-T6 plate exhibiting much lower normalised stress than the 5083-H116 plates. Tensile load curves are presented in Figure 58. The tensile load is given as positive here, if the curves were combined with the equivalent compressive load shortening curves, then one data set would need to be converted to read negative, depending on the coordinate system being used.

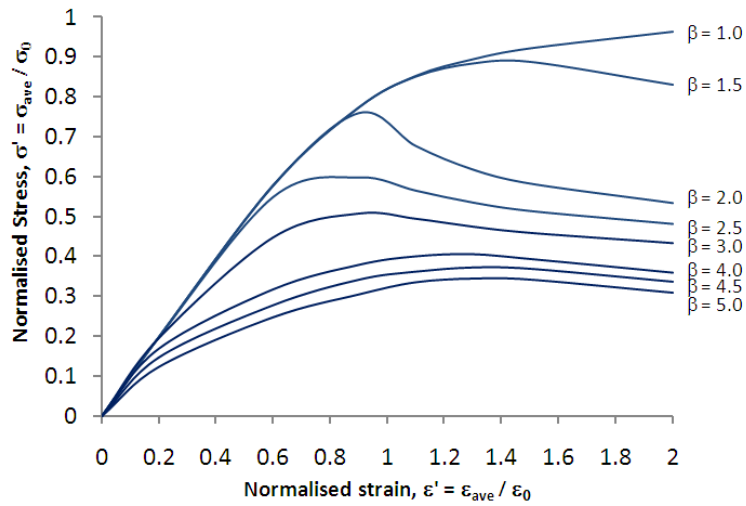


Figure 52 - Normalised stress-strain plates in uniaxial compression - 5083-H116. Slight Imperfection Amplitude

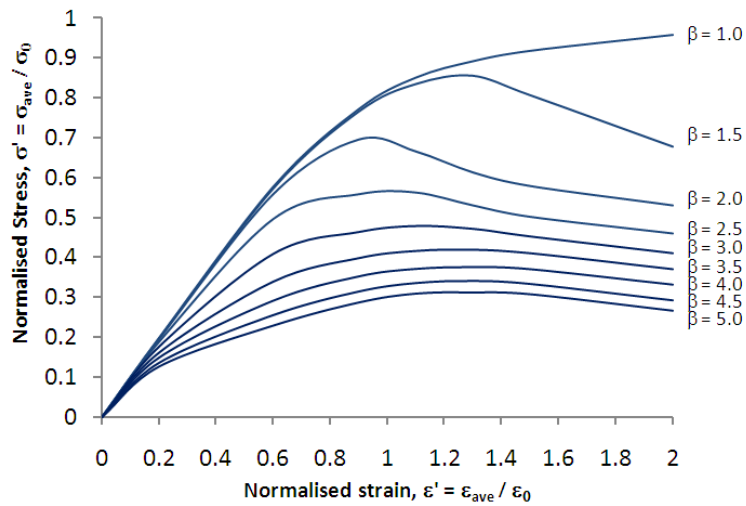


Figure 53 - Normalised stress-strain plates in uniaxial compression - 5083-H116. Average Imperfection Amplitude

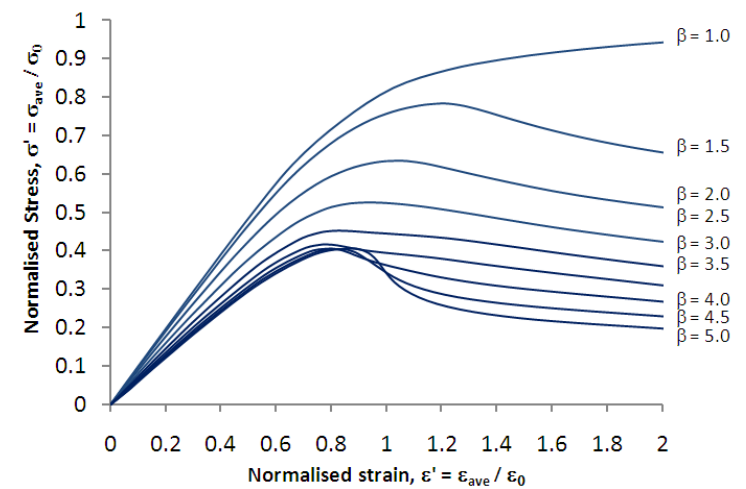


Figure 54 - Normalised stress-strain plates in uniaxial compression - 5083-H116. Severe Imperfection Amplitude

Table 14 – Curve Dataset – 5083-H116, Slight Imperfection Amplitude

Normalised Strain	Normalised Stress, HAZ Ratio = 0.125				
	$\beta=1.5$	$\beta=2$	$\beta=3$	$\beta=4$	$\beta=5$
0.0	0.0	0.0	0.0	0.0	0.0
0.2	0.199	0.199	0.196	0.169	0.124
0.6	0.578	0.578	0.448	0.318	0.248
0.9	0.773	0.760	0.508	0.379	0.306
1.1	0.850	0.677	0.495	0.400	0.336
1.3	0.883	0.618	0.475	0.405	0.345
1.5	0.887	0.583	0.460	0.394	0.343
2.0	0.830	0.534	0.434	0.359	0.310

Table 15 – Curve Dataset – 5083-H116, Average Imperfection Amplitude

Normalised Strain	Normalised Stress, HAZ Ratio, $H_R = 0.125$					HAZ Ratio Multiplication Factor $H_R = b_{HAZ} / b$			
	$\beta=1.5$	$\beta=2$	$\beta=3$	$\beta=4$	$\beta=5$	0.06	0.1	0.16	0.2
0.0	0.0	0.0	0.0	0.0	0.0	1	1	1	1
0.2	0.198	0.195	0.176	0.148	0.127	1.02	1.01	0.99	0.98
0.6	0.574	0.559	0.408	0.291	0.229	1.04	1.02	0.98	0.94
0.9	0.767	0.696	0.463	0.351	0.287	1.05	1.02	0.97	0.94
1.1	0.836	0.666	0.478	0.370	0.310	1.05	1.02	0.97	0.94
1.3	0.857	0.613	0.471	0.375	0.313	1.06	1.02	0.96	0.92
1.5	0.808	0.579	0.452	0.369	0.308	1.06	1.03	0.96	0.91
2.0	0.679	0.531	0.410	0.331	0.267	1.07	1.03	0.96	0.91

Table 16 – Curve Dataset – 5083-H116, Severe Imperfection Amplitude

Normalised Strain	Normalised Stress, HAZ Ratio = 0.125				
	$\beta=1.5$	$\beta=2$	$\beta=3$	$\beta=4$	$\beta=5$
0.0	0.0	0.0	0.0	0.0	0.0
0.2	0.199	0.199	0.196	0.169	0.124
0.6	0.578	0.578	0.448	0.318	0.248
0.9	0.773	0.760	0.508	0.379	0.306
1.1	0.850	0.677	0.495	0.400	0.336
1.3	0.883	0.618	0.475	0.405	0.345
1.5	0.887	0.583	0.460	0.394	0.343
2.0	0.830	0.534	0.434	0.359	0.310

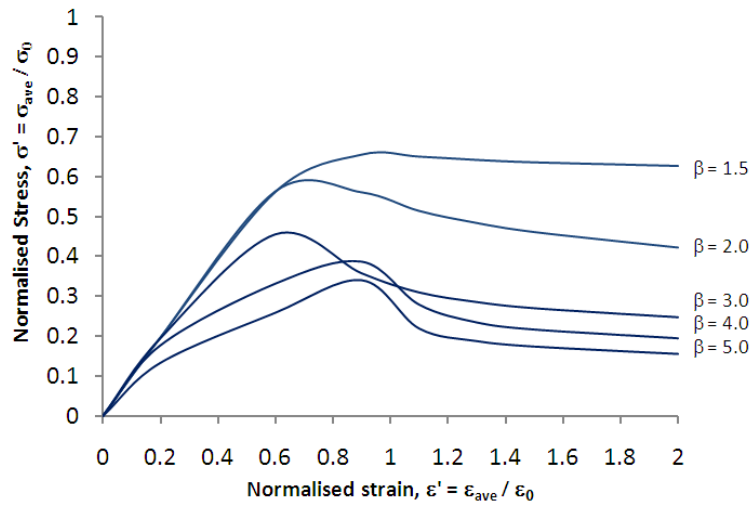


Figure 55 - Normalised stress-strain plates in uniaxial compression – 6082-T6. Slight Imperfection Amplitude

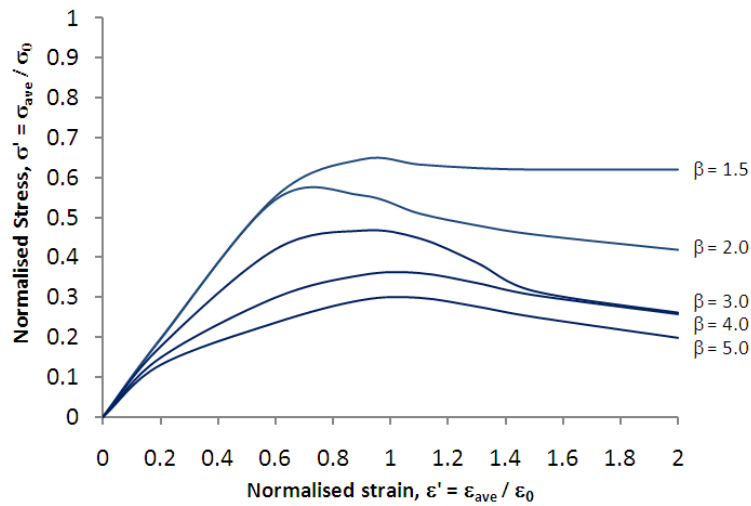


Figure 56 - Normalised stress-strain plates in uniaxial compression – 6082-T6. Average Imperfection Amplitude

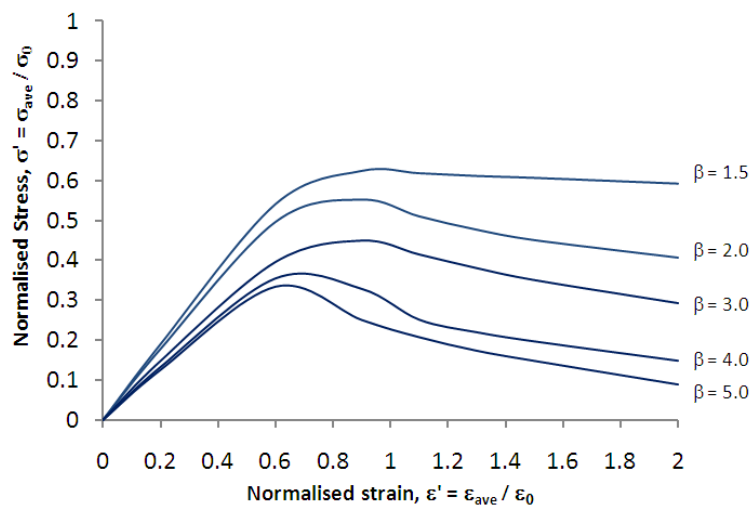


Figure 57 - Normalised stress-strain plates in uniaxial compression – 6082-T6. Severe Imperfection Amplitude

Table 17 – Curve Dataset – 6082-T6, Slight Imperfection Amplitude

<i>Normalised Strain</i>	<i>Normalised Stress, HAZ Ratio = 0.125</i>				
	$\beta=1.5$	$\beta=2$	$\beta=3$	$\beta=4$	$\beta=5$
0.0	0.0	0.0	0.0	0.0	0.0
0.2	0.197	0.197	0.195	0.177	0.133
0.6	0.563	0.563	0.455	0.331	0.259
0.9	0.656	0.561	0.358	0.386	0.341
1.1	0.651	0.514	0.310	0.279	0.220
1.3	0.643	0.484	0.286	0.234	0.188
1.5	0.637	0.461	0.270	0.217	0.175
2.0	0.628	0.422	0.248	0.195	0.156

Table 18 – Curve Dataset – 6082-T6, Average Imperfection Amplitude

<i>Normalised Strain</i>	<i>Normalised Stress, HAZ Ratio, <math>H_R = 0.125</math></i>				
	$\beta=1.5$	$\beta=2$	$\beta=3$	$\beta=4$	$\beta=5$
0.0	0.0	0.0	0.0	0.0	0.0
0.2	0.196	0.194	0.176	0.148	0.130
0.6	0.552	0.544	0.421	0.299	0.235
0.9	0.646	0.555	0.468	0.355	0.291
1.1	0.633	0.509	0.448	0.360	0.297
1.3	0.624	0.480	0.388	0.336	0.275
1.5	0.621	0.457	0.316	0.305	0.249
2.0	0.621	0.418	0.262	0.258	0.198

Table 19 – Curve Dataset – 6082-T6, Severe Imperfection Amplitude

<i>Normalised Strain</i>	<i>Normalised Stress, HAZ Ratio = 0.125</i>				
	$\beta=1.5$	$\beta=2$	$\beta=3$	$\beta=4$	$\beta=5$
0.0	0.0	0.0	0.0	0.0	0.0
0.2	0.189	0.177	0.148	0.133	0.125
0.6	0.540	0.495	0.397	0.355	0.334
0.9	0.624	0.552	0.450	0.329	0.251
1.1	0.618	0.510	0.416	0.252	0.208
1.3	0.611	0.476	0.382	0.220	0.174
1.5	0.606	0.451	0.352	0.197	0.149
2.0	0.592	0.407	0.294	0.149	0.089

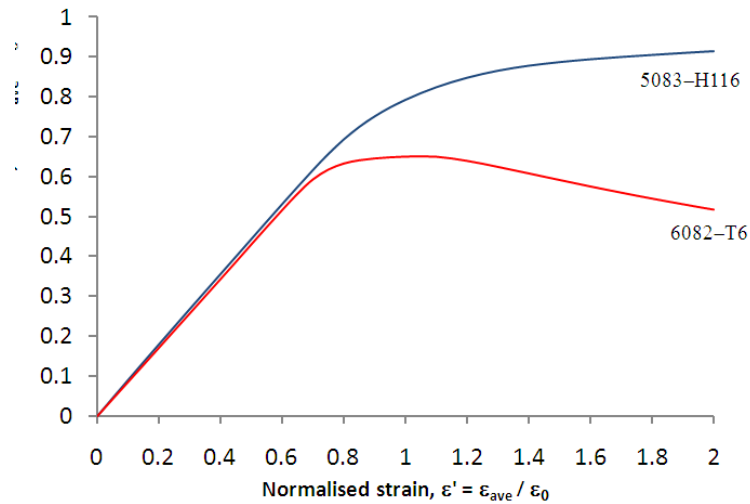


Figure 58 - Normalised stress-strain plates in uniaxial tension – 5083-H116 and 6082-T6.

Table 20 – Curve Dataset – Uniaxial Tension - 5083-H116 and 6082-T6.

<i>Normalised Strain</i>	<i>Normalised Stress</i>	
	5083-H116	6082-T6
0.0	0.0	0.0
0.2	0.180	0.171
0.6	0.531	0.516
0.9	0.751	0.646
1.1	0.823	0.650
1.3	0.865	0.625
1.5	0.886	0.592
2.0	0.914	0.518

#### 4.8. Summary

The detailed analyses presented in this Chapter have shown that the strength behaviour of aluminium plates under a progressively increasing longitudinal load is affected by a number of parameters, including the aluminium alloy, geometric imperfection, HAZ distribution, level of softening, residual stress distribution and secondary load effects. Some of these parameters have been shown to have significant influence on the ultimate strength and load shortening behaviour of a plate. A particularly important finding from the analyses concerns the influence of the HAZ in stocky 6082-T6 plates. If these plates are welded along their short edges, the longitudinal strength is detrimentally affected by a considerable margin because the HAZ formed on the loaded edge fails

plastically. Current design formulae do not account for this localised failure and thus can significantly over predict the plate strength.

The analysis procedure followed in this Chapter has also yielded some important insights with relevance to the analysis of more complex structure using FEM. There is much uncertainty in how to define a representative plate for numerical modelling. However, a representative definition of material and geometric imperfections are an essential part of any FEM analysis. Therefore, the detailed studies of imperfection characteristics and the influence of HAZ have been used to define representative plate properties, which can be used to model a plate with arbitrary dimensions in FEM. This has led to the development of a robust plate modelling procedure within the FEM software, which has important relevance not only when analysing plates in isolation, but also in how they are represented as part of a more complex stiffened panel model.

Using the representative plate modelling approach a parametric dataset of load shortening curves for aluminium plates under uniaxial longitudinal load have been derived. These can be adapted for use in a global assessment of the ultimate strength of an aluminium hull girder in a progressive collapse type analysis. This curve database has an important role in the development of the semi analytical methodology in Chapter 6.

*“Engineering is the art of modelling materials we do not wholly understand, into shapes we cannot precisely analyse so as to withstand forces we cannot properly assess, in such a way that the public has no reason to suspect the extent of our ignorance.”*, A.R. Dykes, British Institution of Structural Engineers [108]

# Chapter 5

## Finite Element Analysis of Orthogonally Stiffened Aluminium Panels

### 5.1. Introduction

This Chapter presents the results of systematic FEM studies of interframe and orthogonally stiffened panels. Special attention is paid to lightly stiffened panels typical of aluminium vessels. These analyses provide a numerical assessment of the influence of the different patterns of collapse in a lightly stiffened panel. The results provide a benchmark to assess the validity of existing analytical panel strength methods and justify the development of a new analytical method to account for both overall and interframe failure modes in a lightly stiffened panel.

The Chapter first describes a rigorous methodology to model panels and hull girder cross sections using ABAQUS. The methodology extends on the findings of the plate analyses described previously to include relevant material and geometric properties including the heat affected zone, residual stress and geometric imperfections. The approach is rigorous in that it allows any prismatic cross

section made up of multiple plates and stiffeners to be modelled accurately and efficiently, with full control of the properties of each element. The method is implemented in various scripts running alongside and external to the ABAQUS graphical user interface (GUI). Although the method is applied exclusively for ABAQUS in this thesis, the general approach is proposed as applicable for use with other FEM software.

The FEM methodology is used to analyse several interframe datasets based on previously published experimental and numerical work including experiments on steel panels [39, 91] and aluminium panels [22]. The interframe model is also compared to the column collapse curves published by Chalmers [76], which form the foundation of the load shortening curves implemented in the NS94 progressive collapse program [45].

The FEM method is extended to orthogonal multi bay stiffened panels where the effects of overall collapse modes are investigated. A new dataset of flat orthogonal stiffened panels are analysed using the same general FEM approach. The dataset focuses on lightly stiffened structure and the results demonstrate the strength reduction and change in the load shortening curve shape due to the influence of overall collapse modes.

## **5.2. Nonlinear FEM Modelling Techniques for Stiffened Panel Structures**

The modelling approach developed to predict the buckling characteristics of an unstiffened plate have been summarised in Chapter 4. This section describes the extension of the approach in order to model stiffened panels; both interframe and orthogonally stiffened. The modelling technique can be used to construct the complete parallel mid-body section of a hull girder over multiple frame spaces. The practical FEM modelling techniques are detailed, which provides a justification of the approach and also summarises the knowledge gained through the present work in effectively developing FEM models for rigorous nonlinear analyses.

The nonlinear FEM method requires the same core modelling principles to be used throughout the structural hierarchy. Thus the approaches developed in the previous Chapter for a plate are equally applicable to a stiffener web, a deck panel and an entire cross section. However, as the complexity increases, the implementation of representative geometric and material imperfections also becomes more difficult. Nevertheless these imperfections must be introduced to all parts of the model to ensure adequate reliability in the solution.

A robust modelling methodology has thus been developed, which enables efficient generation of stiffened panel and hull girder FEM models including all relevant geometric and material imperfections. To enable modelling of an arbitrary sized stiffened panel or hull girder, a general purpose procedure has been developed. Various scripts have been developed to interface with ABAQUS and enable efficient processing of multiple panel variants. The methodology is summarised and critiqued in the following sections.

### **5.2.1. Existing FEM Modelling Approaches**

The approach proposed in the present work is just one of many possible ways to build an FEM model of a hull cross section or stiffened panel suitable for nonlinear analysis. It is difficult to compare the method directly with other studies, as highly detailed descriptions of FEM modelling for such analyses are scarce. This section summarises the general differences between modelling techniques, highlighting key developments in recent years. The review also justifies the motivation for detailing the rigorous methodology developed for use in this study.

Before the advent of “off the shelf” FEA software, numerical research work investigating stiffened panel strength usually used in house programs often written for that specific purpose. One such program is FABSTRAN, which has been previously discussed in Chapter 3. FABSTRAN is a specific FEM approach to solve plate-stiffener combination (PSC) problems. It is therefore specifically developed to incorporate the geometric imperfection features relevant to the potential collapse modes of a PSC.

More recently, the availability of general purpose commercial FEM software packages has removed much of the need to develop special purpose codes. A key advantage of using such software (e.g. ABAQUS, ANSYS or NASTRAN) is that it can be adapted to model many different problem types using the same core principles. However, the use of modern codes also holds new problems for considering nonlinear problems. Using a nonlinear solver to reliably predict panel collapse or ultimate hull girder strength is not a trivial matter. Informed decisions concerning the imperfection characteristics of the panel must be incorporated to adequately represent the model.

There are numerous papers detailing nonlinear FEM results for plated structures in civil and marine applications. Some key papers which detail the FEM modelling approach are discussed here.

Recent ISSC reports have included benchmark FEM studies of steel and aluminium panels. The extents and modelling techniques of the benchmark models are interesting to compare as they provide a good snapshot of current practise. ISSC2003 benchmarks an aluminium panel. All the

studies use a 3 bay model, as shown in Figure 59. Details on the FEM model and results from the benchmark study are published in the ISSC report [109] and other papers [85]. Imperfection is modelled by applying a lateral pressure to the panel and running a preliminary linear analysis, which causes a hungry horse imperfection pattern. As critiqued in section 5.4.6, this method of introducing imperfection is not considered adequate for the present study, as it introduces artificial loads to the structure.

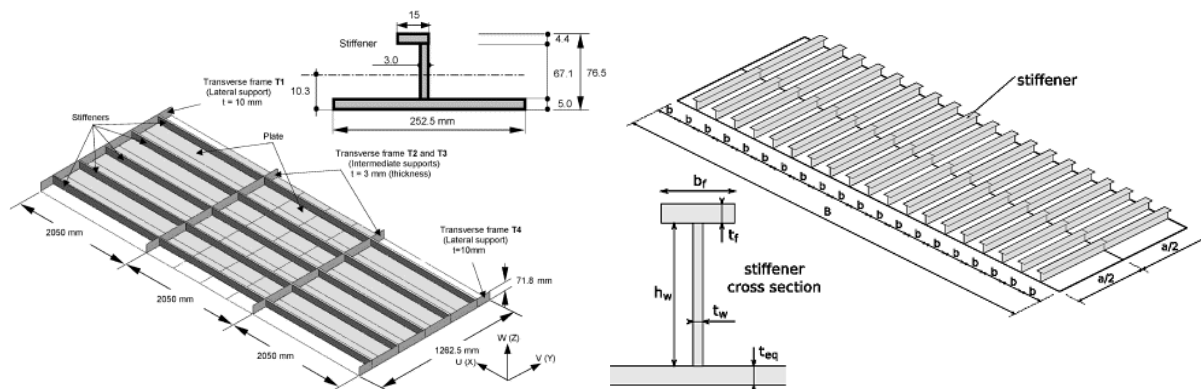


Figure 59 – ISSC 2003 [109] (left) and 2007 [110] (right) benchmark models

ISSC 2009 benchmarks a steel panel using a  $\frac{1}{2} + \frac{1}{2}$  bay model [110]. Various commercial FEM codes are used to compare many aspects of the modelling approach. Imperfection is modelled using Fourier series trigonometric transformations. The method used to apply the imperfections to the numerical model is not detailed, and may have differed between participants in the benchmark, but it can be assumed that nodal translation methods were employed. This technique is detailed in section 5.4.6. Section 5.3.2 discusses the use of  $\frac{1}{2} + \frac{1}{2}$  bay model extents.

Amlashi et al [111, 112] carried out large scale FEM modelling of a bulk carrier under an alternate hold loading condition creating a hogging bending moment. The study provides various details of the FEM model and is a highly useful article for comparing with the approach developed here. ABAQUS is used for the FEM analysis. A  $\frac{1}{2} + 1 + \frac{1}{2}$  hold model extent were chosen to ensure the boundary conditions allow the global bending moment and local loading to correctly transmit through the hull girder. Because the girder is only analysed under vertical bending moment a half model is used with a plane of symmetry specified at the centre plane.

The large size of the model means that mesh size is critical to ensure acceptable computation time. Therefore the model is split into two regions: nonlinear and linear. The nonlinear section, in the bottom structure of the central hold, is modelled with geometric imperfections and a fine mesh. The linear region uses a coarse mesh and geometric imperfections are not included.

Imperfection is applied to the model using an enhanced Eigenmode extraction method. The nonlinear region of the model is sub structured into plate stiffener combinations. Each sub structure is analysed using the linear Eigenbuckling solver to generate an imperfection pattern, following the ABAQUS manual procedure. To ensure specific imperfection modes are captured a special technique is employed, whereby geometric properties are artificially changed to induce specific Eigenmodes in the structure. The technique is critiqued in section 5.4.6.

Amlashi notes that the node translation method is cumbersome when applied to a full hull girder model. However, other studies have shown that the direct translation of nodes is possible. For example, recently published work from DNV [113] uses an in house code to model imperfection throughout a bulk carrier model. Both local deflections of the plate and stiffeners and global imperfection of stiffened panels are modelled. The resulting analyses show that the imperfections have only a small effect in reducing the predicted ultimate strength of the girder. This may be due to the nature of the structure (a heavy framed bulk carrier) and because the ship is only analysed in sagging, where the use of pressure loads on the bottom plating of the hull effectively introduces an imperfection shape.

### **5.2.2. The Building Block Approach**

The parameters of the model are critical to the subsequent analysis and can significantly affect the result. The review of existing methods to FEM modelling demonstrates that techniques are varied, and there is a lack of established procedures available in open literature as guidance. Therefore it was considered appropriate to develop and publish a rigorous methodology for modelling an orthogonal stiffened panel of arbitrary size and orientation. The methodology is then further extended to model a prismatic hull girder compartment, including all relevant features. The procedure, known as the building block approach, is an efficient and robust way of modelling FEM geometry with complete control over imperfections and material properties at the local component level.

The fundamental premise of the building block method is that an orthogonal stiffened panel is a collection of separate plate and stiffener components, which are combined together using Cartesian coordinate translation to form the complete geometry. The method therefore follows the structural hierarchy as described in Chapter 3. Essentially, this means that a structure of arbitrary size is built out of basic “Level 1” components, as shown diagrammatically in Figure 60. Although simplistic, this was found to be an essential conceptual approach to develop a rigorous procedure to efficiently

build nonlinear finite element models. A similar approach is also used to develop the analytical methods as discussed in Chapter 6.

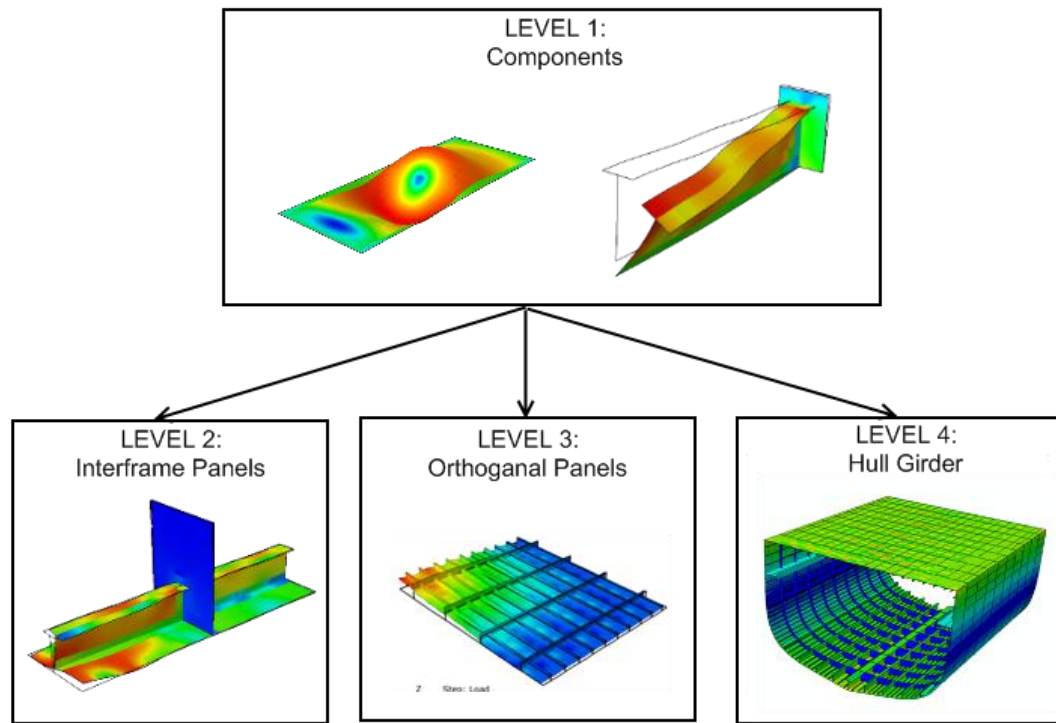


Figure 60 – Graphical representation of the building block approach applied to the structural hierarchy

The diagram demonstrates the modelling process. Each plate and stiffener component, treated as a basic building block, is first modelled separately within the FEM software, and assigned individual geometric and material properties such as initial imperfections, heat affected zone and residual stress. The components are then combined together to form the complete geometry as required.

In addition, the procedure is capable of defining linked imperfection properties over several elements. For example the principal direction of geometric imperfection in adjacent plates (i.e. towards or away from the stiffened side) may be conservatively assumed to alternate, creating a simply supported boundary at the stiffener joint. This effect needs to be properly treated at the modelling stage.

The building block concept is applied practically in ABAQUS CAE. By first defining a series of simple plate and stiffener building blocks, an FEM model of arbitrary extents can be built up by arranging the components using Cartesian translation and rotation. Once arranged the components are then merged into a single geometric model. The merged model is meshed as a single entity, but the individual properties of each component are kept. Furthermore, by utilising the “Sets” feature in ABAQUS, the nodes within each component can continue to be traced after the complete model has

been merged and meshed. This allows control of geometric imperfection of each component in the complete model, taking information from the model input file and applying node translation equations appropriately.

A general purpose procedure, using both internal ABAQUS scripts and external computer code, has been developed to automate much of this process. The program applies equally well to flat panels and complete hull cross sections.

The key steps in the building block procedure, as applied in ABAQUS, are as follows:

1. Determine the required model extents;
2. Write a text “input file” containing details of each plate and stiffener in the model. Details include dimensions, Cartesian coordinate position, imperfection, HAZ and residual stress characteristics of each component;
3. Open a predefined “base” ABAQUS file, which contains building block component models (plates and stiffeners);
4. Build the complete model by replicating each component from the input file and inserting into the global model assembly;
5. Merge the geometric model, set boundary conditions and mesh the geometry. Output the model .inp file;
6. Apply geometric imperfections to each component in the global model;
7. Submit the model to the ABAQUS solver.

### **5.3. Model Extents and Boundary Conditions**

The instability analysis of a ship type stiffened panel needs to produce reliable results which reflect its continuous behaviour as part of a hull girder structure. The model must have an acceptable computation time and include adequate boundary conditions and features to correctly represent the entire panel.

In terms of model extents, a general aim is to keep the number of degrees of freedom within the model manageable whilst ensuring that the characteristic behaviour of the panel is still realised. The number of nodes in the mesh, which closely correlates to the number of degrees of freedom, will

have important consequences for mesh generation, graphics handling, file size and, most importantly, the computation time.

A simple way to minimise the number of nodes is to keep the element size as large as possible without compromising the accuracy of the calculations. For a comparatively simple model, such as a plate, the entire geometry can be meshed adequately without creating an excessive number of nodes. However, a more complex orthogonally stiffened structure becomes computationally heavy if the entire geometry is modelled.

Therefore a sub-model of the structure is usually preferred, whereby the use of appropriate boundary conditions enables a regular arrangement to be represented using a smaller scale model. This enables the extent of the finite element model to be significantly reduced. Reducing the model size also has the benefit of simplifying the definition of geometric and material imperfection parameters, as well as easing the interpretation of results.

### **5.3.1. Plate and Stiffener Models**

Chapter 4 has detailed the FEM modelling extents for unstiffened plate models. A similar component level approach is developed for stiffener “isolation” FEM models. As discussed previously, a stiffener in compression has three fundamental collapse modes: together with the plating (beam-column buckling); by stiffener tripping (torsional-flexural buckling); or by local buckling of the stiffener web. The latter two are local to, and a function of, the stiffener geometry. They can be assumed to be independent of beam-column buckling, which is a function of the combined plate-stiffener geometry. These local characteristics of the stiffener therefore can be predicted in FEM by analysing the stiffener exclusively. A suitable boundary condition represents the connection of the web toe to the plating. A conservative assumption is that the stiffener is free to rotate about the joint axis, thus the boundary condition is simply supported.

However, this support condition can be overly conservative, as the attached plating may affect the rotational restraint along the joint (Figure 61). This is particularly important for a stiffener liable to collapse through tripping, as the rotation behaviour differs from a conventional column in that it occurs about an enforced axis at the stiffener joint, and the attached plate can offer some restraint against this rotation. Hughes [53] defines a rotational restraining coefficient, or stiffness, which comes directly from the plate flexural rigidity.

$$K_{\omega} = \frac{4D}{b} C_r C_{\alpha}$$

where  $K_{\omega}$  is the distributed rotational restraint stiffness which the plating exerts on the stiffener,  $C_r$  is a correction factor due to web bending and  $C_{\alpha}$  is a correction factor for plate aspect ratio (approximated to 1.0 for long plates). For a typical ship type plate  $K_{\omega}$  is usually less than 200GN/m.

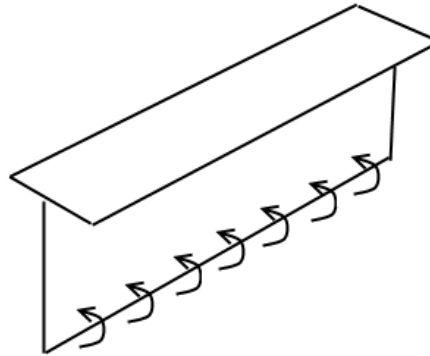


Figure 61 - Stiffener rotational stiffness. The boundary conditions and model extents of the stiffener isolation model are as shown in Figure 62

The model uses a  $\frac{1}{2} + \frac{1}{2}$  bay representation, the reasons for which are discussed in the next section. The joint has a simple support boundary condition except in the z direction, which remains free. This means the stiffener is allowed to buckle as a beam-column, albeit without the influence of attached plating. It is thus assumed that the influence of the attached plating in providing lateral support is small.

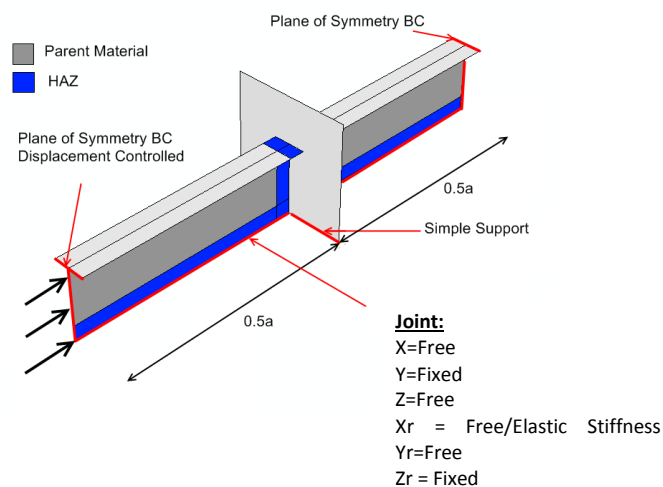


Figure 62 - Stiffener FEM model boundary conditions

### 5.3.2. Plate-Stiffener Combination Models

A conventional assumption in stiffened panel analysis, and also a key assumption in the progressive collapse method, is that transverse frames are relatively strong compared to the longitudinals. Thus they are assumed to not deflect out of plane when the panel is subject to uniaxial compression in the longitudinal direction and the panel fails interframe.

The implication of this assumption in an FEM model is that the transverses can be constrained against out of plane movement. A conventional approach is to set the boundary condition at the transverse frame-plate joint as a simple support.

This means that a panel with regular orthogonal stiffening in both directions can be represented by a simple interframe FEM model. Furthermore, if longitudinal stiffeners are widely spaced relative to the plating thickness, each stiffener can be assumed to act both independently from and identically to adjacent stiffeners.

These key assumptions allow a panel to be represented by a plate stiffener combination model, which consists of a single stiffener with associated plating. Plate-stiffener combination type analyses assume that the behaviour of a single stiffener with attached plating in uniaxial compression will replicate throughout the entire frame space. Thus the analysis can be confined to a single stiffener to determine the behaviour of the entire panel.

There are two different model extents commonly used for a PSC representation in FEM. Figure 63a highlights a single bay representation, modelling the plate and stiffener running between two frames. Figure 63b highlights the  $\frac{1}{2} + \frac{1}{2}$  bay representation.

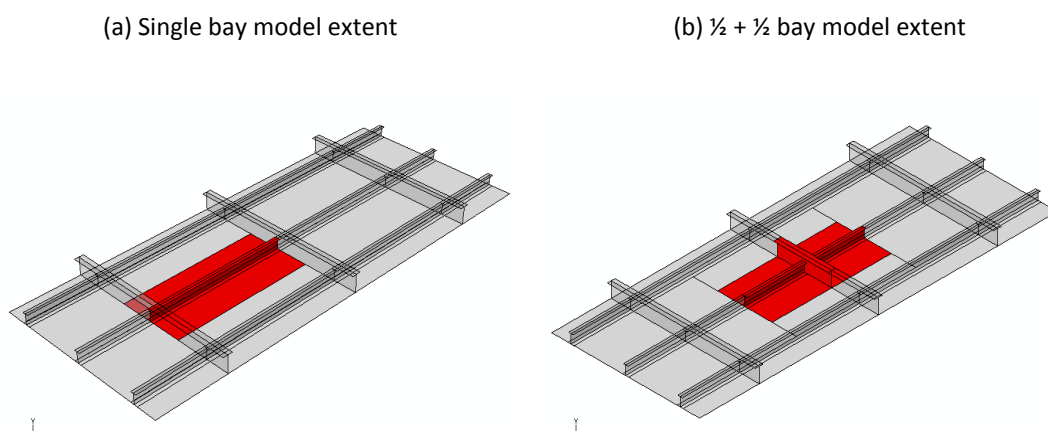


Figure 63 - Modelling extent for plate stiffener combination models

The single bay model extents are used in numerous physical and numerical panel studies including Zha and Moan [27] and Paik et al [19]. The transverse frame is not included in the finite element model, instead appropriate boundary conditions are applied at the bounding edges.

A single bay FEM representation is often used in conjunction with experimental model tests of a similar form. The analysis thus attempts to replicate the exact model extents and boundary conditions used in the physical test. For example, numerical analyses by Zha and Moan [27] are used to compare with experimental single bay panel tests, where the panel ends are simply supported close to the neutral axis of the cross section and load is then applied at this position throughout the collapse test. Similar boundary conditions are applied in single bay aluminium panel tests carried out by Paik [22]. The boundary condition is replicated in FE models, and the numerical results generally show close correlation to the experiment.

However, for the purposes of representing a multi-frame grillage, this assumed simple support boundary condition is not appropriate. This is due in part to the difficulty in following the progressive shift of the neutral axis as the longitudinal stiffener and the included plate begin to buckle, and also due to the presence of the supporting transverse frame and continuous beam interactions between adjacent spans.

In this regard, the  $\frac{1}{2} + \frac{1}{2}$  bay beam-column model (Figure 63b) has a number of advantages. The model accounts for the restraining or destabilizing interaction between adjacent panel bays caused by the direction and magnitude of the buckling in each span, as well as the shift in the neutral axis of the panel and hence the shift in the line of action of the compressive load [39]. The model works as a single stiffener beam-column or when extended to include multiple parallel stiffeners.

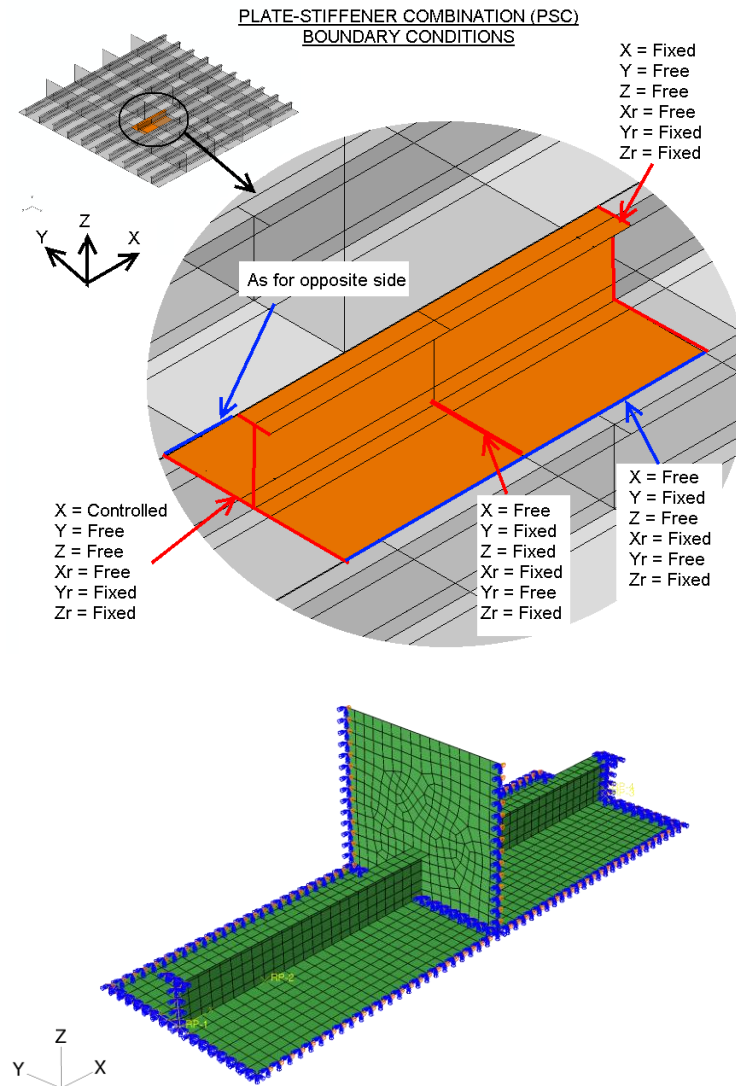


Figure 64 – PSC boundary conditions

The FABSTRAN elasto-plastic beam-column finite element program developed at the A.R.E. uses a  $\frac{1}{2} + \frac{1}{2}$  representation of the complete panel with a single stiffener in isolation (Figure 63b). The plate behaviour is represented by a plate load shortening curve derived from separate analyses and experimental data. Each span has a central plane of symmetry; load is applied using a displacement control. The transverse frame is assumed to be flexurally rigid but torsionally weak; hence a simply supported boundary condition is applied at the frame position.

A PSC type analysis in ABAQUS FEM uses boundary conditions as shown in Figure 64. A typical mesh geometry is also shown. The transverse frame is included to ensure the interaction of longitudinal elements adjacent to the frame behave correctly. This was found to be a more reliable method than using boundary conditions at the stiffener-frame joint.

### 5.3.3. Orthogonal Stiffened Panel

The PSC representation of a flat, orthogonally stiffened panel is unable to include the influence of overall collapse modes, where the transverse frame may shift out of plane and the collapse nucleates over several bays. To adequately assess these effects a more complete FEM model is required including an appropriate number of frames and stiffeners with associated boundary conditions. A complete orthogonal panel is shown in Figure 65. The boundary conditions reflect simple support conditions.

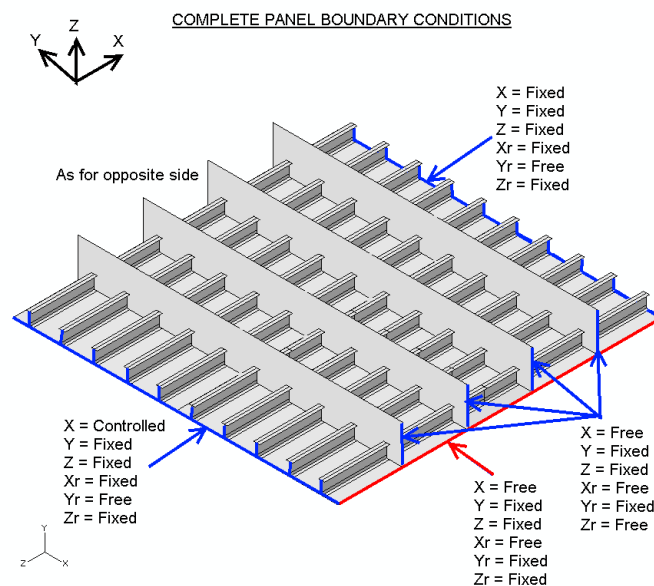


**Figure 65 – Complete panel boundary conditions**

If computing resources are limited, or the panel to be modelled is large compared to the required mesh element size, a half or quarter representation can be used, as shown in Figure 66. These models are acceptable if the panel is generally symmetrical, with regular repeating imperfection patterns. This usually causes overall mode collapse to nucleate into a corresponding symmetrical shape about the central edge. However, the models can sometimes not cope adequately with unsymmetrical issues such as skewed imperfection, which can cause nucleation away from the symmetry boundary condition.

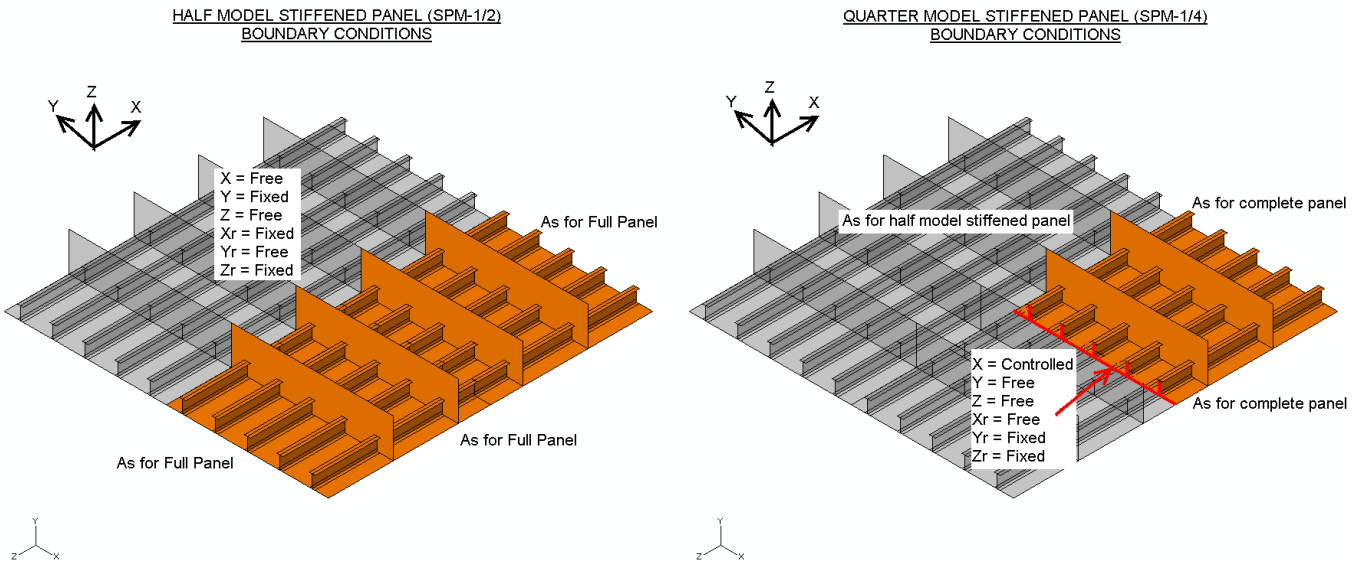


Figure 66 – Half (left) and quarter (right) panel models.

The variability in the panel dimensions, number of stiffeners and number of bays means that the FEM representation of a panel is difficult to standardise. Therefore, to construct a arbitrarily stiffened panel recourse should be made to the building block method described previously. An alternative, which was used in this study due to the large number of models computed, is to construct standard panels. Three standard stiffening arrangements are used in this study:

- $\frac{1}{2} + 3 + \frac{1}{2}$  bay, 10 longitudinals (half panel representation)
- $\frac{1}{2} + 3 + \frac{1}{2}$  bay, 20 longitudinals (half panel representation)
- $\frac{1}{2} + 7 + \frac{1}{2}$  bay, 20 longitudinals (quarter panel representation)

These models are built automatically using a special implementation of the building block method. For panels which do not meet the above configurations the hull girder building block approach is used, which is described further in Chapter 7. The boundary conditions are applied manually using the constraints as shown in Figure 66. The present study focuses on flat panels where all plating lies on the same plane and stiffeners are normal to the plate surface. Although not directly studied, the building block approach is also suitable for curved or other specially arranged panels. For these cases the panel can be built in much the same way as for flat panels. The method can be readily extended to include different types of plate and stiffener.

## 5.4. Geometric Imperfections

### 5.4.1. Geometric Panel Imperfection Parameters

The compressive buckling strength capabilities of thin plated panels are significantly influenced by the presence of as-built geometric imperfections including out of flatness, eccentricity and localised indentations [61]. The causes of geometric imperfection in plates have been previously discussed. The principles extend to stiffened panel structures, where the welding process introduces imperfection characteristics as summarised in the following.

Idealised imperfection patterns are a necessity in nonlinear finite element analysis of stability type problems for stiffened panels because the governing equilibrium equations require an initial geometric nonlinearity to allow progressive buckling and collapse to occur. However, it is well recognised that the magnitude and spatial variation of geometric imperfections in real structures is also subject to significant uncertainty. Therefore statistical approaches are usually coupled to mathematical descriptions of imperfection shape and magnitude to provide an idealised yet realistic pattern suitable for implementation in the FEM mesh.

Typical plate imperfection patterns, and the effects on the plate ultimate strength, are detailed in the previous Chapter. In addition to modelling the plate imperfections, the local imperfections of stiffeners and the global imperfections of the entire panel must also be quantified for the nonlinear analysis of a stiffened panel.

Imperfection amplitude is defined as the translation of any point in the structure from its ideal “perfectly flat” position. In FEM this equates to a particular translation of each node in the mesh normal to the element plane. The nomenclature used in the following text to define the translation of a particular point in a stiffened panel is as defined in Figure 73. Unless a specific panel is being analysed and the exact imperfection pattern is known through detailed measurement of the structure, the geometric imperfection is usually idealised using simplified formulae.

Imperfection patterns using trigonometric functions require a definition of the maximum amplitude over the span in question. The maximum imperfection of a stiffened panel is commonly split into three components: the plate out of plane imperfection ( $w_{opl}$ ), the stiffener out of plane sideways imperfection ( $v_{os}$ ) and the stiffener vertical in-plane column imperfection ( $w_{oc}$ ). The latter is a global imperfection and affects the position of every node in the panel whilst the first two are localised imperfections affecting only the plate and stiffener respectively. The maximum amplitudes are used as scale factors in the definition of the imperfection magnitude at any point in the panel.

### 5.4.2. Plate Imperfection

The plate imperfection is a local imperfection mode quantifying the maximum deviation of the plate from flat in relation to its support structure, as shown in Figure 67. The imperfection over the entire plate surface is commonly described using a Fourier series sine wave shape as detailed in Chapter 4.

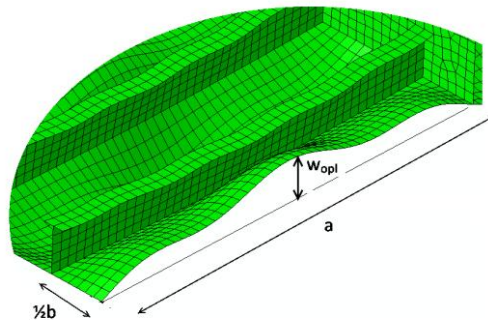


Figure 67 – Maximum plate imperfection amplitude

### 5.4.3. Stiffener Imperfections

The side imperfection of the stiffener,  $v_{os}$ , is a measure of the eccentricity of the otherwise straight stiffener from vertical. The direction of the eccentricity can be arbitrary and can be treated as a local imperfection mode (Figure 68), or it may be coupled to the global mode column imperfection shape, as is the case in the benchmark study of committee III.1 in ISSC2009 [110] (Figure 68). The benchmark study also uses a further local imperfection mode to model the out of flatness of the stiffener web using a square sine wave shape over the stiffener length as shown in Figure 69.

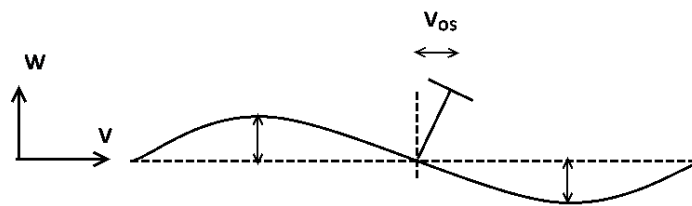


Figure 68 – Stiffener side imperfection

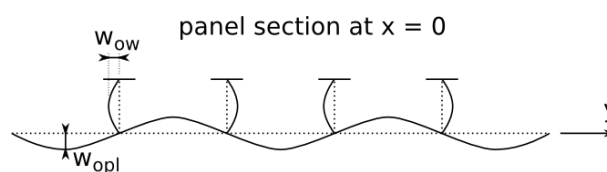


Figure 69 – Stiffener web imperfection

### 5.4.4. Column Imperfection

The vertical column imperfection is a measure of the out of flatness of the entire panel, which spans between transverse frames in the longitudinal direction and end longitudinal supports in the transverse direction. As an example, for a typical deck structure the longitudinal supports might be either the side of the vessel or a deep longitudinal girder. As such the column imperfection is superimposed on top of the local imperfection modes at every point in the panel. Longitudinally, the column imperfection is usually idealised as a single half sine wave between frames, the direction of which can either be towards the stiffener or towards the plating. Two continuity patterns can be used between adjacent frame bays, either an asymmetric condition where the column imperfection direction alternates (Figure 70a), or a symmetric condition as shown in Figure 70b.

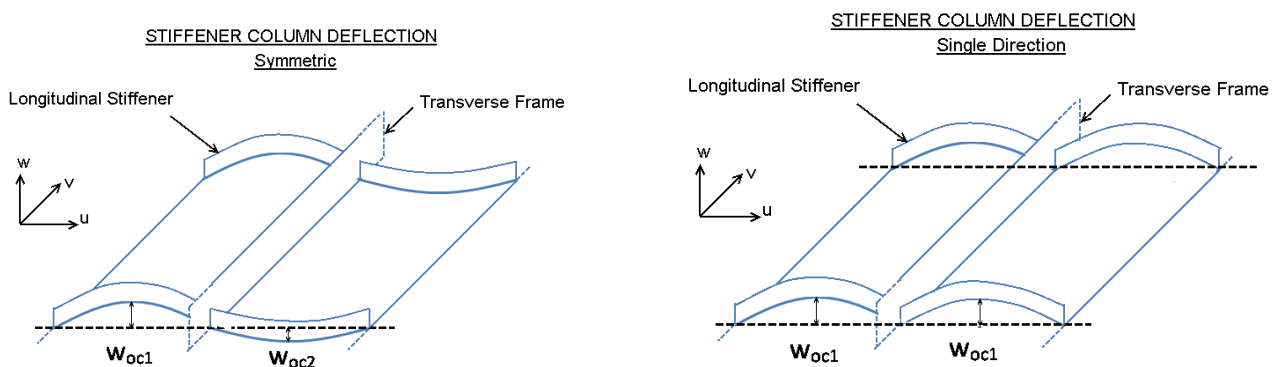
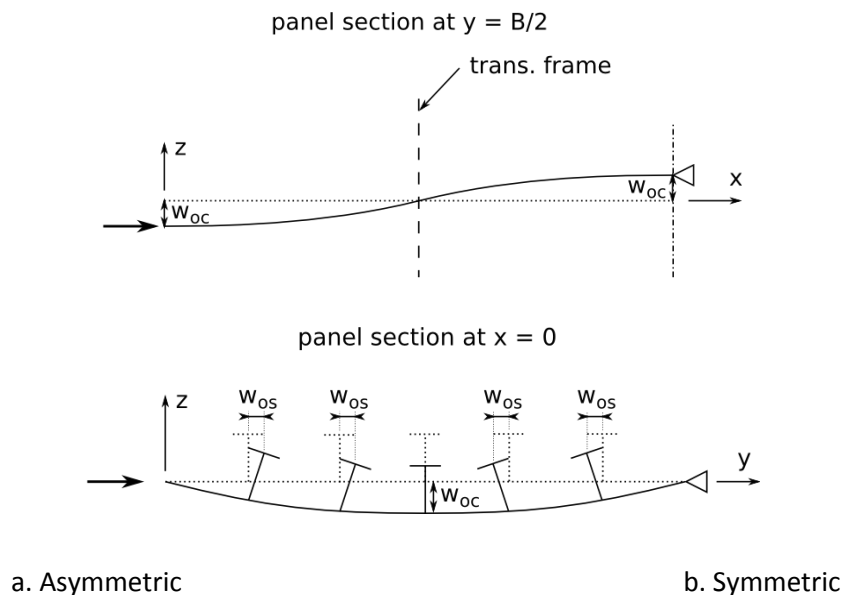


Figure 70 – Stiffener column deflection

Similar to the continuity of the plate imperfection, a symmetric column deflection is equivalent to a clamped boundary condition at the frame intersection, and may be assumed to be appropriate for a panel which supports significant lateral pressure from the plate side, such as hydrostatic or deck loads. However, typical imperfection patterns of British warships measured amongst others by Faulkner [65] showed a tendency for an asymmetric type column imperfection pattern, but with different magnitudes of maximum imperfection in each direction [39]. The following ratios are given to describe the relative magnitudes as shown in Figure 70a.

$$\frac{w_{oc2}}{w_{oc1}} = -0.25 \quad \text{for slight and average imperfection levels}$$

85

$$\frac{w_{oc2}}{w_{oc1}} = -1 \quad \text{for severe imperfection levels}$$

The distribution of the column imperfection in the transverse direction is unimportant for single stiffener beam column type analyses, where the same amplitude can be used across the entire model width, but needs consideration for complete stiffened panel analyses. The benchmark study in ISSC2009 uses a single half sine wave across the 20 stiffener spaces comprising the entire width. An alternate assumption is that the column imperfection amplitude remains constant for a particular cross section and is either included as a distortion at the panel edges or is stepped down to zero using an appropriate shape, such as is shown in Figure 70.

#### 5.4.5. Imperfection Amplitude

Discussion on the statistics of fabrication induced imperfection is detailed in Chapter 4. Extensive measurements of imperfection components have been carried out for steel structures [65] and more recently for marine grade aluminium panels [22]. A summary of formulas to describe slight, average and severe levels of imperfection as given by Smith [39] for steel panels and Paik [22] for aluminium panels is presented in Table 21. There are only marginal differences shown between the statistics for steel and aluminium plates. Obviously, the statistics rely on the type of ship, welding methods and many other factors used in the measurement sample. For example, the aluminium data shown in Table 21 is derived from a sample of panels constructed at the same time and in the same fabrication yard. There is a lack of clear measurement data for aluminium that can be used to derive a generalised set of statistical formulae to cover aluminium ship construction as a whole. Therefore, in lieu of this dearth of statistical data, the imperfection amplitudes used in this study for aluminium plates and stiffeners predominantly utilise the steel based criteria from Table 21. A summary of the

imperfection amplitudes used in this study are given in Table 22. Definitions of the parameters describing imperfection shapes contained in Table 22 are discussed in the next section.

**Table 21 – Formulae to describe fabrication induced initial imperfections in a stiffened panel structure.**

	<b>Smith (1991) – Steel Panels</b>			<b>Paik (2008) – Aluminium Panels</b>		
	Slight	Average	Severe	Slight	Average	Severe
$w_{opl}$	$0.025\beta^2t$	$0.1\beta^2t$	$0.3\beta^2t$	$0.018\beta^2t$	$0.096\beta^2t$	$0.252\beta^2t$
$w_{oc}$ ( $\lambda=0.2$ )		$0.0008a$	$0.0020a$			
( $\lambda=0.4$ )	$0.00025a$	$0.0012a$	$0.0038a$	$0.0016a$	$0.0018a$	$0.0056a$
( $\lambda \geq 0.6$ )		$0.0015a$	$0.0046a$			
$v_{os}$	-	-	-	$0.00019a$	$0.001a$	$0.0024a$

**Table 22 – Imperfection Properties for Steel and Aluminium Plates**

ID	Name	$m$	$n$	$w_{opl}$	Plate	$w_{oc}$	$\frac{w_{oc1}}{w_{oc2}}$	$w_{os}$	$w_{ow}$
S	Slight	$a/b+1$	$a/h_w+1$	$0.05\beta^2t$	$B_1=0.8$ $B_m=0.2$ $B_{m+1}=0.01$	$0.0002a$	-0.25	$0.0004a$	$0.0002a$
A	Average	$a/b+1$	$a/h_w+1$	$0.1\beta^2t$	$B_1=0.8$ $B_m=0.2$ $B_{m+1}=0.01$	$\lambda < 0.2: 0.0008a$ $\lambda < 0.6: 0.0012a$ $\lambda > 0.6: 0.0015a$	-0.25	$0.002a$	$0.001a$
L	Severe	$a/b+1$	$a/h_w+1$	$0.3\beta^2t$	$B_1=0.8$ $B_m=0.2$ $B_{m+1}=0.01$	$0.006a$	-1	$0.005a$	$0.0025a$
ISSC		$a/b+1$		$b/200$	$B_m=1$	$0.001a$	-1	$0.001a$	$h_w/200$

#### 5.4.6. Implementation of Geometric Imperfections

Once the geometric imperfection parameters have been quantified an appropriate idealised pattern needs to be implemented in the finite element mesh. The implementation method should be appropriate to efficiently superimpose the desired imperfection shape onto the initially “perfect” structure. Two methods are readily available: linear superposition of buckling Eigenmodes or direct translation of nodes using trigonometric functions. There are other methods available. For example a number of papers [84, 114] use a pressure loading to impose geometric imperfection in a stiffened panel. However this approach is problematic because it introduces an extra artificial load into the system. It is considered only suitable for imperfection insensitive panels and is not suitable for the analyses conducted in this study.

Geometric imperfection can also be developed using an external 3D CAD program or spread sheet and then imported directly into the ABAQUS CAE for meshing. However, this approach is less

feasible when dealing with large numbers of parametric models because it requires manual input for each model through the transfer between software.

The following sections discuss the relative merits and drawbacks of the Eigenvalue and node translation methods, which essentially do the same thing (translate nodes to a deformed shape prior to nonlinear analysis) but differ in the input technique and the level of control the user has in selecting imperfection shapes. The methods are applied to stiffened panel sub structures, but are also reviewed with consideration given to modelling an entire hull girder section. The node translation method is proposed as the most suitable for use in the present study.

#### **5.4.7. Eigenmode Superposition**

A recommended procedure in finite element buckling analysis of many types of structure is the Eigenmode imperfection approach, first running an Eigenvalue analysis to output critical buckling mode shapes, which are then implemented as node translations prior to applying a nonlinear incremental analysis [101]. Most general purpose finite element analysis programs have the capability to carry out both types of analysis. In ABAQUS the modal results of the Eigenvalue analysis can be passed to the input file of a nonlinear analysis on the same mesh, using appropriate scaling factors to provide an imperfection pattern superimposed onto the original node coordinates.

Eigenvalue buckling analysis is an extended form of the classical Euler buckling procedure. It predicts the theoretical buckling strength of an ideal elastic structure together with the corresponding buckled mode shape of the geometry. Therefore, in isolation, it is only of limited use in assessing the stability of a section because the analysis uses linear elastic theory. Therefore the predicted buckling strength from an Eigenvalue analysis is usually overly optimistic. Furthermore, Eigenvalue analysis is not recommended for solving the buckling strength of more complex structure such as stiffened panels.

However, the analysis is useful in predicting the critical buckling mode shapes of the panel. One of the primary advantages of using the Eigenmodes as inputs in the nonlinear analysis is that the critical buckling mode shapes are used to form the imperfection, thus providing what is likely to be a conservative buckling pattern as the panel deforms under load. The first few Eigenmodes can be considered “worst case” imperfection patterns, as the panel will readily buckle in the Eigenmode shape, usually with the buckle nucleating at one of the imperfection peaks. The use of the primary Eigenmodes as the initial imperfection pattern is less likely to cause an inhibition of buckling by the imperfection shape or exhibit snap through behaviour, whereby the panel switches from one buckling mode to another.

A number of primary and higher order buckling shapes can be combined to form the overall imperfection pattern, allowing for the influence of each included mode in the nonlinear analysis. This is of particular importance if the panel is sensitive to the imperfection shape, which is characterised by a number of Eigenmodes with values of similar magnitude. Therefore, the use of Eigenmodes adds confidence that the nonlinear analysis is a conservative measure of the panel strength.

A set of example Eigenmode plots are given in Figure 71 for subsets of a flat bar stiffened panel with dimensions typical of ship structure. A potential disadvantage of Eigenmode superposition is the lack of control the analyst has in describing the imperfection pattern of the structure. However, this is usually not an issue for simple plates, where the first few Eigenmodes, such as for the plate example given in Figure 71, will give a comprehensive imperfection pattern suitable for superposition in a nonlinear analysis. Eigenmode superposition is also possible for simple stiffened panel models such as the plate stiffener combination (PSC) and single bay panel illustrated in Figure 71.

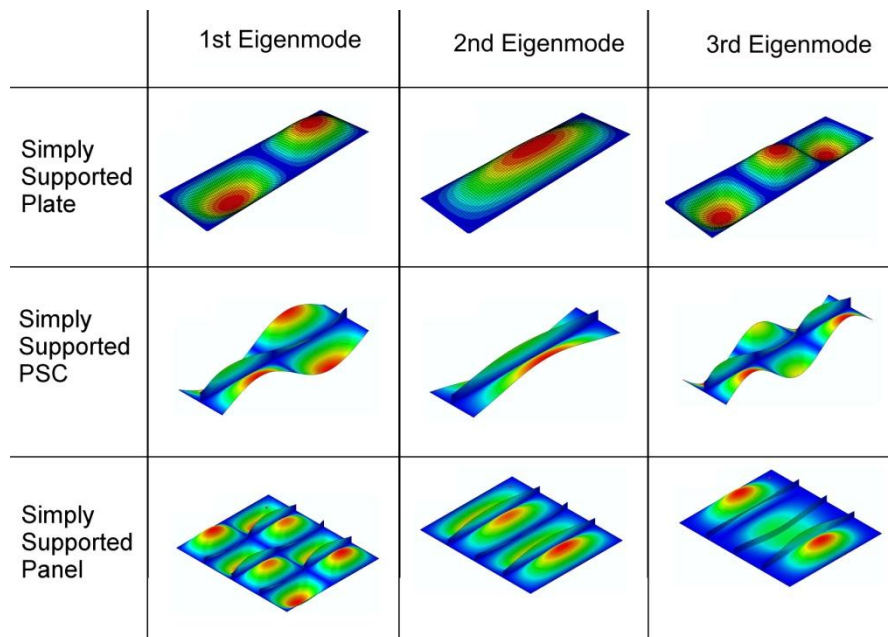


Figure 71 – Example Eigenmode shapes for a 1000mm x 300mm x 10mm plate with 100x10 flat bar stiffener

However, the stiffened panel Eigenmodes are less consistent than those for unstiffened plates. For example, the 3<sup>rd</sup> Eigenmode of the stiffened panel in Figure 71 has an irregular combination of buckling modes: a global imperfection mode across the panel width and local plate imperfection modes in the end plates. Great care must be taken to review each Eigenmode before using as an imperfection superposition – it cannot be assumed that the first few Eigenmodes will provide

suitable imperfection patterns. This is a cumbersome task, and not one well suited to a parametric study involving many analyses of different panel geometries.

This factor is particularly significant if the analyst wishes to create a realistic imperfection pattern based on actual distortion measurements or using statistical information about the nature of the imperfection pattern. Furthermore, the Eigenmodes usually combine plate and stiffener distortion in each imperfection pattern, as is the case for both the PSC and panel shown in Figure 7. This raises a potential difficulty in controlling the relative amplitude of deflection for the plate and stiffener.

In an effort to overcome some of the problems highlighted above, an enhanced method of Eigenmode extraction is proposed by Amlashi et al. [111], whereby specific distortion shapes are encouraged by artificially increasing the thickness of some regions in the structural model, thus altering the buckling behaviour of the panel. For example, the stiffeners can be artificially “thickened” and the resultant Eigenvalue analysis will produce Eigenmodes exhibiting plate buckling only. This method is proposed as advantageous compared to node translation in the construction of an entire hull girder, as the position of the panel edges can be assured through judicious use of boundary conditions and thus an entire hull cross section can be built up incorporating appropriate Eigenmode imperfections into each panel. Amlashi employs the method successfully in a hull girder ultimate strength assessment of a bulk carrier using FEM.

An attempt was made in the present study to replicate this enhanced method to introduce imperfections to a box girder comprising four equally sized panels with the same dimensions as in Figure 71. Example plots of the Eigenmode outputs are given in Figure 72. To produce the region specific imperfections, specific regions in the bottom panel were correctly sized whilst the side and top panels were given an artificially high thickness (in this case 10x the actual thickness). The resulting Eigenmodes produce a variety of relevant critical buckling patterns; the examples in Figure 72 are sample outputs for plate, stiffener and overall panel imperfection modes. The procedure can be repeated as many times as necessary to produce a superposition of the complete imperfection pattern for the box girder.

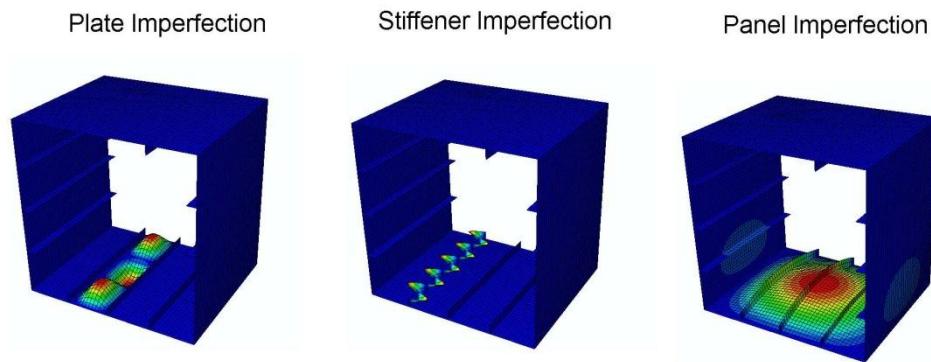


Figure 72 – Box girder Eigenmode buckling patterns with areas of the structure artificially oversized to produce imperfection in specific regions of the model

However, this method also has significant drawbacks, not least the difficulty in appropriately constraining and sizing the model to produce the desired imperfection shape for specific regions. In the example above a number of additional boundary conditions were required at the plate-stiffener joints to produce the plate imperfection shape. For a more complex structure, the Eigenvalue analysis needs to be carefully set up to ensure convergence. Even then, it cannot be guaranteed that the desired imperfection shape can be achieved. A compromise must be made between using *critical* imperfection patterns and *realistic* imperfection patterns.

#### 5.4.8. Direct Translation of Nodes

Eigenmode superposition is a method of translating nodal coordinates prior to a nonlinear analysis by imposing scaled displacements to each node based on the prescribed patterns calculated in the Eigenvalue analysis. The direct node translation method works to the same principle, but rather than using Eigenmode shapes the imperfection is implemented directly using appropriate trigonometric functions. As has been discussed previously, actual imperfection patterns in ship structure can be closely mapped using Fourier expansion series. The Eigenmode imperfection patterns also usually take the form of sinusoidal shapes.

Therefore, direct node translation, using appropriate expressions, can be used to map both realistic and critical imperfection patterns into a finite element mesh of a stiffened panel. This is usually achieved using external software linked to the FEM package [89].

The parameters governing the expressions depend on the availability of actual imperfection information, which if available can be analysed using regression techniques to give appropriate

coefficients in the Fourier expansion formulas. Alternatively, if actual imperfection information is not available, as is likely for a numerically based parametric study, statistical imperfection patterns based on the knowledge of likely imperfection shapes and amplitudes can be used, as have been reviewed in preceding sections of this report.

To impose geometric imperfection by direct translation of nodes a simple program was developed for use alongside ABAQUS. The following is a brief summary of the program method, followed by a description of the trigonometric functions used to describe the translation of each node in the model.

To begin, the panel is constructed in the ABAQUS pre-processor and all the relevant material properties, boundary conditions and dimensions are applied to the model. The model is assembled so that the zero point is positioned as shown in Figure 73. The ABAQUS input file is then written. For each node a transformative set of equations are then applied to translate the original “flat panel” node coordinates to the “distorted panel” coordinates. The equations are applied using an external program developed in the Python programming language, whereby the original input file is opened, each line of node data is passed to the program and the transformative equations are applied. A control file is used to specify the relevant parameters for the imperfection (amplitudes, shape, direction etc). A “distorted panel” input file is then written by the program with the translated node coordinates.

The new input file can be submitted to the ABAQUS solver via the command line. Alternatively, it can be imported into ABAQUS CAE for additional model parameters to be set, or for use as a subassembly in a complex multi panel structure. Other properties within the input file can also be edited by the external code including plate thicknesses and the residual stress distribution. This simplifies the generation of multiple input files in a parametric analysis.

A description of the transformative equations is now given, with the coordinate system as shown in Figure 73. In addition the following nomenclature is used:

M = number of transverse frames

N = number of stiffeners

n = number of imperfection modes applied in the Fourier expansion series

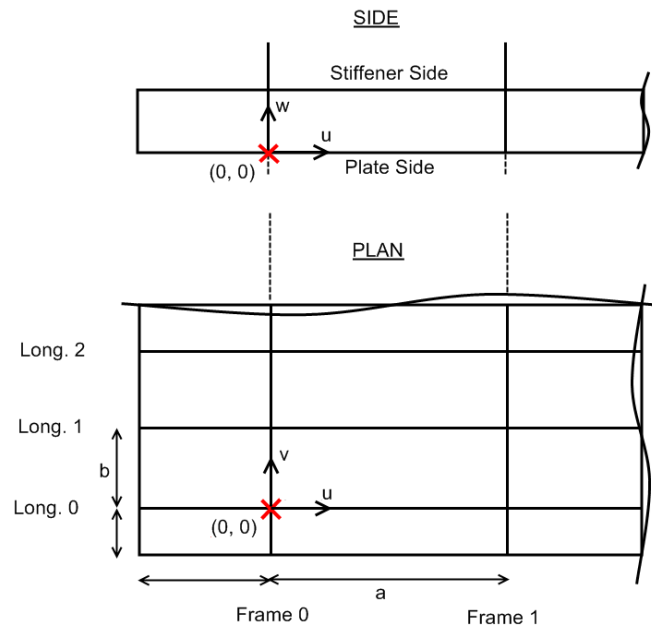


**Figure 73 – Panel coordinate system**

The plate out of plane deflection is applied using a Fourier series expansion formula coupled with a further sine wave function which determines the transverse distribution of the shape.

$$w_{pl} = \left( \sum_1^{i=n} \sin\left(\frac{i\pi U}{a}\right) w_{opl,i} \right) \sin\left(\frac{\pi}{b} V\right) \quad 86$$

If the plate imperfection lobes are single direction (characteristic of hungry horse pattern imperfection) then the above equation is extended by specifying the imperfection is an absolute value:

$$w_{pl} = \left| \left( \sum_1^{i=n} \sin\left(\frac{i\pi U}{a}\right) w_{opl,i} \right) \sin\left(\frac{\pi}{b} V\right) \right| \quad 87$$

To ensure that stiffener flanges are not also deformed by application of the above equation to every node, the Python script includes a limitation to only apply the equations to nodes lying at  $w = 0$ .

The stiffener column deflection must be applied to all nodes in the panel, not just the stiffener nodes, as the deflection propagates throughout the plate width. The deflection follows a Fourier series sine wave shape with zero amplitude at each frame position. Thus:

$$w_c = \sum_1^{i=n} \sin\left(\frac{i\pi U}{a}\right) w_{oc,i} \quad 88$$

If the stiffener column deflection is symmetric (Figure 70a) or asymmetric (Figure 70b), the stiffener deflection lobe alternates direction in each adjacent frame space. If the amplitude of the lobe in the stiffener direction,  $w_{oc,S}$ , is not equal to the amplitude of the lobe in the plate direction,  $w_{oc,P}$ , a scale factor  $F_C$  can be defined where:

$$w_{oc,P} = F_C \cdot w_{oc,S} \quad 89$$

This assumes that the imperfection in the stiffener direction is the larger and is equal to  $w_{oc}$ , which should be the more usual case.

Therefore, Eq. 89 is extended to:

$$w_c = F_C \sum_1^{i=n} \sin\left(\frac{i\pi U}{a}\right) w_{oc,i} \quad 90$$

where  $F_C = 1.0$  for stiffener imperfection in the stiffener direction or as given in Eq. 89 for stiffener imperfection in the plate direction.

If the stiffener column deflection is single direction (Figure 70c), it is usually assumed that all imperfection lobes are directed toward the stiffener (i.e positive direction). In this case, Eq. 90 is extended to be:

$$w_c = \left| \sum_1^{i=n} \sin\left(\frac{i\pi U}{a}\right) w_{oc,i} \right| \quad 91$$

The stiffener side deflection is a function of the stiffener height and can therefore be imposed on all nodes because the  $W$  coordinate of plate elements is zero, thus also making  $v_s$  equal to zero.

$$v_s = F_S \frac{W}{h_w} \sum_1^{i=n} \sin\left(\frac{i\pi U}{a}\right) w_{os,i} \quad 92$$

The total deformed coordinates of the node ( $U'$ ,  $V'$ ,  $W'$ ) are calculated by superimposing the relevant imperfection deflections as a simple summation:

$$U' = U$$

$$V' = V + v_s$$

$$W' = W + w_c + w_{pl}$$

93

Unless stated otherwise, the imperfection patterns as detailed above are used in the parametric studies detailed in this report. Nomenclature is consistent with Figure 73. Imperfection amplitudes are as given in Table 22.

#### 5.4.9. Heat Affected Zone and Residual Stress Field

The heat affected zone and residual stress in the stiffener are modelled in much the same way as for the plate model. The implementation of the residual stress and HAZ in the panel models are the same as for the plate models as discussed in Chapter 4. The tension zone of the residual stress in the stiffener is assumed to equal the HAZ width, which is typically 25mm. A uniform compression zone runs up the remainder of the stiffener height. Some studies prefer to taper the compression zone to zero at the flange; however the influence of this distribution is not considered a critical factor in the present study. HAZ and residual stresses are not considered in the transverse structure.

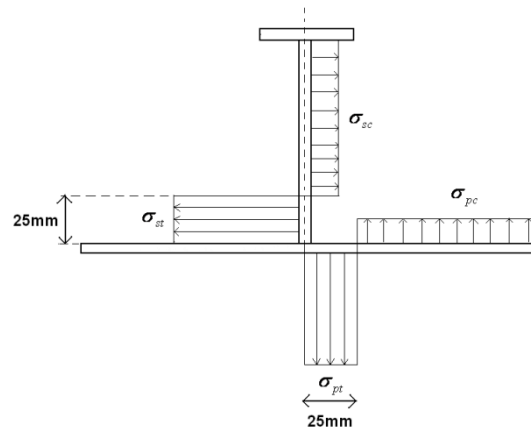


Figure 74 - Residual stress distribution

### 5.5. Analysis of Stiffener Elements

The previous sections have introduced the FEM modelling approach and defined the parameters used to represent the geometric and material imperfections. Now the results of a series of systematic FEM analyses looking at various sub structures of a ship are presented. This section investigates an isolated stiffener model (i.e. with no attached plating) whilst the following sections detail experiment results for interframe and multi bay panels respectively.

Isolated stiffener datasets, along with the plate results derived in the previous Chapter, form the basis of the semi analytical method detailed in Chapter 6. A summary of the datasets are now presented, together with a statistical analysis of the stiffener strength characteristics and discussion of the factors that influence the strength behaviour. The main part of the analysis concerns tee bar stiffeners, as these are more typically used in Naval and high speed craft design. A summary of flat bar, angle and bulb flats is also included.

### 5.5.1. Tee Bar Stiffeners

Tee bar stiffener analyses were completed for 3240 stiffener models, grouped into datasets of stiffener size, imperfection amplitude and magnitude of rotational stiffness at the web toe (Table 23). All the datasets model either Alcan or Admiralty Long Stalk cross sections. The geometric imperfections are as defined in Table 22. Aluminium stiffeners include HAZ along the longitudinal joint and at the connection to the transverse frame. Residual stress width is equal to the HAZ width (25mm). Steel stiffeners include a tensile residual stress field with width  $0.15h_w$ . An example curve series is shown in Figure 75.

Table 23 – Summary of Tee Bar Stiffener Datasets

Dataset ID	$h_{wx}$ (mm)	$t_{wx}$ (mm)	$b_{fx}$ (mm)	$t_{fx}$ (mm)	$\lambda$	Rotational Stiffness (GN/m)	Imperfections	Total
T60	60	3.5	35	5.1	0.2 - 1.2	0 100000 200000	Slight Average Severe	12 (x3)
T80	80	4.5	45	6.2	0.2 - 1.2	“	“	12 (x3)
T100	100	5	50	6.4	0.2 - 1.2	“	“	12 (x3)
T120	120	5.5	55	7.7	0.2 - 1.2	“	“	12 (x3)
T140	140	6	60	8.7	0.2 - 1.2	“	“	12 (x3)
T170	170	6.5	65	10.3	0.2 - 1.2	“	“	12 (x3)
ALS1	69.8	4.4	25.4	6.4	0.2 - 1.2	“	“	12 (x3)
ALS2	104.8	5.1	44.5	9.5	0.2 - 1.2	“	“	12 (x3)
ALS3	113.6	6.65	63.5	13.4	0.2 - 1.2	“	“	12 (x3)
ALS7	235.7	9.1	127	18.3	0.2 - 1.2	“	“	12 (x3)

For each stiffener cross section several idealised curve sets were produced, which measure the effect of the boundary condition at the stiffener-plate joint to account for the rotational stiffness

provided by the plate ( $K_{\omega}$ ). The datasets thus form a parametric curve series, which can be easily used to define a curve for a stiffener of arbitrary length and a given  $K_{\omega}$  using standard interpolation approaches.

The simply supported boundary condition at the joint forms the lower bound result. The results for this case are first presented, followed by a comparison with the rotational stiffness results.

The stiffener ultimate strength under compressive load is found to be a function of a number of defining parameters, including the geometric dimensions, column slenderness ratio and material. This is shown clearly with a plot of ultimate strength versus column slenderness for all the datasets tested for average, slight and severe imperfections (Figure 76). The plots show that, as expected, there is a general trend for strength to reduce as  $\lambda$  increases. However, the highly scattered data indicates that ultimate strength is a function of geometry proportions additional to this single parameter. This is further demonstrated by example comparative load shortening curves in Figure 77, which demonstrate the variability between sections for stiffeners with the same  $\lambda$ . This phenomenon is important to highlight, as the stiffener geometry may be important when defining the strength of the stiffened panel as a whole.

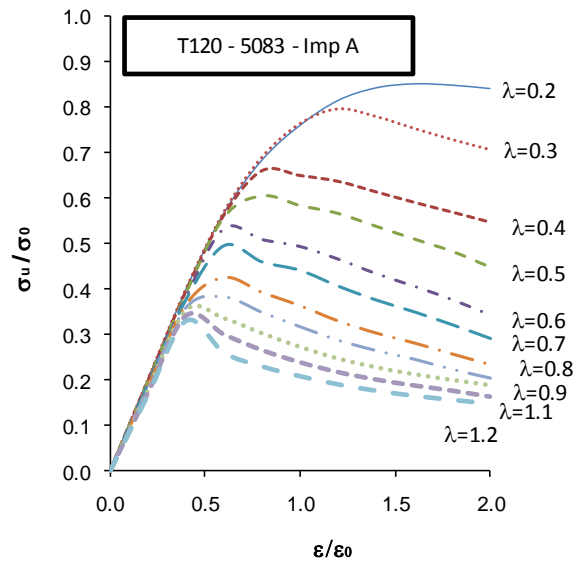


Figure 75 – Tee bar stiffener stress-strain curves , average imperfections, simply supported, varying length

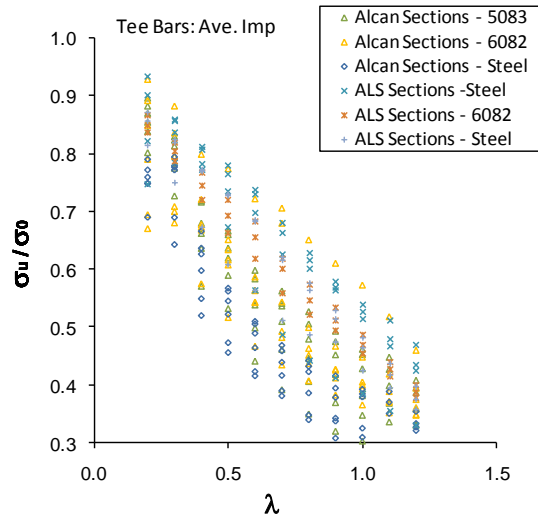


Figure 76 – Tee bar stiffener ultimate strengths vs.  $\lambda$ , average imperfections, simply supported

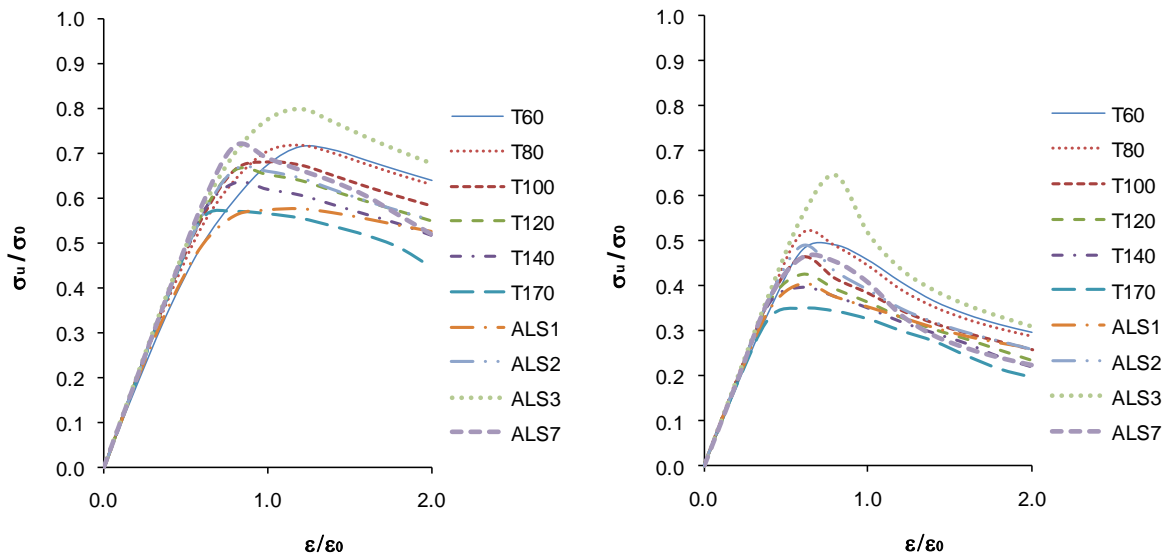


Figure 77 – Load shortening curves for  $\lambda=0.4$  (left) and  $\lambda=0.8$  (right) for different 5083-H116 tee bar stiffener cross sections with average imperfections

The plots indicate that the influence of the stiffener geometry on the ultimate strength can be better quantified to provide a more rational measure of stiffener ultimate strength. Therefore a further non dimensional cross section parameter is proposed which provides a better correlation between datasets, denoted by  $\gamma$  and defined as:

$$\gamma = \frac{h_w/t_f}{b_f/t_w} \lambda$$

The formula recognises that stiffener strength is adversely affected by increasing the stiffener height and decreasing the flange width. The resulting formulation is also multiplied by the column slenderness to give the new cross section parameter,  $\gamma$ .

The ultimate strength values from the stiffener datasets are plotted as a function of  $\gamma$  (Figure 78) and show a much closer correlation. The plot shows some separation between the aluminium and steel results indicating that the material properties are important in defining stiffener strength. Therefore separate regression lines, shown in Figure 88, are fitted through the aluminium and steel data respectively. The general form of the equation is inverse second order:

$$\frac{\sigma_{u,stiff}}{\sigma_0} = C_1 + \frac{C_2}{\gamma} + \frac{C_3}{\gamma^2} \quad 95$$

The coefficients,  $C_1$ ,  $C_2$  and  $C_3$ , depend on the stiffener material and the amplitude of imperfection and are summarised in Table 24. Further analyses were undertaken for different imperfection amplitudes and two rotational stiffness cases ( $K_\phi = 100\text{GN/m}$  and  $200\text{GN/m}$ ), and the regression formula coefficients are summarised in Table 24 –Table6. The regression formula is compared to all the actual data (over 1000 models) in Figure 80, and shows a reasonable correlation with a mean bias of 0.96 and COV of 10%.

**Table 24 – Coefficients for Eq. 95 for stiffeners with simple supports at the web – plate joint**

<i>Material</i>	<i>Rotational Support (GN/m)</i>	$C_1$	$C_2$	$C_3$
5083-H116	0	0.20	0.33	-0.04
6082-T6	0	0.15	0.34	-0.04
Steel	0	0.29	0.32	-0.04
5083-H116	100	0.36	0.27	-0.03
6082-T6	100	0.38	0.21	-0.03
Steel	100	0.29	0.33	-0.04
5083-H116	200	0.37	0.28	-0.03
6082-T6	200	0.40	0.21	-0.03
Steel	200	0.29	0.33	-0.04

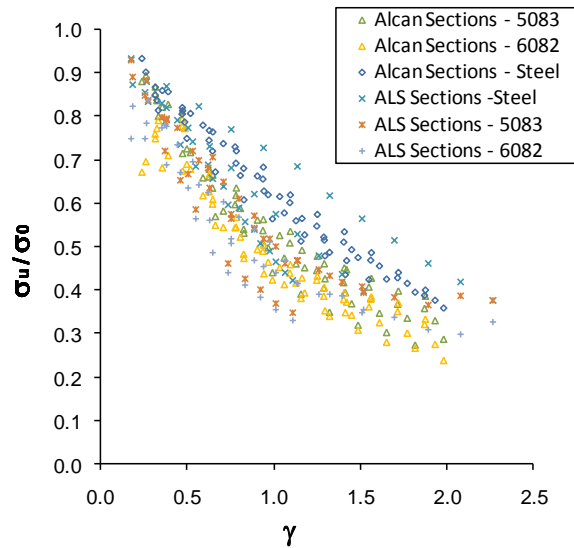


Figure 78 – Tee bar stiffener ultimate strengths vs.  $\gamma$ , all datasets, zero rotational stiffness

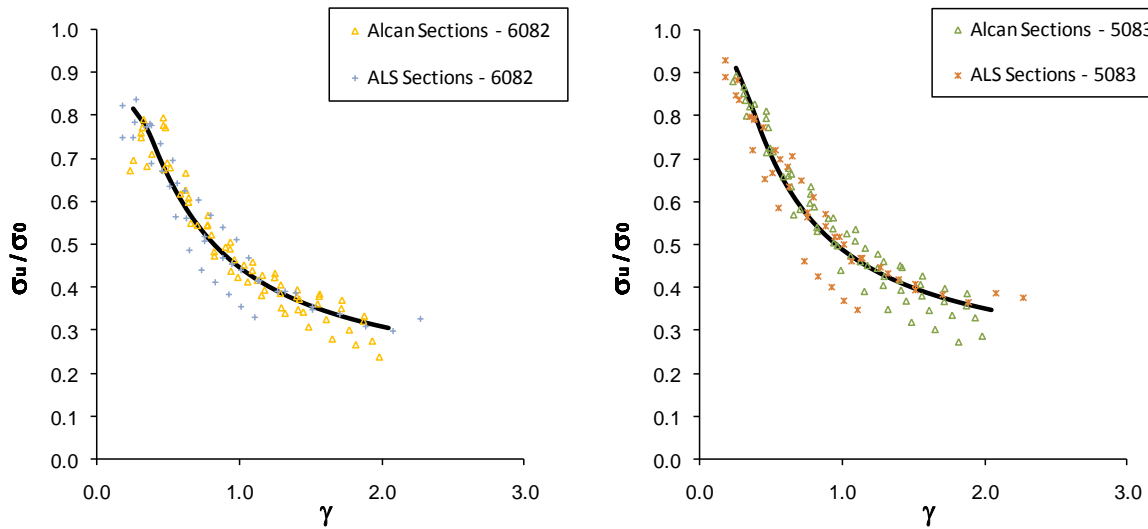


Figure 79 – Tee bar stiffener ultimate strengths vs.  $\gamma$ , A6082-T6 datasets (left) and A5083-H116 datasets (right), zero rotational stiffness, average imperfections

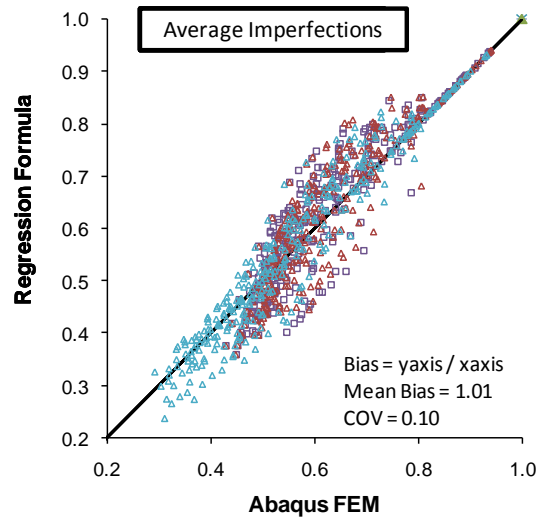


Figure 80 – Comparative performance of regression lines with the ABAQUS FEM predicted ultimate strength of tee bar stiffeners. All datasets, zero rotational stiffness, average imperfections

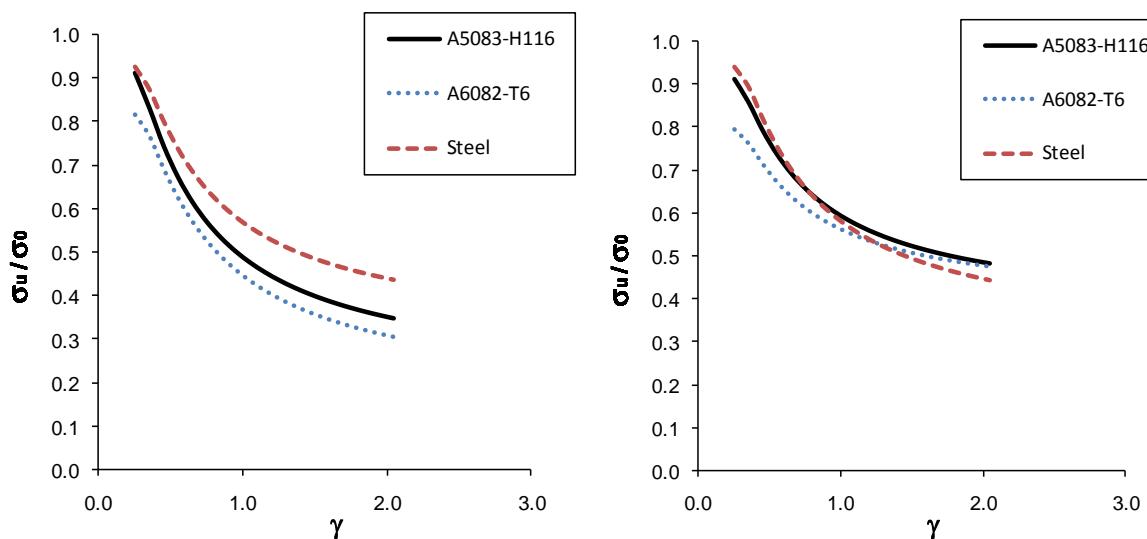


Figure 81 – Comparison of tee bar stiffener regression formulas for average imperfections and  $K_\omega=0$  (left) and  $K_\omega=200\text{MPa}$  (right)

The regression formula allows easy comparison of the effects of material, imperfection and rotational stiffness. Figure 81 presents a comparison of the three materials tested. The steel dataset shows a significantly higher strength as compared to the aluminium datasets with a simple support boundary condition at the web joint. However, the rotational stiffness has a greater effect in increasing the strength of the aluminium stiffeners, and thus the  $K_\omega=200\text{MPa}$  curves are much closer together, with the steel data demonstrating less strength than the equivalent aluminium. This is an interesting result; it suggests that the reduced stiffness of the aluminium stiffeners causes them to be more sensitive to the support conditions at the web joint. This may be due to an increased

susceptibility to stiffener tripping type buckling. This mode of collapse can be counteracted with a restraining moment created by the attached plating. Therefore the stiffener performance can be significantly improved by providing sufficient rotational restraint at the plate-stiffener connection.

The regression formula only predicts the ultimate strength of the stiffener. The shape of the load shortening curve is important when considering the progressive collapse behaviour of a stiffened panel. Figure 82 shows the complete load shortening relationship of stiffeners grouped as a function of  $\gamma$ . The plots are shown for zero rotational stiffness. The plots demonstrate the correlation of the ultimate strength as a function of  $\gamma$ , with a moderate amount of scatter between the curve peaks.

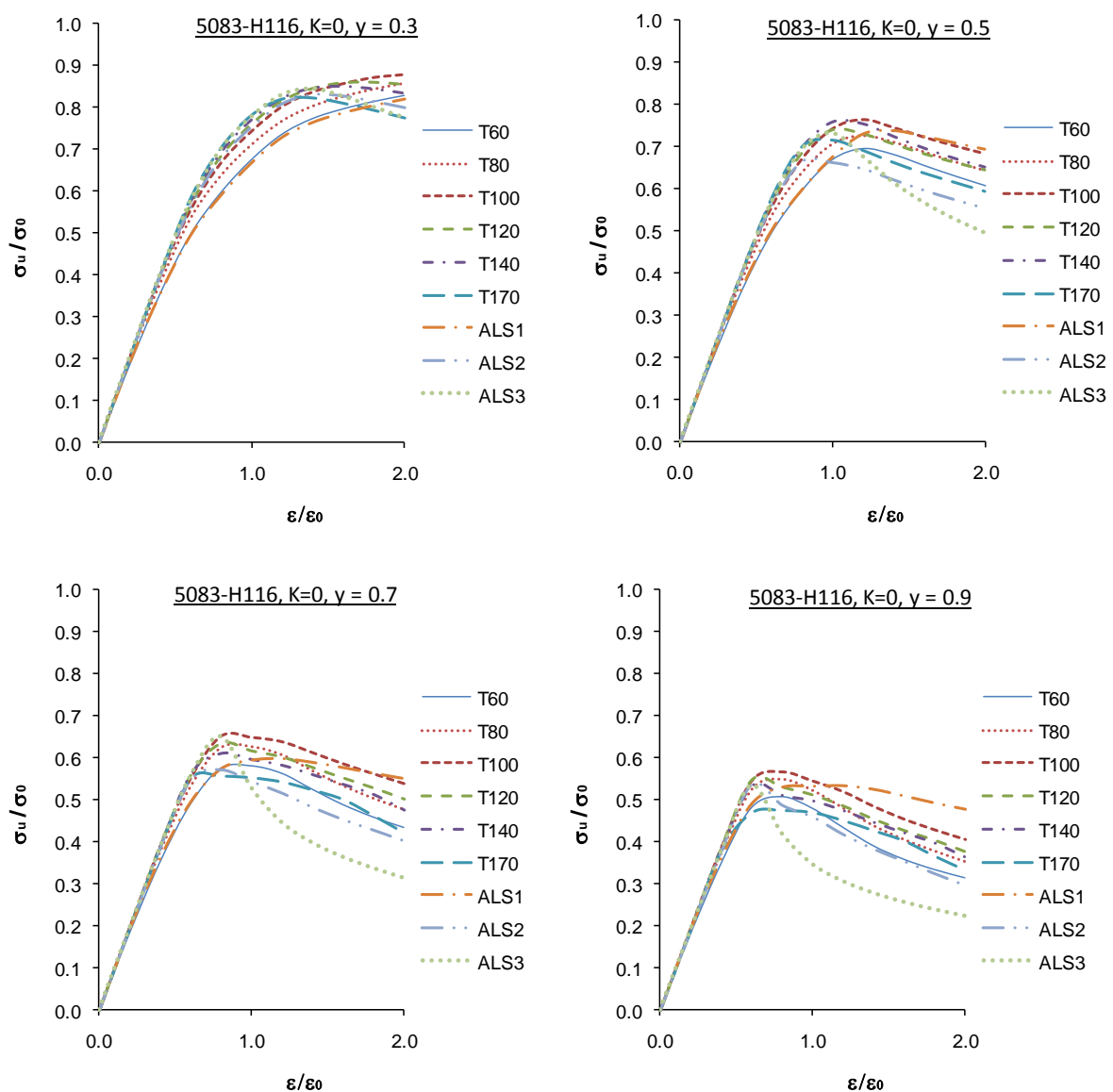


Figure 82 – Load shortening curves for  $\gamma=0.3$  (top left),  $\gamma=0.5$  (top right),  $\gamma=0.7$  (bottom left) and  $\gamma=0.9$  (bottom right) for different 5083-H116 tee bar stiffener cross sections and average imperfections.  $K_\omega = 0\text{GN/m}$ .

The plots also show that the load shortening relationship forms a similar pattern for all stiffeners. The initial curve gradient from the graph zero point is similar across all the stiffeners analysed. As the load approaches the ultimate strength the data begins to show some scatter. The general shape of the curve peaks differ to some extent, with some stiffeners such as ALS1 showing a very shallow peak whilst others, especially ALS3, exhibiting a very sharp peak. In the post collapse region most curves show a fairly linear negative gradient and although there is a moderate amount of scatter between the curves the gradients are generally similar. There are some exceptions, in particular for stiffener ALS3 which has a much steeper unloading characteristic over the range of  $\gamma$  tested.

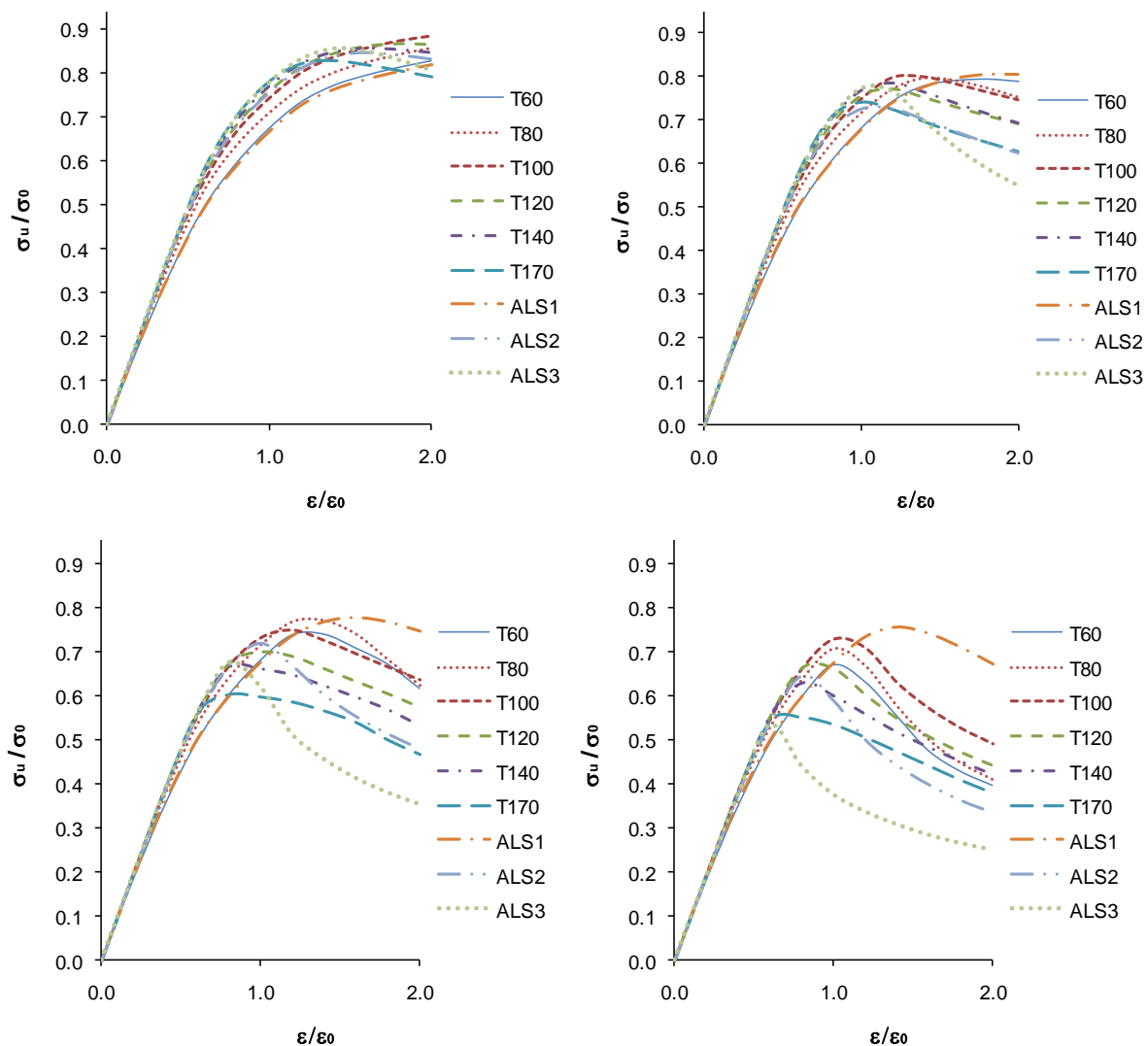


Figure 83 – Load shortening curves for  $\gamma=0.3$  (top left),  $\gamma=0.5$  (top right),  $\gamma=0.7$  (bottom left) and  $\gamma=0.9$  (bottom right) for different 5083-H116 tee bar stiffener cross sections and average imperfections.  $K_{\phi} = 100\text{GN/m}$ .

The results from analyses including a rotational stiffness at the joint of  $100\text{GN/m}$  are shown in Figure 83. The results show close comparison when  $\gamma$  is low. However, at  $\gamma=0.7$  and above, the results show

considerable scatter, with outlying curves such as for the ALS1 and ALS3 stiffeners which are markedly different.

Some of the variation between results can be attributed to factors which are not taken into account by the  $\gamma$  parameter. The influence of the HAZ and residual stress field as a function of the stiffener height has not been accounted for. The rotational stiffness is also shown to have a different effect on different stiffener cross sections, but this is not accounted for. The results indicate that a relationship does exist between the cross section and the resulting strength behaviour. The  $\gamma$  parameter goes some way to quantifying this, and accounting for more parameters may be able to further correlate the data into a general relationship.

For the present study, the correlation between datasets is reasonable and, considering that the stiffener only normally contributes 15-30% of the cross section of a vessel, the data is judged acceptable for use. Therefore, based on these analysis results, a representative curve dataset is derived, which is proposed as valid for an arbitrarily dimensioned tee bar stiffener. The dataset curves are calculated as the averaged curve shape through the individual stiffener results such as is shown in Figure 82 and Figure 83. An example curve set is shown in Figure 84.

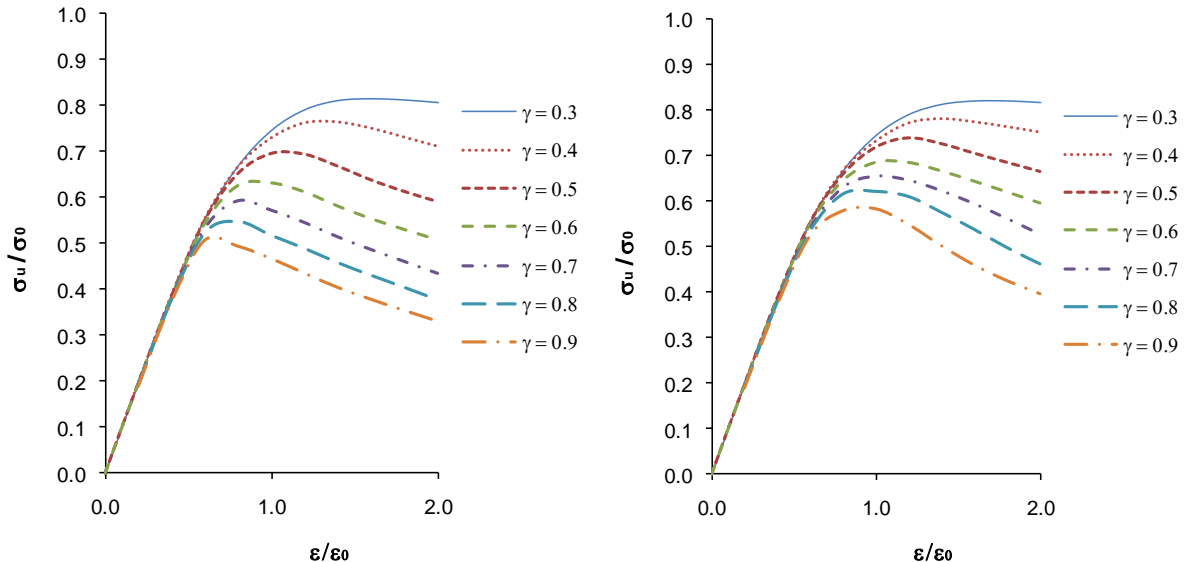


**Figure 84 – Representative 5083-H116 load shortening curves for an arbitrary dimensioned tee bar stiffener, average imperfections.  $K_{\omega} = 0$  (left) and  $K_{\omega}=100\text{GN/m}$  (right).**

These curve sets are suitable for implementation in the semi analytical method presented in Chapter 6. If a more accurate solution for a particular stiffener is required, recourse can be made to the individual datasets for a particular stiffener cross section. The fast solution time and automation of

the FEM analysis also means that a dataset for a different cross section can also be quickly generated. This is worth highlighting because the results presented here cover only a relatively small number of different cross sections, which have been selected as typical of ship fabrications. The use of cross sections which are substantially different to those studied here may demonstrate different characteristics and as such the data curves derived here may not be suitable.

### 5.5.2. Flat Bar Stiffeners

A parametric analysis procedure is carried out for a range flat bar stiffeners, with properties detailed in Table 25. The results for 5083-H116 stiffeners only are summarised in this section. The same approach as applied to the tee bar stiffeners is followed.

Table 25 – Summary of Flat Bar Stiffener Datasets

Dataset ID	hw	tw	$\lambda$	Rotational Stiffness	Imperfections	Total
F1	80	5	0.2 - 1.2	0	Slight Average Severe	12 (x3)
		6		100000		
		8		200000		
F2	100	5	0.2 - 1.2	“	“	12 (x3)
		6				
		8				
F3	120	5	0.2 - 1.2			12 (x3)
		6				
		8				
F4	160	5	0.2 - 1.2	“	“	12 (x3)
		6				
		8				

The resulting ultimate strengths show a similar scatter when plotted against  $\lambda$  (Figure 85). The cross section parameter as defined previously is not suitable for describing a flat bar, therefore a revised parameter,  $\gamma_f$ , is used which only accounts for the ratio of stiffener height to thickness:

$$\gamma_f = \frac{h_w}{t_w} \lambda$$

96

The plot of ultimate strength against  $\gamma_f$  demonstrates improved correlation (Figure 85) and a regression curve is fitted through the data. The general form of the regression line is as given by Eq. 95, with coefficients in Table 26. Similar regression lines are constructed for slight and severe imperfection amplitudes and for different rotational stiffness at the web–plate joint. The regression lines show a similar pattern as the tee bar stiffener results except that the influence of the rotational stiffness was found to be minimal (Figure 86). This indicates that rotational stiffness does not need

to be accounted for when using flat bar stiffeners as part of the semi analytical panel method described in Chapter 6. The data is also used to construct representative flat bar load shortening curves which are given as a function of  $\gamma_f$  as shown in Figure 87.

Table 26 – Coefficients for Eq. 95 for flat bar stiffeners with no rotational stiffness at the web – plate joint

Material	Imperfection	$C_1$	$C_2$	$C_3$
5083-H116	Slight	0.30	0.49	-0.10
5083-H116	Average	0.34	0.40	-0.09
5083-H116	Severe	0.22	0.57	-0.11

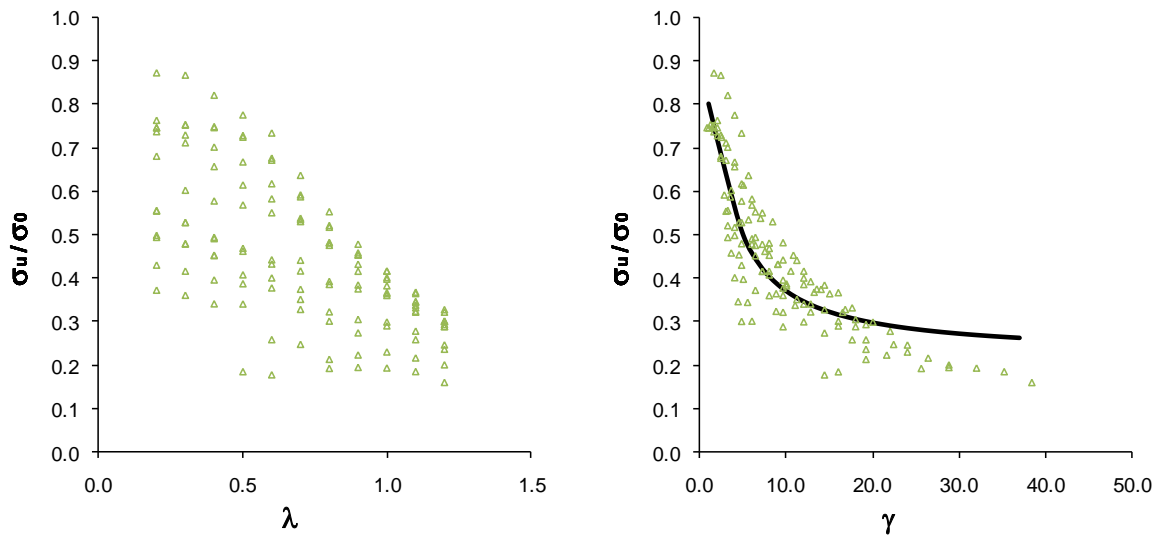


Figure 85 – Flat bar stiffener ultimate strengths vs.  $\lambda$  (left) and  $\gamma$  (right) , all datasets, zero rotational stiffness, average imperfections

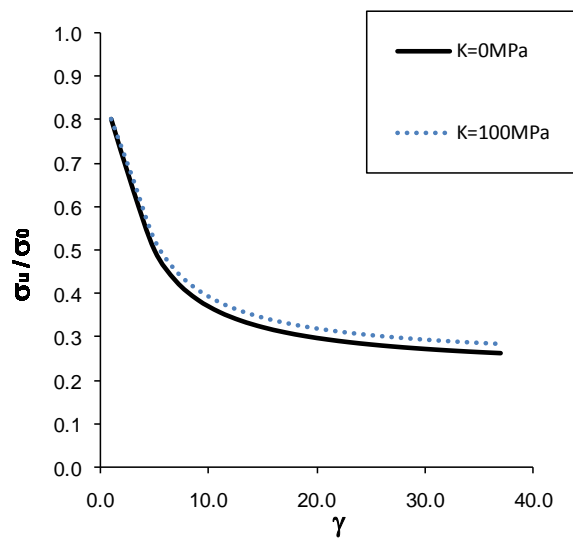


Figure 86 – Comparison of 5083-H116 flat bar stiffener regression formulas for average imperfections

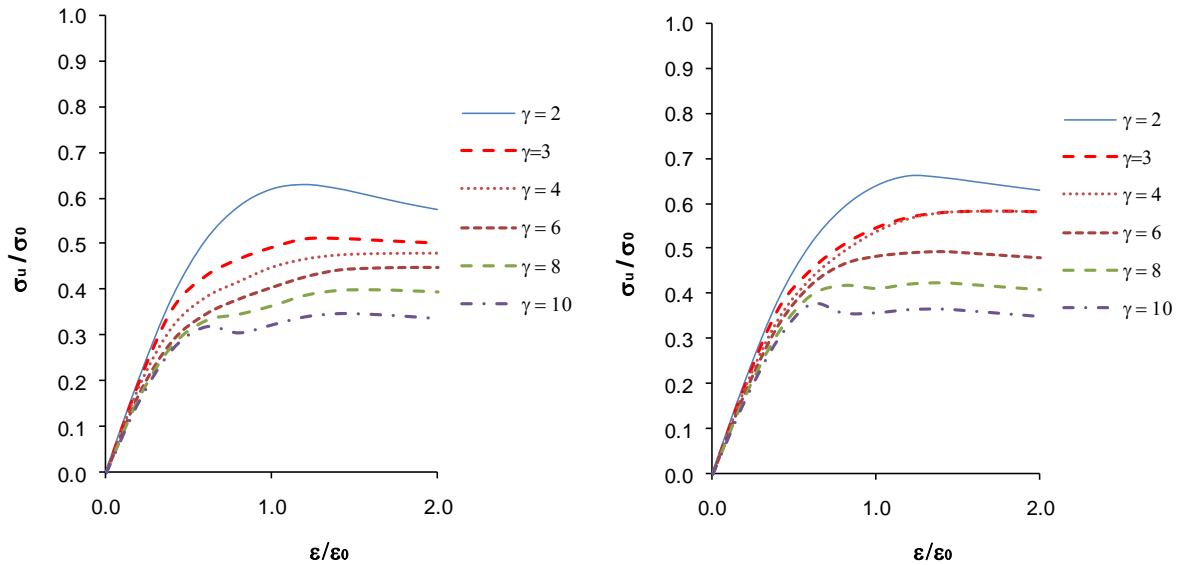


Figure 87 – Representative 5083-H116 load shortening curves for an arbitrary dimensioned flat bar stiffener, average imperfections.  $K = 0$  (left) and  $K=100000$  (right).

## 5.6. Analysis of Plate Stiffener Combinations

The performance of the proposed interframe PSC FEM is assessed by comparison with several experimental test datasets of panels under compressive in-plane load. The PSC is also compared to equivalent published numerical datasets and empirical formulae. The principle aim is to show the applicability of the PSC FEM model for developing a parametric database specific to aluminium. The study also highlights the limitations of the interframe buckling assumption and provides evidence to justify the study of orthogonal panels in the next section.

### 5.6.1. Introduction

Over the past century a substantial number of experimental tests have been undertaken and published to better understand strength and collapse behaviour of stiffened panels. The comparative studies detailed in this section are for only a small subset of the available data; they are chosen to demonstrate the applicability of the FEM model for different metal materials (steel and aluminium) and for a variety of panel cross sections.

A PSC is generally accepted to be an applicable representation of a continuous panel [SMITH], which includes multiple longitudinal stiffeners and several adjacent bays. The limitation, as discussed previously, is that the panel is assumed to collapse interframe, but the  $\frac{1}{2} + \frac{1}{2}$  bay representation means that the rotational effect between adjacent bays is still included. Therefore large scale multi bay panel experiments are of most use for validation. Of course, large scale tests are difficult and

expensive to conduct; thus there are only a few test datasets published in open literature. Details of large scale tests conducted at A.R.E. Dunfermline and Imperial College are widely available and discussed by Smith et al. [39], who use the results for validation of the FABSTRAN FEM model. This is particularly relevant to the present study, as FABSTRAN is linked to the NS94 progressive collapse method.

Smaller scale experimental test data is more widely available, and there have been several experiments concerned exclusively with ship type aluminium panels [22, 86, 87]. These experiments used single span panels, with end supports in the test rig used to represent the transverse frame. Whilst these tests are valuable for examining various buckling phenomena, they are not directly applicable to evaluating the strength of an equivalent orthogonal stiffened panel, for the same reasons as discussed previously for FEM modelling. They are therefore considered less suitable for comparing the performance of the  $\frac{1}{2}+\frac{1}{2}$  bay PSC model.

Nethertheless, a parametric study of welded aluminium panels recently completed at Pusan University (Paik et al. 2008) provides a substantial amount of experimental data. The test data has also been further validated by Collette et al (2011), who provide useful comparisons with various analytical methodologies. Therefore the database is re-analysed using the ABAQUS PSC model and compared directly to the test results and also to other analytical approaches.

There are also numerous FEM studies in literature, of which those most relevant to the present study have been summarised in Chapter 3. A benchmark study carried out by the 2009 International Ship Structure Committee III.1 [110] is a highly useful comparator of the FEM modelling approach used in this study.

### **5.6.2. Steel Panel Experiments**

The A.R.E. carried out 10 full scale steel panel analyses using 4 bay models with 10 tee bar longitudinal stiffeners with typical long stalk tee proportions [115]. Of the 10 panels, 6 are loaded in uniaxial compression only and are presented in this section. The other 4 panels are preloaded with a lateral pressure before applying uniaxial compression. Dorman and Dwight also conducted large scale tests on 12 orthogonal stiffened panels representative of box-girder bridge decks [91]. Eight panels were stiffened by bulb plates and the remaining 4 with flat bar stiffeners.

The FABSTRAN computer code is compared to the two experimental datasets in the paper by Smith et al. [39]. Two sets of FABSTRAN results are presented. The first use typical average imperfections (equivalent to ID A in Table 22), whilst the second set use the actual imperfection characteristics

measured during the experiments. A summary of the comparative results are presented in Table 27. The dataset is highly useful in that both the experiment data and the numerical code results can be compared to the present FEM models.

The panels are analysed with the PSC FEM model using typical average imperfections (A – Table 22) and residual stresses. The numerical results using average imperfections are compared to the experiments and the FABSTRAN average imperfection results in Figure 88. Results are also presented in Table 27 along with the non-dimensional slenderness ratios defining each panel.

The comparisons with the experiment data show that the FEM model is predominantly conservative (bias = 0.95). The data shows reasonable correlation, although the A.R.E. tee bar panels show very poor comparison. The closest correlation is with the Dorman bulb panels, which if compared in isolation show a mean bias of 0.99 and COV of 0.05. The overall COV, including all datasets, is relatively small (0.10). The second comparison shows close correlation between the FABSTRAN and ABAQUS FEM models, with mean bias of 0.97 and COV of 0.06. The tee bar and bulb results show very close correlation if analysed separately, with a mean bias of 1.0 and COV of 0.03.

Table 27 – Test Panel, FABSTRAN and PSC Experiment Results

ID	$\lambda$	$\beta$	Exp.	FABSTRAN Average Imperfection	FABSTRAN Actual Imperfection	ABAQUS Average Imperfection
<b>A.R.E. Tee Bar Panels</b>						
A.R.E.-1a	0.24	2.67	0.76	0.65	0.69	0.64
A.R.E.-2b	0.42	1.48	0.83	0.82	0.82	0.83
A.R.E.-3b	<b>0.70</b>	1.68	0.61	0.71	0.60	0.68
A.R.E.-4a	0.54	1.41	0.82	0.80	0.75	0.81
A.R.E.-5	0.45	3.31	0.72	0.51	0.55	0.56
A.R.E.-7	0.52	3.42	0.65	0.49	0.53	0.49
<b>Dorman Bulb Panels</b>						
Dorman-A1	0.28	1.47	0.90	0.86	0.76	0.86
Dorman-A2	0.30	1.94	0.68	0.76	0.68	0.74
Dorman-B1	0.28	1.47	0.88	0.86	0.77	0.86
Dorman-B2	0.31	1.98	0.70	0.77	0.68	0.73
Dorman-C1	0.27	1.22	0.94	0.89	0.80	0.90
Dorman-C2	0.28	1.49	0.87	0.86	0.77	0.86
Dorman-C3	0.29	1.84	0.81	0.79	0.70	0.77
Dorman-C4	0.28	1.24	0.90	0.88	0.79	0.89
<b>Dorman Flat Bar Panels</b>						
Dorman-A3	0.33	1.50	0.84	0.86	0.75	0.86
Dorman-A4	0.34	1.90	0.73	0.77	0.67	0.82
Dorman-B3	0.35	1.56	0.79	0.84	0.73	0.85
Dorman-B4	0.35	1.90	0.73	0.79	0.68	0.78

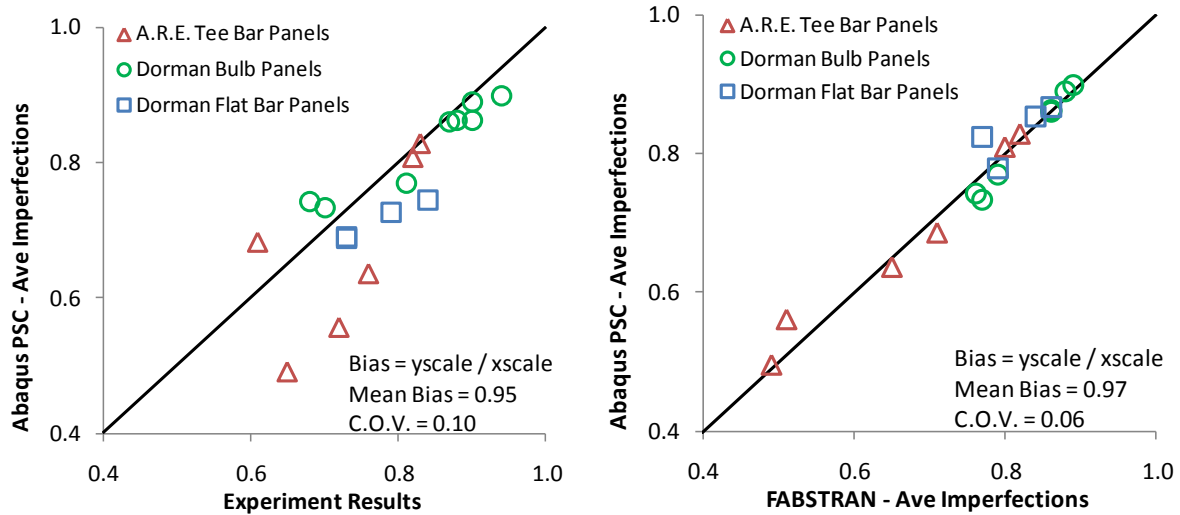


Figure 88 – Comparison of ABAQUS PSC model (average imperfection) with experimental data (left) and FABSTRAN (right)

In addition to the uniaxial test panels, Smith also tested four panels with a pressure load applied prior to the compressive load. These tests are repeated using the ABAQUS PSC model in the same manner as for the other test panels.

The ABAQUS predicted ultimate strengths are compared with the physical experiment results and the FABSTRAN average imperfection results (Figure 89). The ABAQUS model shows fairly good correlation to the experiment, with mean bias and COV both about equal to the non pressure cases analysed previously. FABSTRAN consistently predicts a lower strength compared to ABAQUS and the original experiments (Figure 90).

The results are fairly limited in scope. They provisionally indicate that the PSC model is adequate when dealing with lateral pressure. The PSC model slightly outperforms FABSTRAN in these few cases. It is likely that ABAQUS accounts for lateral pressure more rigorously as the plate is explicitly characterised in the FEM mesh.

Overall, the results suggest that the ABAQUS model is adequately predicting ultimate strength. Similar findings were drawn from the FABSTRAN results [39]. The comparison with FABSTRAN indicates that both approaches work in a similar manner, at least over the range of panels studied, and that the imperfection and residual stress modelling techniques used in the present study are valid. This demonstrates confidence in the larger scale orthogonal panel FEM tests, which use the same principal analysis techniques as the PSC model.

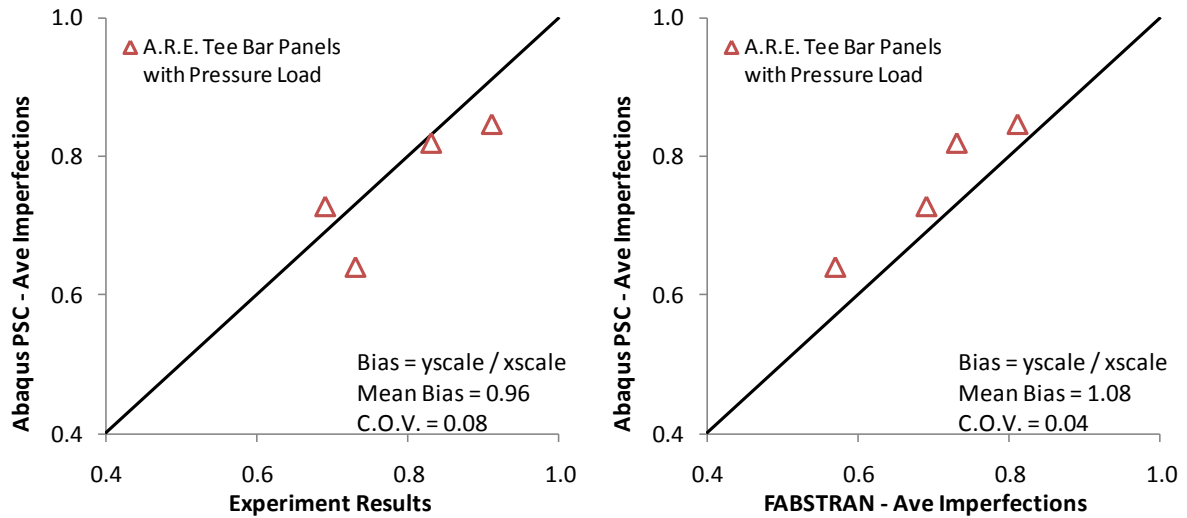


Figure 89 - Comparison of ABAQUS PSC model with experimental data (left) and FABSTRAN (right)

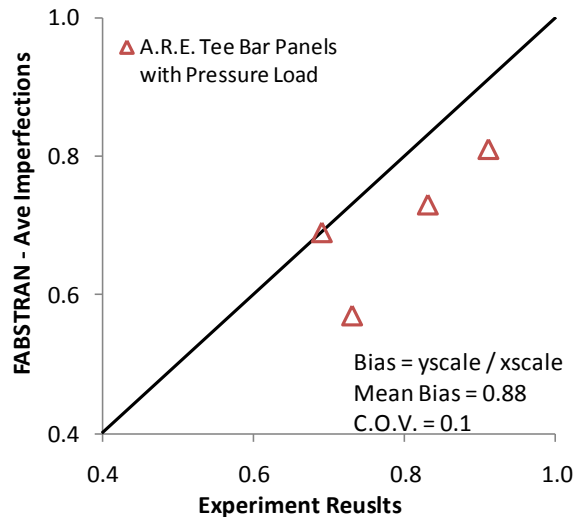


Figure 90 - Comparison of FABSTRAN with experimental data

### 5.6.3. ISSC2009 Benchmark Study

ISSC committee III.1 Ultimate Strength conducted an FEM benchmark study on a single bay stiffened panel constructed from steel. A  $\frac{1}{2} + \frac{1}{2}$  bay FEM model including 20 longitudinal stiffeners was analysed under various load conditions. The effect of the modelling approach and various prescribed conditions were investigated by different researchers on the ISSC panel. A number of different FEM software packages were used including ANSYS and ABAQUS. Factors affecting the panel strength were investigated, including geometric imperfections, residual stress and boundary conditions. The panel dimensions are listed in Table 28.

Table 28 – ISSC2009 Benchmark Panel Dimensions

<i>Dimension</i>	
Length	4300 mm
b	815 mm
$t_p$	17.8 mm
$h_w$	463 mm
$t_w$	8 mm
$b_f$	172 mm
$t_f$	17 mm
$\lambda$	0.303
E	205800 MPa
$\sigma_Y$	315 MPa

The average non dimensional ultimate strength under uniaxial and biaxial compression scenarios are published in ISSC. The imperfection characteristics differ significantly from the “average” levels as used in previous sections and are detailed in Table 22. The ISSC report highlights the sensitivity of the panel to imperfection both in terms of pattern and amplitude. Residual stresses are not included in most of the analyses; instead the effect of residual stress is treated in a separate investigation.

The fundamental comparative analysis in the ISSC study is a simple supported panel at all four edges and with baseline model parameters as reported. The average ultimate strength under uniaxial compression is 0.818, with a small variation (between -1.7% and +2.6%) over the different analyses conducted. A further ISSC analysis using model extents of one stiffener with attached plating shows a slightly reduced strength of 0.79.

In close comparison, the ABAQUS PSC model developed in this study also predicts an ultimate strength of 0.79. A full width model equivalent to the ISSC panel is also tested and results are close to the ISSC study.

Table 29 – ISSC Panel ultimate strength under uniaxial compression. Panel edges simply supported.

<i>Model</i>	<i>Imperfections (see Table 4)</i>	<i>Ultimate Strength</i>
ISSC full width model	ISSC	0.82
ISSC PSC model	ISSC	0.79
ABAQUS full width model	ISSC	0.81
ABAQUS PSC model	ISSC	0.79
ABAQUS PSC model	“average”	0.69

The model is also re-analysed using the “average” imperfection and residual stress characteristics. The predicted ultimate strength reduces by approximately 10% to 0.69. A comparison of the load

shortening curves is presented in Figure 91. The “average” imperfection is slightly more severe and, along with the inclusion of residual stress, means that there should be a negative effect on ultimate strength as compared to the ISSC result.

The comparative analyses with the ISSC 2009 benchmark study demonstrate the validity of the FEM modelling approach and further highlight the applicability of a PSC model to modelling a panel under uniaxial longitudinal compression. The study also shows the limitations of a PSC model in modelling a panel under biaxial compression. A full representation of the panel is recommended to accurately model biaxial load conditions.

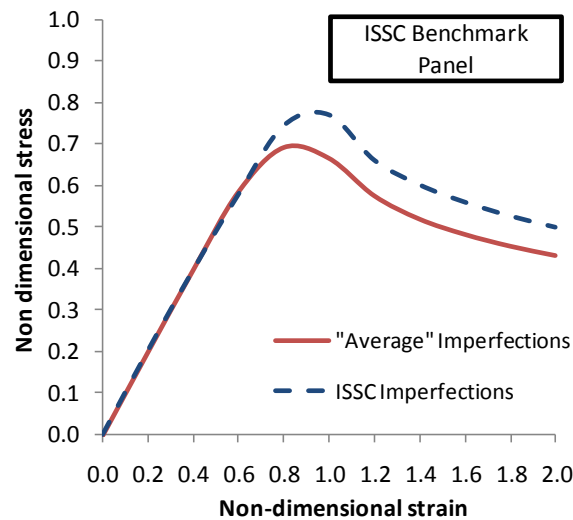


Figure 91 – FEM load shortening curves for the ISSC 2009 benchmark panel. Comparison of imperfection patterns.

#### 5.6.4. SSC451 Aluminium Panels

The 76 aluminium panels detailed in SSC report 451 [22] are re-analysed using the ABAQUS PSC model. The PSC model is not an exact replication of the test setup. As noted previously, the majority of the SSC experiments use single bay panels with a roller bearing to represent the connection to the transverse panel. The roller bearing is positioned at the elastic neutral axis of the panel. However, because of imperfection and subsequent buckling effects, the zero stress line through the panel cross section moves, and thus the roller bearing can induce eccentric loading into the panel [86].

Table 30 – Comparison of methods to predict SSC451 panel strength

<i>Model</i>	<i>Bias</i>	<i>COV (%)</i>
SSC451 FEM (All panels)*	1.06	8.8
SSC451 FEM (Tee Bars only)*	1.07	12.5
Paik and Duran [19]	1.10	21.4
Wang et al. [116]	1.07	15.0
Hughes [117]	1.09	15.2
Aluminium Association Method	1.20	16.0
Aluminium Association Method (80% $\sigma_0$ )	1.12	15.0
<b>ABAQUS PSC (All panels)**</b>	<b>0.94</b>	<b>23.0</b>
<b>ABAQUS PSC (Tee Bars only)**</b>	<b>1.06</b>	<b>11.0</b>
<b>Absqus PSC (Flat Bars only)**</b>	<b>0.74</b>	<b>30.0</b>

\* 2 bay FEM model with column imperfection in the plate direction (CIS). Actual measured imperfections.

\*\*  $\frac{1}{2}+\frac{1}{2}$  bay FEM model with “average” imperfections (A in Table 22)

Collette et al. [118] provide detailed comparative analysis of the SSC data with a number of analytical methods including the Paik and Duran regression formula, ABS panel buckling formulae and Hughes’ beam column method. The tee bar panel results show smaller bias and COV (1.06 and 11.0%) as compared to all the analytical methods computed by Collette (Table 30). In common to the analytical methods, the PSC model shows a tendency to over predict the panel strength. The COV is similar to the steel panel comparison discussed previously.

The tee bar results show a similar bias and COV as compared to the SSC FEM results (1.07 and 12.5%). This was first thought a little surprising, as the FEM models have significant differences. The SSC analyses use an FEM model replicating the actual panel setup along with a Fourier representation of the actual measured imperfections. In comparison, the ABAQUS PSC model is a  $\frac{1}{2} + \frac{1}{2}$  bay representation and standard average imperfections are imposed. Nevertheless, it was found that the different modelling approach produces fairly similar results. This is further highlighted by comparing the FEM models directly (Figure 93), which shows negligible mean bias and a fairly tight COV of 7.0%.

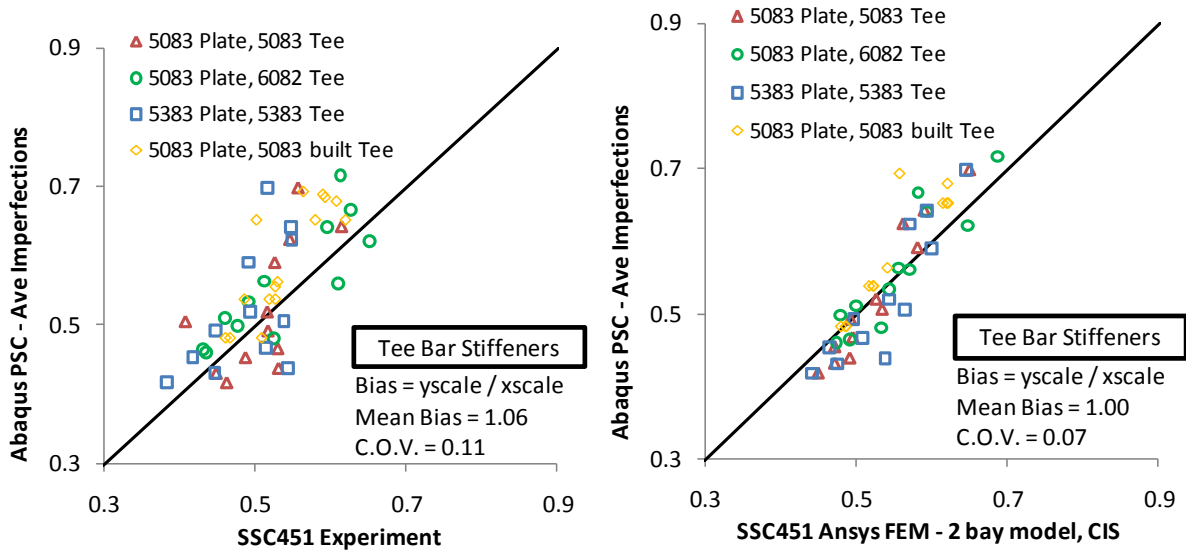


Figure 92 – Comparison of ABAQUS PSC model with SSC451 experimental data (left) and FEM analyses (right)

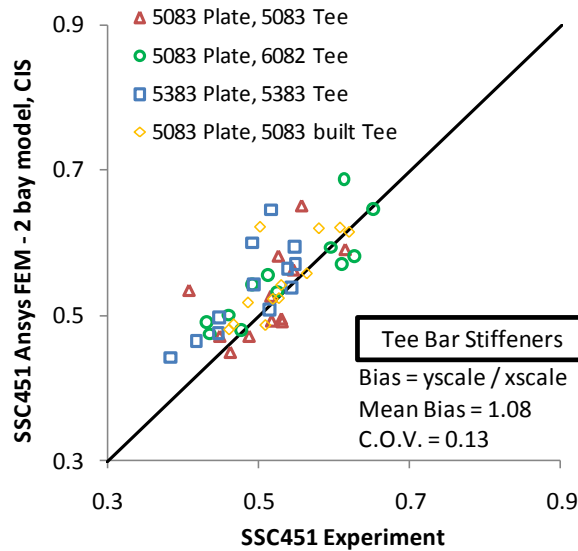


Figure 93 – Comparison of SSC451 ANSYS model (2 bay CIS) with SSC451 FEM analyses – tee bar stiffeners

In contrast to the tee bar results, the ABAQUS flat bar panel analyses demonstrate a very poor correlation with the experiment data and the equivalent SSC FEM (Figure 94). When comparing the PSC model with the experiment Tee data the mean bias is 0.74 with COV of 30%. Thus the PSC model predominantly under predicts the panel strength. The most severe under predictions are for the panels with smallest stiffeners (and hence largest column slenderness). The PSC model shows even worse correlation in comparison with the SSC numerical results, with a mean bias of 0.72 and COV of 34%.

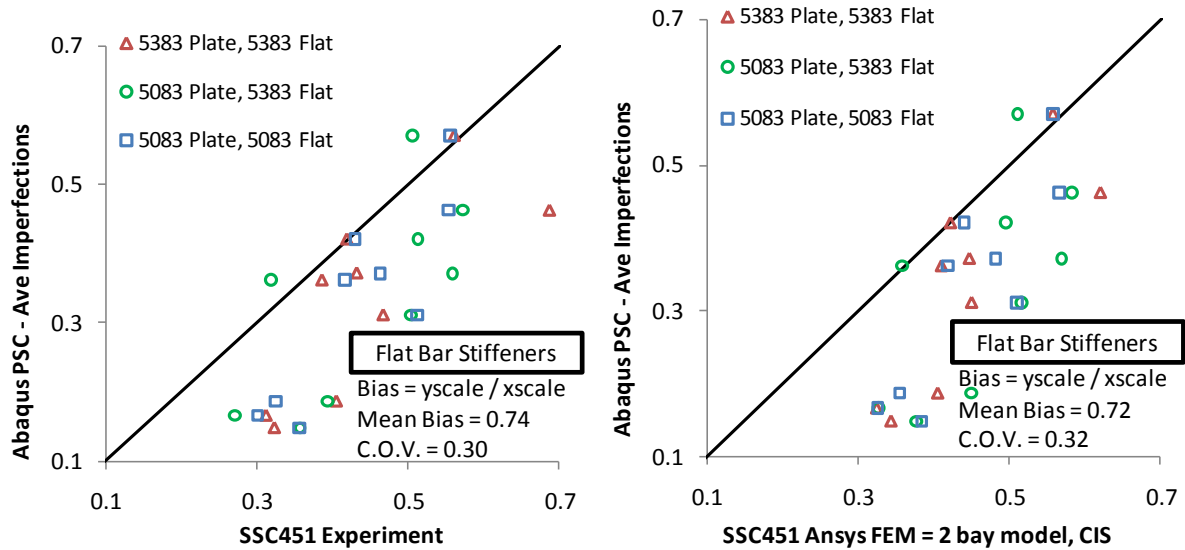


Figure 94 – Comparison of ABAQUS PSC model with SSC451 experimental data – flat bar stiffeners

### 5.6.5. A.R.E. Steel Panel Column Collapse Curves

The comparison with experimental data has shown that the PSC FEM model is an adequate tool for predicting the ultimate strength of a stiffened panel buckling interframe. In this section PSC FEM analyses are compared to steel panel column collapse curves published by Chalmers [76] and expanded upon by Smith [39]. A series of equivalent column collapse curves are then developed for standard tee bar and flat bar stiffened aluminium panels. The effect of different stiffener cross sections is also shown, drawing on the stiffener isolation analysis work previously. The results presented in this section indicate that standard curve series are limited to specific cross sections.

The reason the column collapse curves are of interest is because they are used in existing progressive collapse programs. For example, the NS94 version of the progressive collapse method makes recourse to standard data series for defining the load shortening curves of each element. They also form the background to UK naval design charts, developed by the A.R.E. and published internally and then in open literature by the Ministry of Defence [76]. The charts are in the form of column collapse curves, which show the relationship between ultimate strength and the slenderness ratios defining the panel. The curves are defined for different area ratios ( $A_s/A$ ) and three levels of imperfection consistent with slight, average and severe amplitudes as defined previously in this thesis.

The curve datasets are partially developed from a series of numerical analyses using the FABSTRAN program, which is described by Smith et al [39]. FABSTRAN is also incorporated into the NS94

program. Therefore a comparison between the design curves effectively compares the current FEM approach with FABSTRAN.

A subset of the original design curves are compared with ABAQUS FEM analyses using the same PSC model as described previously. The analyses cover four plate slenderness ratios ( $\beta=1.5, 2.0, 2.5$  and  $3.0$ ) and column slenderness between  $0.2$  and  $1.2$ . The FEM analyses use the same panel dimensions, imperfection properties and residual stress distribution as detailed by Smith [39] and Chalmers [76]. The stiffener is an Admiralty long stalk #2 (ALS2) and the plate is sized to give an  $A_s/A$  ratio of  $0.2$ . Average geometric imperfections and residual stresses are modelled (Table 22), which are equivalent to those used by the A.R.E. in the production of the average datasets.

The ultimate strength from each PSC FEM analysis is output and used to construct column collapse curves equivalent to the original datasets. Second order polynomial regression lines are plotted through the raw data, which show a reasonable close trend through the entire data range. The curves are compared in Figure 95.

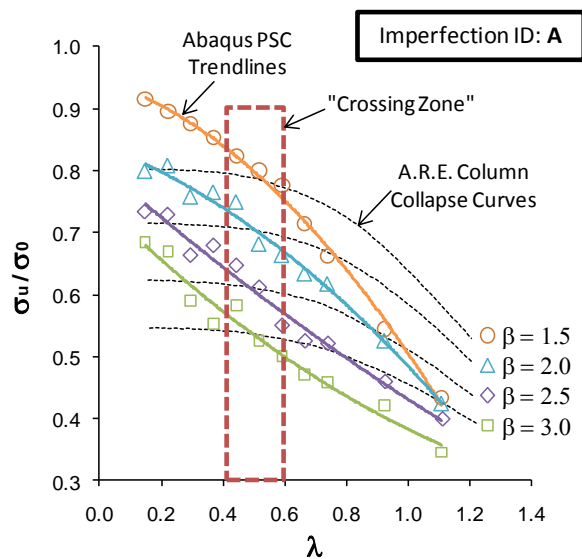


Figure 95 - Steel panel column collapse curves, comparison of FEM with A.R.E. curves

The results show a marked difference between the two sets of data curves. The PSC FEM generated curves are steeper, predicting higher strength for short panels (small  $\lambda$ ) and lower strength for longer panels (large  $\lambda$ ) as compared to the A.R.E. data.

These results are interesting because the previous sections showed that the PSC FEM model generally correlated closely to FABSTRAN results. However, closer inspection of Figure 95 shows that the comparative curves intersect at a similar  $\lambda$  (between  $0.4$  and  $0.6$ ), as highlighted by a “crossing zone”. Within this zone the FEM data shows similar ultimate strength values to the A.R.E. data. The

majority of the A.R.E. experiments compared in the previous section are for panels within or near the  $0.4 < \lambda < 0.6$  zone and therefore provides some explanation as to why, whilst the comparison with experiment and FABSTRAN results show close correlation, the column collapse curves do not.

The disparity between the curve data outside the “crossing zone” may be due to a number of fundamental differences in the numerical approaches (i.e. ABAQUS and FABSTRAN). Although it is difficult to critique the approaches directly, particularly as FABSTRAN is not available to this study, some attempt is made to justify this significant variation between methods.

One fundamental difference between the numerical approaches is the way the attached plating is represented. In ABAQUS, the plate is explicitly included as part of the meshed model. Symmetry boundary conditions are used to represent the repeating arrangement of plates and stiffeners. The plate’s buckling behaviour during the analysis will also influence the rotational stiffness of the joint between plate and stiffener. The out of plane constraint on the plate edge is provided by the stiffener. Therefore, if the stiffener does not provide complete lateral constraint due to beam-column buckling or stiffener tripping, the plate boundary is affected.

In contrast, FABSTRAN models the plate implicitly by assigning plate load shortening stiffness properties to a single “element” at the base of the stiffener. It is unlikely that rotational stiffness provided by the plate to the stiffener is accounted for. Furthermore, and perhaps more importantly, the change in the plate buckling capacity due to a change in the edge boundary condition cannot be accounted for because the plate properties are predefined from the load shortening curve, which assumes continued simple supports at the plate edges throughout the analysis.

This is demonstrated in plots of the collapse for two example panels as shown in Figure 96. Both panels have a stocky plate ( $\beta=1.5$ ). The column slenderness of the left hand panel is low ( $\lambda=0.3$ ) whilst the right hand panel is very slender ( $\lambda=1.0$ ). The stocky panel shows typical plate buckling together with relatively slight out of plane deflection of the plate-stiffener. In contrast, the slender panel shows very little deflection in the plate compared to the large degree of out of plane translation in the mid region of the bay.

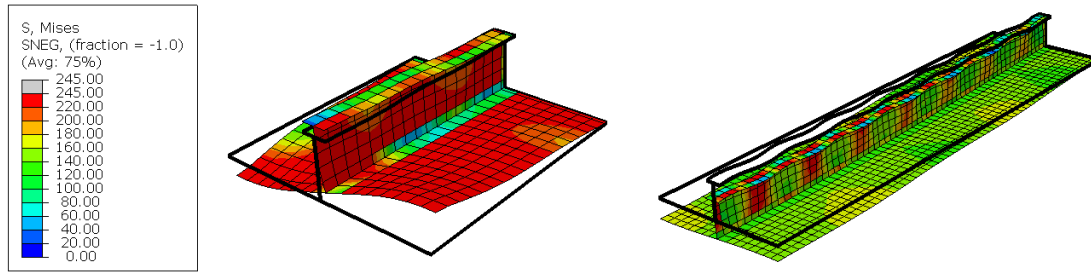


**Figure 96 – FEM of a short PSC panel (left) and long PSC panel (right) under peak ultimate strength uniaxial compression.  $\frac{1}{2}+\frac{1}{2}$  bay representation - only a single  $\frac{1}{2}$  bay is shown. Displacement magnification=10.**

In many ways the FABSTRAN FEM model has similar boundary conditions as the stiffener isolation model used in this study. Therefore, a replication of the FABSTRAN approach is to proportionally sum the appropriate plate strength with the stiffener strength derived in section 5.5. The relative influence of each component is assumed as a proportion of its respective area. This means that if the ratio  $A_s/A$  is increased, the relative influence of the stiffener component load shortening curve is also increased. Rather than taking the ultimate strength of each component, a better approximation is to sum the entire load shortening curves. This procedure is described in further detail in section 6.3.2, as it forms the component strength part of the semi analytical method as derived in that Chapter.

The resulting datasets using this procedure are shown in Figure 97 and demonstrate a much closer agreement to the original column collapse curves. The curve gradients are similar throughout the column slenderness range. For  $\beta=2.0$  and above the ultimate strengths correlate closely. The panels with stocky plates show an increased strength as compared to the original data, which is likely due to the different definition of the plate. FABSTRAN utilises square plate load shortening curves whilst this study uses long plate data. As shown in Chapter 4, this has a greater effect in stocky panels where the differences between square plate and long plate curves are more significant.

These results indicate that the effect of the boundary support on the plate is critical in determining the panel strength. The boundary cannot necessarily be assumed to remain as a simple support throughout the load-shortening range; instead the out of plane deflections of the beam-column can affect the effective strength of the plate component. This is particularly significant at high column slenderness, where the beam column is shown with significant lateral deflection prior and at the collapse point. This conclusion is significant for the development of the semi analytical method and the findings from these analyses are discussed further in Chapter 6.

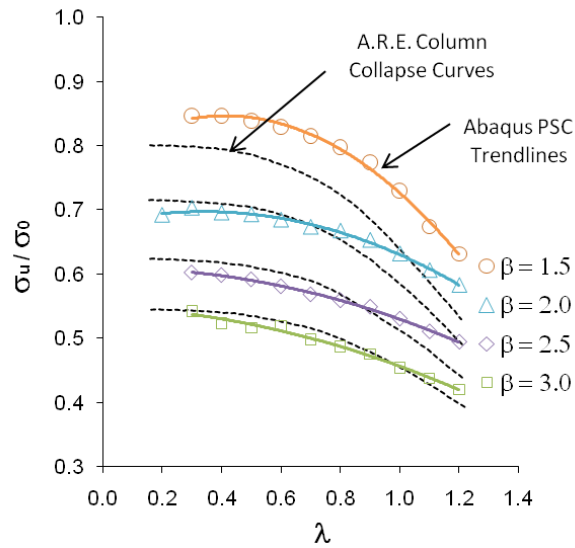


Figure 97 - Steel panel column collapse curves, comparison of FEM

### 5.6.6. Aluminium Panel Column Collapse Curves

The PSC FEM approach is used to calculate a parametric series of standard aluminium panel datasets with a range of plate and column slenderness ratios. The parametric study is used to investigate the factors of influence including:

- Imperfection amplitude;
- Material properties and Heat Affected Zone;
- Stiffener cross section.

In a similar manner to the plate studies presented in Chapter 4, the parameters are compared to a standard panel set. The complete curve sets are presented in Figure 98 and are computed using Alcan T120 stiffened panels with  $A_s/A=0.2$  and three imperfection levels as defined in Table 22. Curves for 5083-H116 and 6082-T6 alloys are given, with properties as defined previously. Most datasets are completed for a range of column slenderness between 0.2 and 1.2 with increments of 0.1. The plates are sized to give slenderness values of  $\beta = 1.5, 2, 2.5$  and 3.

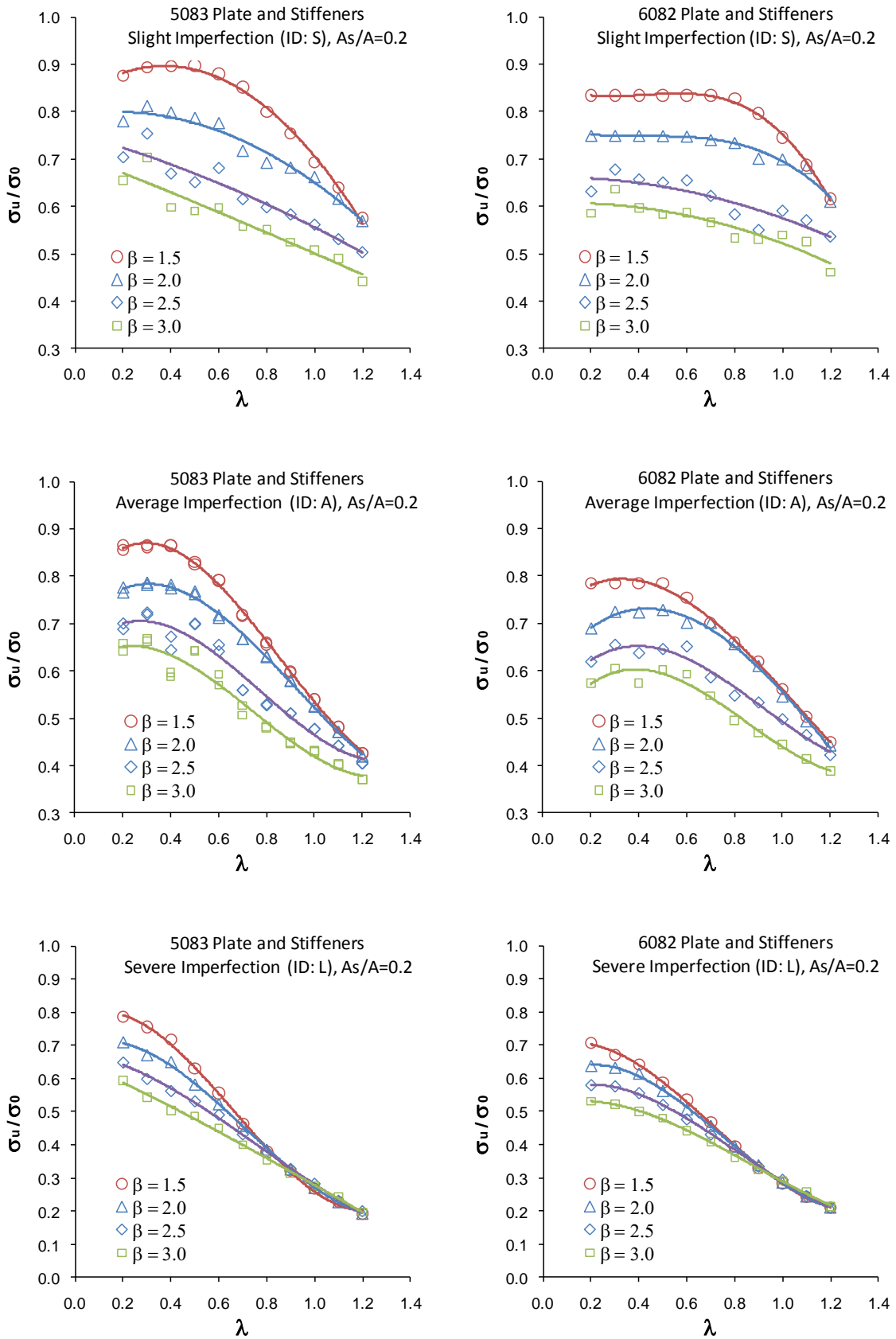


Figure 98 – 5083 (left) and 6082 (right) column collapse curves,  $A_s/A=0.2$

### 5.6.6.1. Imperfection Amplitude

The standard curve sets in Figure 98 clearly demonstrate the negative influence of increased imperfection amplitude on the ultimate strength of the stiffened panels. This is also shown in the plots of Figure 99, which show percentage change in strength due to the use of different imperfection levels. The effect is most pronounced at higher values of  $l$  and for lower values of  $b$ , where the slight imperfection causes an increase in strength by up to 30% and severe imperfection causes a corresponding decrease in strength of up to 55%. At lower column slenderness the effect of imperfection is much less, and in certain cases the difference between slight and average levels are negligible.

Another observed effect of different imperfection amplitude seen in Figure 98 is to change the relative difference between different plate slenderness curves. The results indicate that when imperfection is small, the plate slenderness is a critical factor in determining the overall plate strength. With increased levels of initial imperfection, the difference between curve sets is reduced, particularly at high column slenderness, indicating that the imperfection has a larger influence compared to the actual thickness of the plating.

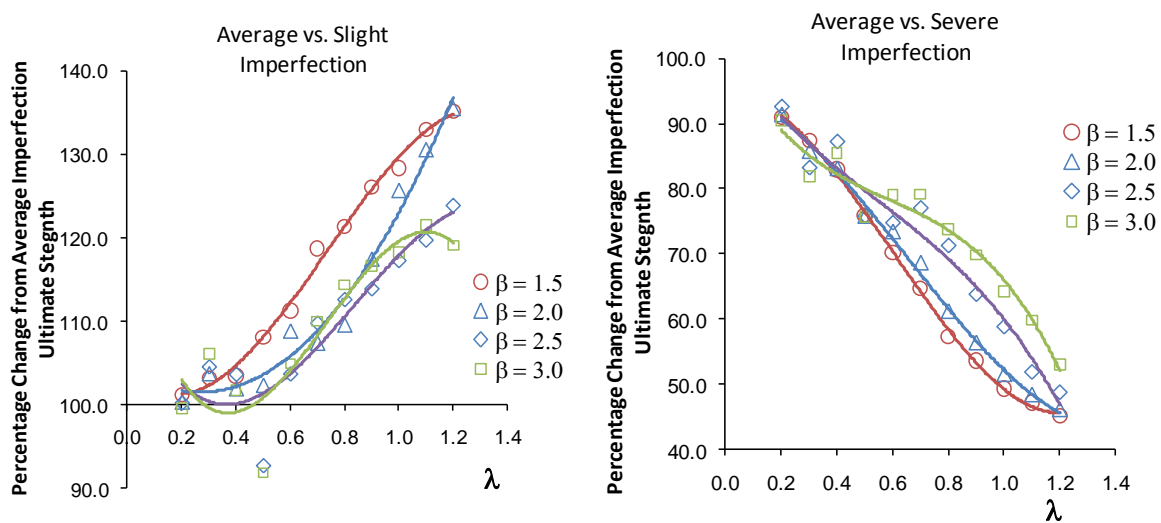


Figure 99 – Percentage difference between average imperfection ultimate strength with slight (left) and severe (right) imperfection amplitudes – 5083-H116 panels

### 5.6.6.2. Material Properties

Four material types for the panel cross section are compared: A5083-H116, A6082-T6, Steel ( $\sigma_y=235\text{MPa}$ ) and a hybrid panel with A5083-H116 plate and A6082-T6 stiffener. The results are presented in Figure 101. These show that the aluminium panels are almost always non-dimensionally stronger than their equivalent steel counterpart. The exception is at very low column slenderness. Above  $\lambda=0.3$  the aluminium panels demonstrate up to 15% additional strength in the range studied.

The differences between the aluminium alloys are less distinct. A5083-H116 performs best at low column slenderness whilst the A6082-T6 alloy is relatively better when the panel is longer. The A6082-T6 panel performance dips markedly at low slenderness, which is likely due to the influence of the transverse HAZ zone at the frame joint, which was shown previously (see Chapter 4) to cause a significant reduction in plate strength at lower slenderness. The strength reduction in the 6082 panels is universal throughout the range of plate slenderness' tested, suggesting that the effect also occurs in the stiffener HAZ zone adjacent to the frame. Although difficult to pick up visually in the FEM post processor, Figure 100 provides some evidence of localised buckling within the HAZ of a short panel.

The hybrid panel with 5xxx series plating and a 6xxx series stiffener is typical of some structural configurations. This demonstrates characteristics of both the other alloy configurations tested, with comparatively good performance at higher slenderness and less strength reduction at low slenderness as compare to the A6082-T6 panel.

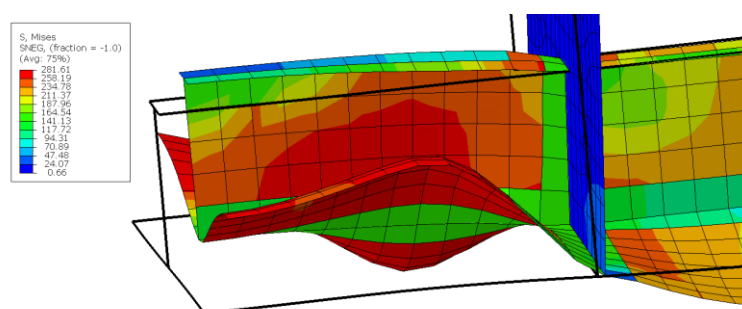


Figure 100 – A6082-T6 PSC model,  $\lambda=0.3$ ,  $\beta=2.0$ , post collapse, showing local HAZ buckling at the transverse joint

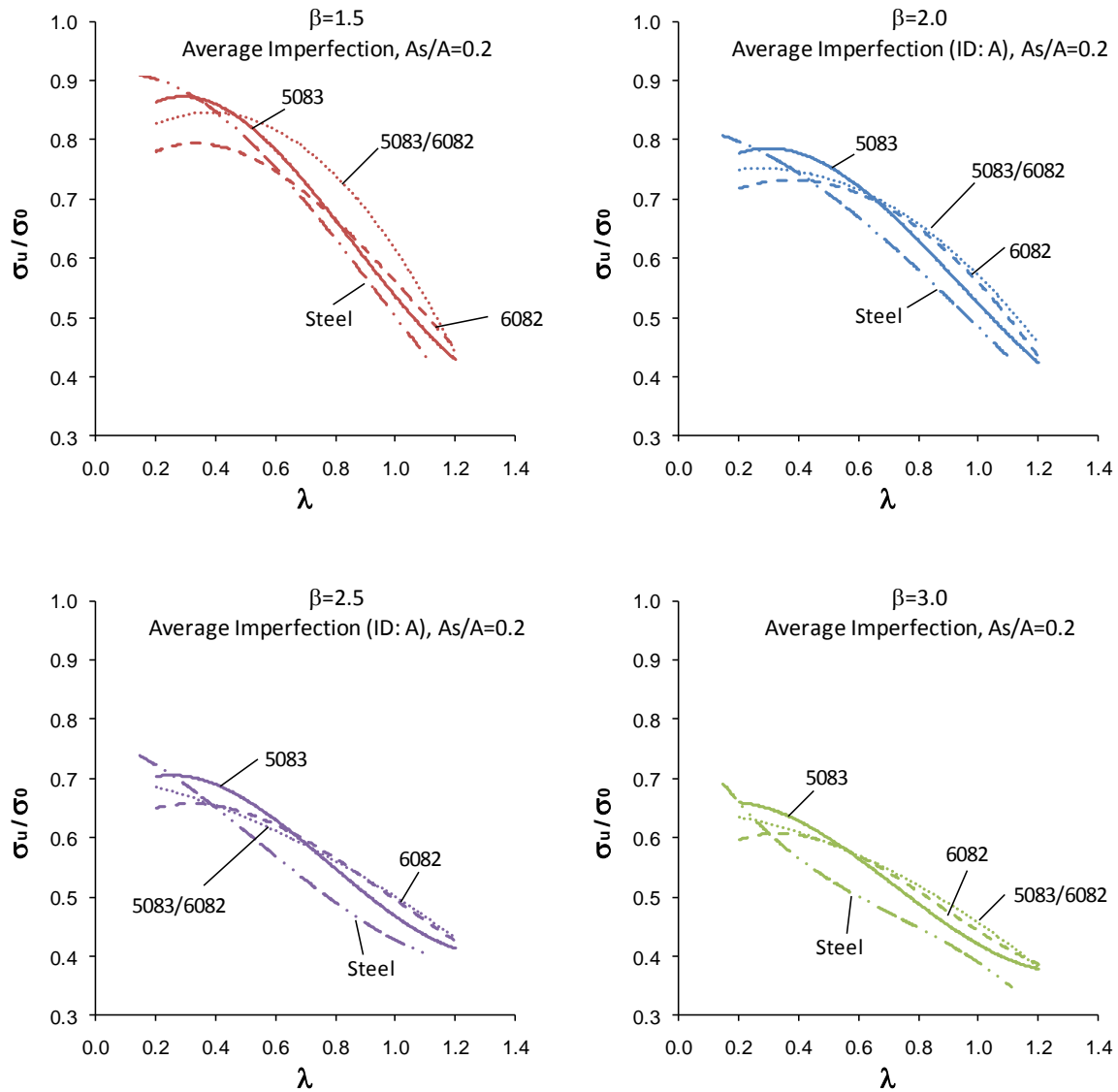


Figure 101 – Comparison of 5083-H116, 6082-T6 and steel column collapse curves,  $A_s/A=0.2$

### 5.6.6.3. Stiffener Cross Section

The stiffener isolation analyses presented in the previous section of this thesis indicated that stiffener behaviour in compression cannot be solely defined as a function of the column slenderness. The two main factors investigated are the rotation stiffness at the joint between the stiffener and the plate and the properties of the cross section.

There is also variation in the ultimate strength and load shortening characteristics of PSCs with the same  $\lambda$  and  $\beta$  values. However, the differences between different panels are less than for the stiffener in isolation. This is because the stiffener only makes up a small proportion of the total PSC cross section.

Example load shortening curves are presented in Figure 102 and Figure 103 for panels with column slenderness of 0.4 and 0.8 respectively. The ultimate strength generally varies by about 10% and tallies reasonably with the  $\gamma$  parameter defined in the previous section. The lower bound result is generally for the T170 panel, which also has a high  $\gamma$  of 3.58. The upper bound is generally the T80 panel, which also has the lowest  $\gamma$  between the panels tested of 2.15. These findings support the potential use of  $\gamma$  as an additional parameter in the determination of panel ultimate strength using analytical methods.

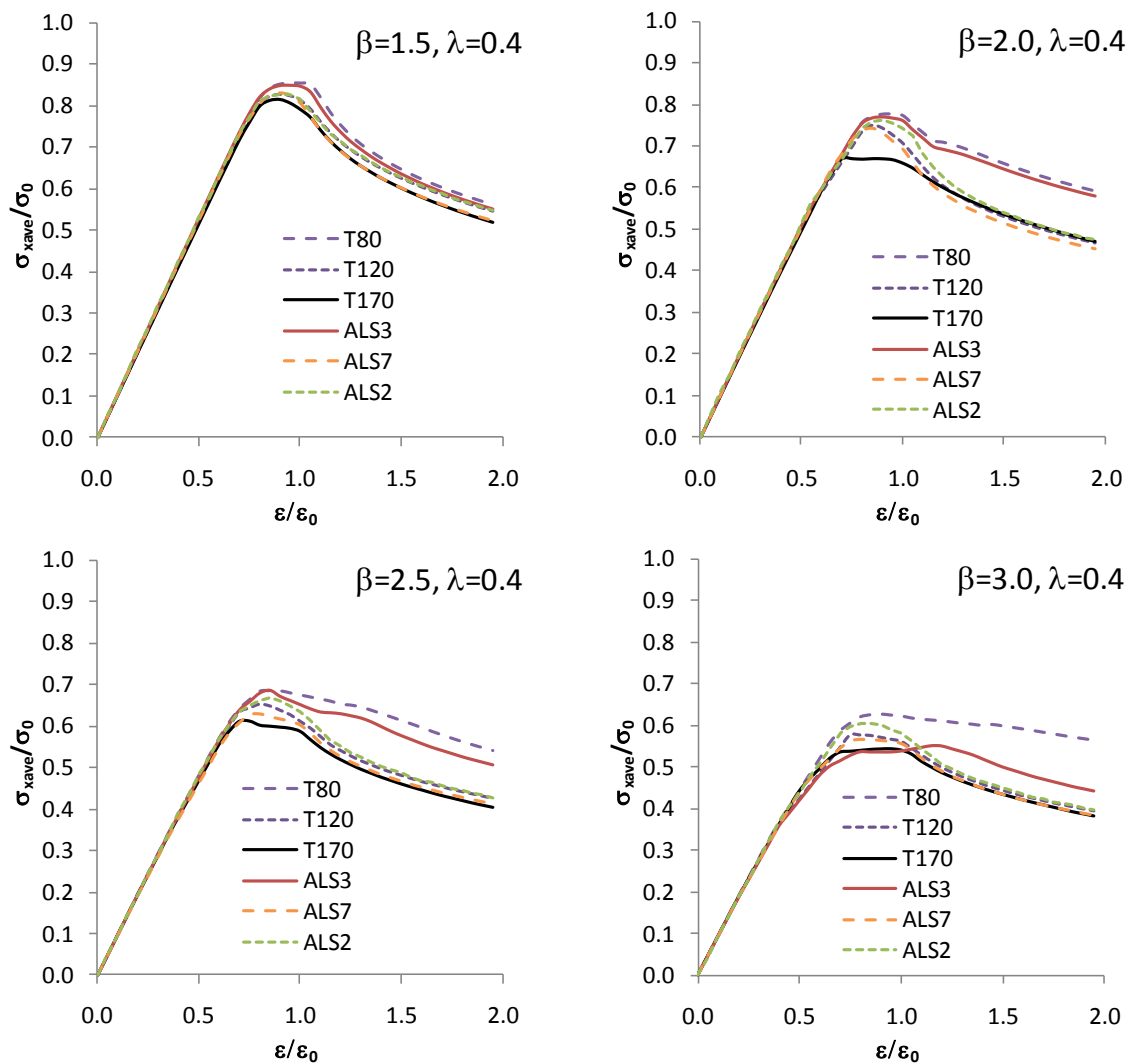


Figure 102 – Load shortening curves for PSCs with different stiffener cross sections ,  $\lambda=0.4$ ,  $A_s/A=0.2$ . 5083-H116 panels

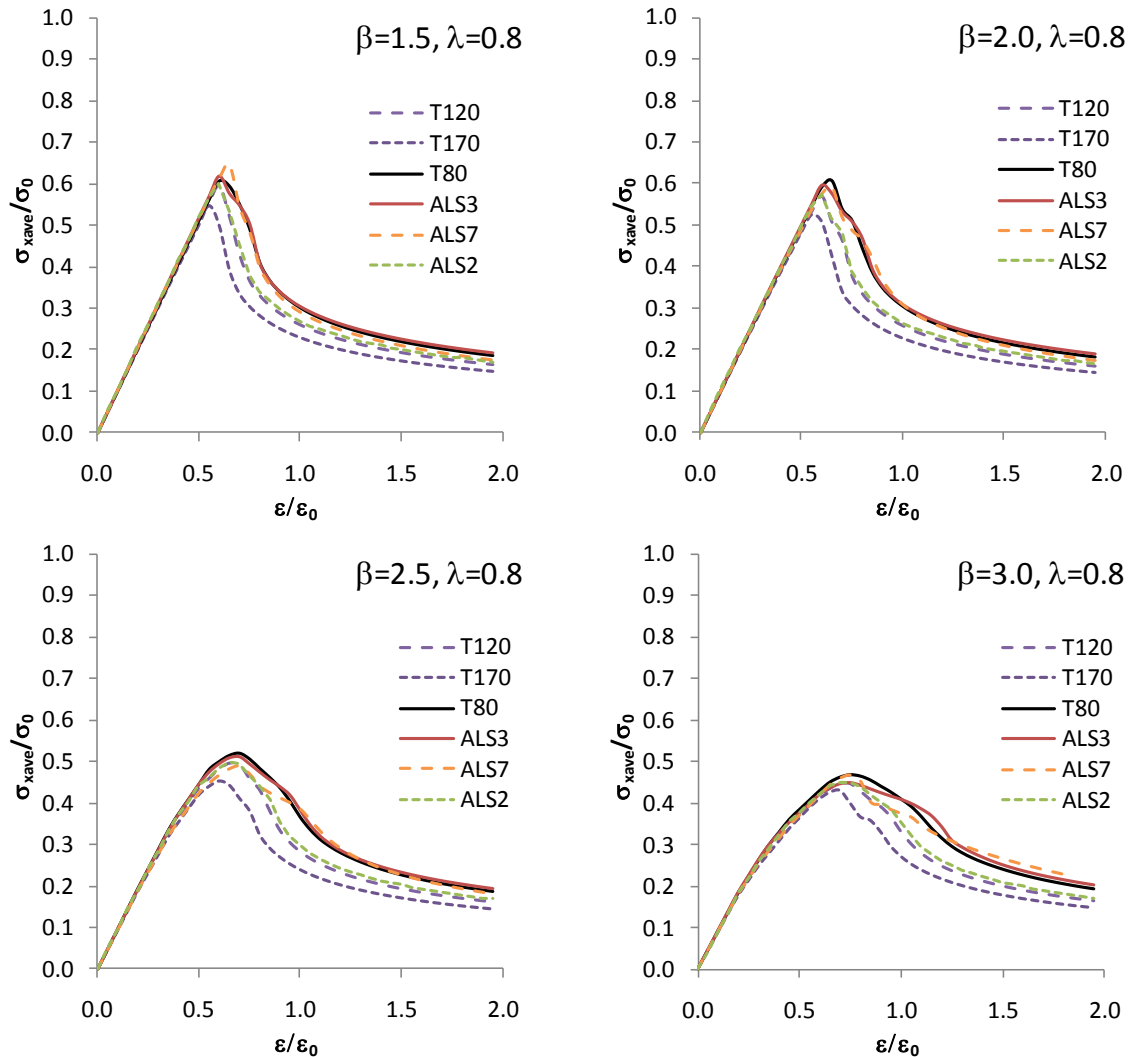


Figure 103 – Load shortening curves for PSCs with different stiffener cross sections ,  $\lambda=0.8$ ,  $A_s/A=0.2$ . 5083-H116 panels

## 5.7. Analysis of Orthogonal Panels

So far the FEM analyses presented in this thesis have focused on interframe panels. The FEM modelling approach also allows a thorough analysis of multi bay stiffened panels, with properties and parameters consistent with the interframe models. In addition, these analyses include the influence of the transverse stiffening and therefore appropriate frame dimensions also need to be selected.

This section documents the results from a series of multi-frame panels, which are analysed together with a range of transverse frame sizes. Unless stated, all analyses use average imperfections and residual stresses as defined previously. The test results detailed in this section demonstrate how various parameters influence the ultimate strength, progressive collapse behaviour and the onset of overall collapse failure modes.

Analyses are undertaken for a series of standard panels, detailed in Table 31. The panel dimensions are selected to give rational measures of slenderness and aspect ratio. Standard stiffener sizes taken from the relevant data tables in Chapter 2 are used. Panels M1-M10 are all constructed from 5083-H116. Panels S1-S4 are constructed from steel with yield strength of 245MPa and  $E=210\text{GPa}$ . The steel panel dimensions are calculated to give the same parameters of  $\beta$ ,  $\lambda$  and  $A_s/A$  as equivalent aluminium.

Table 31 – Multi bay panel test dataset

Dataset ID	Mat.	a (mm)	b (mm)	$t_p$ (mm)	$h_w$ (mm)	$t_w$ (mm)	$b_f$ (mm)	$t_f$ (mm)	$\lambda$ (mm)	$\beta$ (mm)	$A_s/A$
M1	5083	1200	400	14.8	120	5.5	55	7.7	0.62	1.5	0.15
M2	5083	1200	400	11.1	120	5.5	55	7.7	0.56	2.0	0.20
M3	5083	1200	400	8.9	120	5.5	55	7.7	0.53	2.5	0.23
M4	5083	1200	400	7.4	120	5.5	55	7.7	0.50	3.0	0.27
M5	5083	1200	400	14.8	80	4.5	45	6.2	1.09	1.5	0.10
M6	5083	1200	400	14.8	170	6.5	65	10.3	0.38	1.5	0.23
M7	5083	1000	400	14.8	120	5.5	55	7.7	0.52	1.5	0.15
M8	5083	1800	400	14.8	120	5.5	55	7.7	0.93	1.5	0.15
M9	5083	1200	800	14.8	120	5.5	55	7.7	0.81	3.0	0.08
M10	5083	1200	500	14.8	120	5.5	55	7.7	0.67	1.87	0.13
S1	Steel	2281	510	11.6	120	5.5	55	7.7	0.62	1.5	0.15
S2	Steel	2281	510	8.7	120	5.5	55	7.7	0.56	2.0	0.20
S3	Steel	2281	510	7.0	120	5.5	55	7.7	0.53	2.5	0.23
S4	Steel	2281	510	5.8	120	5.5	55	7.7	0.50	3.0	0.27

The transverse frame sizes are selected as a representative range and are detailed in Table 32. T1 and T2 are flat bars whilst T3 is a tee bar. The larger sections can be expected to show less susceptibility to overall collapse in comparative panels. All frames are sized to correspond to the Alcan T120 stiffener, which is used for the majority of the longitudinal cross sections (Table 31). The web height of frames T1 and T3 is typical of a lightly stiffened panel, being 3x the longitudinal stiffener height. The light frame, T2, is deliberately under specified; its cross section area is less than the T120 stiffener. This is perhaps unrealistic for practical design purposes, but provides a useful comparator for the effect of using very light transverse stiffening.

Table 32 – Multi Bay Panel Transverse Frame Dataset

Dataset ID	$h_w$ (mm)	$t_w$ (mm)	$b_f$ (mm)	$t_f$ (mm)
T1	360	10	0	0
T2	180	10	0	0
T3	360	10	100	15

Likewise, the overall panel dimensions have also been chosen to demonstrate the increasing influence of the overall collapse mode as the panel is widened. The length of the panel (i.e. the number of frame spaces) is also varied for comparison. Panel size is denoted by the number of longitudinals and frames. For example, a 10x3 panel consists of 10 longitudinal stiffeners and 3 frames. Half bay lengths are included at each end of the panel to minimise end effects. Half panel models are used for the smaller panel extents such as the 10x3 model, whilst the 20x7 panel uses a quarter model representations. Boundary conditions are as shown in Figure 66.

Figure 104 present the load shortening curves for cross sections M1, M9 and M10, constructed with various overall panel sizes and frame dimensions. All panels have the same stiffener cross section (corresponding to a T120 Alcan cross section) and frame spacing. The plate width between longitudinals,  $b$ , varies as follows: 400mm (M1), 500mm (M10) and 800mm (M9). The variation in  $b$  means the corresponding  $\beta$  also varies between 1.5 and 3.0.

For most models tested, a small multi-frame (e.g. a 10x3 panel) analysis with reasonably large transverse frame dimensions shows similar characteristics to a simple PSC model. An example is for Panel M1, for which a FEM displacement plot and load shortening curve are shown in Figure 104.

Similar characteristics are shown for the small models across the range of panels tested, as summarised by the load shortening plots. These results suggest that, with a relatively small overall panel size, the panel usually fails in an interframe manner predominantly with either beam-column mode or component mode collapse. The additional strength in the multi stiffened panels is likely due to the influence of the side boundary conditions, which will effectively place a hard corner zone adjacent to the panel edge. This effect is neglected in the PSC analysis, which assumes the panel is infinitely wide. Therefore, for such panels, the PSC model is shown to be an adequate representation, and will usually be conservative.

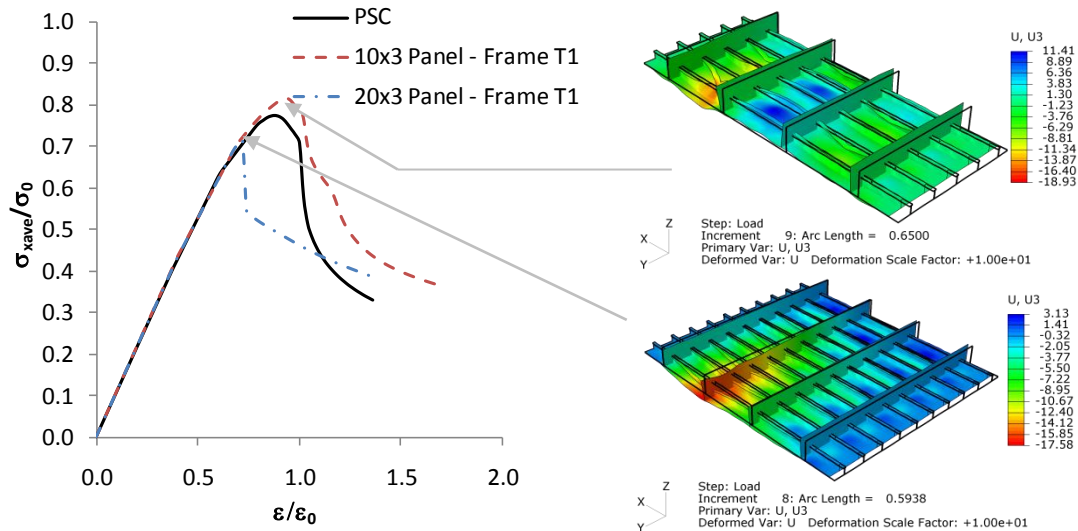


**Figure 104 – Panel M1 3 bay models , 360mmx10mm transverse frames (T1), loaded to ultimate strength, with 10 longitudinals (top right) and 20 longitudinals (bottom right). x10 deflection magnification.**

However, with the panel width doubled to include 20 longitudinals, some panels showed a reduction in ultimate strength. This loss of strength is due to overall panel buckling, which for the case of Panel M1 is highlighted by the displacement plots in Figure 104. The plot shows the mid frame of the larger panel deflecting out of plane, contrasting with the small panel which fails interframe. For this particular example, the overall collapse mode is not dominant. The frame panel in Figure 104 also appears to have buckled with a tripping failure mode at the panel centre, characterised by wrinkles in the frame web.

This is probably due in part to the nucleation of the buckling over two bays, rather than in a single bay as occurs for the smaller model. However, it is not a characteristic of dominant overall buckling, as shown in subsequent plots, in which the frames deflect downwards but do not trip. Instead, this is indicative of a complex interaction between interframe and overall collapse modes where both have similar critical strength. Further cases discussed below show more severe onset of overall collapse for which the gross buckling mode dominates.

Further tests on larger model extents show that strength and failure mode is not only dependent on panel width (B), but also the panel length (L). Note that, for these tests, quarter panel representations are used to provide a more efficient solution time.

The influence of panel length depends on the relative sizing of the transverse frame as compared to the longitudinal. If the critical collapse mode is over only a few frame spaces, which is more common for a heavily framed panel, the length of the panel makes little difference to the overall result. An example is for Panel M1 combined with T3 frames (M1-T3), as shown in Figure 105, which collapses

almost entirely in an interframe manner. An intermediate case is the M1-T1 model, which shows a mixture of overall and interframe collapse. The resulting load shortening curve shows reduced peak strength as compared to the PSC result, but both 3 frame and 7 frame models show similar characteristic ultimate strength, demonstrating that for this particular model the overall length is not a critical parameter. The results also show that the inclusion of a flange on the transverse frame has little influence on the overall panel characteristics.

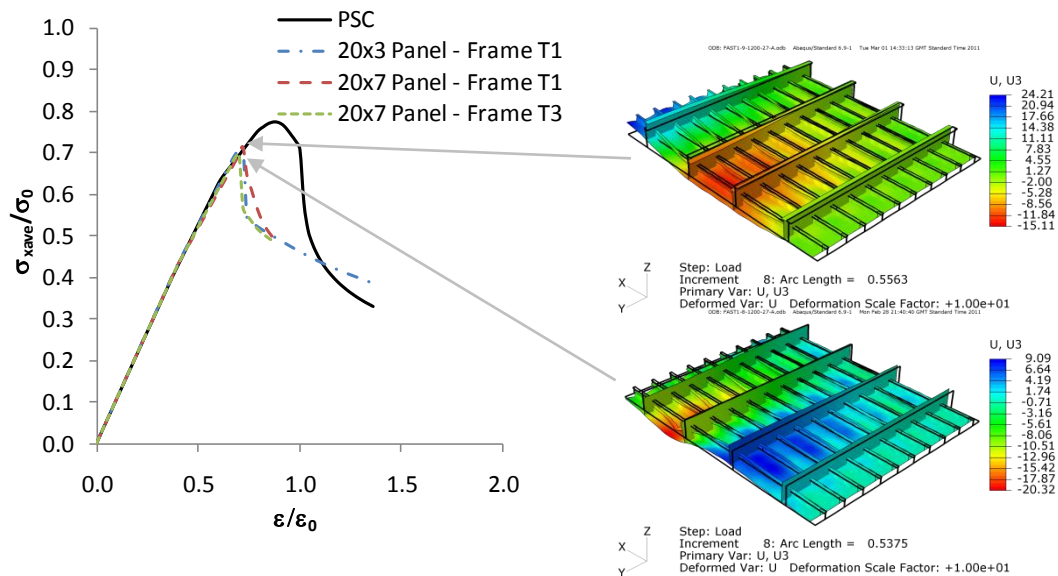
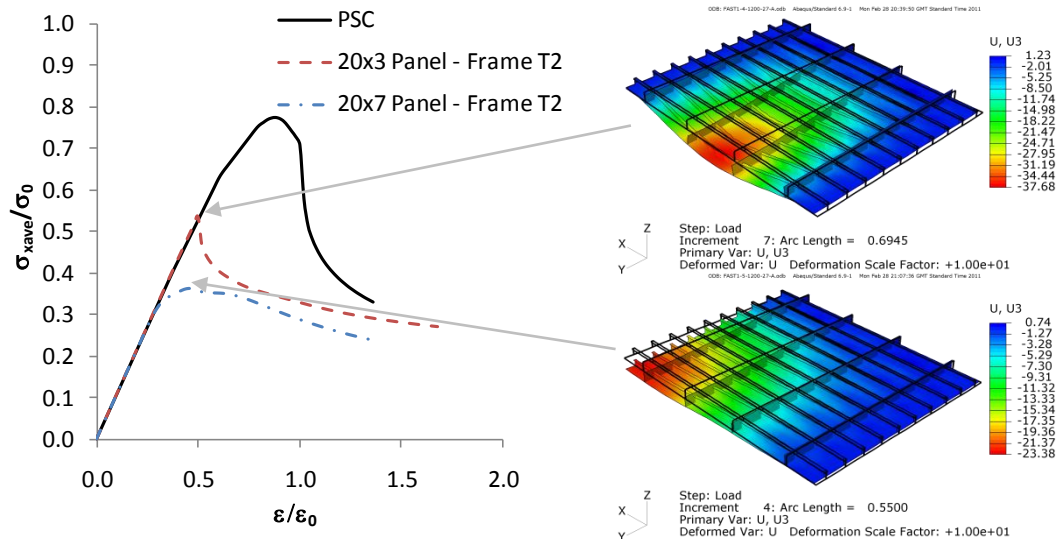


Figure 105 – Panel M1 7 bay models , 20 longitudinals, loaded to ultimate strength, with 360mmx10mm transverse frames (bottom right) and 360mmx10mmx100mmx10mm transverse frames (top right). x10 deflection magnification.

In contrast, when the panel is framed very lightly (T2), increasing the number of frame spaces corresponds directly to a decrease in ultimate strength as the overall mode shape extends over a greater area. This can be likened to the reduction in panel strength as column slenderness increases. This is well highlighted by panel M1-T2 (Figure 106), where the FEM model shows a dominant overall collapse shape. The 3 bay model collapse shape extends over all bays, whereas the 7 frame model collapse extends over 5 bays. This corresponds to a further reduction in peak strength for the 7 frame model.



**Figure 106 – Panel M1 20 longitudinal models , 180mmx10mm transverse frames, loaded to ultimate strength, 3 bay (left) and 7 bay (right). x10 deflection magnification.**

Comparisons between panels M1, M2, M3 and M4 show the effect of increasing the plate slenderness ratio. Except for the plate thickness, which is used to control  $\beta$ , all panels have identical geometric dimensions. The figures present both the 360x10 and 180x10 transverse frame cases for a 20x7 panel. Table 33 provides a further comparison of the ultimate strength for each panel, which is taken as the peak of the corresponding load shortening curve.

The results demonstrate that the stockier panels, where plate slenderness is low, have a greater susceptibility to overall collapse. The onset of overall collapse on these panels has a greater weakening effect on the ultimate strength. The ultimate strength of Panel M1 is less than half the PSC strength when constructed with 180x10 transverse frames and 20 longitudinals.

The mesh displacement plots (Figure 111 and Figure 112) further demonstrate the differing influence of the overall collapse mode for panels of different plate slenderness. For panel M1, with 180x10 transverse frames, the overall mode is observed well before the ultimate strength is attained. However, with the frame height increased to 360mm, the panel shows more complex buckling mode up to the ultimate strength. Only in post collapse does the overall mode become dominant. For panel M3 the 180mm frame height also shows overall buckling forming at the ultimate strength increment and into the post collapse region. However, contrasting with panel M1, the overall buckling shape does not form well before collapse. For the 360mm transverse frame model, the overall collapse mode is not prevalent throughout the load range.

Table 33 – Ultimate Strength Results – 5083-H116 Panels

Panel ID	Frame Dimensions (mm)	Panel Size	Ultimate Strength	% Ultimate Strength to PSC Strength
M1	-	PSC	0.77	-
M1	360x10	20x7	0.71	92%
M1	180x10	20x7	0.36	47%
M2	-	PSC	0.73	-
M2	360x10	20x7	0.66	90%
M2	180x10	20x7	0.46	63%
M3	-	PSC	0.60	-
M3	360x10	20x7	0.61	102%
M3	180x10	20x7	0.47	78%
M4	-	PSC	0.56	-
M4	360x10	20x7	0.56	100%
M4	180x10	20x7	0.46	82%
M5	-	PSC	0.47	-
M5	360x10	20x7	0.38	81%
M5	180x10	20x7	0.24	52%
M6	-	PSC	0.86	-
M6	360x10	20x7	0.80	93%
M6	180x10	20x7	0.50	58%
M7	-	PSC	0.83	-
M7	360x10	20x7	0.67	81%
M7	180x10	20x7	0.38	45%
M8	-	PSC	0.58	-
M8	360x10	20x7	0.50	85%
M8	180x10	20x7	0.40	69%
M9	-	PSC	0.52	-
M9	360x10	20x7	0.33	63%
M9	180x10	20x7	0.23	45%
M10	-	PSC	0.71	-
M10	360x10	20x7	0.47	67%
M10	180x10	20x7	0.34	48%

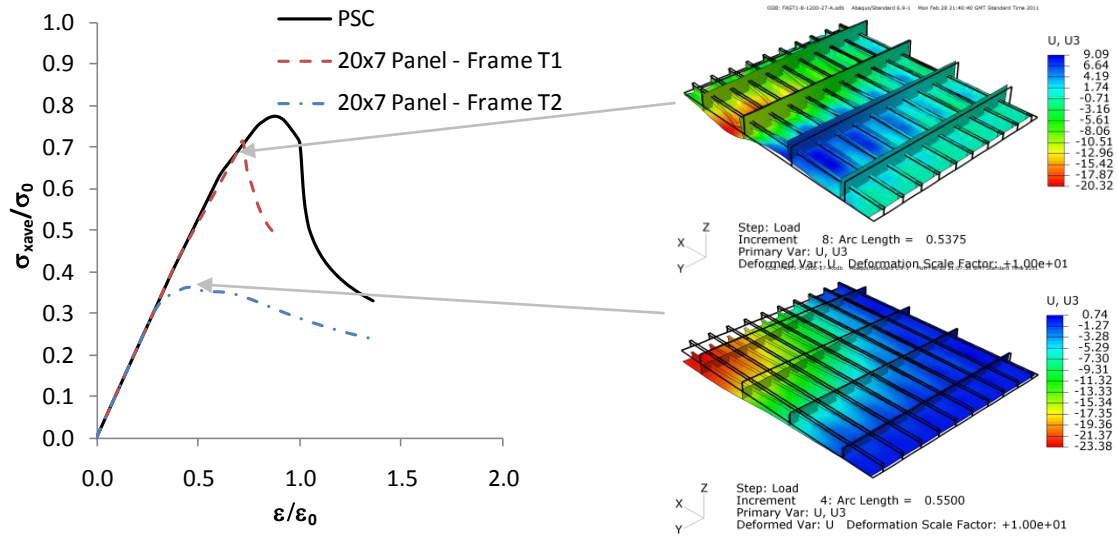


Figure 107 – Panel M1, comparison of transverse frame size 360x10 (top right) and 180x10 (bottom right)

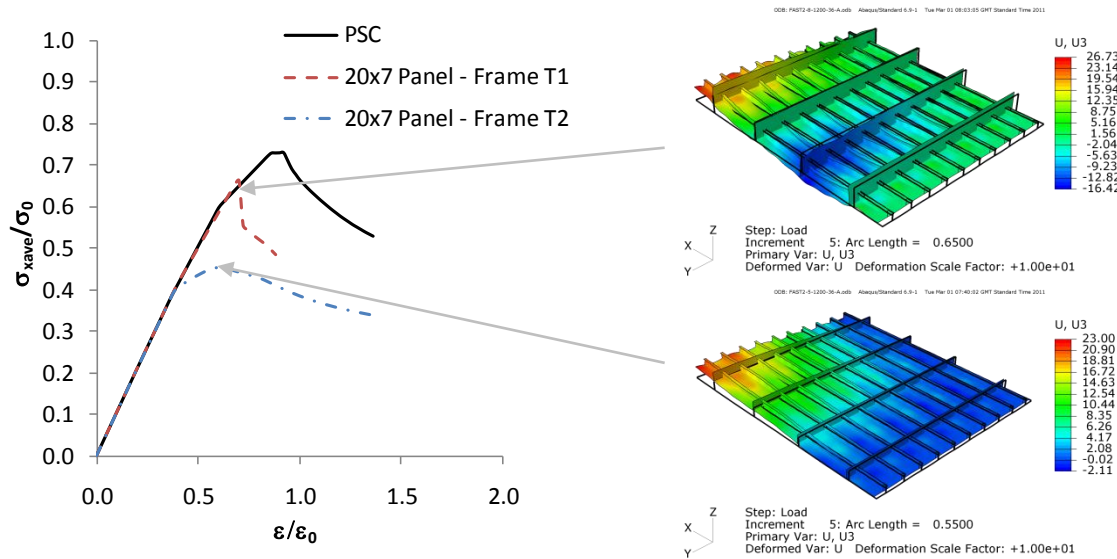


Figure 108 – Panel M2, comparison of transverse frame size 360x10 (top right) and 180x10 (bottom right)

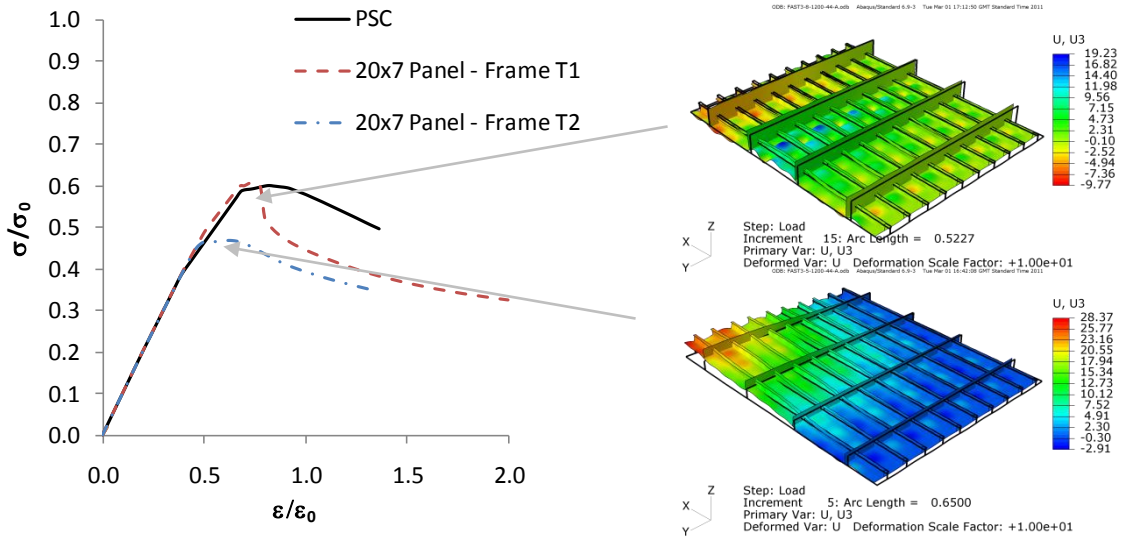


Figure 109 – Panel M3, comparison of transverse frame size 360x10 (top right) and 180x10 (bottom right)

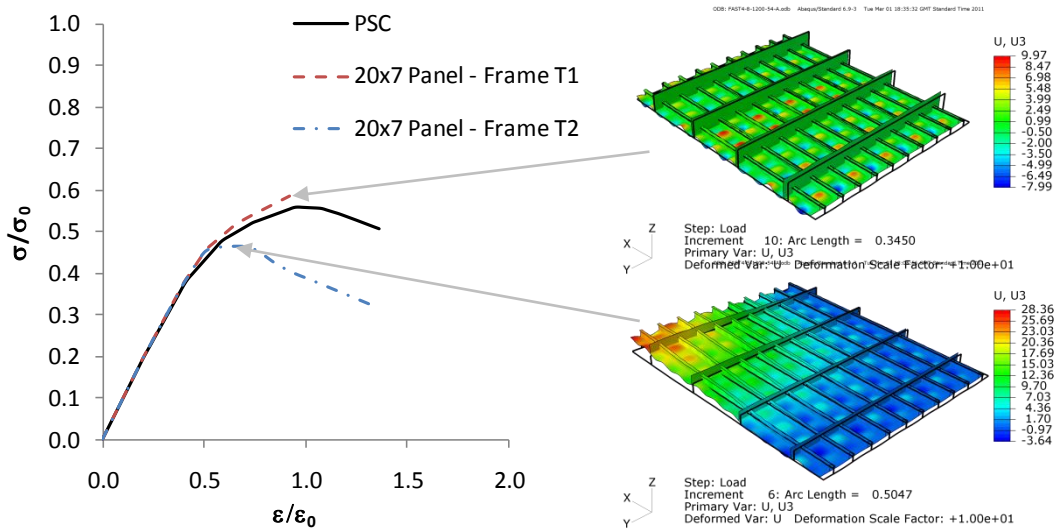


Figure 110 – Panel M4, comparison of transverse frame size 360x10 (top right) and 180x10 (bottom right)

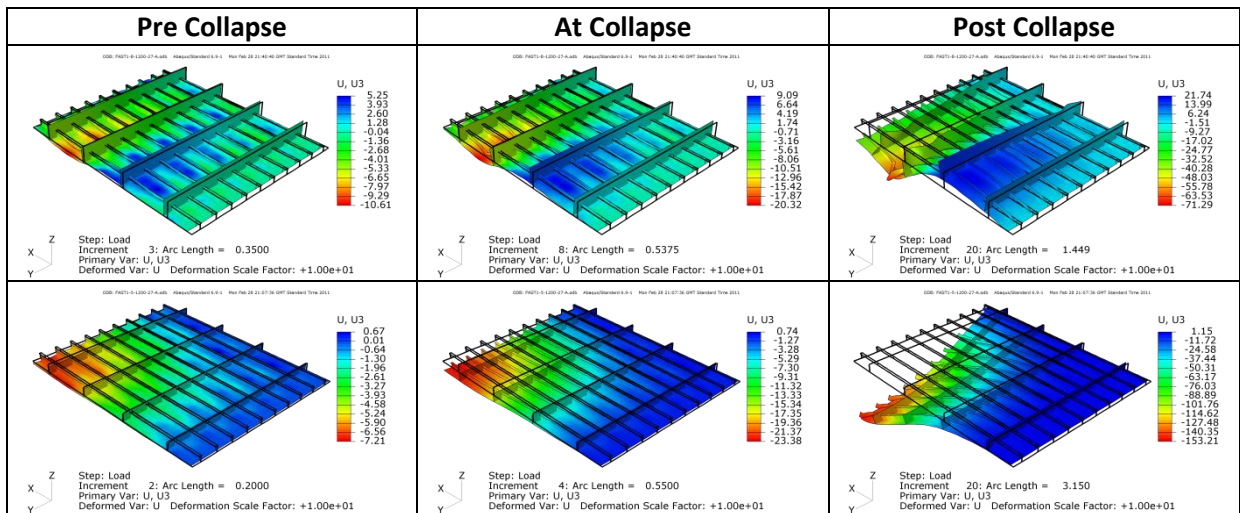


Figure 111 – Panel M1 displacement plots showing the nucleation of the collapse from interframe to an overall mode. With 360x10 transverse frames (top) and 180x10 transverse frames (bottom)

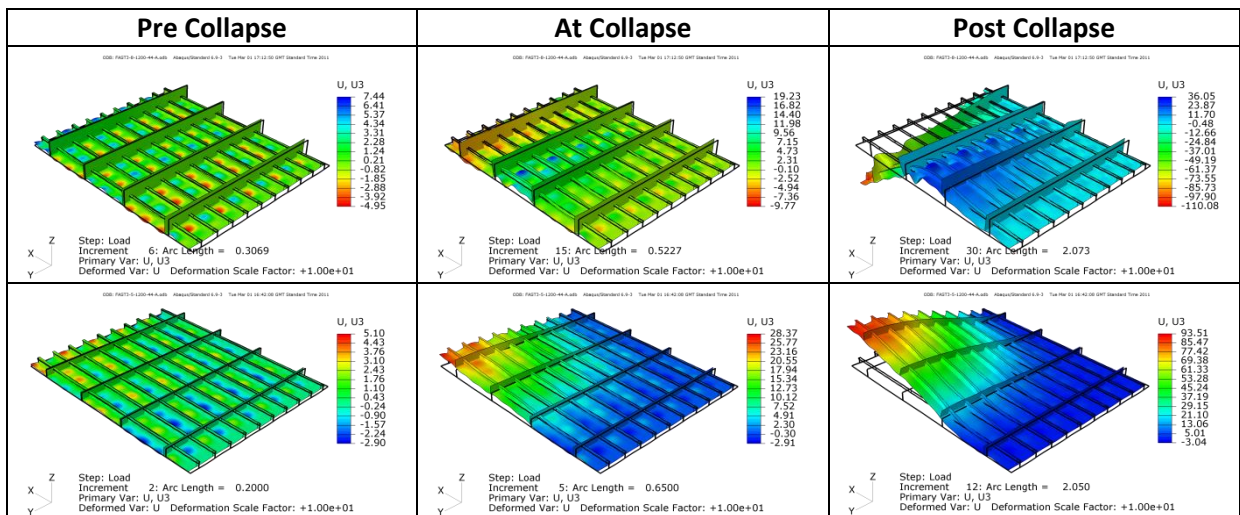


Figure 112 – Panel M3 displacement plots showing the formation and nucleation of the collapse mode. With 360x10 transverse frames (top) and 180x10 transverse frames (bottom)

Comparisons between panels M1, M5 and M6 show the effect of changing the stiffener dimensions (Figure 113). Three standard Alcan stiffener cross sections are used: M1 uses T120, M5 uses T80 and M6 uses T170. The PSC curve is also included to show the influence of overall collapse modes in each case. The comparative plot shows that changing the longitudinal stiffener profile will cause a corresponding change in ultimate strength, but the influence of overall collapse modes remain. This suggests that the influence of overall collapse modes is less dependent on the longitudinal cross section compared to the influence of the transverse frame.

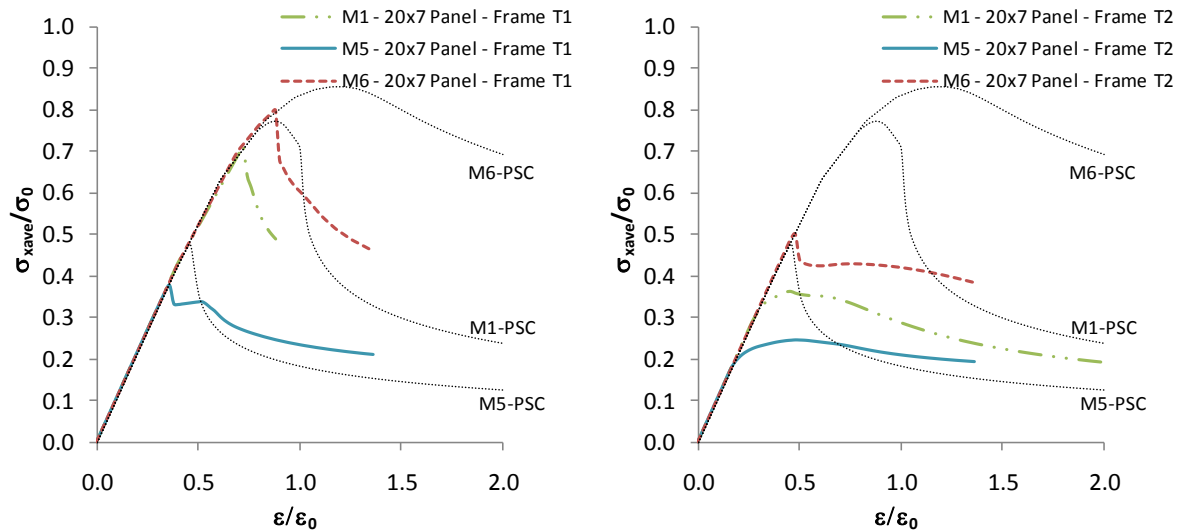


Figure 113 – Comparison of panels M1, M5 and M6 with 360x10 transverse frames (left) and 180x10 frames (right).

The effect of transverse frame spacing is also investigated by comparing panels M1 ( $a=1200\text{mm}$ ), M7 ( $a=1000\text{mm}$ ) and M8 ( $a=1800\text{mm}$ ).

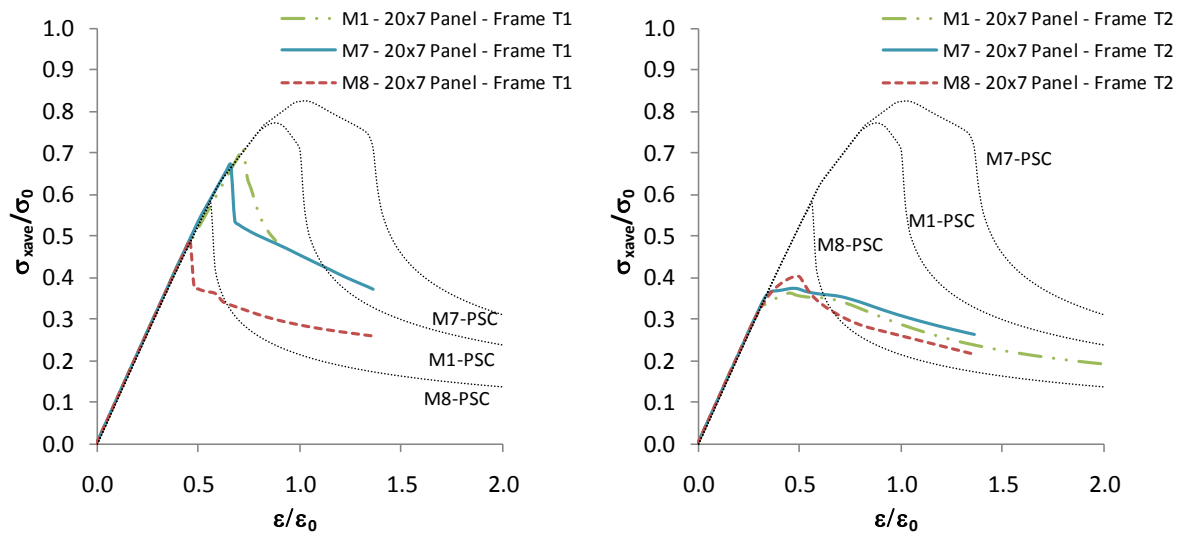


Figure 114 – Comparison of panels M1, M7 and M8 with 360x10 transverse frames (left) and 180x10 frames (right).

Equivalent steel panels are compared with the 5083-H116 results in Figure 115 and Table 34. All panels have the same stiffener cross sections and imperfection characteristics. The imperfection of the plate is average using Smith's formula ( $0.1\beta^2t$ ), which means the steel panels imperfection amplitude is effectively less than the equivalent aluminium panels because plate thickness is reduced to maintain the same plate slenderness. The panel slenderness ratios are set equal by altering the plate breadth and thickness for the steel panels until the ratios match the equivalent

aluminium panel. This ensures a comparison of like for like panels with the only difference being the material.

The plots show that, for these cases, the steel panels are less susceptible to overall collapse than equivalent sized aluminium panels. The 180x10 frame (T2) causes the aluminium panel to lose a significant proportion of its ultimate strength for all four panels tested. A significant strength reduction is also seen in the steel panel with low plate slenderness ratio (S1). However, this is not the case for the other three panels. The percentage reductions in Table 34, and the corresponding load shortening plots, show that the steel panel maintains its strength closer to the interframe value whereas the aluminium panel with 180x10 frames still shows a significant reduction in strength due to overall collapse mode.

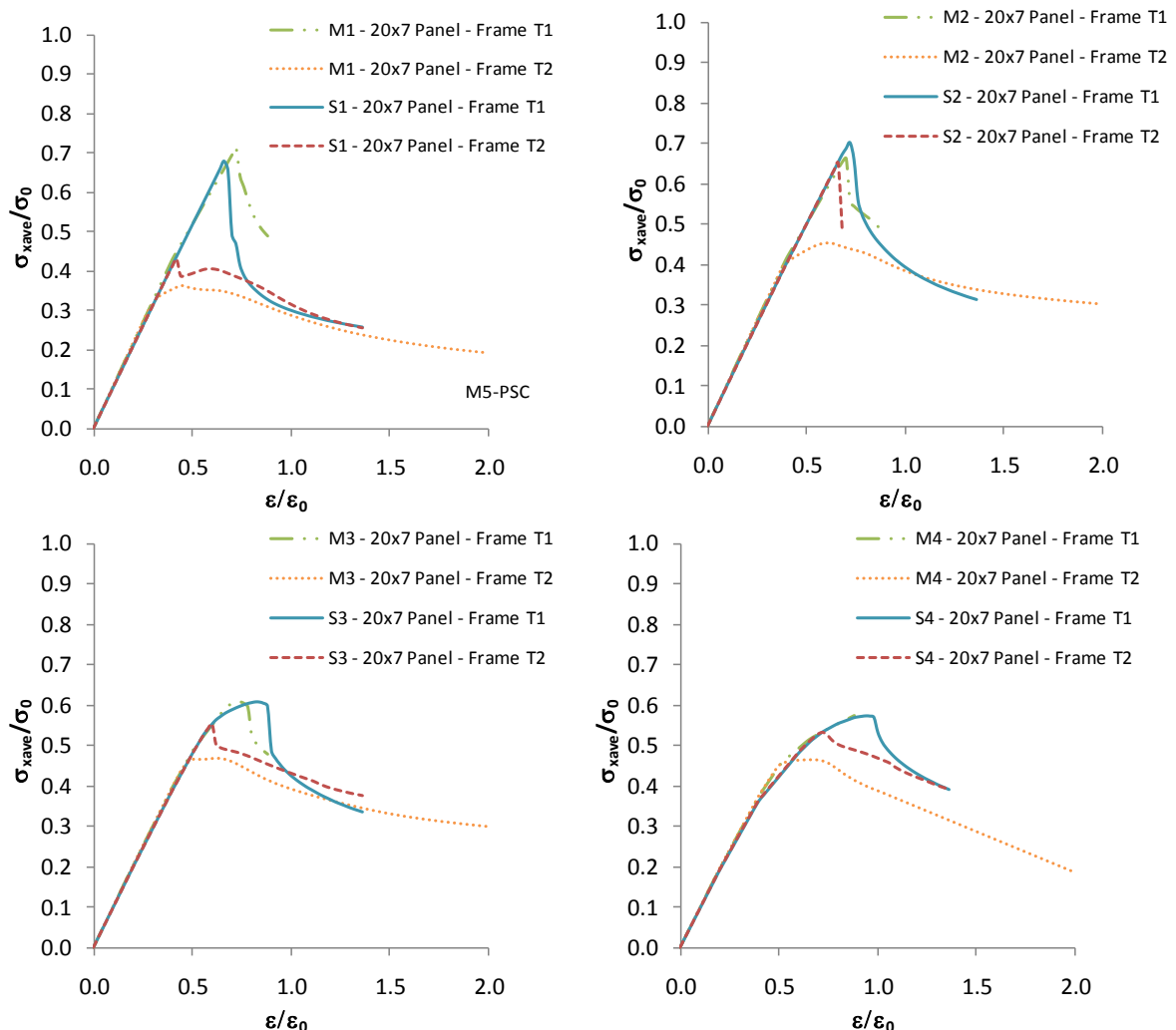


Figure 115 – Steel Panels S1-S4 compared to 5083 panels M1-M4. 20x7 panel size

**Table 34 – Ultimate Strength Results – 245MPa Steel Panels**

Panel ID	Frame ID	Panel Size	Ultimate Strength	Reduction from PSC	Equivalent 5083 Panel ID	Equivalent reduction for 5083 panel
S1	-	PSC	0.70	-	M1	-
S1	T1	20x7	0.68	97%	M1	92%
S1	T2	20x7	0.43	62%	M1	47%
S2	-	PSC	0.66	-	M2	-
S2	T1	20x7	0.71	102%	M2	90%
S2	T2	20x7	0.65	94%	M2	63%
S3	-	PSC	0.58	-	M3	-
S3	T1	20x7	0.60	103%	M3	102%
S3	T2	20x7	0.55	94%	M3	78%
S4	-	PSC	0.55	-	M4	-
S4	T1	20x7	0.58	104%	M4	100%
S4	T2	20x7	0.43	96%	M4	82%

## 5.8. Summary

A series of nonlinear large deflection finite element analyses have been carried out on lightly stiffened panels typical of high speed vessel deck or bottom structures, investigating their uniaxial in-plane compressive strength assuming interframe and overall collapse modes.

Panels are first modelled assuming interframe collapse, with the frames represented as a simple support constrained against out of plane movement. Comparisons of the non-dimensional ultimate strength of two different aluminium alloy panel constructions showed the same general pattern compared to equivalent existing steel column collapse curves.

A set of multi-frame panels were then modelled to assess the influence of overall collapse modes on the ultimate strength characteristics of the overall panel. The results suggest that aluminium panels have a significantly increased possibility of overall collapse compared to equivalent steel panels. Furthermore, the onset of overall buckling modes has an adverse effect on the overall strength and post collapse behaviour of the panel. To summarise it is useful to quantify some common patterns found in the results which are pertinent when considering the influence of different collapse modes.

Firstly, if the transverse frame is sized to be significantly larger in relation to the longitudinal structure, the panel will collapse interframe. In these cases, a PSC model is usually sufficient in representing the panel. An exception is when the panel only contains a few longitudinals. In these cases the close proximity of the boundary conditions to the central region of the panel may provide some additional strength. The influence of the overall collapse mode is increased when the

transverse frame size is decreased or when the longitudinal cross section is strengthened (usually by decreasing either  $\beta$  or  $\lambda$ ). This conclusion drawn from the quantitative results can be furthered by qualitative reasoning. When the longitudinal strength is increased, for example by increasing the plate thickness, the comparative size of the transverse frame is effectively reduced. This has the effect of increasing the interframe collapse strength whilst decreasing the relative overall collapse strength.

The results also show that aluminium panels with the qualities described above have significantly greater susceptibility to overall collapse than equivalently dimensioned steel panels. This must be due to the lower stiffness and hence the greater flexibility of aluminium; this lowers the threshold at which the transverse frame loses out of plane rigidity and deflects, causing an overall collapse pattern to form.

*“Experience serves not only to confirm theory, but differs from it without disturbing it, it leads to new truths which theory only has not been able to reach”, D’Alembert [119]*

# Chapter 6

## **A Semi Analytical Panel Strength Methodology**

### **6.1. Introduction**

The FEM studies detailed in the previous Chapter demonstrate how gross panel buckling modes adversely affect the load shortening behaviour and ultimate strength of an orthogonally stiffened flat panel. The FEM approach has proved capable of describing the load shortening behaviour with an arbitrary arrangement of stiffening across the panel width. This is achieved by a robust modelling approach which adequately accounts for geometric and material imperfections in the structure. However, as discussed previously, FEM solutions can be numerically expensive and also require rigorous pre and post processing. In comparison, a major advantage of simplified methods is the rapid setup and solution time. This not only improves convenience, but also extends the practicality of the solution method for use in applications requiring rapid analysis. For example, a rapid solution time means that the effect of changing parameters can be quickly identified, which is an essential quality for reliability analysis.

In the current work the purpose of developing panel load shortening curves is for input into an extended progressive collapse methodology, which can be programmed to accept any suitable dataset describing the load shortening behaviour of an element. Therefore, if necessary, the FEM solution for a panel can be assigned to elements in the girder cross section. This is certainly a viable option if a PSC FEM model is a sufficient representation of the panel as a whole. However, there are several drawbacks. Firstly, the progressive code must be linked to a suitable nonlinear solver such as ABAQUS. This reduces the portability of the progressive collapse program. Secondly, although a single PSC FEM solution is reached in a few minutes, the total analysis time will still be raised considerably if there are a large number of elements making up the hull girder. Thirdly, the FEM solver is not completely reliable in providing a realistic solution. Instabilities in the FEM mesh can cause snap bucking and even a reversal of the load direction. Each load shortening curve would need to be checked to make sure such errors were not present. Finally, and perhaps most importantly, the FEM solution depends on many parameters including the imperfection characteristics, the solution step size and the mesh. Therefore, as has been shown in the previous Chapters, there is a degree of variability in the resulting load shortening curve, and it is difficult to provide a true representative result without running several analyses to check the influence of the imperfection parameters.

These arguments become even more important when considering multi bay stiffened panels. The long simulation time together with the detail required in the initial model setup means it is unfeasible to use FEM results for an orthogonal panel directly in the progressive collapse code. Furthermore, the FEM solver requires close attention to ensure a complete load shortening curve is achieved. As has been shown previously, orthogonal panel FEM analyses can easily break down before the peak load is attained, due to the complex instabilities occurring across the mesh. A rapid method to predict of the load shortening curve for a stiffened panel element is thus an essential requirement for an extended progressive collapse methodology.

The literature review in Chapter 3 discusses potential simplified approaches for application to multi bay stiffened panels. The large deflection orthotropic plate method is the only reviewed method which directly takes into account the transverse structure of a stiffened panel. However, the established approach is only applicable to very lightly stiffened panels [82] because the panel orthotropy is calculated using the elastic properties of the material and geometry. The method is thus able to predict elastic buckling but is unable to account for the elasto plastic complexities typically observed in the collapse behaviour of stockier ship type panels.

This Chapter describes a method to include elasto-plastic effects in the orthotropic plate method, which extends its capability to include panels which are not adequately assessed by the standard

approach. The extended orthotropic plate method underpins an incremental, semi analytical method to predict the load shortening curve for an arbitrary dimensioned stiffened panel. The methodology is called semi-analytical because it uses pre-established numerical results from plate and stiffener analyses to define the instantaneous stiffness of the components making up the panel. These are derived from the FEM analysis results for the plate and stiffener components, as presented in Chapters 4 and 5 respectively, and are encapsulated in a series of standard parametric datasets covering different materials (specifically aluminium alloy and steel) together with a range of plate slenderness and column slenderness ratios.

The semi analytical method applies an incremental in-plane longitudinal compressive load to the panel, which is increased using displacement control. At each increment, the corresponding maximum overall resistance of the panel is compared to the resistance at the interframe level. The minimum determines the instantaneous level of resistance of the panel and indicates the current mode of failure. In the present study, the semi analytical method is developed for uniaxial longitudinal compression only, although the orthotropic plate method is presented in a generalised form for biaxial load problems.

## 6.2. Rationale

This section sets out the rationale for developing the orthotropic plate method to account for elasto-plastic material properties.

The general principles of the established large deflection orthotropic plate method have been summarised in Chapter 3. The method calculates the ultimate capacity of the panel when represented as a single entity, with the properties of the individual plating and stiffener elements combined to make an equivalent responding “panel plate”. It is useful to briefly examine the limitations of the established classical method in order to justify further developments which are required to meet the objectives of this study.

The established orthotropic plate method is closed form. Therefore it only calculates the ultimate strength; it does not directly calculate the complete load shortening response of the panel to progressively increasing compressive load. This means that the method has to be implemented as part of an extended approach, which derives the complete panel load shortening curve using other methods and uses the orthotropic approach to define the curve peak.

As already mentioned, the existing orthotropic plate method also has limitations for application to ship type stiffened panels. Very lightly stiffened panels, for which the orthotropic plate method has been validated, are assumed to buckle elastically under in-plane compressive load. Panels typical of a ship structure are usually relatively stocky and thus buckling generally moves into the elasto-plastic region. The standard orthotropic approach only uses the initial material properties to derive elastic constants for the panel cross section. Therefore the overall buckling strength of the panel can be substantially over predicted.

In reality, as the panel is incrementally loaded and as it approaches collapse, the “instantaneous” material and assumed geometric properties do not remain constant. These elasto-plastic effects are included in the orthotropic plate method by using the instantaneous stiffness of the components (derived from the component load shortening curves) to replace the elastic constants in the orthotropic calculations. The properties of both the material and the assumed geometry across the entire panel change due to the behaviour of the constituent parts, specifically because of their loss of effectiveness. As the panel is compressed, individual component plates and stiffeners within the panel follow a nonlinear load shortening relationship.

The stiffness of the components are described by, and contained within, the plate and stiffener component load shortening curves. Therefore, if the plate and stiffener behaviour can be estimated when in “isolation”, this can provide useful information on the instantaneous effectiveness of the component parts of the panel. The parametric FEM datasets for stiffeners and plates provide this information for a wide range of structure, and because the datasets are given for non dimensional slenderness parameters, they provide excellent data which can be applied to an arbitrary dimensioned panel (within the limits of the datasets).

Once the instantaneous stiffness of each component is known, it can be applied in the orthotropic plate method to re-evaluate the material and geometric properties. In the original orthotropic plate method, the panel properties are described by “elastic constants”. In the extended methodology presented here, these elastic constants are re-evaluated at each increment and technically they are neither elastic nor constant. However, to keep the description of the calculation method clear, they are still referred to as “elastic constants”.

The result of updating the elastic constants is that the elasto-plastic properties of the components are reflected in the orthotropic plate calculations. As further increments of end displacement are applied the stiffness of the components reduces, causing a corresponding reduction in the ultimate strength prediction for overall buckling.

## 6.3. Calculation Methodology

### 6.3.1. Calculation Principles

The principles of the semi analytical method are best described using a case study of a large scale orthogonally stiffened panel. The top deck of the aluminium multihull, which is described in detail in Chapter 7, provides an excellent example. A base case model, together with several variants, are analysed. The base case (Deck A) is as shown in Figure 116. It is a very wide panel, stiffened with closely spaced stringers (200mm spacing) and intermittent deep longitudinals (spacing shown for top deck of cross section shown in Figure 163). The frames are flat bars and are spaced at 1200mm intervals. A seven bay deck length is modelled, thus representing a midship region compartment space of 8.4m. In reality the compartment may be substantially longer than this, but the addition of more bays increases the FEM computation time. A seven bay compartment is considered adequate for the purposes of demonstrating overall failure modes. The effect of increasing the compartment length is investigated in the next Chapter.

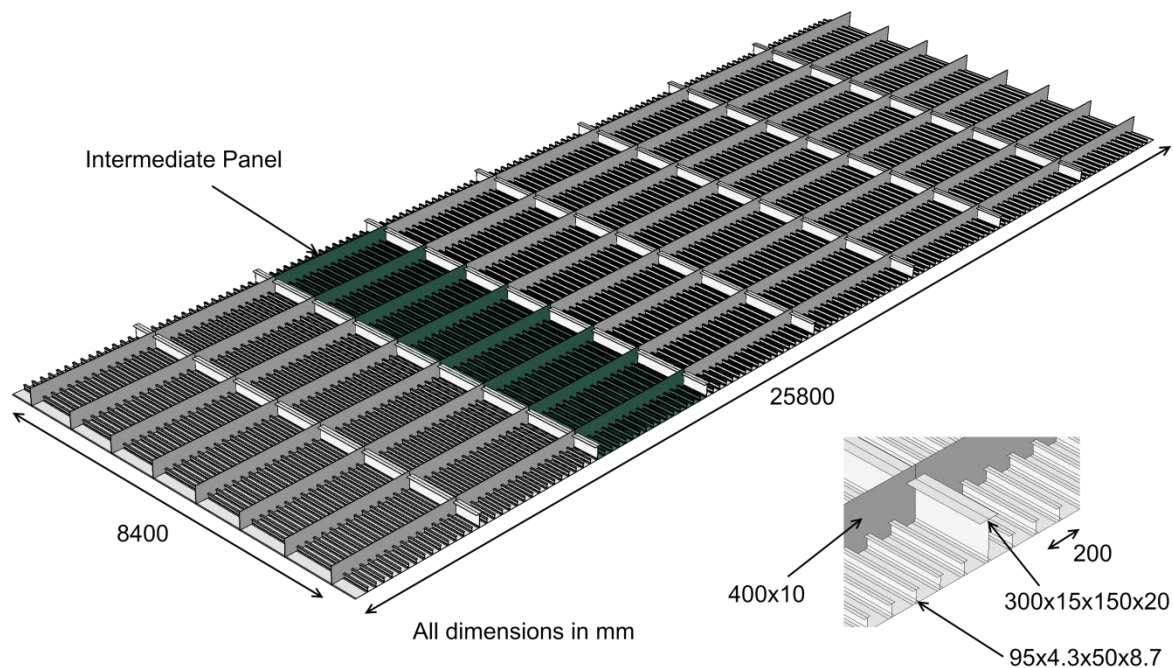


Figure 116 – Aluminium multihull top deck.

Three variant models are also developed to demonstrate the effect of changing the stiffening arrangement in the deck:

- Deck B has the same overall dimensions as Deck A but the deep longitudinals are replaced by regular stringers, thus creating a uniformly stiffened span.

- Deck C is arranged identically to Deck A except the deep longitudinals are doubled in size (600x30x300x40 tee bars) to add additional lateral support at the intermediate positions.
- Deck D is identical to Deck A except the central stiffener is replaced with a much heavier section (900x30x450x40) in an attempt to prevent a single half wave buckling shape over the entire deck width.

The deformed mesh plots in Figure 119 show the scantling arrangements for each panel.

To provide comparative results, the decks are first analysed with FEM. A series of three different representations of Deck A are compared, as shown in Figure 116:

- PSC – Provides a baseline load shortening curve which would be typical of that used to represent each plate-stiffener element in the conventional interframe progressive collapse method.
- Intermediate Panel – this model assumes that the deep longitudinals provide sufficient lateral support to provide a simply supported boundary condition. Therefore the structure between the deep longitudinals is analysed in isolation. The panel width is 3.4m. The model extents are  $\frac{1}{2}+7+\frac{1}{2}$  bays in length with a 3.4m width (the distance between the deep longitudinals).
- Whole Deck – FEM representation of the entire deck with simple supports at the edges only. The deck is represented by a  $\frac{1}{2}+7+\frac{1}{2}$  model length, together with a half deck width of 12.9m. A plane of symmetry boundary condition is specified for nodes at the longitudinal centreline.

All deck variants for the case study have the same longitudinal stiffeners and thus have the same PSC load shortening curve.

The FEM analyses follow the procedures outlined in the previous Chapter. Average imperfections and residual stresses are introduced into the geometry using the building block method. The boundary conditions are set appropriately to give simple supports at the panel edges and symmetry conditions at centrelines where required. Load is applied with displacement control.

The results from the FEM analyses are shown in Figure 117. The combination of large width and light scantlings means that the deck has an overall critical collapse mode. This is most clearly seen in the deformed mesh plot, which shows the buckled shape of the deck at the ultimate capacity. The comparative load shortening curves output from the FEM analyses also demonstrate that the non-

dimensional strength of the whole deck is significantly reduced as compared to an equivalent PSC representation. The intermediate panel representation is also an inadequate representation of the whole deck. It fails interframe and the resulting load shortening curve is similar to the PSC result.

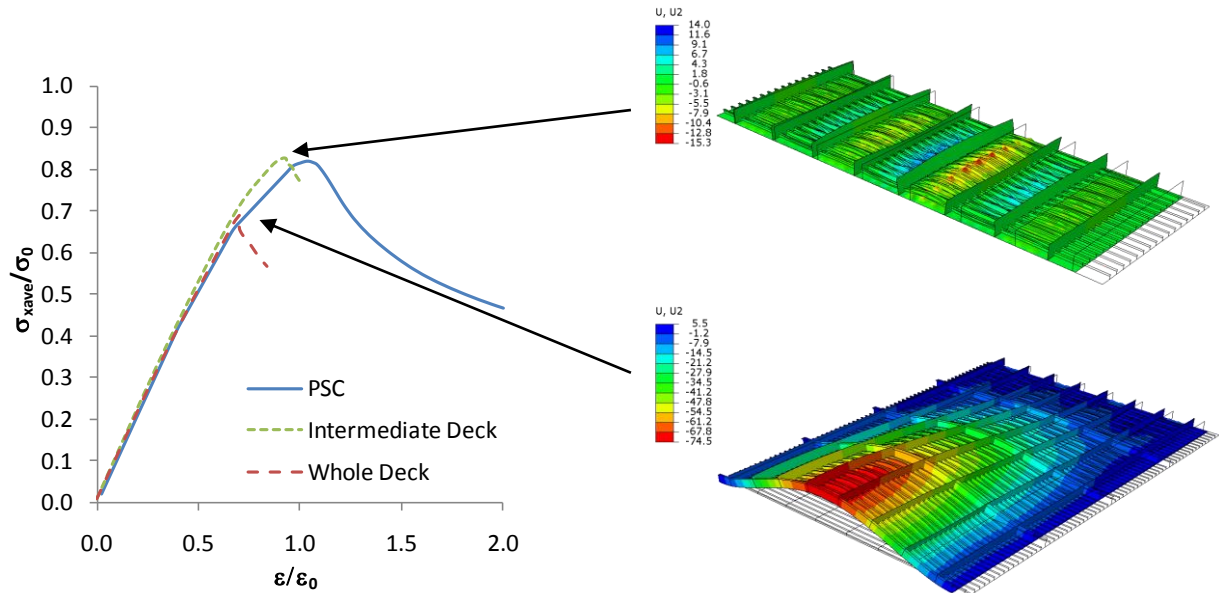


Figure 117 – Deck A load shortening curves

A comparison of the load shortening curves for the variant decks is shown in Figure 118. Deformed mesh plots at ultimate strength are shown in Figure 119. A description of the failure pattern in each deck is as follows:

- Deck B fails overall; the ultimate strength is slightly less than the base case result. The shape of the buckled panel is also different to the base case, with a combination of three half wave and single half waves shape over the panel length.
- Deck C shows that increasing the size of the deep longitudinals provides sufficient lateral support to cause the panel to fail interframe. The ultimate strength is therefore equivalent to the PSC result.
- Deck D fails overall but with a nucleated shape over half the total deck width; the centreline deep longitudinal providing sufficient lateral support to change the buckling mode shape as compared to the base case. However, the ultimate strength is only improved slightly with this configuration.

The purpose of the semi analytical method is to efficiently determine the load shortening behaviour of an arbitrarily stiffened panel such as the four examples shown above. Therefore an important

requirement for the method is to determine both the critical collapse mode and the extent of the collapse. This procedure is complicated by differently sized stiffeners in the panel cross section which may or may not provide sufficient lateral support to act as edge boundaries within the panel.

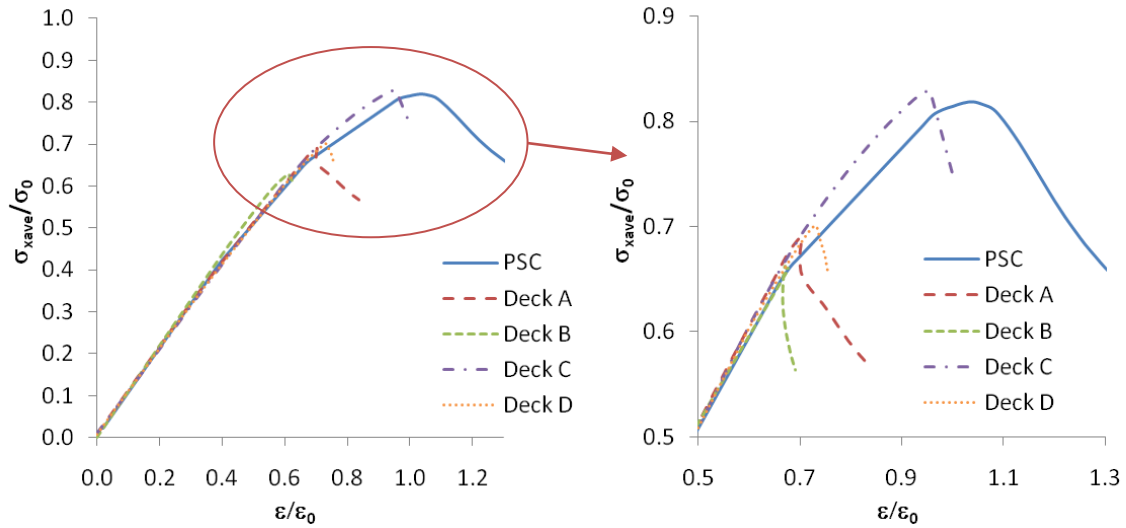


Figure 118 – Variant deck load shortening curves

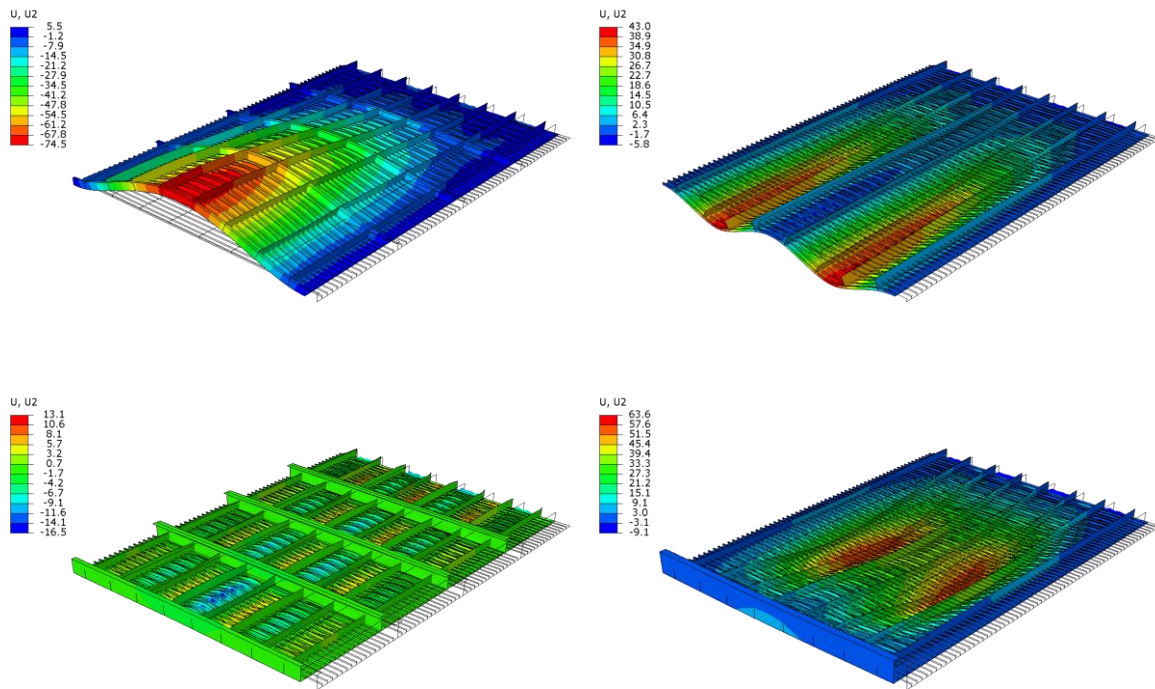


Figure 119 – Variant deck mesh plots. Deck A (top left), Deck B (top right), Deck C (bottom left) and Deck D (bottom right)

The aluminium deck provides an interesting example in this respect and gives an indication as to how the simplified methodology must operate. Deck A, the base case, is predicted to buckle across

its entire width and length. The deep longitudinals do not provide sufficient lateral resistance to be considered as boundary supports. This means that this particular deck arrangement cannot be represented by either a PSC or the intermediate deck extents.

A conservative assumption, which is relatively easy to replicate in a simplified approach, is to neglect the presence of the deep longitudinals and assume a uniformly stiffened panel across the entire deck width (Deck B). This can result in a pessimistic prediction of ultimate strength, although in the case shown above it is a reasonable representation of the base case load shortening behaviour.

However, if the deep longitudinals are sized large enough the lateral support is sufficient for the longitudinals to act as simply supported boundaries. This is the case in Deck C, for which an intermediate deck representation (and hence a PSC representation) is sufficient to predict the whole panel load shortening response. For this case the uniformly stiffened representation (Deck B) would be overly conservative as it neglects the support provided by the deep longitudinals. Deck D also shows a different response to the other models due to the increased sizing of the centreline stiffener.

The deck example demonstrates that the simplified method needs to calculate the strength of a large flat panel at several levels:

- Firstly, the PSC strength of the panel needs to be quantified. If the panel is sized appropriately, with sufficiently stocky transverse frames, it will fail interframe and the PSC representation should be sufficient for representing the response over the entire panel width, even for a very large panel such as the example deck shown above.
- The second level analysis should account for the regular structure between deep longitudinals, assuming that the stockier stiffeners provide sufficient lateral support. The load shortening behaviour of this intermediate panel should be compared to the PSC strength and, if the strength is reduced, this gives a more appropriate representation of the panel as a whole.
- The third level analysis considers the panel extents over several deep longitudinals, checking whether they are actually able to provide sufficient lateral support to the panel and thus be assumed to act as simple supports. If they do not, the buckling behaviour over several deep longitudinals must be predicted.

- Subsequent analysis levels may also be required to introduce further stiffening structure and further increase the overall width of the panel. For example, Deck D would need to be analysed at three levels in total.

At each level the extents of the panel are chosen to be between points which can be considered to be a simple support. The next level then assesses the validity of this assumption. The analysis continues until the assumption is proved to be valid, or the maximum extents of the panel are reached (for example by analysing an entire ship deck).

These requirements mean that the orthotropic plate method must be further adapted to account for the latter level analyses, where the panel extents include several stiffener sizes. The established orthotropic plate method is only suitable for assessing a regularly stiffened panel. Because of this, the description of the semi-analytical approach is split into two parts. Firstly the approach used to analyse a regularly stiffened orthogonal panel is described (sections 6.3.2-6.3.7). The proposed approach is then further adapted to deal with the effects of deep longitudinals and other irregular stiffening arrangements in section 6.3.8.

### **6.3.2. Calculation Procedure – Regular Stiffened Panel**

This section sets out the calculation procedure of the semi analytical method for analysing an arbitrarily sized panel with evenly spaced identical stiffeners. The procedure first derives the component plate and stiffener load shortening curves. These are combined to predict the interframe PSC strength and then also provide the instantaneous stiffness in the orthotropic calculation of overall panel strength.

The calculation procedure is incremental and is thus able to predict the instantaneous resistive strength of a panel under a specified level of end shortening. At each increment the corresponding instantaneous level of panel resistance is calculated. The panel load shortening curve is derived by repeating the procedure over a full range of increments. The number of increments and step size are chosen so as to provide sufficient detail to adequately describe the panel behaviour.

The calculation descriptions in this section use the terms “resistance” and “instantaneous strength”, which are worth defining to ensure there is a clear distinction between them:

- The resistance of a panel (or component) is the amount of force required to compress the panel by the specified end displacement. The resistance is always less than or equal to the ultimate strength of the panel.

- The instantaneous strength of a panel is associated with a particular mode of collapse and is the maximum capacity, or ultimate strength, for that collapse mode. The strength is instantaneous and can change depending on the end displacement applied to the panel.

The methodology is clearly described by separating the calculation process into steps. At each monotonically increasing increment of end shortening the calculation method is as follows:

1. The plate resistance,  $R_{plate}$ , is evaluated from the parametric FEM curve database;
2. The stiffener resistance,  $R_{stiff}$ , is evaluated from the parametric FEM curve database;
3. The corresponding local component resistance ( $R_L$ ) is calculated by combining  $R_{plate}$  and  $R_{stiff}$ ;
4. The interframe panel strength  $R_C$  is derived from the relevant column collapse curve. This provides an upper bound ultimate strength which is compared with the component resistance. The interframe resistance,  $R_i$ , is the minimum of  $R_L$  and  $R_C$ ;
5. The instantaneous panel strength over two frame bays ( $R_{p,1}$ ) is evaluated using the modified orthotropic plate approach with the number of transverse frames set to unity ( $n=1$ ) and the panel length,  $L$ , equal to  $a(n+1)$ ;
6. Calculations are repeated for integer values of  $n$  from 1 up to the total number of actual transverse frames in the entire panel (i.e. the compartment length);
7. The instantaneous panel resistance ( $R_O$ ) is taken to be the minimum of  $R_i$  and  $R_{p,n}$ . At each increment,  $R_O$  provides an additional point for the panel load shortening curve;
8. If the ultimate strength is reached (i.e.  $R_C$  or  $R_{p,n}$  becomes the minimum) a separate algorithm is initiated to predict the post collapse portion of the load shortening curve.

The interframe resistance,  $R_i$ , should normally be the minimum for small end displacements. The combination of the plate and stiffener component load shortening curves enables tracking of nonlinear behaviour in the pre collapse region. As end displacement progressively increases either the interframe or overall panel strength may become the minimum, indicating that the panel collapses in that mode. The incremental procedure is halted and a post collapse algorithm is invoked to estimate the post collapse behaviour of the panel.

The approach is developed in a computer program to automate the calculation process. A calculation flow chart is presented in Figure 120. The code can either be run as a standalone

application or called from an external program. The standalone version calls a user generated datafile in which the panel properties are detailed. An output file is written containing the panel load shortening curve and other relevant information. Alternatively the code can be invoked by an external program, in which the panel properties are predefined. For this study the program is developed specifically for incorporation in the progressive collapse code developed in Chapter 7. It can therefore be called automatically by the progressive collapse program and output is produced in a format suitable for direct implementation in the progressive collapse calculations.

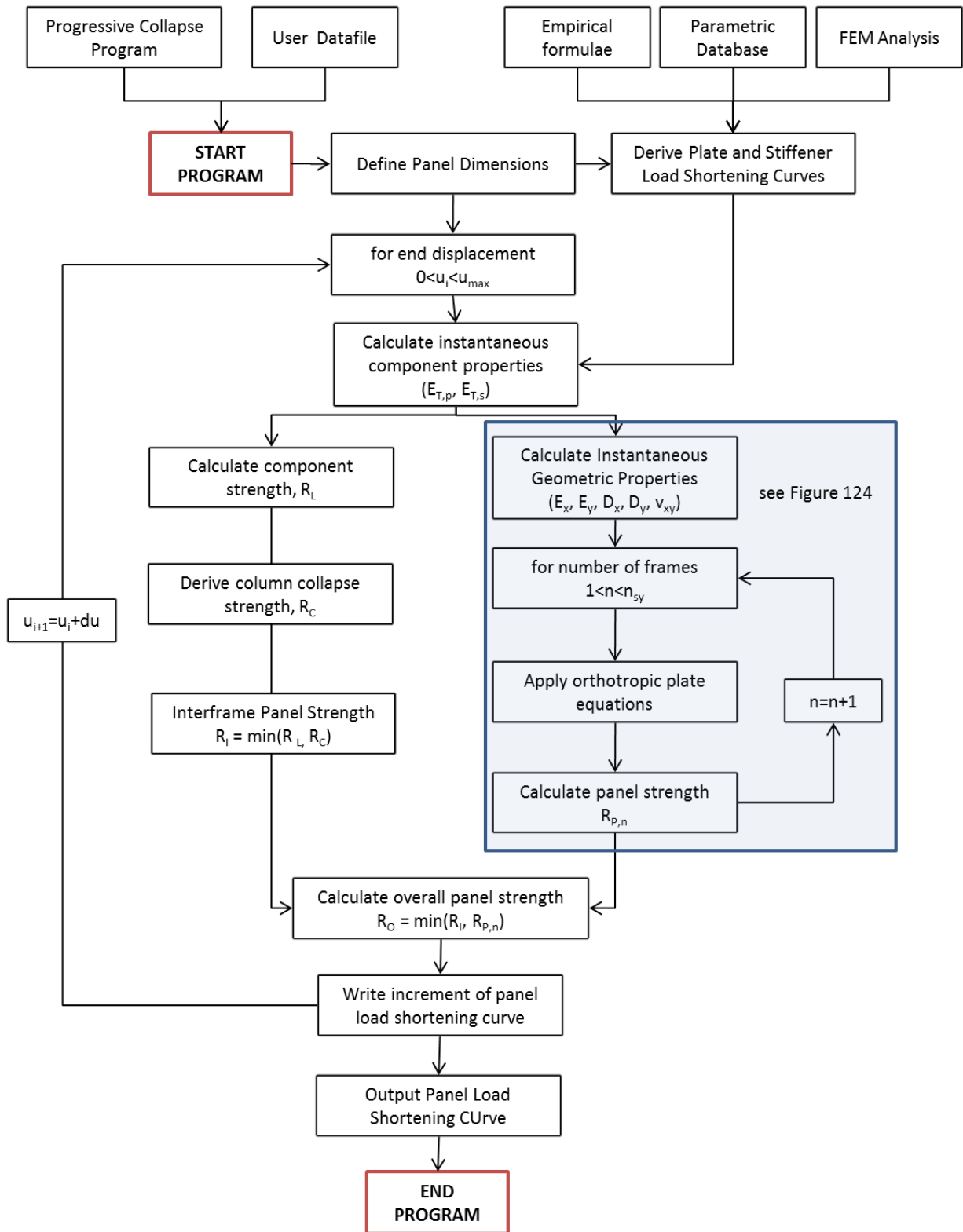


Figure 120 –Semi analytical method calculation flow chart

### 6.3.3. Plate and Stiffener Load Shortening Curves

The individual plate and stiffener load shortening curves are derived by interpolating within the numerical datasets developed in previous Chapters. Linear interpolation gives adequate accuracy as long as the datasets are sufficiently detailed.

The dataset limits in the present study are:

- Materials: 5083-H116, 6082-T6 and Steel
- Plates:  $\beta=1.0-5.0$  with  $H_R=0.06-2.0$
- Stiffeners:  $\lambda=0.2-1.2$  and  $\gamma=0.3-0.9$  with  $K_{\omega}=0-200\text{GN/m}$
- Stiffener sections: Tee Bar, Flat Bar

For the purposes of the semi analytical method, the plate load shortening curves (presented in Chapter 4) form a fairly efficient dataset and covers most typical midship plating found in conventional and lightweight vessels. As is concluded in Chapter 4, plates can be defined by their slenderness ratio,  $\beta$ , material properties and HAZ ratio (if the plate is a welded aluminium alloy). All these properties are accounted for within the dataset.

As has been detailed previously, the stiffener load shortening curves are less easy to condense into a discrete dataset. It has been shown that the stiffener cross section influences the load shortening behaviour, meaning that arbitrarily dimensioned stiffeners with the same  $\lambda$  may exhibit significantly different behaviour under compressive load. The cross section ratio,  $\gamma$ , is defined which provides a reasonable measure of the influence of the cross section. Therefore, a representative curve dataset is created which can be used to define the load shortening curve for an arbitrarily dimensioned stiffener. These curves are given as a function of  $\gamma$ , and can be accessed by the semi analytical method. Alternatively, the individual stiffener data sets for a particular cross section can be used. These datasets are suitable for use if the cross sections match or are roughly similar. However, they are not as suitable for an arbitrarily dimensioned stiffener. For these individual datasets, the curves are defined as a function of  $\lambda$ .

The plate and stiffener component curves are used to give a measure of the instantaneous resistance of the component to a given end displacement. The curves are also used to define the instantaneous tangent stiffness of the components ( $E_{T,p}$  and  $E_{T,s}$ ). Tangent modulus is the

instantaneous stiffness of the element (the gradient of the load shortening curve at a given strain). An example plate curve is presented in Figure 121 with a visual definition of the tangent modulus.

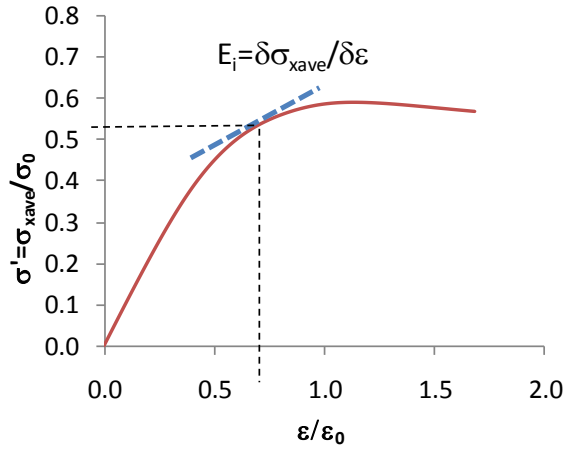


Figure 121 – Example measurement of component resistance and tangent modulus

### 6.3.4. Interframe Panel Strength

This section describes the formulations used to derive the behaviour of the interframe panel in the semi-analytical method. This is achieved by combining the predefined component load shortening curves. As already discussed, the component information used in this study is calculated using FEM. However, the flexibility of the method means that any relevant dataset can be used. Therefore, if more refined information on the component strength is available, the semi analytical method can be easily extended to incorporate this data.

The determination of the unstiffened plate resistance,  $R_{plate}$ , at a given panel end displacement,  $u$ , is derived using the representative load shortening curve obtained from FEM generated datasets as detailed in Chapter 4. The datasets as published in this thesis give the non-dimensional stress-strain relationship of each plate as normalised ratios ( $\sigma'$ - $\epsilon'$ ) using the material proof stress and proof strain (or yield stress/strain for steel). The plate resistance,  $R_{plate}$ , is thus a function of the end shortening displacement and is calculated by converting the normalised stress-strain relationship to a load shortening relationship:

$$R_{plate}(u) = \sigma'_s(u) \cdot \sigma_0 \cdot b \cdot t_p \quad 97$$

where:

$$u = \epsilon' \cdot \epsilon_0 \cdot a \quad 98$$

Likewise, the stiffener resistance is also derived using a representative predefined dataset and converted into the load-shortening format as follows:

$$R_{stiff}(u) = \sigma'_s(u) \sigma_0 (h_w \cdot t_w + b_f t_f) \quad 99$$

The contribution of the stiffener and the plate to the combined local panel resistance,  $R_L$ , is proportional to the relative sectional area of the two components and can be calculated as:

$$R_L(u) = \frac{R_{plate}(u) \cdot b \cdot t + R_{stiff}(u) \cdot (h_w \cdot t_w + b_f \cdot t_f)}{b \cdot t + h_w \cdot t_w + b_f \cdot t_f} \quad 100$$

As discussed previously, this approach can be assumed to give an approximation of the PSC strength and has been shown to produce reasonable correlation with the A.R.E. column collapse design curves, which were ostensibly produced using a similar approach. However, the results do not compare closely to equivalent PSC FEM analyses, which produce much lower predictions of strength at higher column slenderness ratios. A conclusion from the previous Chapter suggests that the assumption of simple supports on the longitudinal edges of the plate, which are used for the generation of the component load shortening curve, is not necessarily suitable when used to predict the behaviour of the plate supported by the actual stiffeners in the panel. This is presumed to be because the stiffener does not maintain a simple support boundary condition on the plate throughout the compressive load range, which is not reflected in the plate load shortening curve.

In the present study a simple approach is adopted to provide an adequate PSC solution. The column collapse curves as derived using FEM analyses are used to define a limiting PSC strength. These curves have been derived for different material combinations and levels of initial imperfection, and thus provide a reasonable For this study the PSC FEM curves as derived in the previous Chapter are utilised. The load shortening behaviour up to the ultimate strength must still be derived using the previous formulation, meaning that the interframe panel resistance,  $R_I$ , thus becomes:

$$R_I(u) = \min \left( R_L(u), R_C \left( \lambda, \beta, \frac{A_s}{A} \right) \right) \quad 101$$

where  $R_C$  is the limiting ultimate strength of the PSC as a function of the column slenderness ( $\lambda$ ), plate slenderness ( $\beta$ ) and stiffener area ratio ( $A_s/A$ ) and can be derived from a suitable column collapse curve.

The semi analytical approach gives a lower bound prediction of the ultimate strength. This is demonstrated by using the above formulation to rework the steel column collapse curves as shown

in Figure 122. Because the method uses the datasets produced using the PSC FEM analyses the resulting column collapse curves are also very similar. At low column slenderness the predicted ultimate strength is more conservative, using the component strength formula. At higher slenderness the PSC FEM datasets predict lower strength, and thus the curves drop off more steeply as slenderness increases.

The ultimate strength is only a single measure at a specific point on the load shortening curve. The entire load shortening relationship is required for input to the progressive collapse method. The pre collapse portion is well described by Eq. 101. If the limiting ultimate strength is never surpassed, then Eq. 101 is used throughout the load range and thus also predicts the load shortening curve beyond the ultimate strength and into the post collapse region. In these instances the collapse mechanism is due to localised buckling of the plate and stiffener components in isolation.

Alternatively, if  $R_L$  reaches the limiting ultimate strength the formulation breaks down and the panel collapse mode is assumed to be by beam column failure. In these cases a further algorithm is required to provide an adequate estimate of the post collapse behaviour. This must adequately represent the characteristics of the failure mode, which is important for progressive collapse analysis.

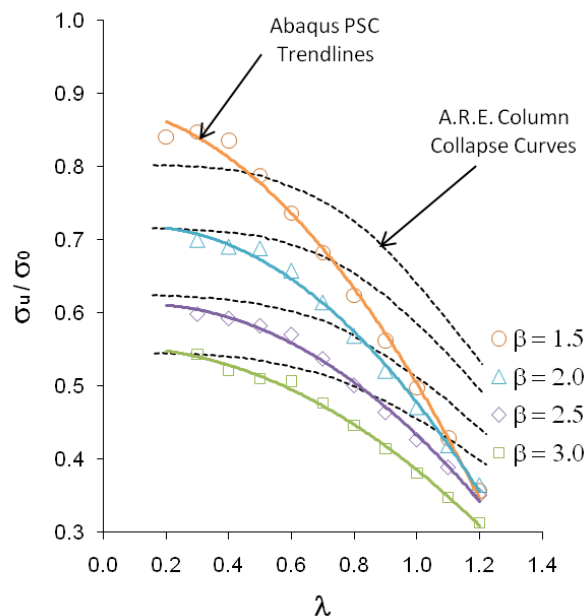


Figure 122 – Column curves for steel PSCs constructed using Eq. 4. The dotted lines show the original A.R.E. curves [76].

Analysis of the post collapse region of the PSC FEM curves show that the unloading gradient depends on the predominant collapse mode of the panel. A shallow unloading gradient generally occurs when collapse is driven by local failure of either the plating or the stiffeners. This is similar to

the general shape of the component plate and stiffener load shortening curves. Steep unloading is indicative of beam column type collapse, where plating and stiffeners fail as a single unit. This type of failure is more sudden, and often occurs when the component stiffness is in the elastic region.

For a beam column collapse mode, the post ultimate strength portion of the load shortening can be assumed to be linear. This simplifies the algorithm, although the FEM results in the previous Chapter show that a linear relationship is not always the case. In some instances (for example panel M1) the post collapse behaviour is characterised by a steep unloading immediately after the ultimate strength is reached which then flattens out at some point further along the post collapse range.

A conservative approximation is to give a close match to the initial unloading curve causing an under prediction of capacity at large displacement. Using this assumption, it was found that an acceptable agreement with FEM results was achieved by taking the negative of the curve gradient immediately before the ultimate strength is reached.

Example load shortening curves predicted using the above formulations are compared to equivalent PSC FEM results in Figure 123. The panel dimensions are as given in Table 31. The FEM and simplified curves show close correlation; the general shape of the semi analytical curve matches closely to the FEM result and all show very similar ultimate strength prediction. The post collapse characteristics are also acceptable. Panels M1 and M2 are predicted to fail with a predominantly beam column collapse mode. Their unloading curve is steep, which shows reasonable similarity to the FEM results, although the ultimate strength of panel M'' is predicted to be lower.

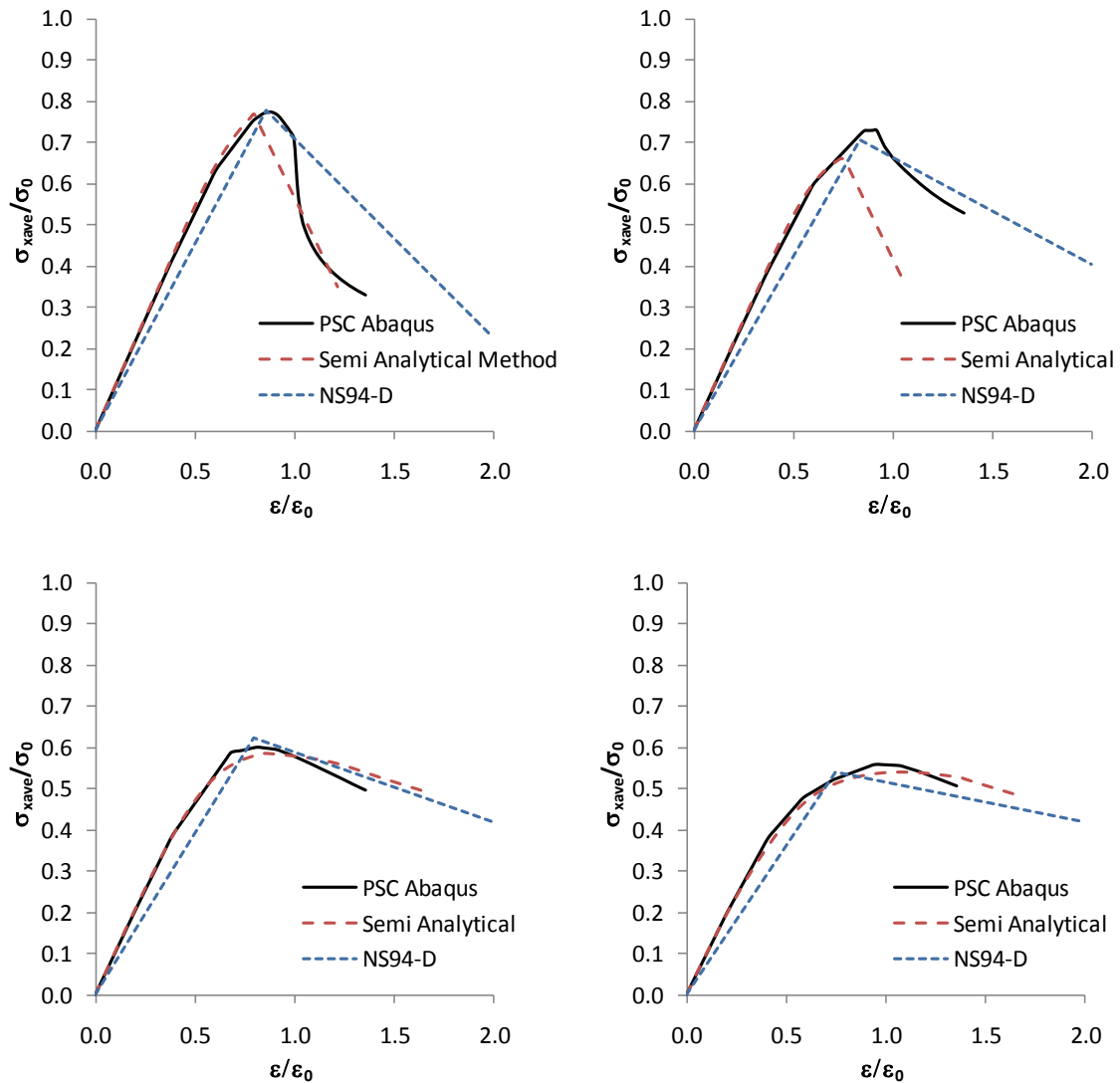


Figure 123 - PSC load shortening curves for Panel M1 (top left), M2 (top right), M3 (bottom left) and M4 (bottom right)

### 6.3.5. Overall Panel Properties

The published large deflection orthotropic plate approach includes elastic constants to describe the plate orthotropy, including the stiffness ( $E_x, E_y$ ), flexural rigidity ( $D_x, D_y$ ), Poisson ratio ( $\nu_x, \nu_y$ ) and torsional rigidity ( $H$ ). The constants reflect the orthotropy of the resulting plate when including the equivalent “smeared” effect of the individual stiffeners. The equations are derived using the governing nonlinear differential equations of large deflection orthotropic flat plate theory. In the classical method these quantities are functions of the panel geometry and the material Young’s modulus. The method assumes that the material properties remain elastic when placed under load. The method thus predicts the elastic response of the panel only.

This assumption is reasonable for very light stiffened panels, where buckling and collapse occurs with average edge stress well below the material yield point. However, this assumption is less acceptable when applied to more stocky stiffened panels. In these cases the response of the panel involves elasto-plastic collapse mechanisms.

For the proposed method, the effective equivalent elastic and flexural properties of the panel components (plates and stiffeners) are recalculated from these previous values at each progressive increment of end displacement using the current instantaneous properties of the components. As the panel end displacement increases, the local tangent modulus of the component stress strain curve reduces, causing a corresponding reduction in the orthotropic plate stiffness values. Similarly, and often more importantly in determining the strength, the flexural rigidity of the components are also affected.

All equations in the following derivation assume a regularly spaced stiffened panel with dimensions as defined previously.

The instantaneous stiffness for the panel under longitudinal compressive load are reworked as follows:

$$E_x = \frac{E_{T,p} B t_p + E_{T,s} n_{sx} A_{sx}}{B t_p} \quad 102$$

$$E_y = \frac{E_{T,p} L t_p + E n_{sy} A_{sy}}{L t_p} \quad 103$$

$E_{T,p}$  is the instantaneous tangent modulus from the plate component load shortening curve. Likewise,  $E_{T,s}$  is the tangent modulus from the stiffener load shortening curve. It is assumed the longitudinal plate tangent stiffness adequately represents the plate in the calculation of  $E_x$  and  $E_y$ , although strictly speaking  $E_{T,p}$  only describes the longitudinal stiffness of the panel. This was considered a reasonable assumption because biaxial plate tests, detailed in Chapter 4, show a reduction in plate stiffness in the transverse direction if a load has previously been applied in the longitudinal direction.

However, this assumption cannot be applied to the transverse frames. The transverse stiffeners are represented by  $E_{(\sigma-\epsilon)}$ , which is the tangent modulus of the material stress-strain curve. This is usually equivalent to the elastic Young's modulus for steel and the tangent modulus of the Ramberg Osgood stress-strain curve for aluminium. This assumes that the transverse frame does not experience high levels of strain, which is reasonable when the load is in the longitudinal direction only.

If the panel is under a biaxial or a transverse load condition then Eq. 103 can be reworked to include both the transverse plate and transverse frame stiffness:

$$E_y = \frac{E_{T,p,transverse}Lt_p + E_{T,s,transverse}n_{sy}A_{sy}}{Lt_p} \quad 104$$

The orthotropic Poisson's ratio equation is similarly reworked as follows:

$$M = \frac{E_y}{E_x} \left( \frac{E_{T,p}t^3}{12} + E_{T,p}tz_{0x}^2 + \frac{E_{T,s}I_x}{b} \right) - \frac{E_{T,p}t^3}{12} - E_{T,p}tz_{0y}^2 - \frac{EI_y}{a} \quad 105$$

$$N = \frac{E_{T,s}I_x}{b} \left( \frac{E_y}{E_x} \right)^2 - \frac{EI_y}{a} \left( \frac{E_y}{E_x} \right) \quad 106$$

$$v_x = c \left[ \frac{M}{N} \right]^{0.5} \quad 107$$

$$v_y = \frac{E_y}{E_x} v_x \quad 108$$

$$v_{xy} = \sqrt{v_x v_y} \quad 109$$

The neutral axis positions and second moment of areas are calculated using Eq. 10.

The calculation of the orthotropic Poisson ratio can break down as the component stiffness progressively reduces. If Eq. 107 or 108 become negative then the solution of Eq. 107 is no longer real. This usually occurs when the panel has surpassed the peak collapse load, and thus only impacts on the post collapse part of the load shortening curve. Therefore, to mitigate the problem, the incremental procedure checks for negative values of M and N at each successive increment and, if either becomes negative, then the previous increment value is used in Eq. 107 to keep  $v_{xy}$  real.

The tangent and torsional rigidities and the shear modulus of the orthotropic plate are also reworked as follows:

$$D_x = \frac{E_{T,p}t^3}{12(1-v_{xy}^2)} + \frac{E_{T,p}tz_0^2}{1-v_{xy}^2} + \frac{E_{T,s}I_x}{b} \quad 110$$

$$D_y = \frac{E_{T,p}t^3}{12(1-\nu_{xy}^2)} + \frac{E_{T,p}tz_0^2}{1-\nu_{xy}^2} + \frac{EI_y}{a} \quad 111$$

$$G_{xy} = \frac{\sqrt{E_x E_y}}{2(1 + \sqrt{\nu_x \nu_y})} \quad 112$$

$$H = \frac{1}{2} \left( \nu_y D_x + \nu_x D_y + G_{xy} \frac{t^3}{3} \right) \quad 113$$

### 6.3.6. Overall Panel Strength

At each increment of end shortening, the revised “elastic” constants are applied in the orthotropic plate calculations. The orthotropic method outputs the instantaneous strength of the panel in the overall mode ( $R_{p,n}$ ) and the critical buckling shape of the overall mode. To reiterate, these calculations output the panel strength, NOT the panel resistance. Section 6.3.7 explains how the instantaneous panel strength is used to determine the incremental panel resistance (i.e. the panel load shortening curve).

The calculation method is summarised as a flow diagram in Figure 124. The orthotropic plate calculations are repeated for an integer number of frame spaces up to the number of bays over the entire panel length. In a compartment level analysis this is usually the number of transverse frames between bulkheads. The critical collapse strength,  $R_{p,n}$  is the minimum value that is calculated with the associated mode indicated by the corresponding value of  $n$ . The minimum is not necessarily found to be over the entire compartment length; hence the calculations must be repeated for intermediate numbers of frame bays.

Firstly, the critical buckling mode shape is calculated. This is defined by the buckling mode numbers  $m$  and  $n$ , which are derived by finding the minimum values satisfying the following equations:

$$D_x \frac{m^2}{L^2} + 2H \frac{1}{B^2} + D_y \frac{L^2}{m^2 B^4} \leq D_x \frac{(m+1)^2}{L^2} + 2H \frac{1}{B^2} + D_y \frac{L^2}{(m+1)^2 B^4} \quad 114$$

$$\left( \frac{B}{L} \right)^4 \leq \frac{D_y}{D_x} n^2 (n+1)^2 \quad 115$$

Once  $m$  and  $n$  are known the discrete solution of the third order equation for the added deflection,  $A_m$ , can be calculated. The third order equation is derived by substituting the Airy stress function into the governing orthotropic equations (see Chapter 3) to yield:

$$C_1 A_m^3 + C_2 A_m^2 + C_3 A_m + C_4 \quad 116$$

The Galerkin method is used to derive the solution to the constants in the discrete equation for longitudinal or transverse in-plane compression load cases. These equations are generalised here in order to apply to combined load cases:

$$C_1 = \frac{\pi^2}{16} \left( E_x \frac{m^4 B}{L^3} + E_y \frac{n^4 L}{B^3} \right) \quad 117$$

$$C_2 = \frac{3\pi^2 A_0}{16} \left( E_x \frac{m^4 B}{L^3} + E_y \frac{n^4 L}{B^3} \right) \quad 118$$

$$C_3 = \frac{\pi^2 A_0^2}{8} \left( E_x \frac{m^4 B}{L^3} + E_y \frac{n^4 L}{B^3} \right) + \frac{m^2 B}{L} \sigma_{xav} + \frac{n^2 L}{B} \sigma_{yav} + \frac{\pi^2}{t} \left( D_x \frac{m^4 B}{L^3} + D_y \frac{n^4 L}{B^3} + 2H \frac{m^2 n^2}{LB} \right) \quad 119$$

$$C_4 = A_0 \frac{m^2 B}{L} \sigma_{xav} + A_0 \frac{n^2 L}{B} \sigma_{yav} - \frac{16LB}{\pi^4 t} p \quad 120$$

The solution of the third order equation can be found using standard algebraic methods and results in:

$$A_m = \frac{C_2}{3C_1} + k_1 + k_2 \quad 121$$

where:

$$k_1 = \left( -\frac{Y}{2} + \sqrt{\frac{Y^2}{4} + \frac{X^3}{27}} \right)^{1/3} \quad 122$$

$$k_2 = \left( -\frac{Y}{2} - \sqrt{\frac{Y^2}{4} + \frac{X^3}{27}} \right)^{1/3} \quad 123$$

$$X = \frac{C_3}{C_1} - \frac{C_2^2}{3C_1^2} \quad 124$$

$$Y = \frac{2C_2^2}{27C_1^2} - \frac{C_2C_3}{3C_1^2} + \frac{C_4}{C_1} \quad 125$$

Once  $A_m$  has been solved, the stress distribution over the whole orthotropic panel is computed as:

$$\sigma_{xmax} = \sigma_{xav} - \frac{m^2 \pi^2 E_x A_m (A_m + 2A_0)}{8L^2} \quad 126$$

$$\sigma_{xmin} = \sigma_{xav} + \frac{m^2 \pi^2 E_x A_m (A_m + 2A_0)}{8L^2} \quad 127$$

$$\sigma_{ymax} = \sigma_{yav} - \frac{n^2 \pi^2 E_y A_m (A_m + 2A_0)}{8B^2} \quad 128$$

$$\sigma_{xmax} = \sigma_{yav} - \frac{n^2 \pi^2 E_y A_m (A_m + 2A_0)}{8B^2} \quad 129$$

The non-dimensional von Mises stress criterion can be used to assess the stress state at any point in the plate. The maximum stress in a uniaxial compressed orthotropic plate is at the midpoint of the longitudinal edges. At this point the von Mises stress,  $\sigma_{MISES}$ , is:

$$\left( \frac{\sigma_{xmax}}{\sigma_0} \right)^2 - \left( \frac{\sigma_{xmax}}{\sigma_0} \right) \left( \frac{\sigma_{ymin}}{\sigma_0} \right) + \left( \frac{\sigma_{ymin}}{\sigma_0} \right)^2 = \frac{\sigma_{MISES}}{\sigma_0} \quad 130$$

Collapse is indicated when the von Mises stress equals the material yield or proof stress (i.e.  $\sigma_{MISES}/\sigma_0=1$ ). If the von Mises stress is less than yield then the assumed average edge stress is too low. A von Mises stress greater than yield indicates the opposite. The calculations are therefore looped with revised predictions of  $\sigma_{ave}$  based on the results of Eq. 130. The program developed in this thesis uses a simple trial and error convergence loop to find the required  $\sigma_{ave}$  to satisfy the von Mises yield criterion with sufficient accuracy.

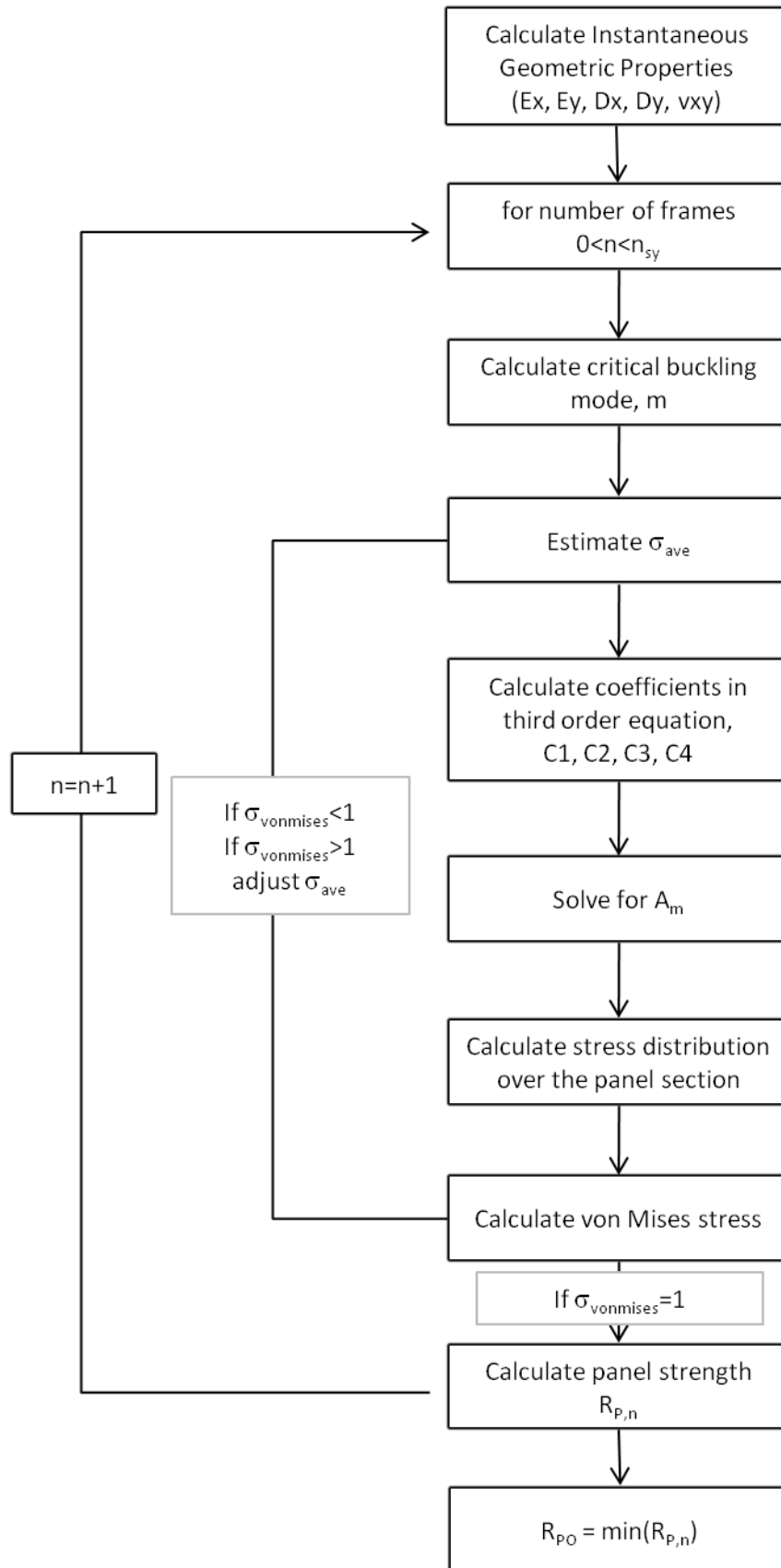


Figure 124 – Orthotropic plate calculation flow chart

### 6.3.7. Panel Load Shortening Curve and Post Collapse Response

Once the orthotropic plate calculations are completed, the method must determine if the panel will fail in an overall manner or continue with interframe PSC behaviour. Therefore, at each increment of end displacement, the instantaneous overall panel resistance,  $R_{\text{OVERALL}}(u)$  is determined as the lesser of  $R_{\text{PO}}$  and  $R_{\text{L}}$ .

In the first (pre collapse) increments of the calculations,  $R_{\text{L}}$  should remain the lesser value. The panel stiffness remains positive and the load shortening curve follows the PSC representation.  $R_{\text{PO}}$  is usually a fairly high value, particularly if the panel is reasonably stocky. This is because the component properties are in the elastic region and the orthotropic calculations are thus reporting the elastic overall buckling strength of the panel.

As end displacement increases, several possibilities may occur. In some instances the overall panel resistance remains higher than the PSC resistance throughout the displacement range. If this is the case the panel is judged to collapse interframe and the PSC curve is used to represent the panel behaviour throughout. This is shown graphically in Figure 125a, which plots the PSC curve together with the panel strength determined over the entire displacement range.

In other instances, the PSC resistance exceeds the instantaneous overall panel strength prior to interframe collapse. This signals a switch from interframe to an overall mode of failure, and also usually determines the ultimate strength of the panel. This is shown in Figure 125b - Figure 125d. The overall failure mode becomes critical where the panel strength curve intersects with the PSC load shortening curve. At this point a separate post collapse algorithm is invoked, which will be explained below.

The switch from the PSC to overall buckling can be due to several different phenomena predicted by the extended orthotropic plate calculations. In some cases the elastic properties of the orthotropic plate are such that the overall mode of collapse starts from a low value. The very light panels examined in Chapter 3 using the original orthotropic plate calculations are typical examples. Thus the positive gradient PSC curve slope meets the overall panel strength curve which remains horizontal (Figure 125b).

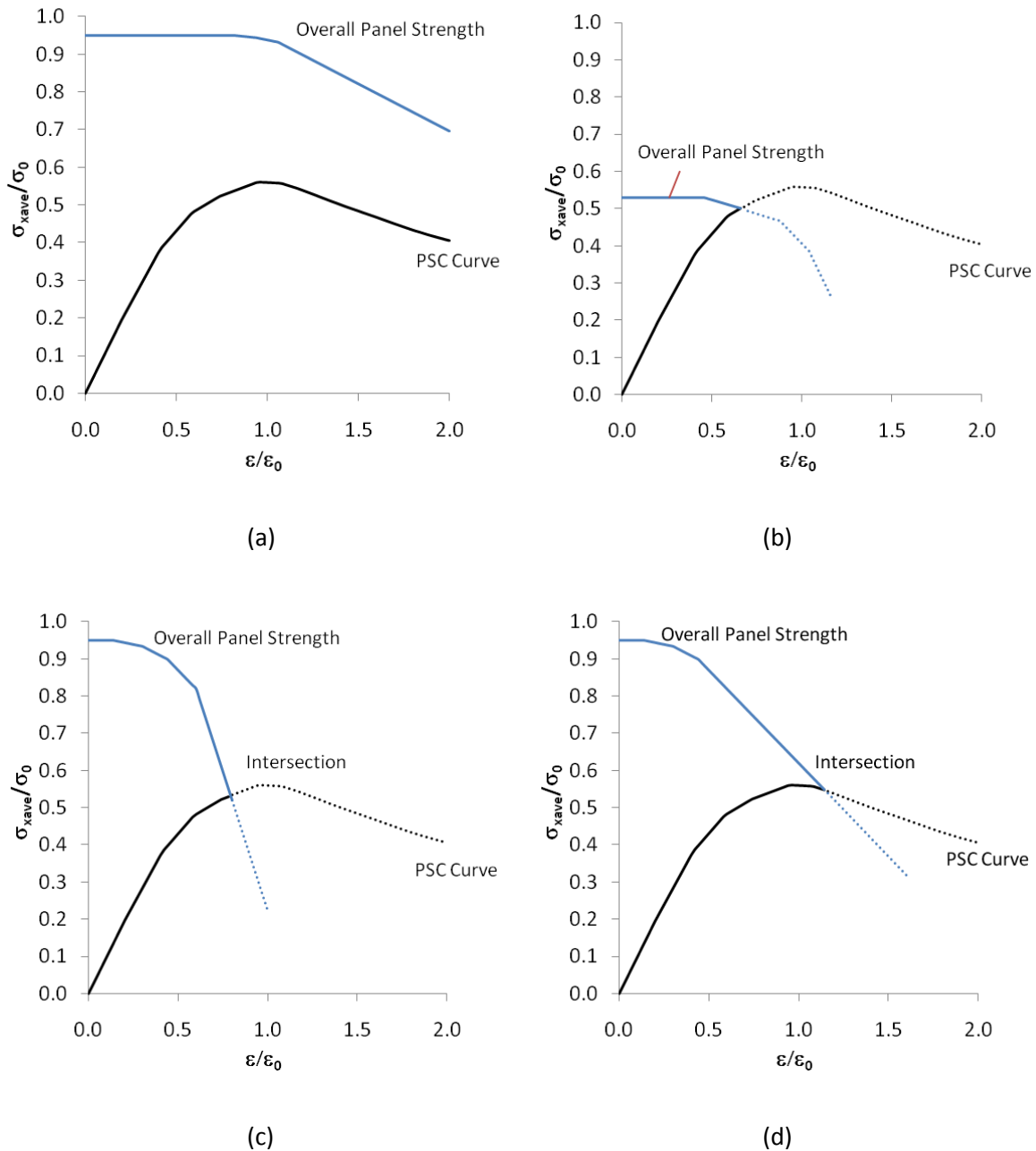


Figure 125 – Example PSC and overall panel strength curves

In other instances the overall panel strength curve initially predicts a high ultimate strength. However, the reduction in the stiffness properties of the components causes the strength curve to descend as shown in Figure 125c and Figure 125d. This often occurs quite rapidly, as either the plate or stiffener start to reduce in stiffness and approach their local buckling points. In this case the intersection with the PSC curve is due to the negative gradient in the overall panel strength curve. The intersection point may occur prior to the PSC ultimate strength point (Figure 125c) or after the PSC ultimate strength point has been passed (Figure 125d).

The intersection point determines the ultimate strength of the orthogonal panel and indicates an overall collapse mode. The post collapse behaviour of the panel is also required to complete the load shortening curve prediction over the entire displacement range. For a progressive collapse analysis, the shape of the post collapse region of the load shortening curve is highly important. As has been summarised previously, the failure of individual elements does not necessarily cause the failure of the entire hull girder and therefore the post collapse behaviour of elements can significantly affect the progressive collapse solution.

One potential way for predicting the post collapse behaviour is to continue calculating the orthogonal panel strength with further increases in end displacement, thus following the overall panel strength curve. An example is shown in Figure 126a. In the example, the method starts to predict a steep negative gradient. This is consistent with FEM predicted post collapse behaviour when the overall panel buckling is preceded by localised plastic buckling in the components. However, at larger increments of end displacement the orthogonal plate calculations become less reliable, partly due to the negative stiffness of the components once they have buckled. This results in a fairly chaotic load shortening curve, which is not close to the actual likely behaviour.

Therefore a simpler post collapse curve can be postulated by taking the initial gradient from the post collapse point and assuming a linear post collapse curve shape (Figure 126b). The gradient of the post collapse response is thus determined by the orthotropic plate behaviour in the ultimate strength region only. This was found to give an adequate prediction of the post collapse response. Thus a steep post collapse gradient is predicted when overall panel strength drops steeply due to plasticity in the components. When the panel is very lightly framed, and the ultimate strength point is well within the elastic region, the post collapse gradient is much shallower. An example of this type of collapse is shown in Figure 125b.

The post collapse response is further explored in the example cases presented in section 6.4.

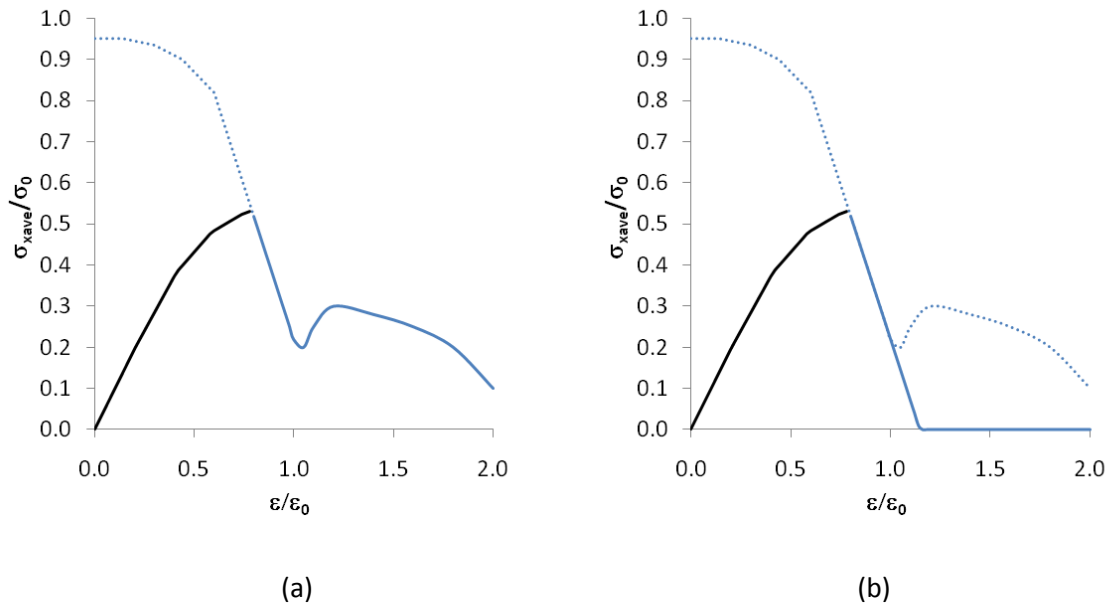


Figure 126 – Post collapse region curve prediction methods

### 6.3.8. Irregular Stiffened Panels

Up to this point, the semi analytical method has been described for a regularly stiffened panel. For panels with several different stiffeners making up the cross section, such as the deck introduced in section 6.3.1, a further extension of the semi analytical methodology is required.

The primary inputs to the semi analytical method are load shortening curves which describe the component behaviour. In the method as described so far, these components are simple flat plates and single stiffeners. The stiffener shape is important for determining the second moment of area of the panel and hence the panel slenderness. However, the actual shape of the plate component is not so important. Therefore, an “equivalent” plate can be used, which is actually a span of stiffened structure.

The output of the method is orthotropic plate strength, where the individual plates and stiffeners are treated as a single entity, which is then used to construct a load shortening curve for the panel.

This approach fits neatly into the hierarchical procedure proposed in section 6.3.1. It allows an irregular stiffened panel to be analysed by using multiple passes through the orthotropic plate method. Each pass uses larger model extents to encompass more structure. The previous model extents are represented by the associated load shortening curve and are treated as equivalent to a simple plate. After each pass the strength of the larger model is compared to the previous intermediate model. A reduced strength behaviour indicates that the stiffeners in the larger model do not provide sufficient lateral support and must be included as part of the panel buckling analysis.

This is clearly shown using the diagram in Figure 127 for the example deck panel. A span of regularly stiffened plating between deep longitudinals is first analysed using the semi analytical method. This sub panel is assigned a load shortening curve from the results of the first pass analysis. The intermediate span is then treated as an equivalent plate attached to the deep longitudinals, with the plate behaviour represented by the intermediate level panel load shortening curve. A second pass through the orthotropic calculations is completed.

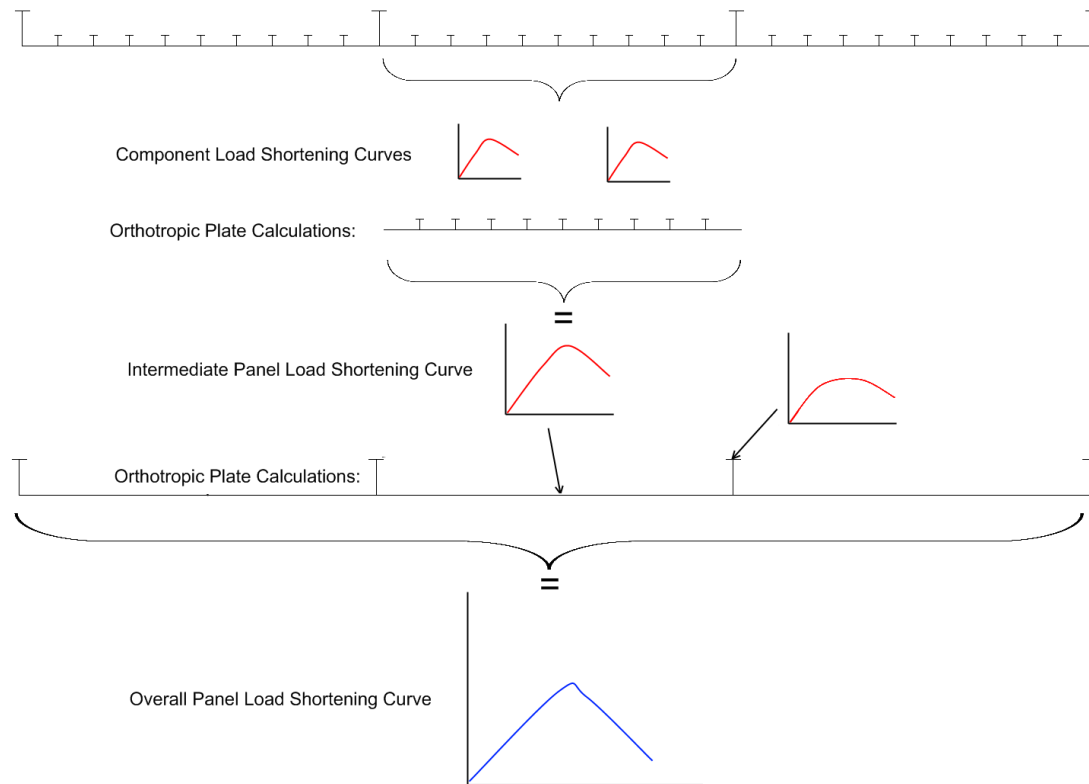


**Figure 127 – Irregular panel calculation method**

Analyses of the example aluminium deck panel show the calculation method in practice. Analysis of Deck A requires two passes through the orthotropic plate calculations. Firstly, the local PSC load shortening curve is derived. This is shown in Figure 128 and compares very closely to the equivalent FEM result. The intermediate deck structure (i.e. between adjacent deep longitudinals) is then analysed using the orthotropic plate calculations. The same results as found by the FEM analysis is predicted. The interframe structure shows no difference to the PSC result. The resulting load shortening curve predicted by the semi-analytical method is the same as the PSC result in Figure 128.

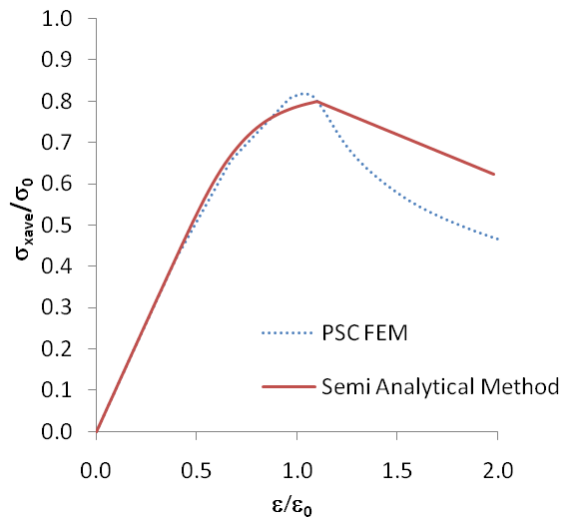
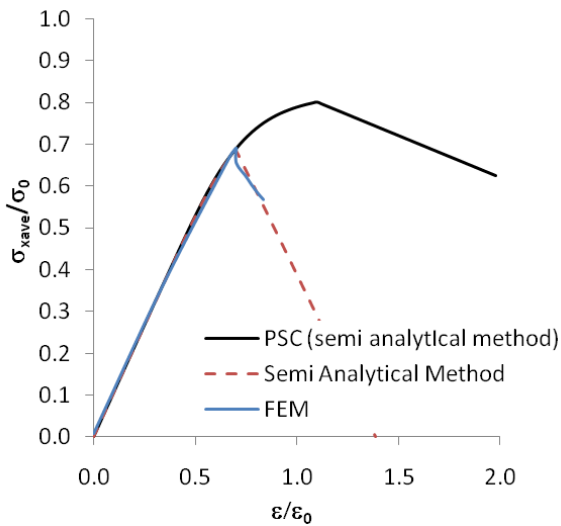


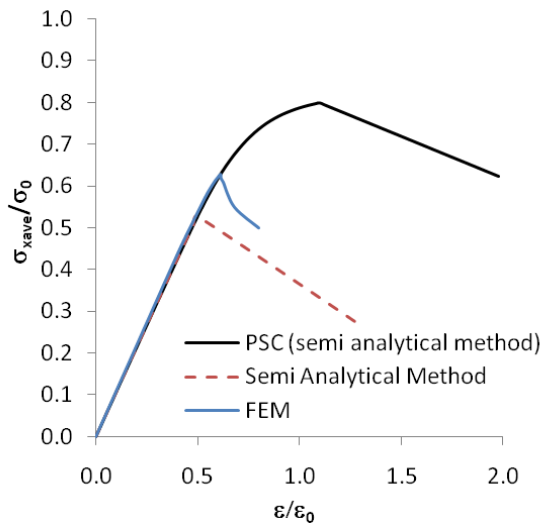
Figure 128 – PSC load shortening curve predicted by the semi analytical method for the aluminium deck structure

The intermediate deck result is then used as an input to the second pass orthotropic plate calculations, which models the entire deck with 7 deep longitudinals connected to an equivalent plate which is described by the load shortening curve in Figure 128. The resulting panel load shortening curve is shown in Figure 129.

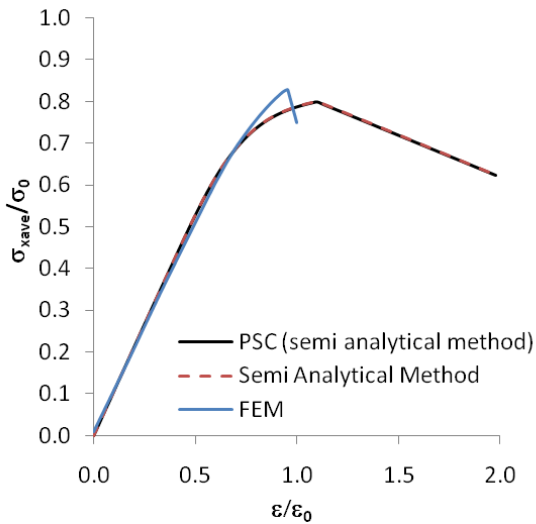
The results show that the deep longitudinals are adequately accounted for in the semi analytical methodology. As shown earlier with the FEM analyses, the size and location can have a significant effect on the collapse strength of the panel. Deck C, the most heavily stiffened panel, has overall characteristics identical to the interframe PSC. The other 3 variants all show reduced strength and correspond well to the equivalent FEM panel analyses. The results for Decks A and D show remarkably close agreement to the FEM both in terms of the ultimate strength prediction and the post collapse curve shape. The result for Deck B, which is the lightest structure with no deep longitudinals, has a semi analytical prediction of the ultimate strength somewhat below the equivalent FEM panel result. However, the general shape of the curve is similar. The difference in ultimate strength prediction may be because the panel is stiffened so lightly, which increases its sensitivity to the overall panel width. If the panel width is reduced only slightly, the overall strength increases markedly.



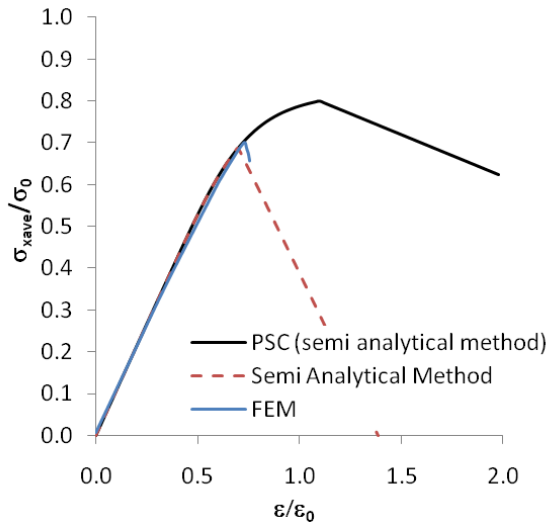
(a) Deck A



(b) Deck B



(c) Deck C



(d) Deck D

Figure 129 – Panel load shortening curves predicted by the semi analytical method for the variant aluminium deck structures

### 6.4. Case Studies – Multi Bay Stiffened Panels

So far, the calculation steps involved in the semi analytical method have been explained using just one example aluminium deck. This provides only one validation case. Therefore, the purpose of this section is to further validate the method by applying it to the dataset of orthogonally stiffened panels previously computed using FEM and reported in Chapter 5. All the panel dimensions and geometric properties are as defined in section 5.4.

Of primary importance to this study is the behaviour of aluminium ship structures, and for this reason the performance of 5083-H116 stiffened panels are first compared. The correlation between the results of the FEM studies in Chapter 5 and the proposed semi analytical method can be judged using several comparative measures. A first comparison is of the ultimate strength values, which are listed in Table 35 and also shown in Figure 130. The figure shows that the methods correlate reasonably well. The semi analytical method is conservative with a mean bias of 0.93. The COV is 0.14, which is of the same order as was found when comparing FEM with experiment. This is relevant because it must be considered that the FEM results are subject to an amount of variation due to the various parameters that define their imperfection characteristics.

**Table 35 – Ultimate Strength Results – 5083-H116 panels**

Panel ID	Frame Dimensions (mm)	Panel Size	Ultimate Strength (FEM)	Ultimate Strength (Simplified)
M1	360x10	20x7	0.71	0.69
M1	180x10	20x7	0.36	0.43
M2	360x10	20x7	0.66	0.63
M2	180x10	20x7	0.46	0.46
M3	360x10	20x7	0.61	0.57
M3	180x10	20x7	0.47	0.40
M4	360x10	20x7	0.56	0.51
M4	180x10	20x7	0.46	0.40
M5	360x10	20x7	0.38	0.42
M5	180x10	20x7	0.24	0.25
M6	360x10	20x7	0.80	0.76
M6	180x10	20x7	0.50	0.55
M7	360x10	20x7	0.67	0.73
M7	180x10	20x7	0.38	0.40
M8	360x10	20x7	0.50	0.53
M8	180x10	20x7	0.40	0.38
M9	360x10	20x7	0.33	0.16
M9	180x10	20x7	0.23	0.22
M10	360x10	20x7	0.47	0.48
M10	180x10	20x7	0.34	0.24

Table 36 – Ultimate Strength Results 6082-T6 panels

Panel ID	Frame Dimensions (mm)	Panel Size	Ultimate Strength (FEM)	Ultimate Strength (Simplified)
N1	360x10	20x7	0.35	0.41
N1	180x10	20x7	0.53	0.65
N2	360x10	20x7	0.38	0.41
N2	180x10	20x7	0.58	0.62
N3	360x10	20x7	0.41	0.42
N3	180x10	20x7	0.58	0.56
N4	360x10	20x7	0.42	0.37
N4	180x10	20x7	0.53	0.50

Table 37 – Ultimate Strength Results – Steel panels

Panel ID	Frame Dimensions (mm)	Panel Size	Ultimate Strength (FEM)	Ultimate Strength (Simplified)
S1	360x10	20x7	0.44	0.47
S1	180x10	20x7	0.69	0.72
S2	360x10	20x7	0.66	0.50
S2	180x10	20x7	0.71	0.67
S3	360x10	20x7	0.55	0.53
S3	180x10	20x7	0.61	0.60
S4	360x10	20x7	0.53	0.51
S4	180x10	20x7	0.58	0.53

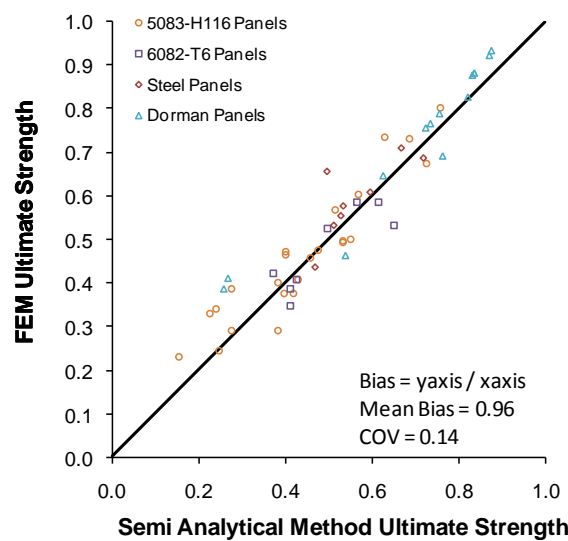


Figure 130 – Comparison between FEM and semi analytical ultimate strength prediction – 5083-H116 panels

For the purposes of providing input to the progressive collapse method, the curve shape produced by the simplified method is also highly important. Example load shortening curves for panels M1-M4 are shown in Figure 131 - Figure 134. The plots show that the semi analytical method generally predicts a reasonable curve shape over the entire load range. In the pre collapse region of the curve, the semi analytical method tracks closely to the PSC result.

The ultimate strength point forms a sharp transition into the post collapse curve. The sharp peak is always more pronounced than the more rounded peak of the FEM results. This is particularly noticeable for the lightly framed (T2) results, where the FEM curve departs from the PSC track for a period before the ultimate strength is reached. The equivalent semi analytical result cannot predict this effect. The linear post collapse relationship as predicted by the semi analytical method shows reasonably close correlation to the FEM results. Even where the ultimate strength is not well correlated, for example in panel M3-T2, the gradient of the post collapse curve is well predicted.

Overall, the semi analytical method shows good correlation to the FEM results and provides an excellent method for implementing load shortening curve generation for the progressive collapse method.

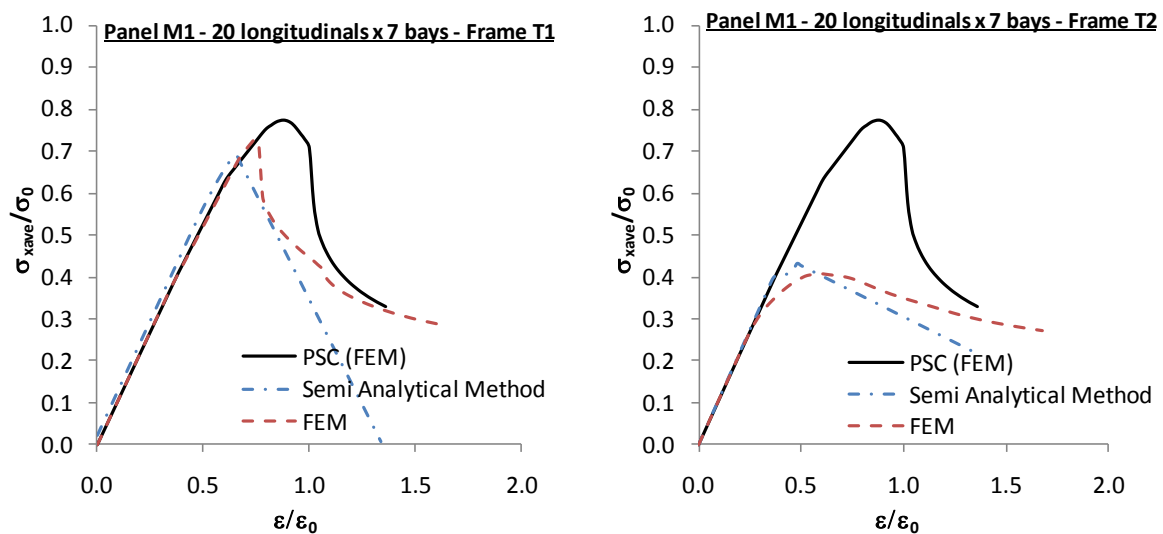


Figure 131 - Panel load shortening curves : comparison of semi analytical and FEM results, Panel M1

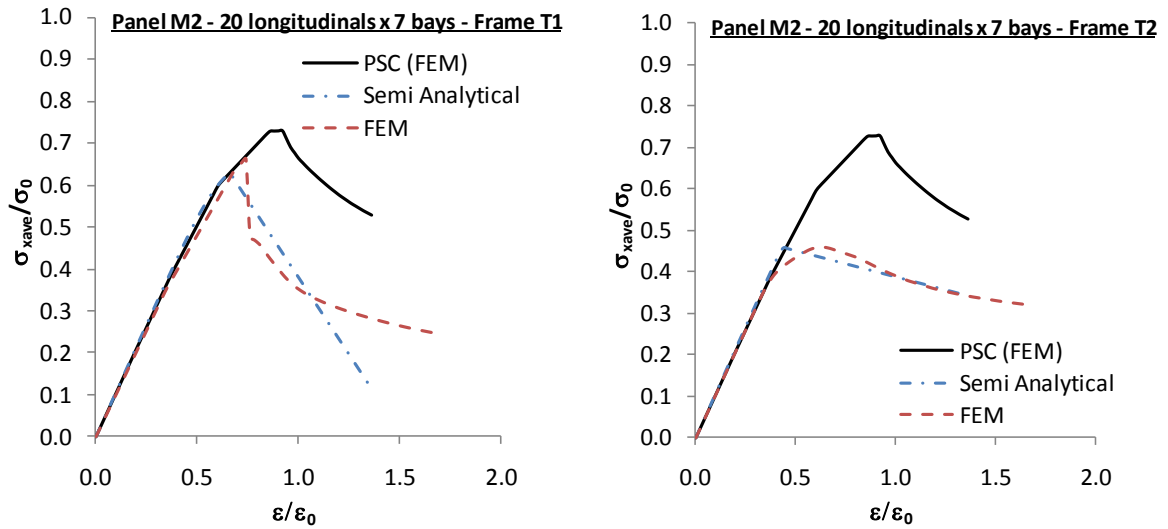


Figure 132 - Panel load shortening curves : comparison of semi analytical and FEM results, Panel M2

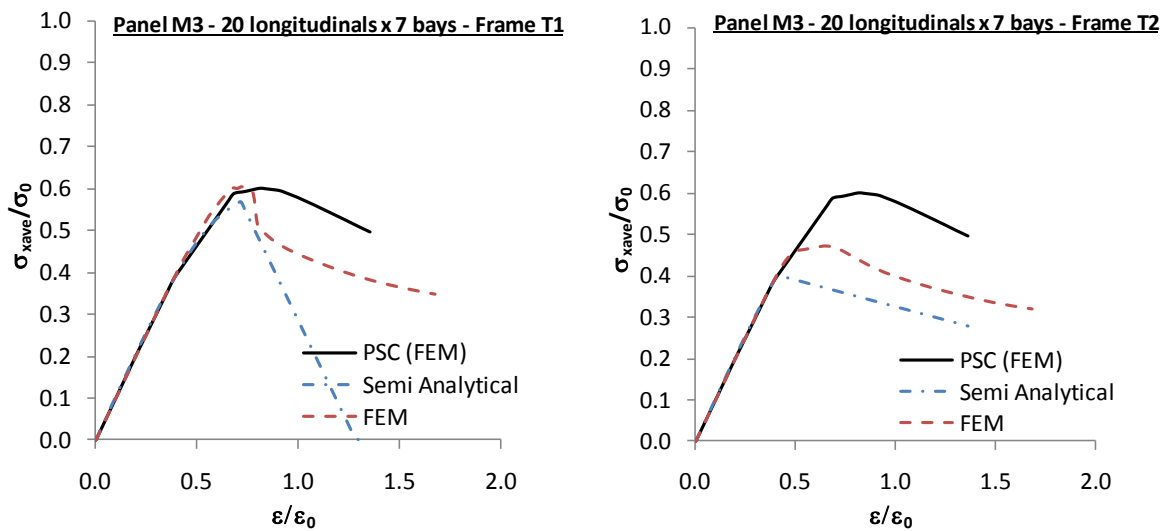


Figure 133 - Panel load shortening curves : comparison of semi analytical and FEM results, Panel M3

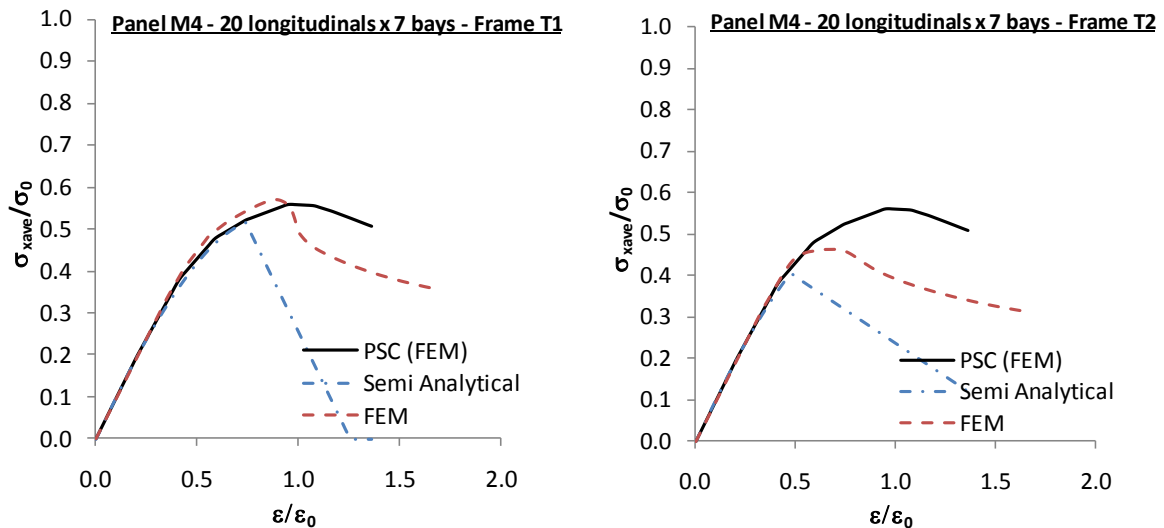


Figure 134 - Panel load shortening curves : comparison of semi analytical and FEM results, Panel M4

## 6.5. Summary

The semi analytical method as summarised in this section is capable of predicting the onset of overall and local buckling modes for a multi bay stiffened panel in uniaxial compression. Comparisons with FEM analyses have shown good correlation throughout a range of end shortening up to and beyond the peak ultimate strength.

The experiments show that overall buckling modes can have a significant effect on the load shortening characteristics of a panel and that PSC models may not always be sufficient in representing the behaviour of a structure in a progressive collapse type method. If overall buckling modes are expected then an enhanced ultimate hull girder strength analysis method which includes the effects of the panel characteristics is needed.

The procedure described in this Chapter has been primarily developed and tested for a uniaxial longitudinal load condition. Further developments are envisaged to extend the methodology to deal with multiple load combinations including lateral pressure loads and biaxial in-plane compression.

*“...the most useful and valuable experience is that derived from failures and not from successes”,*  
Isambard Kingdom Brunel [40]

# Chapter 7

## Hull Girder Progressive Collapse Methods

### 7.1. Introduction

The previous Chapters have shown how the structural arrangement and sizing of stiffened panels will affect the failure mode and progressive collapse characteristics under in-plane compressive load. The extents of the structural model have been increased from simple plate components (Chapter 4) up to a complete deck structure (Chapters 5 and 6). This Chapter completes this progression through the structural hierarchy; investigating hull girder under global load scenarios.

Previous studies have demonstrated that the interframe progressive collapse method is a capable approach to predict the ultimate strength behaviour of a hull girder when collapse is wholly interframe [120]. An extension of the interframe method is proposed to take into account the collapse characteristics of a lightweight structure, which are not necessarily equivalent to conventional steel ships and may include compartment level buckling modes. The extended progressive collapse method can account for both interframe and overall buckling modes. The

method is thus a compartment level approach, being applicable to predicting the strength of a girder between bulkheads or other discontinuous transverse structure.

The first part of the Chapter describes the calculation procedure for the Smith progressive collapse method and details how the approach is extended to account for gross panel buckling. The nonlinear FEM modelling approach, which is used to validate the simplified method, is summarised. A series of validation studies are then presented, comparing the bending moment-curvature prediction of various stiffened cross sections using the conventional progressive collapse method (ProColl-I), extended progressive collapse method (ProColl-O), nonlinear finite element analysis and, where available, physical experiment results.

Five models are used to provide validation of the proposed methods:

- IST box girders [121];
- 1/3 Scale Frigate Model [120];
- “Collette” Box Girder [5];
- Aluminium box girders (based on the panels examined in section 6.4);
- Pacificat catamaran [16].

## **7.2. The Interframe Progressive Collapse Method**

The general principles of the Smith progressive collapse method are detailed in Chapter 2. A summary of the calculation procedure proposed by Dow [45] is now presented, which deals with biaxial bending and unsymmetrical sections.

The progressive collapse method can be used to determine the longitudinal strength of any closed shell girder structure, and can be used to determine the strength at any point along the girder length. In a ship the midship cross section is usually of greatest interest as the maximum wave bending moment is normally found at or around amidships. For the purposes of constructing a progressive collapse model the cross section is divided into discrete elements. The element size must be small enough to provide sufficient fidelity in the solution. A fundamental assumption of the progressive collapse method is that plane sections remain-plane. This means that curvature about the neutral axis only imparts in-plane loads on the continuous longitudinal structure. Therefore, each element is assumed to bear in-plane tensile or compressive loads only.

A second assumption of the progressive collapse method is that the elements behave independently. This means that each element is assigned a pre-determined load shortening curve which is unaffected by the relative strength of adjacent elements. An element is usually considered to be one of two types: it either buckles in compression or, if it is sufficiently stocky to avoid buckling, follows the material stress-strain relationship. The latter is normally only assigned to elements adjacent to corners, which will not buckle due to the localised rigidity of the corner shape. Hard corner elements are often assumed to extend a distance of  $30.t_p$  from the corner point. The tensile properties of the element are also usually assumed to follow the material stress-strain curve.

With the exception of hard corners, all elements are assumed to buckle under compressive load. It is usual for an element to be assigned a load shortening curve derived for a single stiffener with attached plating, which has been shown in Chapter 5 to provide a representative average compressive strength for a wide interframe panel. However, the element itself does not have to be the same shape or extents as the equivalent PSC model used to define the load shortening curve. Figure 135 provides some example element sizes. A standard element is directly equivalent to a PSC, comprising a single stiffener with attached plating. However, a smaller element size can be used, such as an individual plate or stiffener (see Figure 135). Although the element itself is not proportioned as a PSC, it is still assigned the equivalent PSC load shortening curve. In the same manner a larger element size, encompassing multiple stiffeners, can also be employed. The advantage of smaller elements is to improve the accuracy of the solution. The concept of separating element size and equivalent panel size for defining the load shortening curve is particularly important for the extended progressive collapse method proposed in the next section.

The contribution of each element to the overall bending strength of the girder is calculated using a simple incremental approach. Increments of bending moments ( $\Delta M_H$ ,  $\Delta M_V$ ) are related to incremental curvature ( $\Delta \phi_H$ ,  $\Delta \phi_V$ ) using the instantaneous tangent rigidities of the cross section ( $D_H$ ,  $D_V$ ,  $D_{HV}$ ). The method assumes that incremental bending moment / curvature occurs about an instantaneous neutral axis, which is a function of the instantaneous tangent stiffness and area of each element. The relationship between bending moment and curvature is split into vertical and horizontal components:

$$\begin{bmatrix} \Delta M_H \\ \Delta M_V \end{bmatrix} = \begin{bmatrix} D_H & D_{HV} \\ D_{HV} & D_V \end{bmatrix} \begin{bmatrix} \Delta \phi_H \\ \Delta \phi_V \end{bmatrix} \quad 131$$

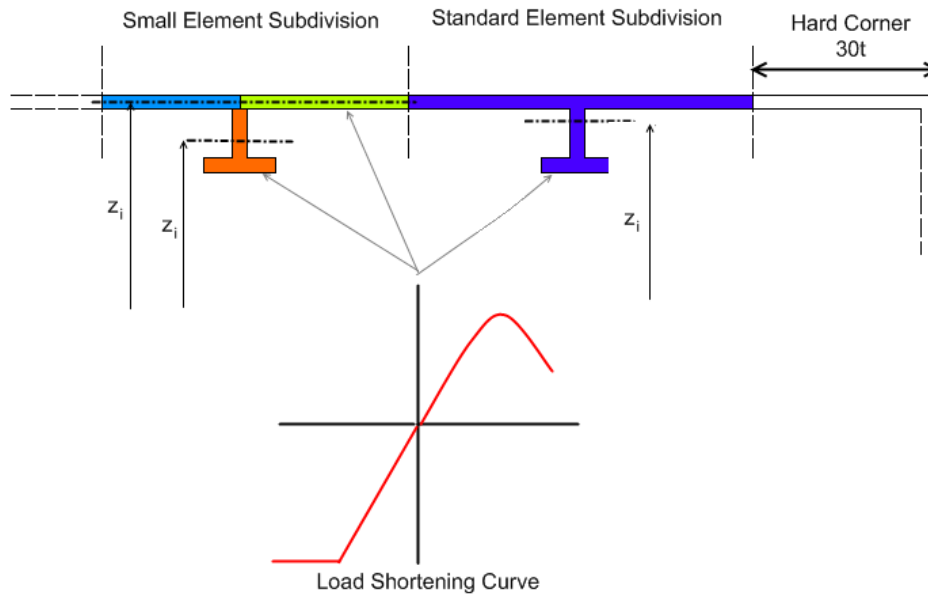


**Figure 135 – Element subdivision in the progressive collapse method**

The above formulation is suitable for calculating incremental bending moment for fixed increments of curvature. The method can be used directly to calculate bending moment well into the post collapse region. However, this approach is not always suitable for biaxial bending moment problems, as the proportion of horizontal and vertical bending moments are unconstrained and will not necessarily follow a prescribed ratio. Therefore the equations can be rearranged to calculate curvature over fixed increments of bending moment:

$$\begin{bmatrix} \Delta\phi_H \\ \Delta\phi_V \end{bmatrix} = \begin{bmatrix} D_H & D_{HV} \\ D_{HV} & D_V \end{bmatrix}^{-1} \begin{bmatrix} \Delta M_H \\ \Delta M_V \end{bmatrix} \quad 132$$

Expanding this equation yields:

$$\begin{bmatrix} \Delta\phi_H \\ \Delta\phi_V \end{bmatrix} = \begin{bmatrix} \frac{D_V}{|A|} & \frac{-D_{HV}}{|A|} \\ \frac{-D_{HV}}{|A|} & \frac{D_H}{|A|} \end{bmatrix} \begin{bmatrix} \Delta M_H \\ \Delta M_V \end{bmatrix} \quad 133$$

where:

$$|A| = \begin{vmatrix} D_H & D_{HV} \\ D_{HV} & D_V \end{vmatrix} = D_H D_V - D_{HV}^2 \quad 134$$

This formulation breaks down when the maximum bending moment is reached, which is signalled when the determinant of A becomes negative. Thus the procedure must switch to applying incremental curvature if the post collapse behaviour is also required.

The contribution of each element to the overall bending strength of the girder is encapsulated in the tangent rigidity formulations.  $D_H$ ,  $D_V$  and  $D_{HV}$  describe the instantaneous inertia of the cross section including the effects of the tangent stiffness of each element:

$$D_H = \sum_i E_i A_i y_i^2 \quad 135$$

$$D_V = \sum_i E_i A_i z_i^2 \quad 136$$

$$D_{HV} = \sum_i E_i A_i y_i z_i \quad 137$$

These equations assume that each element is relatively small and therefore its own inertia can be neglected.  $y_i$  and  $z_i$  are the component distances of the element centroid from the vertical and horizontal position of the instantaneous neutral axis. In the first increment the instantaneous neutral axis is equivalent to the elastic neutral axis because all elements are assumed to have elastic stiffness. However, the stiffness of the element changes as the end displacement increases. To derive the tangent modulus ( $E_{t,i}$ ) of each element, the strain in each element is first calculated incrementally as:

$$\Delta \varepsilon_i = \Delta \phi_H y_i + \Delta \phi_V z_i \quad 138$$

$$\varepsilon_i = \varepsilon_{i-1} + \Delta \varepsilon_i \quad 139$$

The instantaneous stress ( $\sigma_i$ ) and tangent modulus is then derived from the element load shortening curve using appropriate interpolation methods (see Figure 136).

The tangent modulus is also used to determine the shift in the instantaneous neutral axis. In the first increment the elastic neutral axes of the cross section are used to define the initial curvature axes. In subsequent steps the method assumes that incremental bending moment/curvature occurs about instantaneous neutral axes, which are a function of the instantaneous tangent stiffness and area of each element. Thus as the stiffness of elements change, the position of the axes shift according to the following formulae:

$$\Delta NA_V = \frac{\sum_i E_i A_i z_i}{\sum_i E_i A_i}, \quad \Delta NA_H = \frac{\sum_i E_i A_i y_i}{\sum_i E_i A_i}$$

140

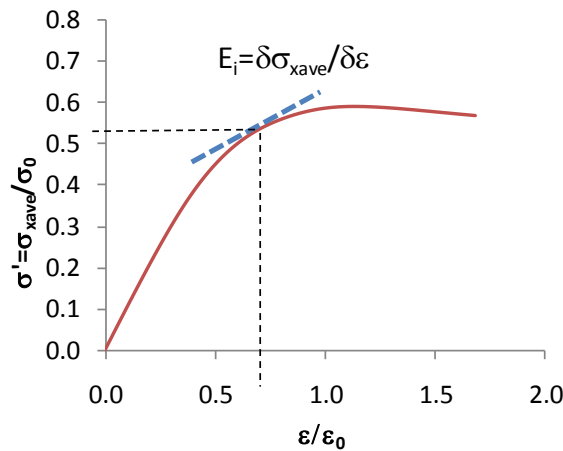


Figure 136 - Example element load shortening curve.

### 7.3. The Extended Progressive Collapse Method

Previous Chapters of this thesis have emphasised that it is critical to define representative load shortening curves for the stiffened panel elements in the progressive collapse method. Established progressive collapse codes have therefore developed several methods to predict the load shortening behaviour of a plate stiffener combination. For example the original code developed by Dow [45], known as NS94, has options to utilise a parametric database of load shortening curves, which have been derived using a combination of physical test results and beam column finite element analyses. Alternatively, element load shortening curves can be derived using empirical approaches [116, 122], analytical methods [123] or by the nonlinear finite element method (FEM) [39] as have been reviewed in Chapter 3.

The common assumption for all these established approaches is that the panel fails interframe and that each plate-stiffener element acts independently. This allows the elements in the progressive collapse methodology to be subdivided and assigned load shortening curves as shown in Figure 135. However, the figure also demonstrates that the actual shape of the element is arbitrary so long as the load shortening curve assigned to it is representative of how that element will behave when placed under in-plane load.

This means that the progressive collapse method is not restricted to calculating interframe collapse of a hull girder cross section if the load shortening curves can be suitably adjusted to reflect compartment level behaviour. The semi analytical method described in the previous Chapter

provides such a means to derive compartment level panel load shortening curves. Therefore, the extended approach proposed here follows the same overall principles and calculation procedure as the original progressive collapse method. The difference between the extended approach and the original interframe method is the way the elements are defined, subsequently requiring load shortening curves which reflect overall and interframe collapse modes.

The approach keeps the assumption that plane sections remain-plane. This is required because the load shortening curves derived using the semi analytical method can only deal with in-plane load conditions. This means that elements are still assumed to resist incrementally increasing in-plane loading only. The plane section assumption is valid as long as curvature continues to be small relative to the total compartment length.

Elements are subdivided into small components using the same approach as the standard method. However, the assumption that elements act independently from adjacent structure is removed. Furthermore the element length stretches over the entire compartment rather than interframe. Thus the approach differs in the way the load shortening curves are derived and then implemented in the calculations.

The elements are grouped into “panel sets” which defines the overall extents of orthogonal stiffened panels (usually flat panels) within the structure. The choice of panel extents is usually dictated by the form of the overall girder geometry, and follows a similar process as used in the semi analytical method. The panel width must encompass all the structure which may fail in an overall manner. For example, a deck panel may run the entire width of the ship, or the panel may be intersected by deep longitudinal frames or longitudinal bulkheads, thus creating several panel sets with reduced width.

The panel length is usually equal to the compartment length between bulkheads. As has been shown in the previous Chapter, the semi analytical method can predict the critical collapse mode, which may be interframe or overall. Therefore, if all the elements are found to be critical interframe, the load shortening curves will reflect this and the extended progressive collapse methodology will calculate the same girder response as the conventional approach.

The proposed method is developed into a progressive collapse program (ProColl) with a direct interface to the semi analytical orthotropic plate method. A user manual for ProColl is presented in Appendix A. The program follows a two step process. Firstly the load shortening curves for all the elements are calculated and secondly the progressive collapse calculations are invoked to calculate the incremental bending moment-curvature relationship. The program can complete either an interframe analysis (ProColl-I) or a compartment level analysis (ProColl-O). If ProColl-I is invoked, the

semi analytical method is restricted to calculating the interframe strength of each panel set, which effectively restricts the elements to PSCs. ProColl-O uses the full capabilities of the semi-analytical method and therefore requires information on the compartment length and the transverse frame size.

The program calls a user generated datafile, which contains details of the panel sets and a list of elements making up the hull girder cross section. The panel sets are defined separately, although they may have the same dimensions as elements. The semi analytical method is invoked to calculate the load shortening curves for each panel set. Each element is assigned to a panel set or can be defined separately as either a PSC element or a hard element. If the element is part of the panel set then it is assigned the load shortening curve of that set. If the element is designated as a PSC, then the semi-analytical method is called to derive an interframe PSC load shortening curve. If the element is steel and is designated as a hard point an elastic-perfectly plastic load shortening curve is assigned with the material yield/proof stress used as the plasticity point in both tension and compression. A Ramberg-Osgood representation of the material properties is used for aluminium elements.

The element load shortening curves are read by the incremental progressive collapse program, which follows the incremental approach as detailed in section 7.2. An output file is written containing the bending moment and curvature results. In addition, the program has capabilities to produce basic 2D contour plots of the instantaneous element tangent stiffness at a given increment of curvature/moment. An example contour plot is shown in Figure 137. The plot shows the position of the instantaneous neutral axis and highlights elements which have failed (i.e. those where the element tangent stiffness is less than zero) in red. Hard corners are highlighted yellow when they reach the yield/proof stress. Elements which are close to their ultimate strength are highlighted green.

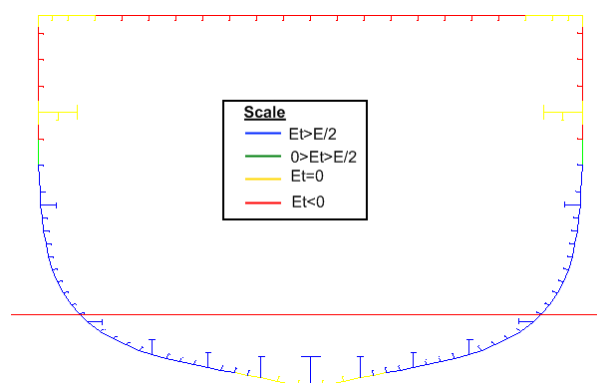


Figure 137 – Example ProColl element stiffness plot for the 1/3 scale frigate (see section 7.5.2)

## 7.4. FEM Methods

Continuing the procedures developed in Chapter 5, the simplified methods proposed in this thesis are validated using nonlinear FEM analysis.

The component and orthogonal panel FEM analyses have clearly demonstrated the effects of initial imperfections, residual stresses and heat affected zone on component level structure. These properties must continue to be represented adequately in a global hull girder FEM model. For this reason the hull girder FEM models are constructed using the building block approach, which has previously been summarised in section 5.2.2. This enables full control of the imperfection characteristics of individual plates and stiffeners throughout the global model. The global model extents must be set carefully to ensure that all possible failure modes and interactions are properly accounted for. Several example model extents are shown in Figure 138, ranging from a single bay interframe model to a large 3 compartment representation. The choice of model extents is fundamentally linked to the way the boundary conditions are represented, as will be explained in the following text.

A single bay representation, which is used by a number of published research studies [2, 124], is the simplest model in terms of mesh density and model setup. The single bay model does not require information about the transverse frame size. It assumes the frames are relatively strong and can thus be represented by rigid body boundary conditions. However, this assumption causes a significant problem with a single bay model. It ignores continuous beam interactions, which are important for the same reasons as highlighted for the single bay panels critiqued in section 5.3.2. A single bay does not adequately represent the rotational restraint provided by the transverse frames, which are not modelled explicitly but are instead represented by the boundary conditions placed on the model.

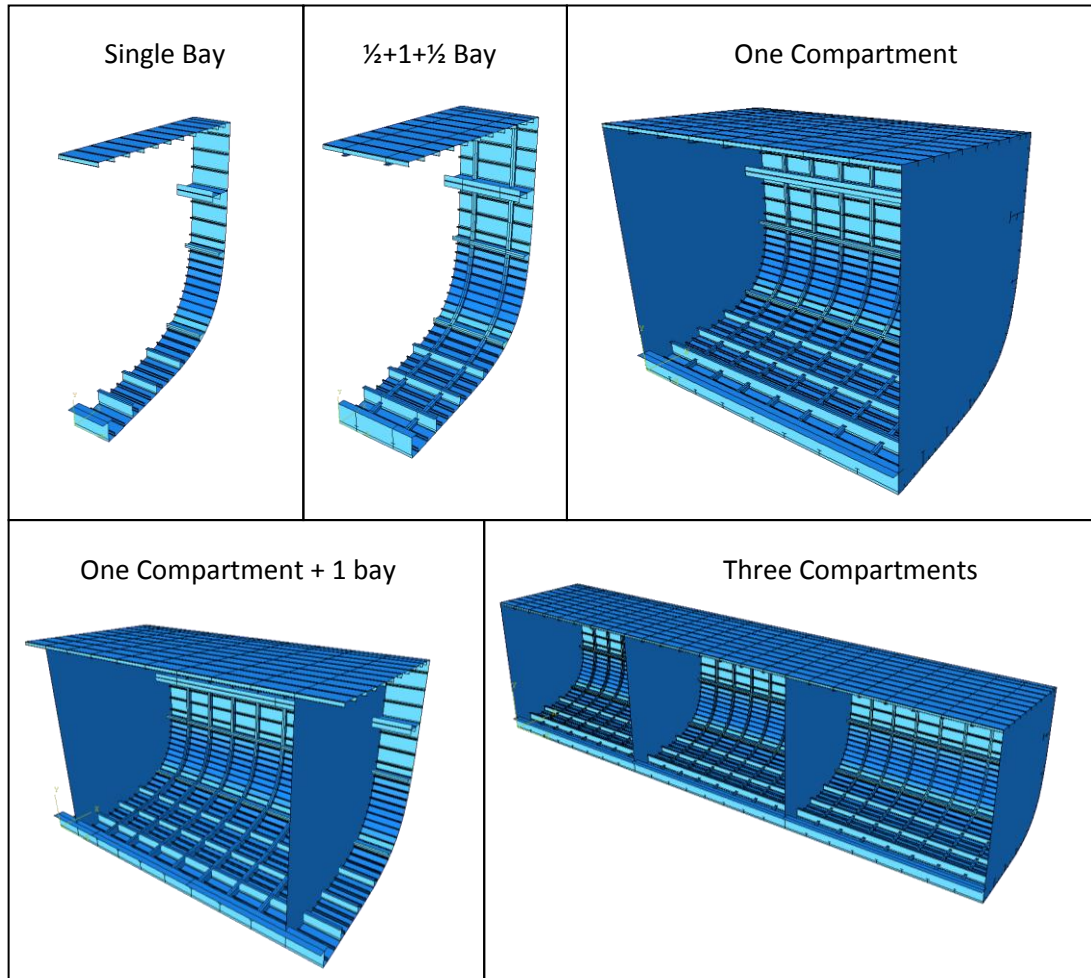


**Figure 138 – FEM extents for hull girder models**

Unlike the stiffened panel model, the hull girder is placed under bending moment, rather than axial compression. This means that, unlike the PSC models, this issue cannot be solved by using a  $\frac{1}{2} + \frac{1}{2}$  bay representation as the symmetry boundary conditions are impossible to model adequately. Therefore, an extended  $\frac{1}{2}+1+\frac{1}{2}$  bay model is employed to include the influence of the transverse frames whilst keeping the overall model size to a minimum.

However, the use of only a few frame spaces in the FEM model can be problematic for applying a pure bending moment over the cross section. A well recognised issue with modelling girder bending moment in FEM, and also in physical experiments, is ensuring that the neutral axis is allowed to shift as areas of the structure buckle. If the bending moment is applied about a fixed axis at the initial neutral axis of the section, the load application point becomes separated from the instantaneous neutral axis once plasticity and buckling start to spread.

A commonly employed solution is to ensure that the model extents are sufficiently large and sized in such a way so that the collapse occurs well away from the load application point. This allows the load path to readjust to the instantaneous neutral axis in the frame bays where collapse occurs. To ensure collapse occurs within the central part of the section length, the outermost frame spaces can be sized with thicker sections and/or have zero geometric imperfections, thus artificially increasing the section strength in these areas. This means that at the outer extents the instantaneous neutral axis remains at or near the elastic position whilst in the central zone the neutral axis readjusts to account for buckling effects. An example is sketched in Figure 139.

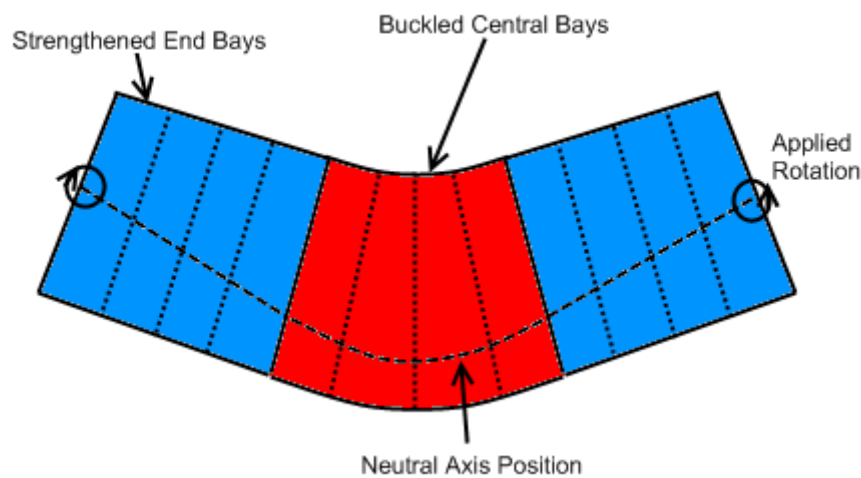


**Figure 139 – Neutral axis position across multiple frame spaces**

However, this approach has several drawbacks, not least that it requires a multi-frame model to predict an interframe collapse mode and, if overall collapse is expected, the model must extend beyond a single compartment, even requiring a three compartment FEM mesh (see Figure 138). This leads to very high simulation times because the mesh must be modelled fine enough to adequately represent the imperfection and buckling effects at least in the section of interest and also in the surrounding bays to avoid highly distorted mesh elements.

A further problem encountered in this study when dealing with multi-frame FEM models is that the FEM solution is liable to terminate due to equilibrium problems. It is difficult to ascertain the exact cause of the equilibrium errors, especially as the information available from the ABAQUS program is limited to standard output from the FEM solver. It is suggested that equilibrium is difficult to maintain because of the complicated buckling patterns which form in the structure. For example, if the component plates in the top deck of a sagged girder all buckle within the same increment, the solver has difficulty nucleating the collapse into a single frame space, which would effectively prevent buckling in the adjacent frames. Instead, the buckling patterns often look like the example

given in Figure 140, where a regular buckling pattern forms simultaneously over the entire deck. This example FEM analysis terminated shortly after this point.

This issue was found to be more prevalent in hull girder structures, whereas regularly sized box girder cross sections are less susceptible. This indicates that the level of complexity in the scantlings has a large influence on how successful the FEM analysis is likely to be. Because very few full scale fine mesh nonlinear FEM analyses of hull girders are reported in the literature, it is difficult to ascertain if similar problems are found in other finite element simulation attempts. Similar problems are evident in compartment level FEM studies of a cargo ship reported by Kippenes et al. [113], who use the ABAQUS arc length solver.

The problems highlighted above meant that an alternative approach, which avoids the need to model multiple frame spaces, was investigated as a suitable way to model interframe hull girder collapse. The approach is based on the method used to correct the neutral axis problem as given by Hughes and Paik [2], who provide a method similar to that used in the progressive collapse method to account for the neutral axis shift at each load increment in an FEM analysis. This corrective method is proposed as suitable for a single bay model. Rotation is applied at a single point located at the outer bottom or upper deck of the model and the rotation point is tied to all the nodes on the outermost extent of the model to create a rigid plane. The rotation point is allowed to translate, and thus it does not need to be located at the centroid of the cross section. The instantaneous neutral axis position of the cross section can be calculated by outputting the longitudinal stresses at every node at the outermost boundary and then calculating the moment of the stress from the base point. The instantaneous neutral axis is then obtained in a similar way to Eq. 140 and the moment about the neutral axis position can then be calculated.

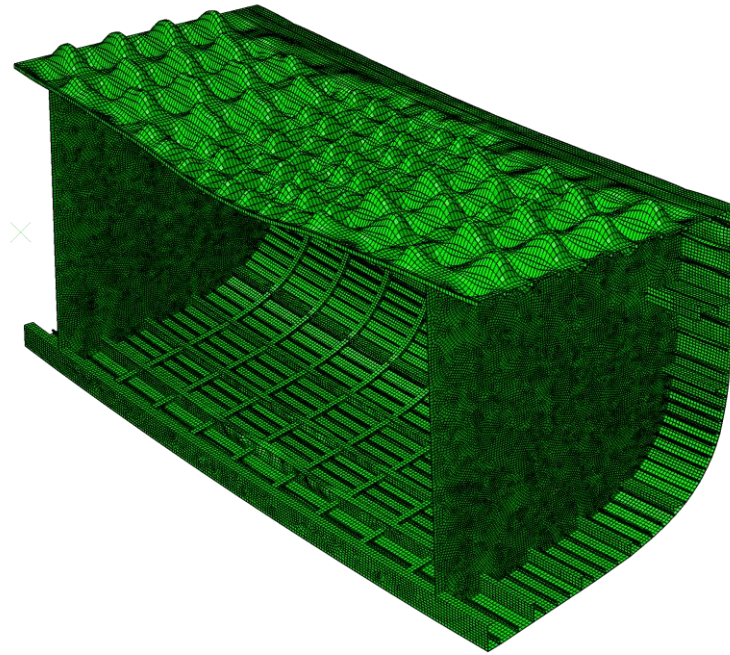


**Figure 140** – Example of a compartment level hull girder model (1/3 scale frigate) with a sag bending moment, showing a repetitive formation of buckling in the top deck. The model is sized as shown in Figure 151 with heavier scantlings in the outer bays.

This type of approach is highly useful because it does not matter where the rotation is applied from, because the rigid plane automatically accounts for any shifts in the neutral axis. However, care must still be taken to ensure that the rigid body does not interfere with the buckling capacity of the cross section. The approach is still unsuitable for a single bay model because the rigid body will effectively provide a clamped condition at the transverse frames and will not account for continuous beam effects.

Therefore the principles are extended in ABAQUS, with boundary conditions set as presented in Figure 141. The end planes of the model are constrained as rigid bodies and the boundary conditions are set so that the girder acts as a cantilever. End 2 is clamped by constraining all the nodes in 6 degrees of freedom. The nodes at End 1 are tied to a reference point using the “\*Rigid Body” constraints. The tie constraint propagates translation and rotation constraints placed at the reference point to all the associated nodes, whilst keeping the relative position of the nodes to the reference point fixed. Pure bending moment is applied by controlling the rotation of the reference point. The remaining degrees of freedom are left free, allowing the end nodes to translate. This automatically accounts for the shift in neutral axis and ensures a pure bending moment is applied on the girder. The position of the reference point is arbitrary and does not affect the resulting solution.

The approach is suitable for  $\frac{1}{2}+1+\frac{1}{2}$  bay FEM models and above. Care must still be taken to ensure buckling occurs in the central bay. One method used successfully in this study is to only introduce imperfection into the central bay, thus encouraging buckling to nucleate into this zone.

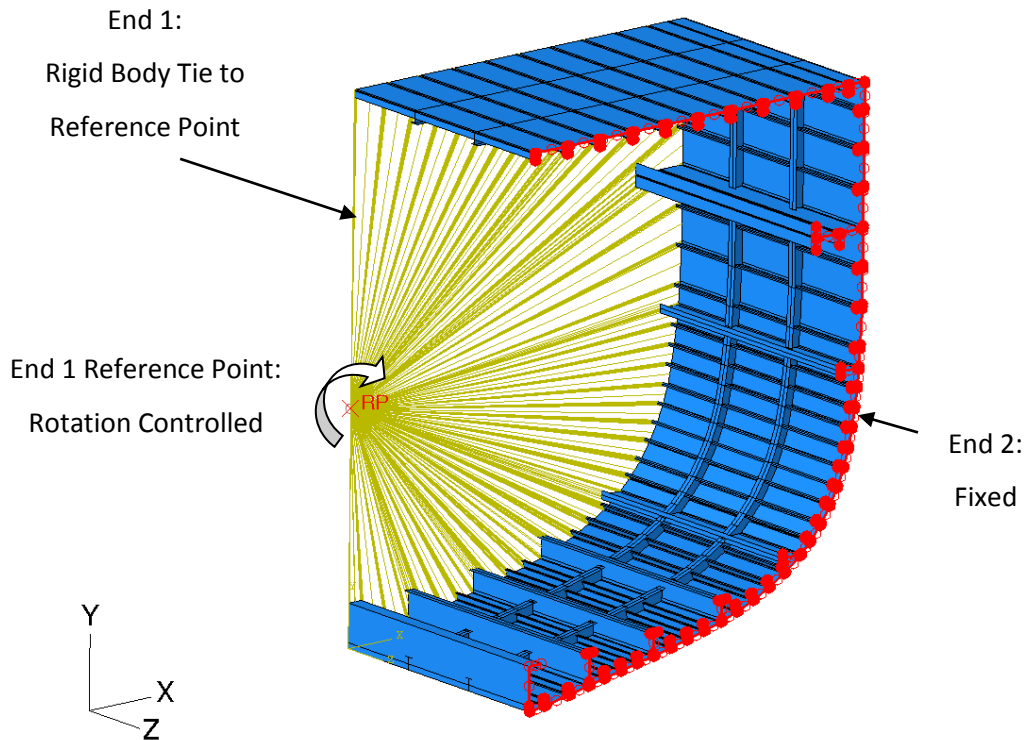


**Figure 141 – Hull girder boundary conditions (half model shown)**

So far, the discussion has centred on modelling interframe collapse. If compartment level buckling is expected or needs to be accounted for then the model must be sized accordingly. For the same reasons as outlined above, there is less perceived need to increase the extents much further beyond a single compartment. A 1 bay + 1 compartment model is thus deemed sufficient for predicting interframe and overall collapse modes in a hull structure. Unfortunately, the problems of solver equilibrium as highlighted above are still to be expected in compartment level models. As before, simple box girder models were found to be less susceptible to equilibrium errors. Furthermore, lightly framed hull structures (such as the aluminium multihull presented in section 7.7) which exhibit overall failure modes were much more successful compared to models such as the 1/3 scale frigate which is expected to collapse predominantly in an interframe manner.

For pure vertical bending moment cases, a half model can be used, such as is shown in Figure 141. This halves the number of elements in the model and therefore improves computation time considerably. The half model requires a symmetry boundary condition on the centreline nodes.

Mesh size and the distribution of fine and coarse mesh areas were also found to be important in determining the success of the finite element model. In areas where compressive in-plane load is expected a relatively fine mesh is required. The exact mesh length depends on the overall model size, but usually a mesh length equal to or less than the HAZ width should be used to ensure the effects of residual stress and reduced HAZ strength are adequately modelled. The mesh should also be fine enough so that at least two elements span the stiffener web height. In the tension portion of the hull girder a coarser mesh size can be used to reduce the overall number of elements in the model. The use of coarse mesh in tension regions was actually found to improve the reliability of the FEM solution.

In summary, this section has highlighted some of the complexities of modelling a hull girder in a nonlinear collapse analysis under primary bending. The discussion provides some qualitative evidence to justify the continued development of simplified models, which do not encounter some of the instability problems associated with FEM analysis. This feature of FEM is further highlighted in the next sections, which provide comparisons between the FEM results, simplified approaches and actual test results.

## **7.5. Validation with Existing Physical and Numerical Experiments**

Physical experiments can provide an invaluable resource for validating theoretical models. However, in terms of hull girder collapse analysis, experimental data is extremely limited, primarily because of the impracticalities and expense in testing large scale girder models in primary bending. There are a small number of experimental tests on large scale box girder structures subjected to pure bending moments which are described in open literature. Reckling [125] carried out seven steel box girder tests. Model no. 23, which had the largest number of longitudinal stringers, has been further analysed numerically by a number of research studies [126]. Experimental box girder tests have also been completed by Dowling [127], Ostapenko [128] and Nishihara [129]. A series of box girder tests have recently been carried out at the Technical University of Lisbon [121].

There are very few experiments which use actual ship structures. The only, and therefore highly important, laboratory test result available in open literature is that of a 1/3 scale frigate model, which was loaded up to and beyond collapse under a vertical sagging bending moment [120]. The test was conducted in a large test frame, which is essentially a large cellular steel structure which can be closed to form a reaction box with a roof and strong concrete floor.

The Energy Concentration, which has been discussed in the introduction to this thesis, also provides a usable case study of an actual ship cross section, although this is only because the circumstances of

the hull collapse were unusual. The hull girder broke in still water conditions and, furthermore, the loading condition at the time of the accident was known. Therefore the collapse scenario is close to an experimental test type of Rutherford and Caldwell [4] use this to calculate the applied bending moment at the time of failure.

For the present study, existing experimental data from two models are used: the small scale box girders tested by Gordo and Guedes Soares and the 1/3 scale frigate model tested by Dow. Both of these models exhibit predominant interframe failure modes. They provide a number of insights into the theoretical approaches and enable validation of the FEM and simplified methods.

### **7.5.1. IST Box Girders**

Simple multi-frame box girder structures were tested at the Technical University of Lisbon (IST) [121], using a four point bending rig as pictured in Figure 142. The girders were built simply; because it is a small scale model the stiffeners are placed on the outside of the shell to enable welding access during construction. In total three girders were tested; all have the same cross section (see Figure 142) but with different spacing between frames:

- F200 - Specimen Length = 1000mm, frame spacing = 200mm;
- F300 - Specimen Length = 1100mm, frame spacing = 300mm;
- F400 - Specimen Length = 1400mm, frame spacing = 400mm.

The test specimen length includes a 100mm span at each end which is then connected to the bending rig by a heavy bulkhead. Load is applied through hydraulic jacks connected to a strong box which in turn rests on the outer supports of the bending rig. All the supporting structure is constructed from thick high tensile steel. The test specimen is welded between the outer supports whilst the outer edges of the supports rest on the floor. The rig thus produces a four point bending load, with the central section under pure bending moment.

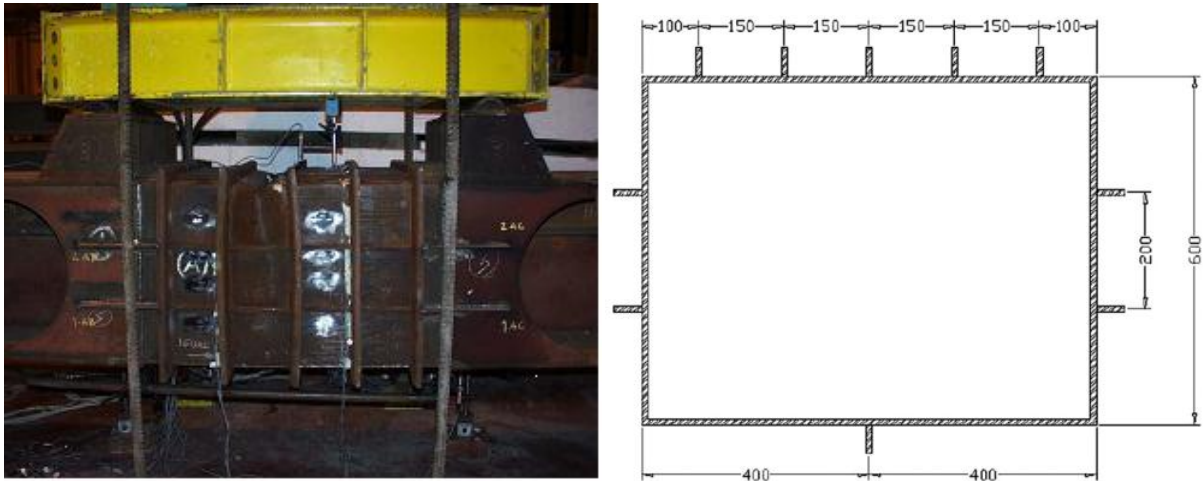


Figure 142 – Lisbon box girder test experimental setup (left) and specimen cross section (right) [121]

#### 7.5.1.1. Implicit FEM Analyses

The results from theoretical analyses of the F200 and F300 IST box girders using a standard implicit FEM methodology are now presented. The test setup is replicated in ABAQUS using two model extents. The first includes a representation of the entire structure, including the outer supports. This allows load to be applied in the same manner as the physical experiment. The model extents and mesh discretisation of the F200 model is shown in Figure 143. The second model is of the test section only which is set with boundary conditions as specified in Figure 141. Both models are built using the standard building block approach. The initial imperfections of the welded specimens was not measured; therefore average imperfection characteristics (Table 22) are assumed.

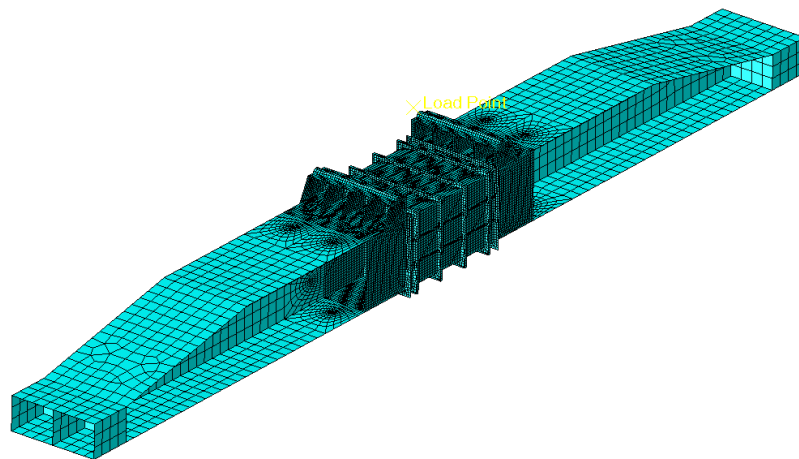


Figure 143 – Complete FEM model extents

The primary purpose of modelling the bending rig in its entirety is to compare with the equivalent boundary conditions when modelling the test section in isolation. Figure 144 shows the bending moment-curvature relationship from the FEM analyses for the 200mm frame space model. The

results show very good correlation between the two FEM models but poor correlation with the experiment.

The very close comparative results between FEM models indicates that the idealised boundary conditions in the test specimen model is a capable technique to model a pure bending moment in a multi stiffened girder. In addition to close comparative bending moment – curvature relationships, the FEM mesh plots in Figure 145 show that the models buckle with a near identical pattern, with failure predominantly interframe and nucleating in the central frame space.

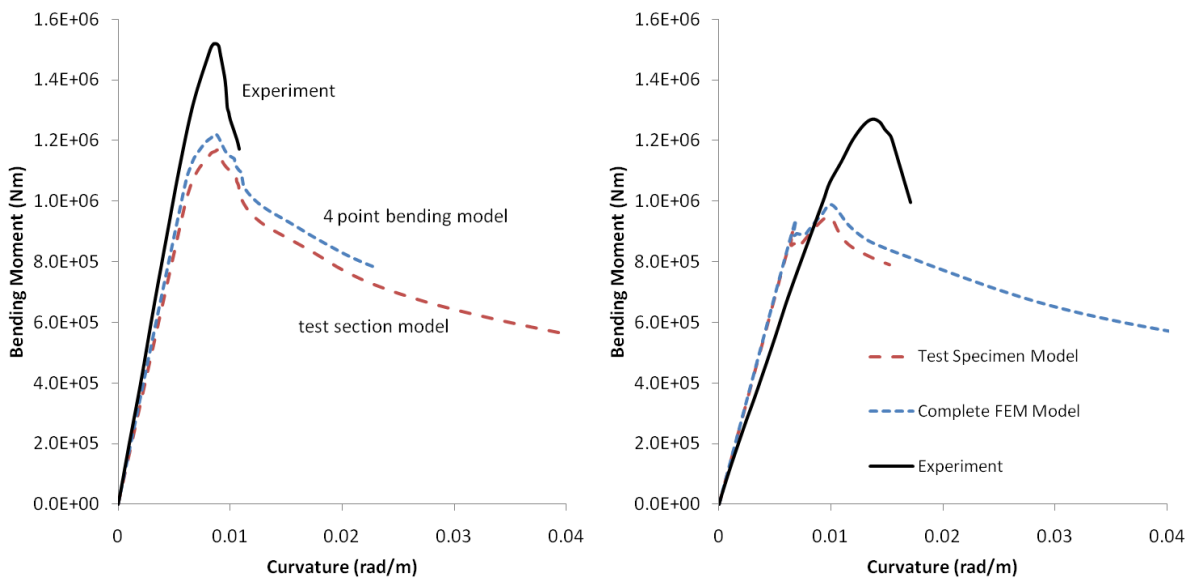


Figure 144 – IST box girder experiments comparison with FEM models . F200 (left) and F300 (right)

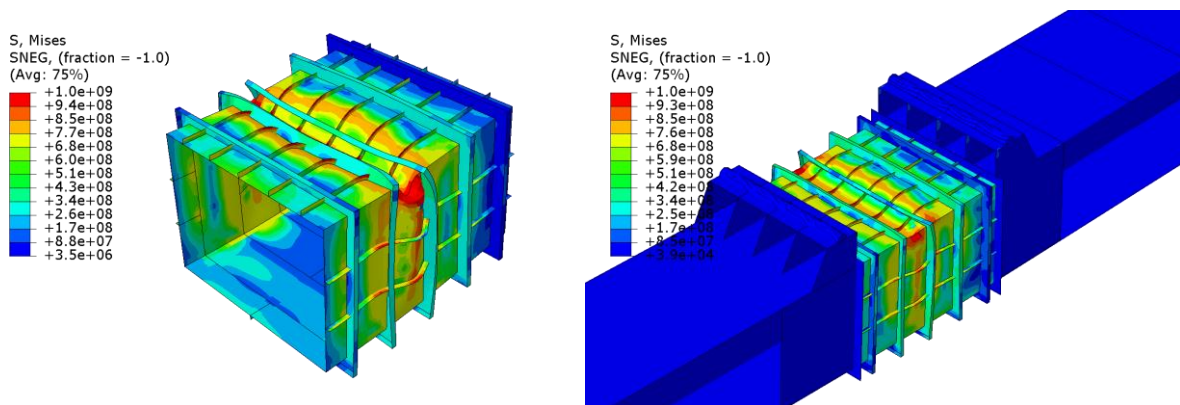


Figure 145 – FEM mesh plots for F200 test - specimen model (left) and complete model (right)

An explanation of the poor correlation between the experiment and FEM data can only be made based on the limited information regarding the experiment setup contained in [121]. A simple hypothesis for the discrepancy is proposed, which is based on observation of the load application setup used in the physical experiments. The connection between the load box and the bending rig

uses simple half cylinder bearing surfaces at the vertical load edges, as shown in Figure 146. During the application of load the top of the box girder is compressed, causing the top flange to pull in. The load edges will also pull in, but the simple bearing with the strong box above may produce a frictional resistance to the pull in force. This would effectively provide a restraint to delay the buckling response of the top flange, effectively strengthening the structural model.



**Figure 146 – Load points for four point bending [121]**

To test this hypothesis an artificial friction restraint was modelled using a nonlinear spring attached to the support edges in the full structural model. Two spring models were compared. In the first the restraint is modelled with a linear spring constant, which is calculated using the unrestrained force-displacement at the support in the four point bending FEM model. Analysis of the unrestrained F200 FEM model found that the load edge displaces horizontally by approximately 0.5mm with about 6MN of force applied. Assuming a frictional coefficient of 0.3 between the force and the displacement gives a horizontal frictional stiffness of 200 MN/m.

A second model uses a nonlinear spring, which assumes the friction coefficient is constant up to the collapse point of the structure but then decreases back to zero in the post collapse region, as shown in Figure 147. This assumes that, when the box begins collapsing, the frictional restraint reduces because the collapse is dynamic, thus the contact force between the support and the strong box reduces rapidly. The boundary conditions of the 4 point bending model means that the displacement at the two load application points is different, with End 1 displacing further than End 2.

Results are presented in Figure 148 for the F200 and F300 models. Both show a much closer correlation between the numerical model and the experiment and similar characteristics between numerical results. The linear spring model shows an initial collapse forming at about the same bending moment as the experiment ultimate strength. However, the continued restraint at the load edges prevents the box from failing completely and the post collapse behaviour is highly unrealistic.

The nonlinear spring corrects this problem by switching to negative stiffness when the box surpasses the ultimate strength point and collapses. This produces a very close correlation with the experiment data.

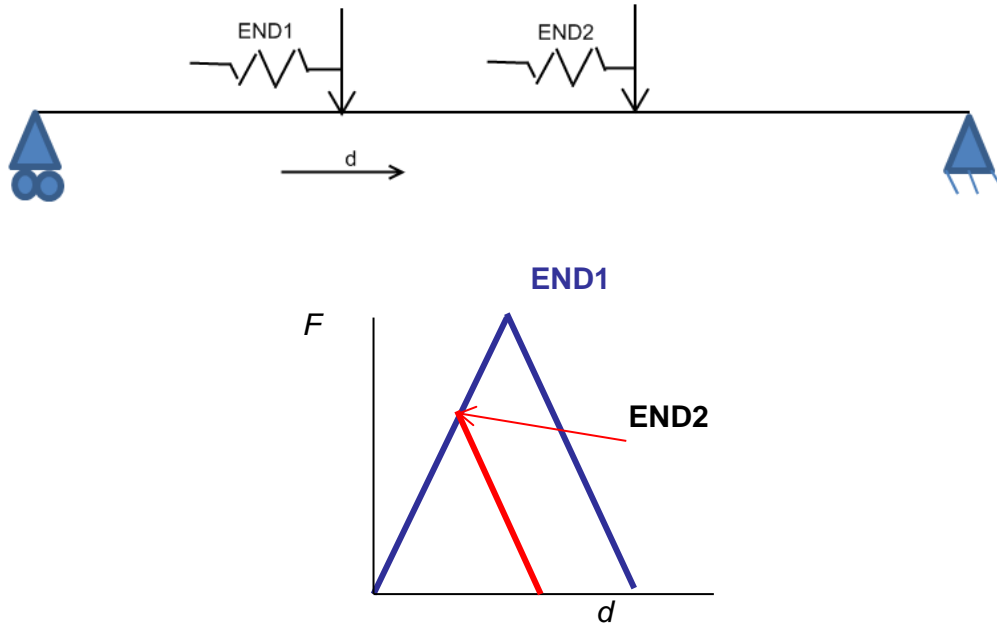


Figure 147 –Representation of the spring boundary conditions used to model the horizontal load point friction in the IST box girder tests.

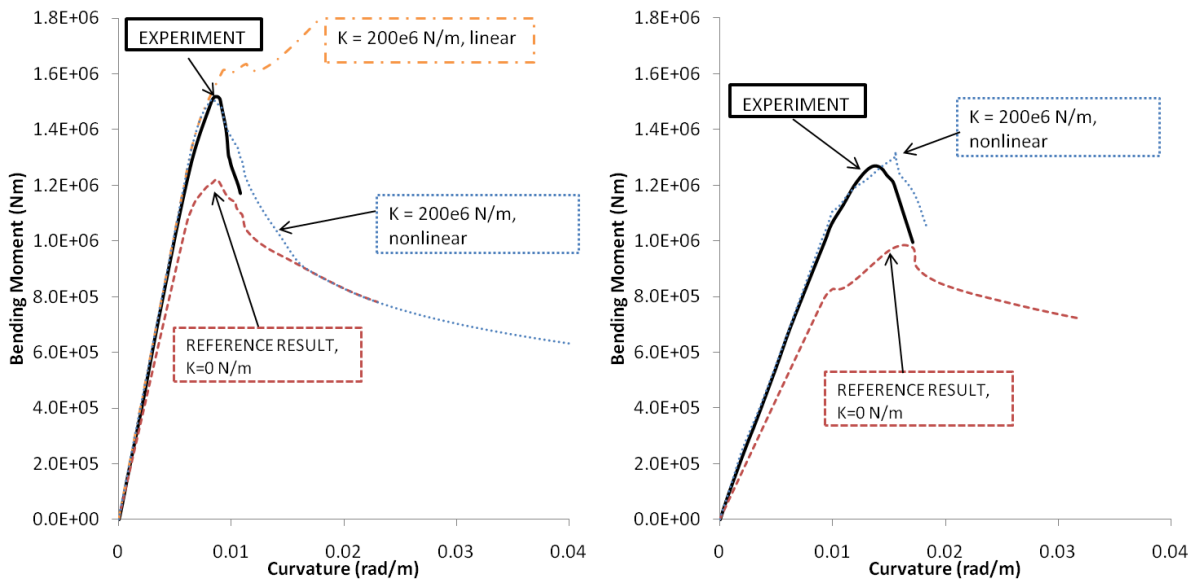


Figure 148 – Comparative results showing the effect of spring . F200 (left) and F300 (right)

#### 7.5.1.2. Explicit FEM Analyses

The test report by Gordo and Guedes Soares [121] describe the dynamic nature of the box girder collapse. In particular, the F200 girder collapses quite suddenly with a quick discharge of load and large deformations in the collapsed zone. This highly dynamic failure contrasts sharply with the way the FEM analysis is solved, and therefore raises the question of whether a dynamic solver may produce a different collapse mechanism and hence give different results.

Most FEM analyses documented in this thesis use the Riks arc length approach in an implicit static, incremental analysis. The post collapse is therefore represented quasi-statically. Curvature continues to be controlled and the load shedding must follow an equilibrium path. This is considered acceptable if it is assumed the post collapse characteristics are relatively smooth. Conversely, in a dynamic FEM solution, the stresses do not have to equilibrate. A negative aspect of explicit solvers is that the mass and damping properties of the structure must be included, adding a layer of complexity to the setup and analysis. In addition an explicit solver is usually less efficient than an equivalent implicit analysis. Nevertheless some research studies have used explicit solvers to analyse the progressive collapse of box girder structures [130].

The quasi static Riks method is therefore compared to an equivalent nonlinear explicit FEM analysis to demonstrate the suitability of the quasi-static post collapse characterisation. The small size of the IST box girders means that they are perfectly suited to an efficient analysis. Although the inclusion of the nonlinear springs improves the correlation with the experimental results, it is equally relevant to compare any like for like representation, and therefore a simple model with no restraints is used for comparison. The results are presented in Figure 149. The implicit and explicit approaches produce almost identical behaviour; the results are even closer than originally expected and may be due in part because the same software package and hence the same FEM architecture has been used to formulate the solutions. The findings indicate that the quasi static Riks approach is an acceptable solver method. The results are so close as to suggest that the dynamic analysis proves that collapse is quasi static, even when the peak of the bending moment curve is sharp and the unloading portion of the curve is steep.

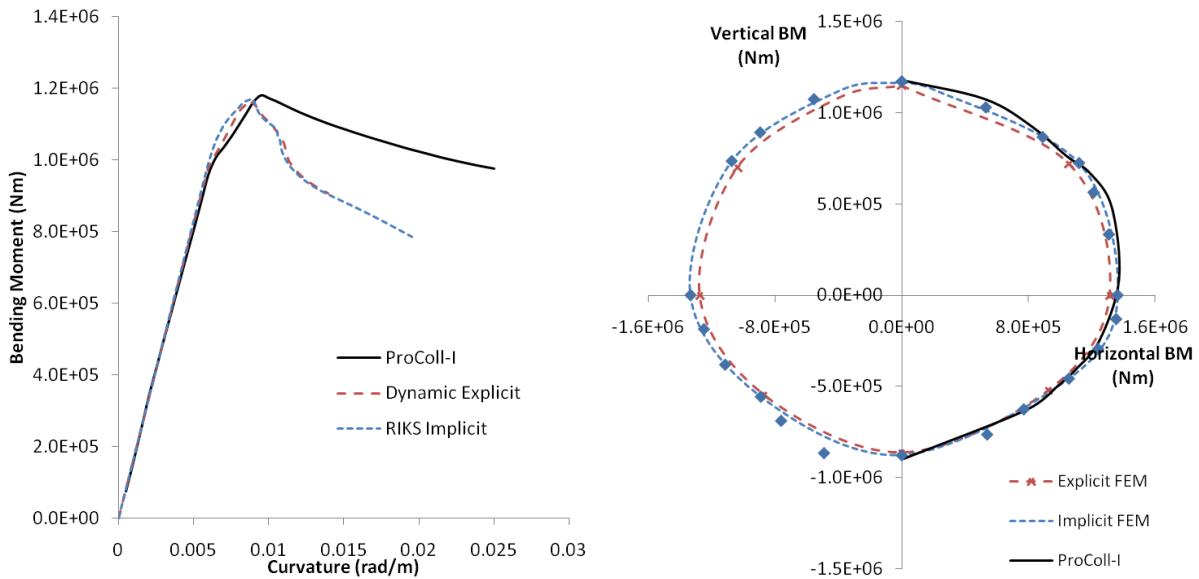


Figure 149 – Comparison of implicit and explicit FEM solvers for the F200 box girder model. Vertical bending moment-curvature relationship (left) and interaction diagram (right)

### 7.5.1.3. Simplified Progressive Collapse Analyses

The FEM analyses of the IST box girders also compare closely to interframe progressive collapse analyses using ProColl-I. Example results are shown in Figure 149. The progressive collapse representation is relatively simple, with hard corners extending 30t from the four box corners and the remaining structure represented with simple PSC elements. Because the box is very small the side plates are split into 6 elements to ensure the progression of collapse into the side shell is correctly represented.

In summary, the IST box girder analyses presented here demonstrate a number of key features of the FEM and simplified methodologies. The theoretical results compare well to the experimental data when the boundary conditions in the physical tests are properly taken into account. The FEM study has shown that a prismatic section can be constrained adequately to impart pure bending moment across the section. The analyses have also demonstrated that implicit and explicit FEM solvers can produce very similar results when used to model a progressive collapse failure of a box structure. Finally, the results provide a first validation of the progressive collapse method. It is important to note that the progressive collapse results compare closely to the FEM analyses but not to the original experiment data. This is an important finding because it provides a case in point that physical test results must be critiqued as intensely as equivalent numerical results to ensure that the boundary conditions are not influencing the result unduly.

### 7.5.2. 1/3 Scale Frigate

A primary purpose of laboratory tests of ultimate strength is to validate simplified theoretical approaches. This was a key objective of the hull girder test carried out at A.R.E. Dunfermline in the 1980s, which was used to validate the conventional progressive collapse method. The test has since proven a highly valuable resource because it is the only openly available experimental result from a large scale ship structure subjected to a controlled primary bending moment.

The test was conducted on a 1/3 scale prismatic ship section which was based on a Leander class frigate. The scale was probably set so that the structure would fit inside the large test frame at A.R.E. Dunfermline. The total length of the test model was 18 metres and consisted of five full compartments (Figure 150). The ends of the cross section were connected to thick bulkheads through which horizontal loads were applied by hydraulic jacks. These were calibrated to create a pure bending moment over the cross section. The actual test section consisted of 6 bays in the central compartment between frames 41 and frame 49. The structure surrounding the test section was built from high tensile steel and sized to ensure failure in the test section whilst maintaining the elastic neutral axis position.

Only one moment/curvature test result is reported in [120], with the girder placed under a sagging bending moment. In the subsequent test reports this was shown to correlate well with the theoretical prediction using the Smith progressive collapse method. The deviation between the predicted ultimate strengths is only 4%. Further analyses by several studies using interframe simplified methods [124] have also shown good agreement with the original test results.

In addition to the experiment data, Dow [120] reports the results from various theoretical calculations of the main strength deck, including an estimation of the overall grillage buckling strength using an orthotropic plate approach. These indicated that the likely mode of failure for the central compartment was overall. During the experiment the strength deck was observed to exhibit fairly large overall deflections which were considered consistent with the theoretical predictions. However, it was surmised that the overall buckling behaviour did not have a significant effect on the bending moment – curvature relationship. The theoretical progressive collapse calculations appear to substantiate this finding because they show close agreement to the experimental results.

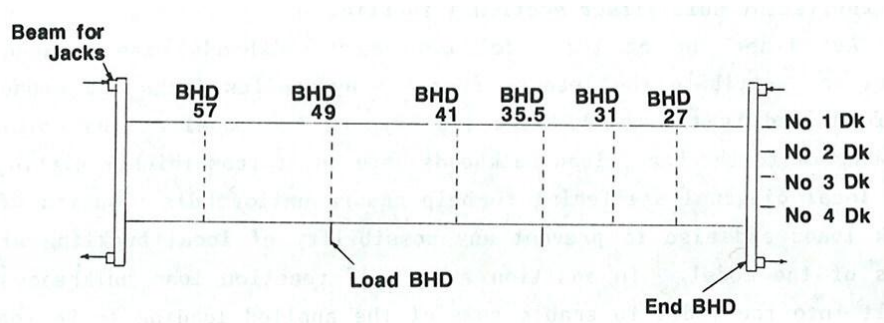


Figure 150 – Profile of frigate test section, taken from [120]

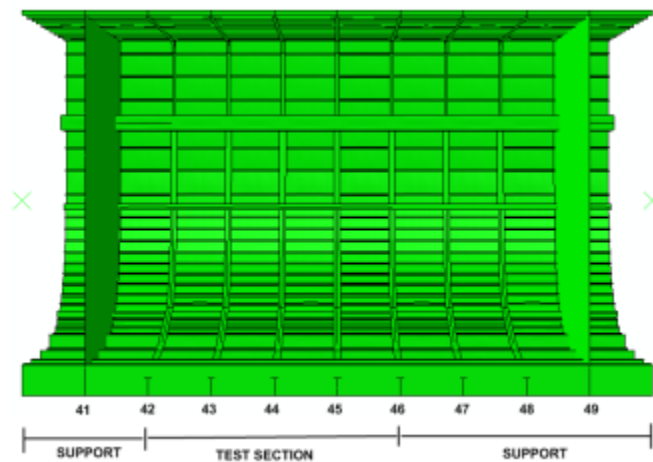


Figure 151 – Structural arrangement in the central compartment of the 1/3 scale frigate

The scantlings of the frigate model are taken from the original sketch in Dow’s 1991 paper and are reproduced in Figure 152. A detailed coordinate breakdown of the stiffener positions within the model is provided by Hughes [2]. The plating is predominantly 3mm thick except in the mid part of the main deck where the thickness is reduced to 2mm. All stringers are 38.1x1.8x14x3.3 tee bars. The hull bottom has several deep longitudinal tee bars ranging from 114mm-228mm web height. The structure is relatively lightly framed with 63.5x2x50x5 tee bars in the main deck and side shell spaced at 457.2mm intervals.

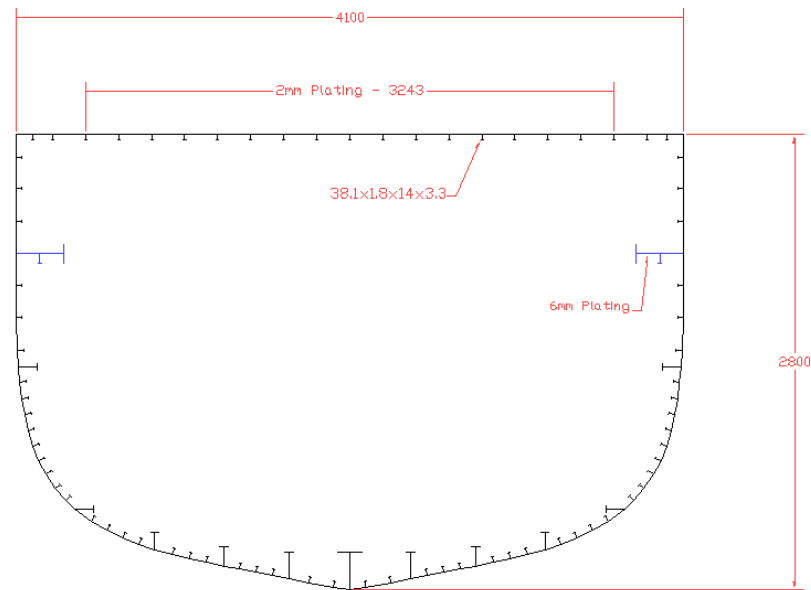


Figure 152 – 1/3 scale frigate scantlings

For the purposes of this study the experiment test result provides a basis for several key research objectives. Firstly the FEM modelling approach can be compared and thus validated with an actual physical test result. Secondly, the scantlings can be investigated to see whether overall collapse modes have any influence in the structure, and how the transverse frame size can affect the result. This provides some initial data for comparison between FEM, the conventional progressive collapse method and the extended progressive collapse method.

The frigate has been re-analysed with several finite element representations. As well as producing some comparative results, the numerical experiments also provides insight into the difficulties inherent in the FEM approach when used to analyse a complex structure in overall bending. This is highly useful in providing a framework for rigorous FEM analysis of box and hull girders. The problems encountered with FEM are emphasised because, as has been shown in previous sections of this thesis, solving an orthogonal stiffened structure using nonlinear FEM is a difficult task. The insights developed throughout the course of the present work, which are highlighted in this section, provide a contribution to current understanding of suitable techniques for hull girder FEM analysis. The frigate model provides an excellent example to demonstrate the limitations of the FEM tool for predicting progressive collapse behaviour. This provides justification for the continued development of simplified tools, which in many instances provide a faster and more reliable prediction of progressive collapse behaviour.

### 7.5.2.1. Interframe Analyses

An interframe strength model of the frigate under a sag bending moment is predicted using a  $\frac{1}{2} + 1 + \frac{1}{2}$  bay, half model FEM representation. This model provides the baseline result for comparison with other model extents and solutions. The geometry extents are as shown in Figure 141. Average geometric imperfections and residual stresses (Table 22) are introduced using the building block procedure as outlined in Chapter 5. The material is steel with a yield stress of 245MPa and Young's modulus of 210GPa. The material stress-strain relationship is idealised as bilinear, with 1% isotropic strain hardening in the plastic region. This was found to help stabilise the FEM increments. A tensile residual stress zone with magnitude 240MPa is modelled together with an equilibrating compressive zone of  $0.15\sigma_0$ . Geometric imperfection is only included in the central bay; outer bays remain perfect. This is to encourage nucleation of the collapse in the central bay. Example magnified imperfection patterns are shown in Figure 153. A fine mesh is modelled in the top deck and upper side shell whilst a coarser element size is used in the bottom structure where the girder experiences tensile in-plane forces.

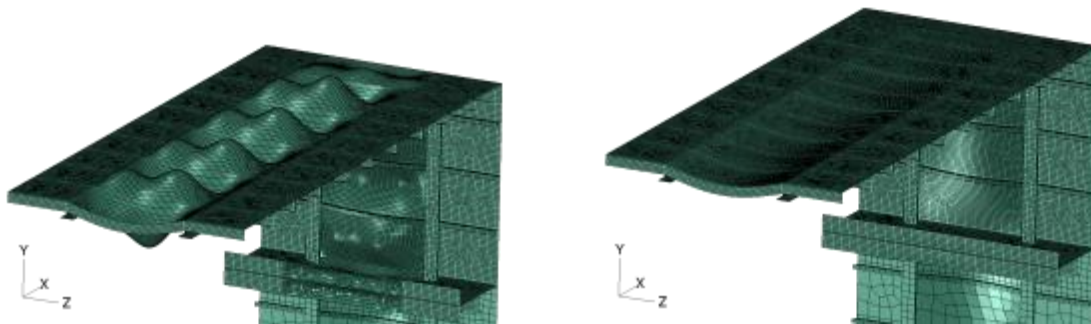


**Figure 153 – Geometric imperfection in the  $\frac{1}{2}+1+1/2$  bay frigate model . Plate imperfection (left) and column imperfection (right)**

Two equivalent interframe progressive collapse models are developed for comparison with the FEM result. The first model utilises the semi-analytical method to calculate the load shortening curve for each plate-stiffener element in the model. The second model uses the load shortening curves originally developed in FABSTRAN and reported by Dow [120] . This provides a simple check of the ProColl program as compared to the original NS94 calculations. The two load shortening curve sets are shown in Figure 154. The curves are mostly similar except for the top deck outer where there is a large discrepancy. This has only a small influence in the results because this region is a relatively small proportion of the total cross section.

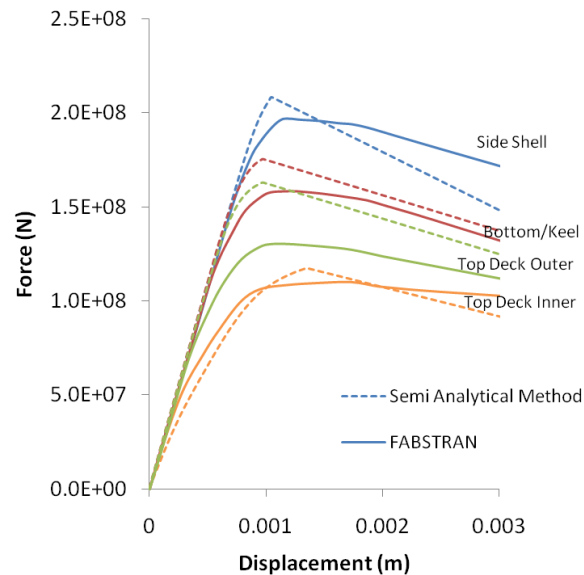


**Figure 154 – Load shortening curves for the 1/3 scale frigate output from FABSTRAN and the semi analytical method**

The resulting bending moment - curvature plots are compared with the experimental result in Figure 155. In addition a deformed mesh plot of the  $\frac{1}{2}+1+\frac{1}{2}$  bay FEM analysis is shown. As can be seen from the plots the various theoretical solutions demonstrate reasonable correlation with each other and with the experimental result. In particular, the NS94 and ProColl-I solutions are very close when using the same load shortening curves, which indicates that the correct formulations are used in ProColl.

Although the prediction of ultimate strength across all theoretical models is similar, the two ProColl-I results differ in their prediction of initial stiffness and the post collapse gradient. This is explained by the shape of the load shortening curves shown above. The semi analytical curves have a more pronounced peak, meaning that the element stiffness prior to collapse is greater. The post collapse characteristics are also steeper, which will produce a steeper unloading in the corresponding bending moment – curvature plot.

The  $\frac{1}{2}+1+\frac{1}{2}$  bay FEM solution shows close correlation to the ProColl-I and experimental curves. The initial stiffness matches the experiment up to about 90% of the ultimate strength. At this point both the ProColl and FEM results exhibit a transition with the bending moment stiffness reducing considerably. This is due to failure of elements in the top panel which is clearly seen by observing the contour plots in Figure 156, which show that the elements close to the deck corner fail first followed by the central region. This is interesting because the plating close to the corner is thicker than in the central region and therefore the panel is stronger. However, the load shortening curve peak is at a lower strain and therefore, although the elements contribute a greater amount of resistance to bending, they actually fail earlier than the weaker central plating.

The ultimate strength point is attained when the entire top deck and the side shell up to the first deep longitudinal have all failed. The FEM plot in Figure 155 and the middle contour plot in Figure 156 both show this characteristic. The FEM and ProColl-I results diverge in the post collapse region, with the collapse further propagating down the side shell in the ProColl analysis. This contrasts with the FEM analysis in which the resulting bending moment curve is much flatter indicating that the collapse is smoother with less propagation. In this respect the ProColl-I result is more closely representative of the actual experimental result.

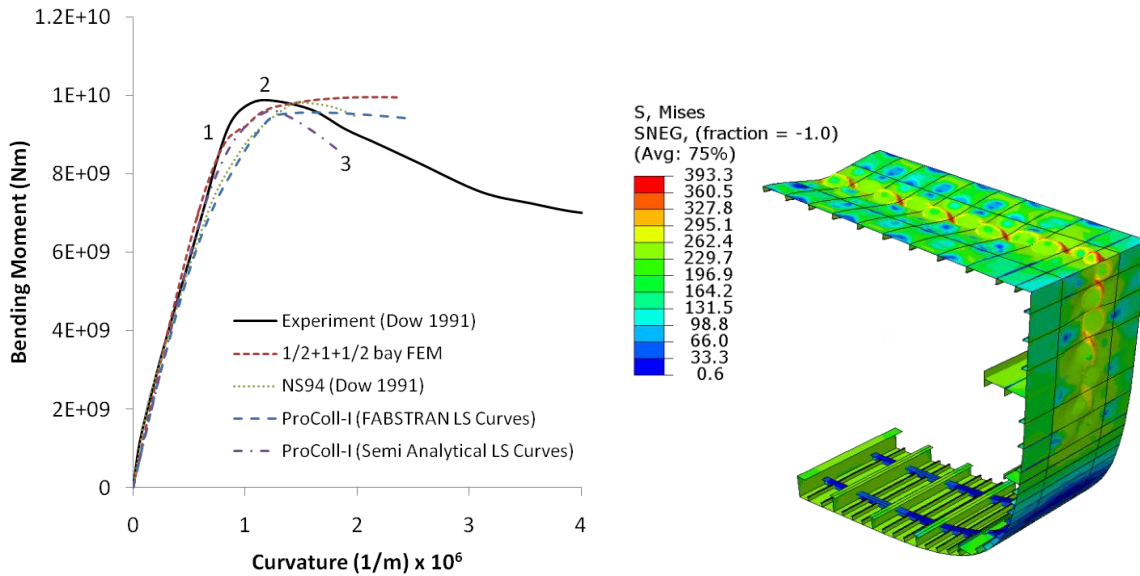


Figure 155 – Interframe bending moment – curvature plot for the 1/3 scale frigate (left), 1/2+1+1/2 bay FEM mesh plot at collapse (right)

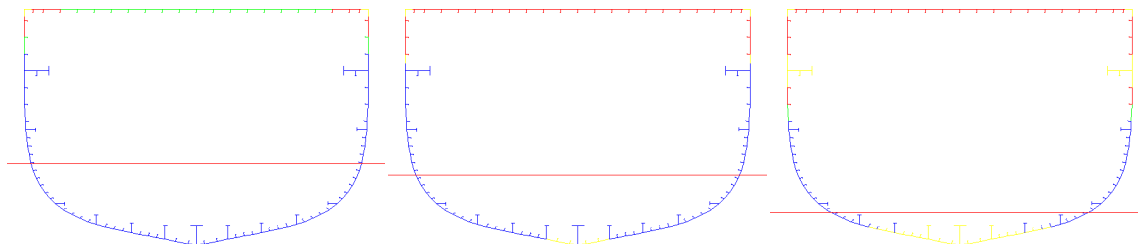


Figure 156 – ProColl element stiffness contour plots for the interframe 1/3 scale frigate analysis at the positions shown in Figure 155. Position 1 (left), 2 (centre) and 3 (right). Scale is as shown in Figure 137.

### 7.5.2.2. Compartment Analyses

In general, the theoretical analyses show good correlation with the experimental test. However, the interframe methods cannot assess whether the overall collapse mode observed in the main deck has a substantial effect on the progressive collapse behaviour. Therefore a series of compartment level theoretical analyses are also attempted. However, significant problems were encountered in the FEM analyses and a high number of tests terminated prior to the ultimate strength. The following discussion summarises qualitative reasoning as to why this particular cross section presented such difficulties. The ProColl-O prediction of the compartment level strength is also presented.

All the FEM models were set up using the general building block principles to construct the imperfect mesh. This allowed the imperfection and residual strength characteristics to be controlled at the component level. Initially, the same imperfection characteristics as used in the interframe analyses were employed although other imperfection patterns and amplitudes were also attempted. Various mesh sizes were used, with the fine mesh in the compression portion of the girder sized to ensure that elements in the HAZ regions are not distorted. This means the element length is approximately 20mm.

Despite the use of a rigorous modelling approach, a high number of the analyses failed prematurely with insufficient increments to predict either ultimate strength or the post collapse characteristics. In many cases the applied curvature reverses at an instability point, producing a relationship such as the example shown in Figure 157. Based on observations of the analyses, it appears that the instability problems are not due to one particular reason, but are perhaps more likely to be due to a combination of the complexities of the model and the way the solver handles buckling and instability. Some possible reasons for the instability problems are as follows.

Observations of the unsuccessful FEM analyses indicate that the model either terminates or reverses (see Riks method below) at a critical instability point. The deformed mesh plot shows that at this position significant out of plane deformation of the top deck plating has occurred in a regular repeating pattern (Figure 157). The instability could therefore be due in part to an unclear nucleation of buckling into a single bay. This problem may be particularly prevalent in structure where buckling is predominantly interframe.

The Riks method is used because it has capabilities to solve for equilibrium even with sharp discontinuities in the load displacement relationship. However, the method is also found to be problematic when reaching very sharp instabilities which cause a snap reversal of the load direction. This has been previously observed in the component plate analyses, although the solver mostly finds

the new equilibrium path in the correct load direction. However, when dealing with a complex global model, the method is found to sometimes continue the reversal direction back to the zero point and beyond, as shown in Figure 157. There are no restraints on the ABAQUS solver to prevent this. The cause of the snap back is perhaps associated with the nucleation problems highlighted above.

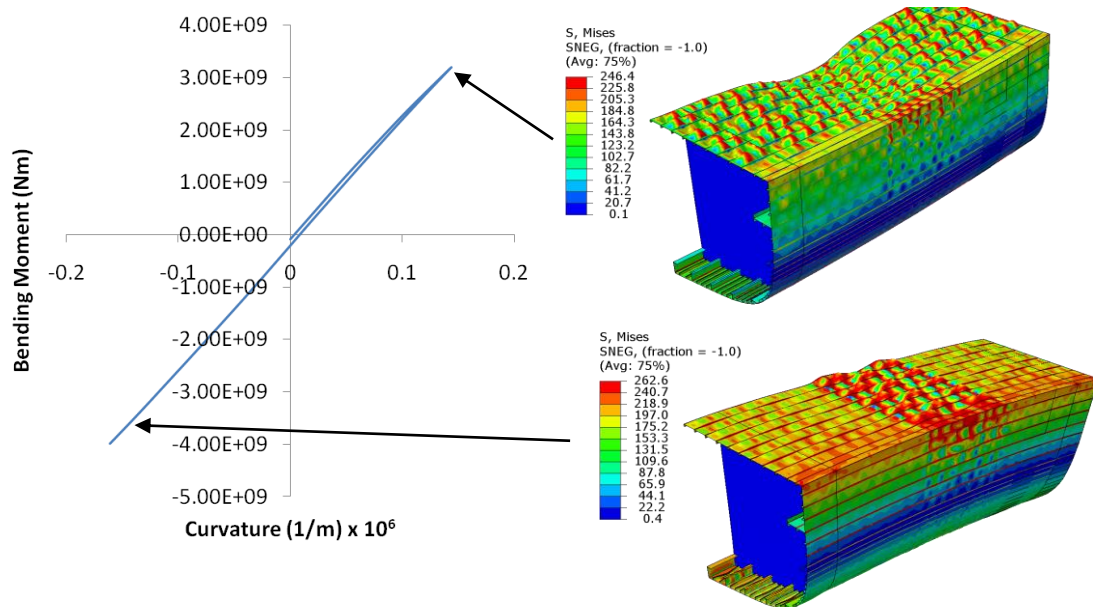


**Figure 157 – Example of an unsuccessful FEM analysis on a half model of the 1/3 scale frigate**

The Riks method was found to be unsuccessful for all compartment level analyses attempted on the 1/3 scale frigate model. Instead, a successful compartment level study was achieved by using the modified Newton Raphson approach with an artificial stabilization damping factor added to enable the solution to continue into the post collapse region. This is a recommended approach by the ABAQUS manual [101] and has been previously shown to produce good results by other investigators [113]. However, the choice of the damping factor is difficult to quantify and there is scarce information provided to help calculate a suitable value. In general, the damping factor should be as small as possible to minimise its effects on the solution. In this case the default values provided by were used.

The model was sized as shown in Figure 151 to replicate the central compartment used in the actual experiment test. The test section is 6 frames in length with the remaining bays specified with thicker plating. The resulting curvature plots are shown in Figure 158 and deformed mesh plots in Figure 159. Note that the axes on Figure 158 do not start at zero so that the results can be clearly seen.

Both the FEM and the ProColl-O analyses indicate that the top deck fails with an overall collapse mode and that this reduces the ultimate strength of the girder.

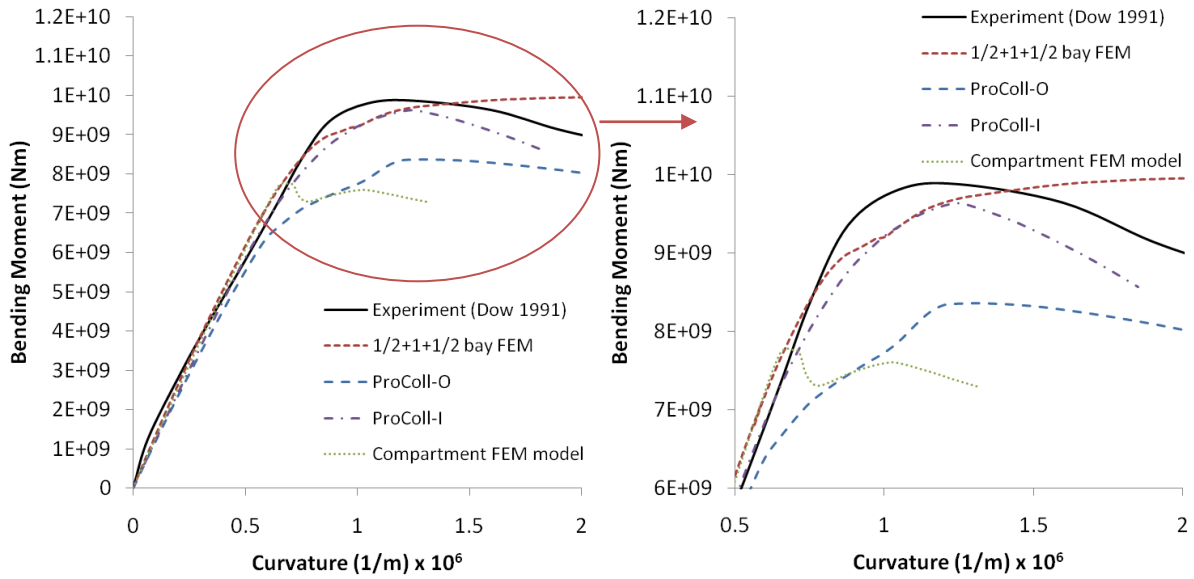


Figure 158 – Compartment level progressive collapse curves for the 1/3 scale frigate predicted by FEM and simplified methods

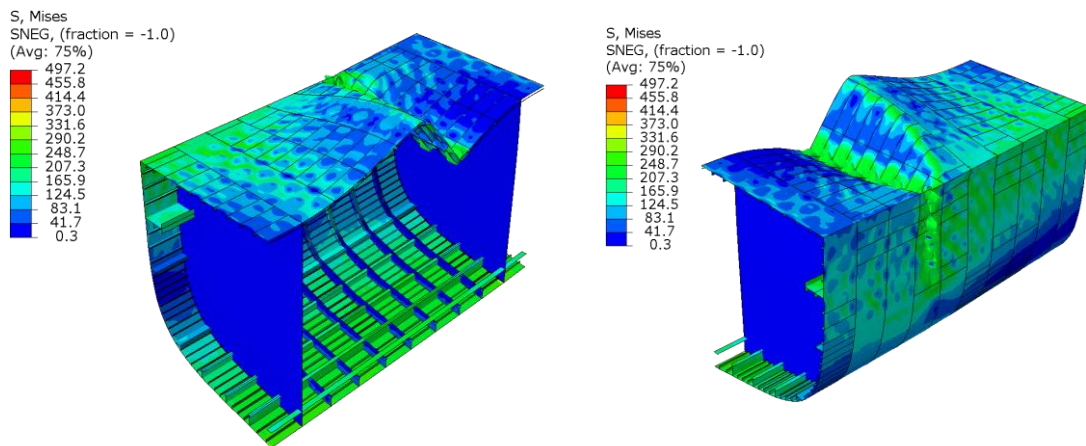


Figure 159 – Compartment level FEM deformed mesh plots. Magnification x10

The progressive collapse result indicates a strength reduction of about 10%, with the overall collapse causing the ProColl-O curve to diverge from the ProColl-I curve at about 70% ultimate strength. The FEM result predicts a lower strength, and overall collapse is exhibited as shown by the mesh plots. However, the predicted failure is still predominantly interframe, which is indicated by the sharp peak of the progressive collapse plot. The overall failure mode develops in the post collapse region. The mesh plots show that the mechanism of collapse is interesting, with a full sine wave type shape across the test section length. This contrasts with the type of overall failures seen in the previous

Chapters and is perhaps a further indicator of possible instability problems which may have caused the problems in the FEM analyses.

In summary, the compartment level analyses have demonstrated that whilst the nonlinear FEM approach is an acceptable tool for predicting the collapse behaviour under primary bending moment, it has numerous issues concerning the solution stability. The interframe results show that the FEM approach gives a reasonable validation of the simplified progressive collapse method. However, the discussion of the compartment level analyses has qualitatively highlighted some of the problems faced by the FEM analyst when attempting to model a complex structure which behaves with high nonlinearity. The unreliability of the FEM approach in attaining sufficient solution stability must be taken into account when comparing results with simplified theoretical methods and experimental data, particularly for complex whole ship models.

## **7.6. Box Girder Case Study**

The previous section has principally validated the interframe progressive collapse method. The next two sections provide a validation of the compartment level capabilities of the extended method. As has been previously shown, the complexity of the cross section under consideration has a large bearing on the successful completion of an incremental FEM solution of primary girder strength. Therefore, rather than using an actual ship structure, the interframe progressive collapse method (ProColl-I), extended progressive collapse method (ProColl-O) and nonlinear FEM analyses are first compared using a much simpler case study box girder with properties typical of a large aluminium vessel. The results are presented in this section. The next section then provides a further validation of the methods using an actual compartment level ship structure which is typical of a large aluminium multihull.

The dimensions of the box girders are similar to the types of arrangement used in other studies investigating ship type aluminium structures [5]. They are constructed using the orthogonal panel dimensions previously studied in Chapters 5 and 6. These panels showed different overall buckling characteristics depending on the size of the transverse frames. They are therefore highly suitable for assessing their strength as part of a 3D box girder structure. The load shortening curves predicted by the semi analytical method, which are accessed directly by the ProColl-O analyses, are all previously discussed in section 6.4 and are therefore not repeated here.

The overall box girder is square in cross section with a side length of 8.4m, stiffened by 20 longitudinals spaced 400mm apart on each side. Four cross sections are considered, which are sized and named consistent with orthogonal panels M1-M4 (see Table 31). The frames are also consistent

sizes with the panel analyses. The compartment length is set at 7 frame spaces, which is sufficient to show compartment level buckling characteristics. All FEM models use a 1 compartment + 1 bay representation (see Figure 138). The bulkheads are modelled with very large thickness to keep the compartment ends straight. The boundary conditions are as given in Figure 141. Geometric and material imperfections are applied over the entire box using methods and amplitudes consistent with the panels discussed in the previous section. A 50mm element length is used to mesh the geometry, which was found through a mesh refinement study of box M1 to give sufficient convergence in the results.

The results are compared to the extended progressive collapse methodology. The results can be compared both in their prediction of the ultimate strength of the box and the prediction of the entire load shortening relationship. The ultimate strength results are summarised in Table 38 and show close agreement. The results reflect similar characteristics to the panel strength results presented previously. If the transverse stiffening is lightened or the longitudinal stiffening is made stockier, the influence of the overall collapse mode is increased. Box girder M1 shows the most dramatic decrease in strength when framed with the light T1 flat bar (180x10) with a drop in ultimate strength of 39%.

**Table 38 - Box Girder Ultimate Strength Results**

ID	Frame Size	ABAQUS (MNm)	ProColl-O (MNm)	Bias
M1	Interframe	-	279.1	
	T1	158.7	170.7	0.93
	T2	253.8	248.2	1.02
M2	Interframe	-	191.0	
	T1	134.1	139.7	0.96
	T2	169.0*	191.0	0.99
M3	Interframe	-	148.8	
	T1	115.2	118.8	0.97
	T2	144.9	148.8	0.97
M4	Interframe	-	130.0	
	T1	99.9	104.4	0.96
	T2	121.7	130.0	0.94
Mean Bias = 0.96, C.O.V. = 0.03				

Table 39 – Box Girder Panel Dimensions

Dataset ID	Mat.	a (mm)	b (mm)	$t_p$ (mm)	$h_w$ (mm)	$t_w$ (mm)	$b_f$ (mm)	$t_f$ (mm)	$\lambda$ (mm)	$\beta$ (mm)	$A_s/A$
M1	5083	1200	400	14.8	120	5.5	55	7.7	0.62	1.5	0.15
M2	5083	1200	400	11.1	120	5.5	55	7.7	0.56	2.0	0.20
M3	5083	1200	400	8.9	120	5.5	55	7.7	0.53	2.5	0.23
M4	5083	1200	400	7.4	120	5.5	55	7.7	0.50	3.0	0.27

Dataset ID	$h_w$ (mm)	$t_w$ (mm)	$b_f$ (mm)	$t_f$ (mm)
T1	360	10	0	0
T2	180	10	0	0
T3	360	10	100	15

Of course the ultimate strength prediction is just a measure of a single point on the bending moment – curvature plots. The entire progressive collapse behaviour of the four girder models are shown in Figure 160. The plots demonstrate the applicability of the extended progressive collapse method in firstly predicting the onset of overall collapse in stiffened panels making up a longitudinally stiffened structure, and secondly predicting the subsequent effect on the overall progressive collapse characteristics of the structure under primary bending. The curves show remarkable correlation of the ultimate strength, although the curve characteristics near to the peak do have some significant differences. In particular, the FEM analyses show a much more gradual transition from the interframe mode to overall, which is characterised by a reduced gradient in the bending moment curve. In comparison, the ProColl analyses maintain a fairly linear relationship up to near the ultimate strength, at which point the curve diverges more sharply into an overall mode. This is a similar characteristic as found in the panel analyses, and thus the difference can be attributed to the way the semi-analytical method predicts the influence of overall collapse at the panel level.

Plots of the FEM mesh at the ultimate strength point of the analysis for girders M1 are shown in Figure 161. These show that the box collapses with an overall mode of failure in the top and side panels. Overall collapse occurs with both transverse frame sizes. As would be expected, the more lightly stiffened girder (T1) shows an increased influence of gross panel buckling between bulkheads and thus suffers a more severe degradation in strength as compared to the interframe result.

Plots of the FEM mesh at the ultimate strength point of the analysis for girders M3 are shown in Figure 162. This girder uses thinner plate, thus the longitudinal cross section is “lighter” than girder M1. The results show a degradation of strength in the lighter framed girder (T1), although the reduction is less than the equivalent result for girder M1. With the 360x10mm frames (T2), the box

collapses interframe. This demonstrates that the influence of overall collapse is dictated by the longitudinal structure as well as the absolute sizing of the transverses.

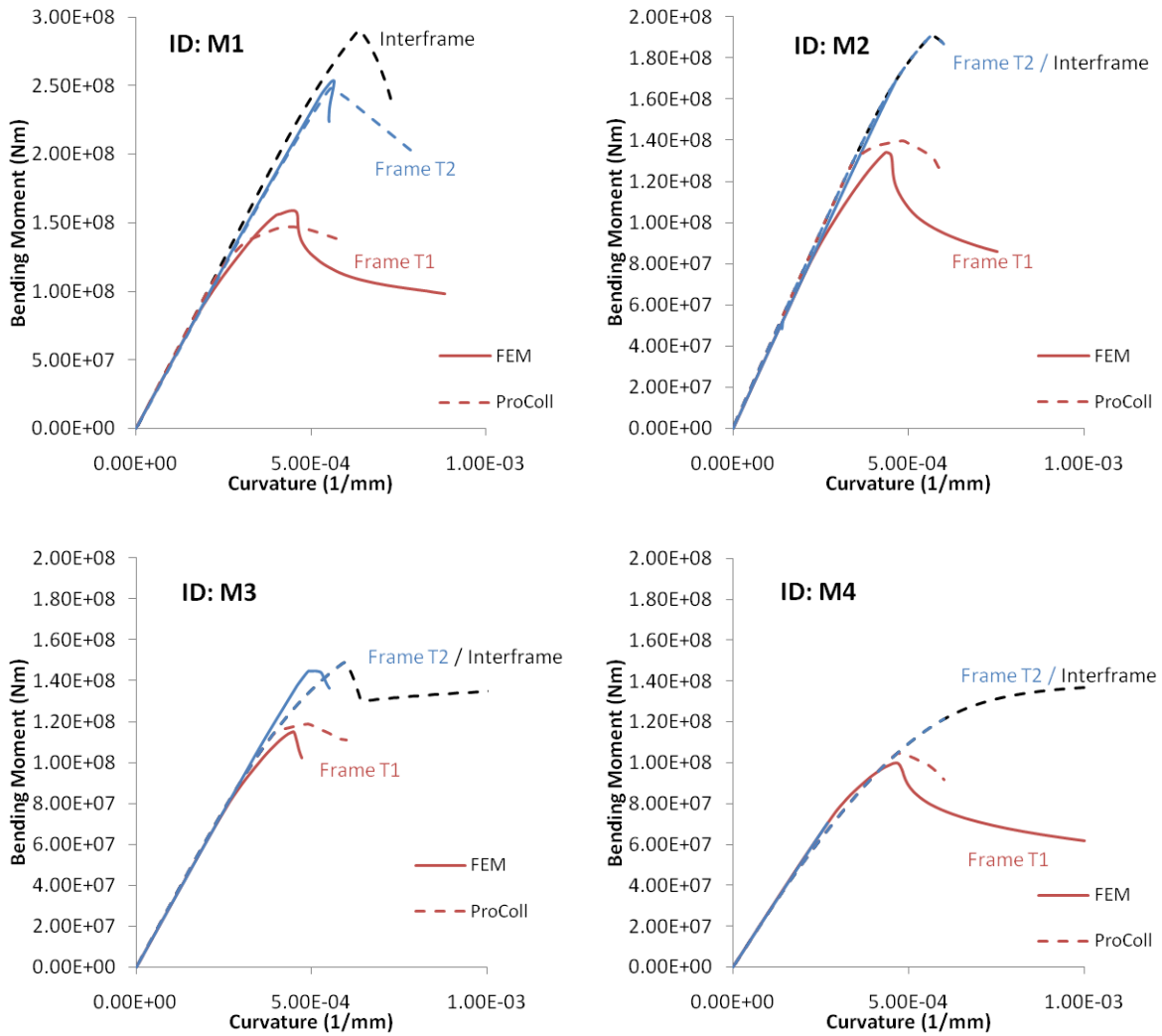


Figure 160 - Progressive collapse under vertical bending of the four box girder models

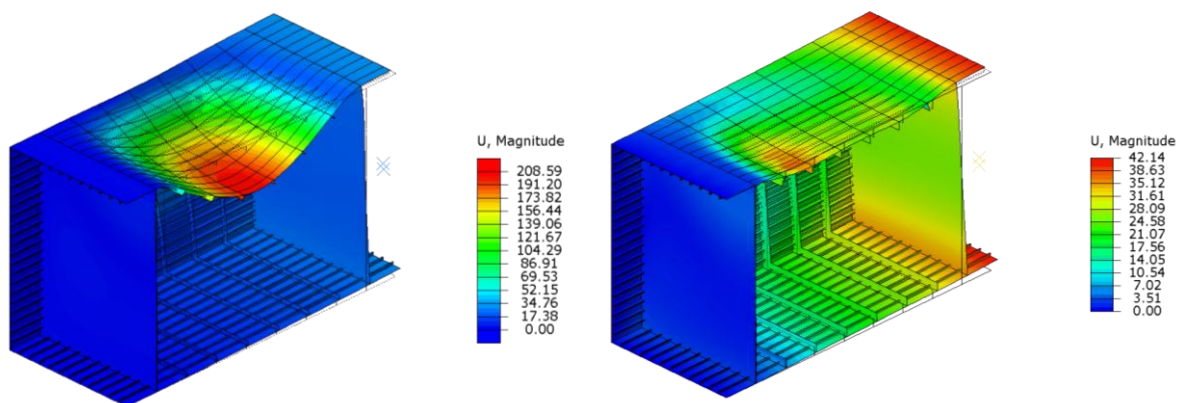


Figure 161 – Deformed mesh plots of box girder M1 with frames T1 (left) and T2 (right), magnification x3

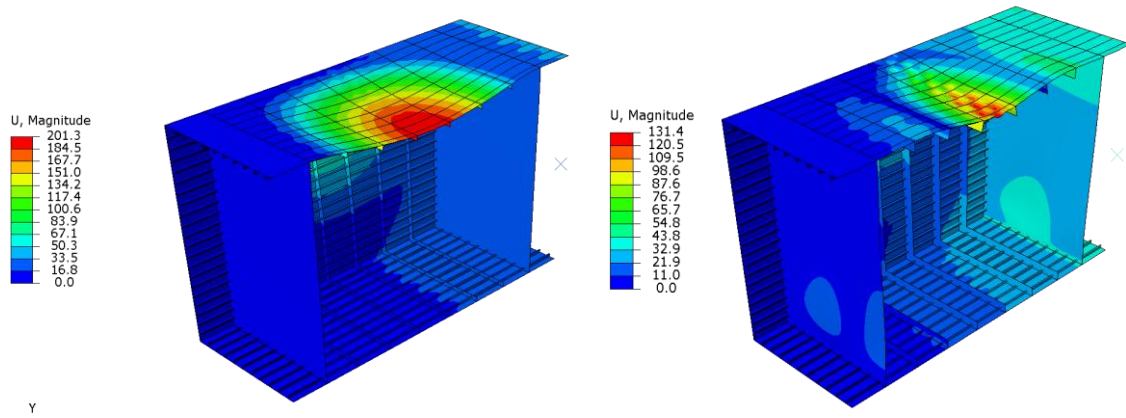


Figure 162 – Deformed mesh plots of box girder M3 with frames T1 (left) and T2 (right), magnification x3

## 7.7. Case Study – Aluminium Multihull

The methods developed in this thesis are directed towards large lightweight marine structures. Therefore, the study of a realistic aluminium ship structure provides a good culmination of all the aspects in the present work. Therefore, this case study investigates the strength characteristics of a typical aluminium multihull under primary longitudinal bending.

Based on the limited information contained in ship structure report SSC-438 [16], a typical multihull cross section is developed with scantling details as shown in Figure 163. These scantlings are not the exact configuration of the Pacificat hull investigated in the SSC report, for which a detailed structural layout is not openly available. The hull shape is broadly similar and was developed by scaling from a small scale general arrangement drawing contained in the SSC report. Similarly, the stiffener sizes and spacing were estimated based on reported information, but are not necessarily an accurate reproduction of the actual vessel scantlings. Therefore no inference from the results in this thesis should be transferred to the actual vessel.

It is recognised that longitudinal bending moment is not necessarily the critical load condition for a multihull of this size. The critical load in such a vessel is usually the prying moment between the two demi-hulls. However, for the purposes of comparing the methodologies developed in this thesis the application of a longitudinal bending test as a theoretical case study is considered valid, particularly because the scantlings are such that overall and interframe failures occur in different areas of the cross section.

The structural details are specified to enable a concise assessment of component level strength of plate and stiffener combinations. The plate thickness ranges from 8mm in the decks to 20mm at the keel. Four stiffener sections are used with webs 95mm – 140mm high and are spaced between 200mm-275mm. Stocky longitudinals with 300mm webs are positioned intermittently along the

decks at about 3000mm intervals. The transverse frames are 400mmx10mm and are spaced at 1200mm intervals. In total the cross section contains 13 distinct panel sizes, which are summarised in Table 40 with the panel locations indicated in Figure 163. The material is 5083-H116 throughout.

**Table 40 – Aluminium Multihull Panels**

Dataset ID	b (mm)	tp (mm)	hw (mm)	tw (mm)	bf (mm)	tf (mm)	nsx	$\beta$	$\lambda$
P1	250	10	120	5.5	55	7.7	7	1.39	0.48
P2	212	10	120	5.5	55	7.7	7	1.17	0.46
P3	270	20	120	5.5	55	7.7	6	0.75	0.60
P4	275	12	140	6	60	8.7	13	1.27	0.42
P5	270	8	120	5.5	55	7.7	13	1.87	0.46
P6	270	8	120	5.5	55	7.7	17	1.87	0.46
P7	270	8	120	5.5	55	7.7	9	1.87	0.46
P8	200	8	95	4.3	50	8.7	14	1.39	0.55
P9	200	8	95	4.3	50	8.7	15	1.39	0.55
P10	200	8	95	4.3	50	8.7	16	1.39	0.55
P11	200	8	95	4.3	50	8.7	11	1.39	0.55
P12	200	8	95	4.3	50	8.7	10	1.39	0.55
P13	200	8	95	4.3	50	8.7	9	1.39	0.55

The hull girder is first assessed in vertical bending assuming interframe collapse. A  $\frac{1}{2}+1+\frac{1}{2}$  bay FEM model is analysed under vertical hog and sag. The boundary conditions are consistent with those used previously. The FEM analysis includes average imperfections and residual stresses (Table 22). The geometric imperfections are only introduced into the central bay for the same reasoning as discussed for the 1/3 scale frigate model.

The section is also analysed using ProColl-I. Hard corners are assumed to extend 30 times the plate thickness from the deck corners and knuckle points. For the purposes of an interframe progressive collapse analysis, several of the panels listed in Table 40 have identical properties (Panels P5-P7 and P8-P13). These panels only differ in the number of longitudinals making up the total panel, which is irrelevant if assuming each PSC acts independently. Therefore there are only 6 PSC combinations. PSC FEM and semi analytical method generated load shortening curves for these panels are compared in Figure 164. The PSC FEM analyses use the methodology described in Chapter 5 with average imperfection levels. The curves show close agreement, further demonstrating the applicability of the semi analytical method for predicting interframe PSC strength.



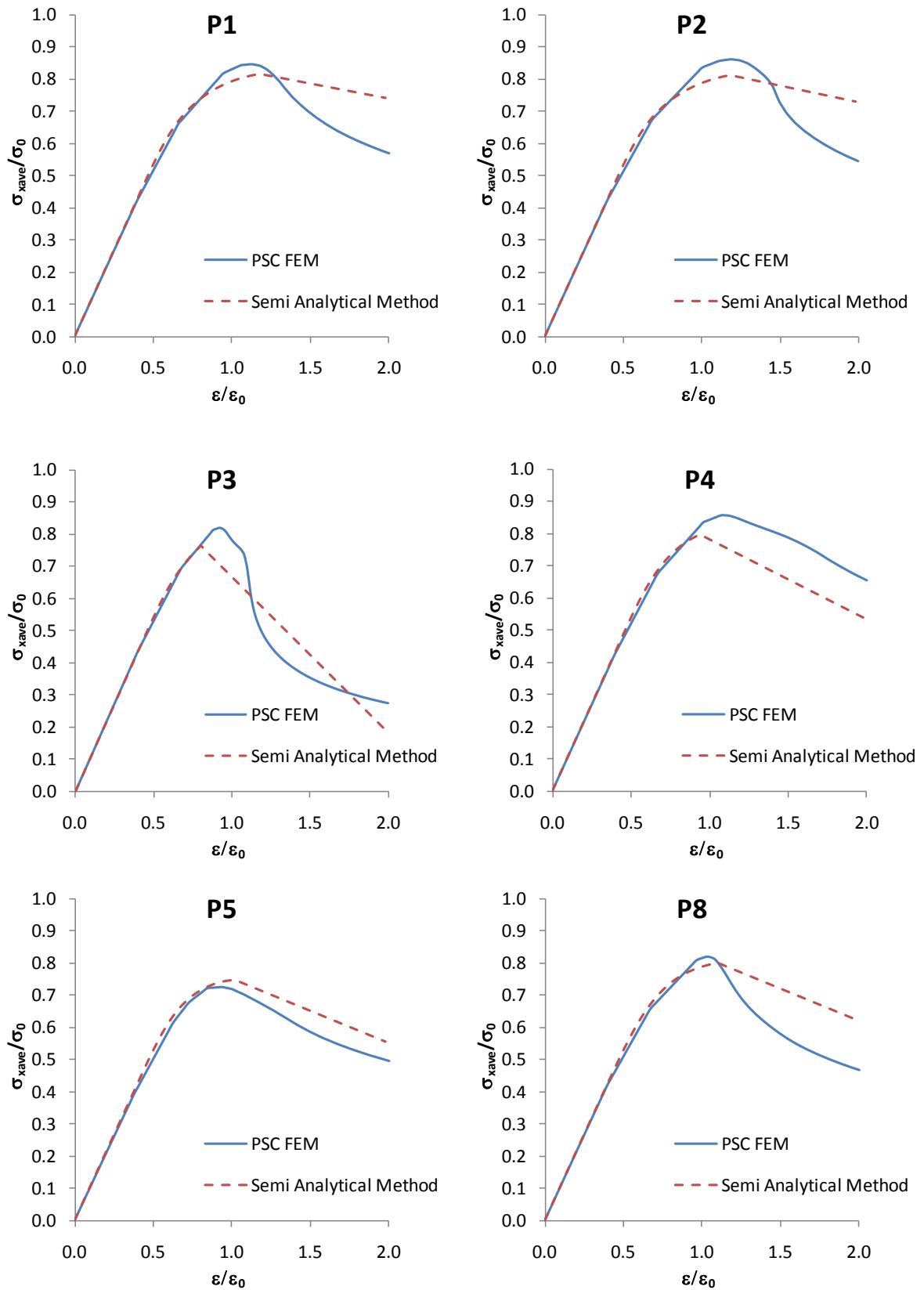


Figure 164 – Aluminium multihull PSC curves

These PSC load shortening curves together with deformed mesh plots from the FEM analysis and 2D section plots from the ProColl-I program are compared in Figure 165. The results show remarkably good agreement with the close correlation of the load shortening curves matched by the same pattern of buckling in the FEM and ProColl-I section plots. There are three clear transition points highlighted on the load shortening curve.

The bending moment – curvature relationship is almost linear up to position A at a curvature of  $0.6 \times 10^6 \text{m}^{-1}$ , at which point the top deck and the uppermost area of side shell begin to buckle. The ProColl plot shows that the side shell is the first to collapse and a similar pattern is observed in the FEM plot although the exact areas which have collapsed are less distinct. The failure in these regions does not trigger complete collapse of the hull girder, but instead causes the bending moment curve gradient to drop considerably. A further effect of the loss of tangent stiffness in the top deck area is to lower the instantaneous neutral axis, which causes additional loads in the upper portions of the cross section.

The ultimate strength is reached at a curvature of approximately  $0.8 \times 10^6 \text{m}^{-1}$  (position B) at which point the entire top deck and side shell between the top deck and middle deck has collapsed. The collapse is triggered by the decrease in tangent stiffness of the middle deck, although the ProColl-I analysis shows that this deck has not actually collapsed at the ultimate strength point but instead has lost effective stiffness below half the elastic modulus. This is validated by the FEM mesh plot, which shows that buckling has not nucleated into the middle deck at the ultimate strength point.

The ultimate strength point is characterised by a clear transition on the FEM load shortening curve whereas the ProColl-I result is much smoother. However, the general characteristics are still broadly similar. The collapse is not as gradual as found for the 1/3 scale frigate, which is perhaps due to the influence of buckling in several decks rather than just a single main deck. The post collapse curves predicted by ProColl-I and FEM are closely correlated. The mesh plots show that buckling spreads across the entire middle deck and continues propagating down the side shell. The ProColl-I plot demonstrates the same pattern.

In summary, the interframe analysis demonstrates two key factors that result in a close correlation between FEM and the simplified method. Firstly, the element load shortening curves are closely matched between FEM and the semi analytical method. The elements in the progressive collapse method are therefore closely replicating the behaviour of the compressed portion of the global FEM model. Secondly, the pattern of the collapse and the spread of buckling in the cross section are

similar between the FEM and simplified analyses, showing that the methods are broadly representing the curvature about the instantaneous neutral axis in a similar manner.

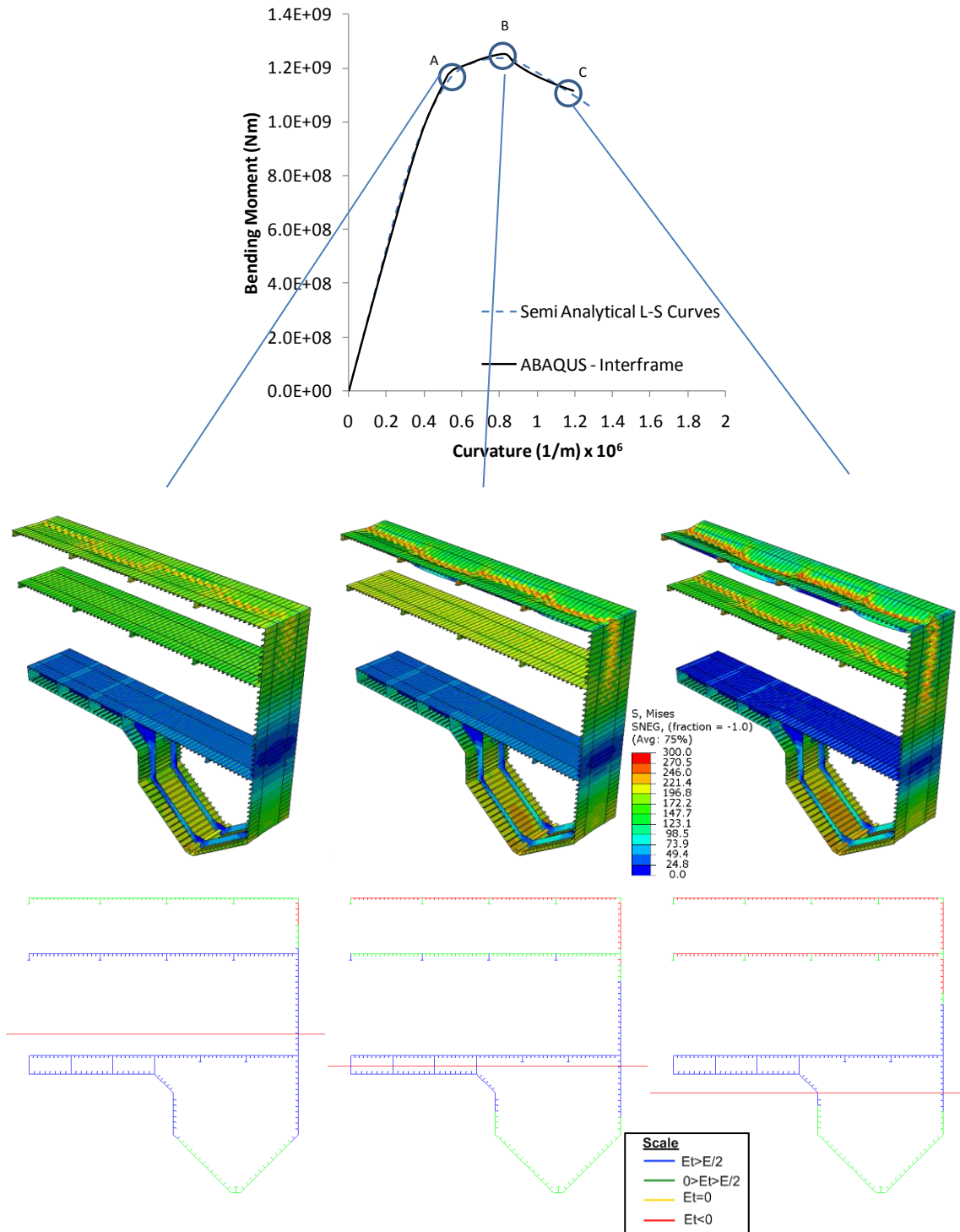


Figure 165 – Interframe bending moment – curvature of the aluminium multihull . FEM plots are magnified x10.

The hull girder is also assessed using a compartment level FEM model and is compared to the ProColl-O predicted result. The previous Chapter has shown that the two uppermost decks in the aluminium multihull are predicted to fail in an overall manner and that their ultimate strength characteristics are significantly reduced as compared to equivalent interframe strength. This means that the compartment level hull girder model also shows significantly reduced primary strength. This means it is an excellent comparator of the capabilities of the extended progressive collapse method.

The FEM model has 1 compartment + 1 bay extents with boundary conditions as given in Figure 141. A half model is used with a symmetry boundary condition along the centreline. The imperfection and residual stress magnitudes are the same as used for the interframe model and also the same as introduced into the deck analyses presented in Chapter 6. The imperfections are introduced across the entire compartment. The mesh size is varied from fine elements in the top decks and the upper portion of the side shell to a coarse discretisation in the bottom structure. This was instigated following the findings from the 1/3 scale frigate modelling and also to reduce the number of nodes and hence the solution time for the model.

The FEM solution does not experience the same problems as found for the 1/3 scale frigate model, providing a clear bending moment – curvature relationship up to and beyond ultimate strength. This is perhaps due to a significant difference between the two models in the mode of collapse. Whereas the 1/3 scale frigate buckles predominantly in an interframe manner, albeit with some overall failure of the top deck, the multihull model fails clearly in an overall mode in the wide decks. This means that potential nucleation problems are much reduced because the collapse nucleates over the entire compartment rather than attempting to buckle interframe.

The FEM results are compared to the equivalent ProColl-O and ProColl-I bending moment curves in Figure 166, together with associated mesh plots at critical points. The compartment level analyses show very good correlation. Although the ultimate strength of the FEM analysis is slightly higher than the ProColl-O prediction, the general shape of the curve is similar, showing that the propagation of the buckling is similar in both models. As expected the hull girder shows a significant loss of ultimate strength (approximately 25% compared to the interframe result), which is due to overall buckling of the two uppermost decks.

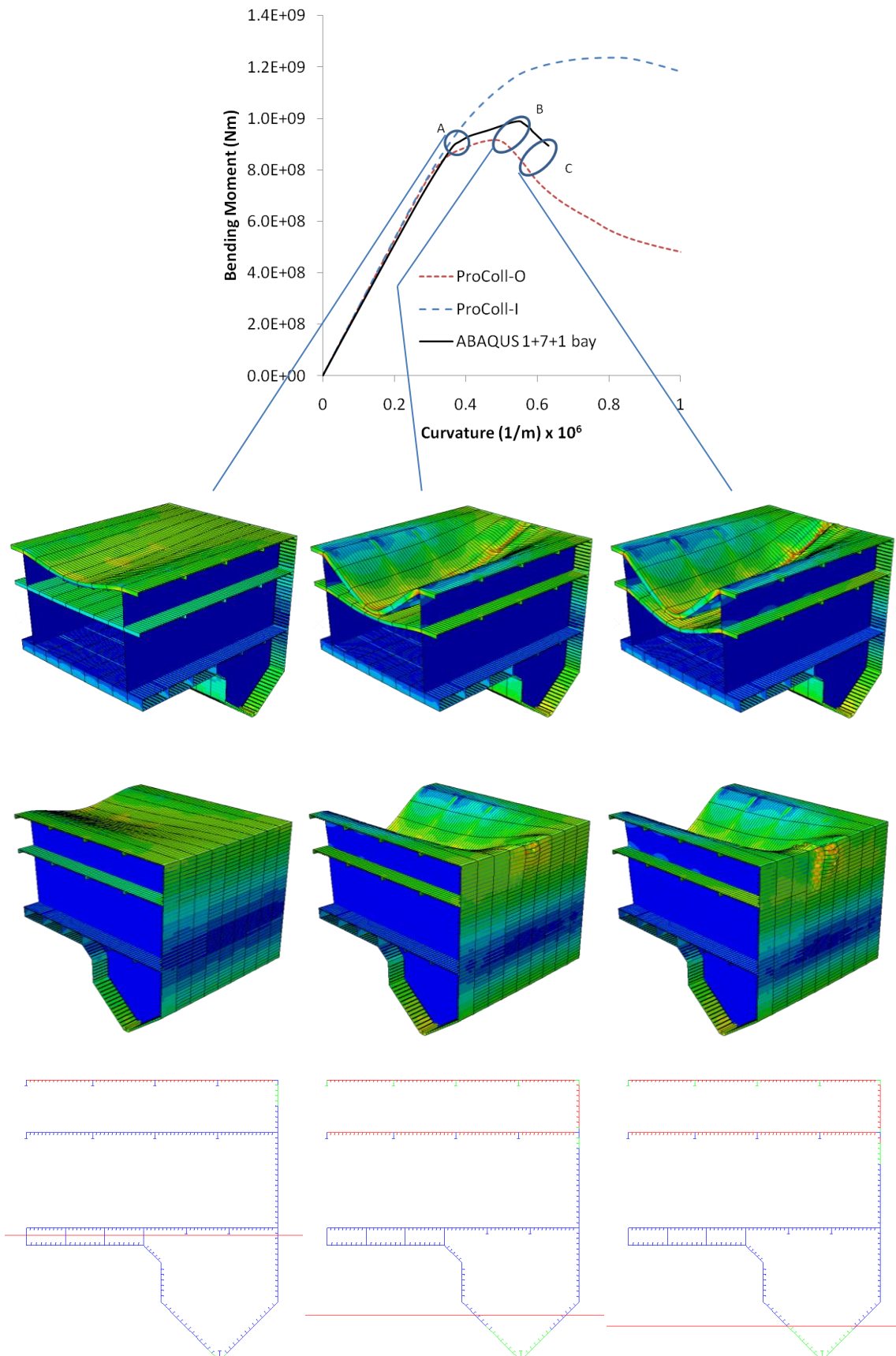


Figure 166 – Overall bending moment – curvature of the aluminium multihull . FEM plots are magnified x10.

The plots show two clear transition points where each of the upper decks buckles overall. The top deck collapses first (position A in Figure 166) which causes a drop in the bending moment curve stiffness. This is similar to the girder behaviour in the interframe analysis. The ultimate strength is reached when the middle deck also fails. Both decks collapse in a clear overall pattern with the same general shape as found for the panel analyses in Chapter 6. The side shell fails in an interframe mode, which is predicted by both the FEM and the extended progressive collapse method.

The post ultimate strength behaviour shows the propagation of the collapsed region continuing down the side shell. The neutral axis continues to drop. The ProColl-O analysis can continue for a long period after ultimate strength has been surpassed, although the continued validity of the predicted bending moment curve at high curvature is questionable because the calculations rely on the reserve strength of the buckled members, which is difficult to quantify accurately in the load shortening curves. In contrast, the FEM analysis terminates shortly after the ultimate strength is surpassed.

## **7.8. Summary**

This Chapter has proposed an extended progressive collapse method which utilises the semi analytical method developed in Chapter 6 to re-evaluate the load shortening curves used in the progressive collapse calculations. The extended method has been shown to predict the overall buckling characteristics for a range of box and hull girders. The method has proved to give representative results and encapsulate the characteristics of the overall collapse mode in lightly stiffened compartments under primary bending moments.

*“The major difference between a thing that might go wrong and a thing that cannot possibly go wrong is that when a thing that cannot possibly go wrong goes wrong, it usually turns out to be impossible to get at and repair.”, Douglas Adams, Mostly Harmless. [131]*

# Chapter 8

## Conclusions and Recommendations for Future Work

### 8.1. Conclusions

This thesis investigates the different collapse modes of lightweight hull girders, focusing on the effect of compartment level buckling modes on the progressive collapse behaviour of the longitudinal structure. The research contributes to the theory of hull girder progressive collapse with several important insights.

Firstly, it is shown that the buckling strength and mode of collapse of a stiffened panel is influenced by the orthogonal scantling arrangement together with the stress-strain relationship of the material, which in a lightweight vessel is commonly aluminium alloy rather than conventional shipbuilding steel. The buckling strength is further affected by the welding induced effects on the material properties, which are shown to be markedly different in aluminium than in equivalent steel.

Secondly, the thesis highlights the need to account for the possibility of compartment level overall collapse modes in a lightweight ship structure and demonstrates how these modes can have a detrimental effect on the progressive collapse behaviour of the hull. Through numerical analyses, the research has demonstrated that gross panel buckling over an entire compartment space is a realistic collapse mechanism in typical lightweight stiffened panels. Further analyses of representative girder cross sections has shown that compartment level collapse modes can result in a significant reduction in the ultimate strength of a hull when compared to the equivalent interframe strength.

Thirdly, in response to these findings, a novel compartment level progressive collapse methodology is proposed. The method is able to account for the specific properties of both steel and aluminium welded scantlings and is capable of determining the effect of interframe and overall buckling modes on the progressive collapse behaviour of a hull girder over an entire compartment.

The findings of the research have an important impact on the applicability of progressive collapse methodologies to predict the ultimate capacity of a hull girder. A fundamental assumption of established progressive collapse methods is that the transverse frames provide sufficient support to be treated as boundaries and thus panel buckling is interframe. It has been shown in this research that this assumption is no longer acceptable if gross panel buckling over an entire compartment is a possible collapse mode.

In fulfilling the overall aims of this research, the following objectives are achieved:

1. Current methodologies for quantifying the ultimate strength and progressive collapse behaviour of lightweight hull structures are reviewed, with a focus on marine grade aluminium;
2. A rigorous nonlinear FEM approach suitable for analysing the ultimate strength and collapse characteristics of ship structures under primary load conditions at the component and global level is developed;
3. Quantification of the strength of welded aluminium plates and stiffened panels under in-plane compressive loads using a nonlinear FEM approach. Investigate the effects of imperfections, residual stresses and the welded heat affected zone on the progressive collapse characteristics of component structure;

4. A semi-analytical approach is developed to predict the load shortening behaviour of an orthogonally stiffened panel under compressive axial load including the effects of interframe and overall buckling modes;
5. The semi-analytical approach is incorporated into a compartment level progressive collapse methodology, extending the Smith interframe approach;
6. The extended progressive collapse method is validated with equivalent nonlinear FEM and experimental test data.

The review of existing ultimate strength methodologies and experimental test results for stiffened panel structures has shown that, although the overall mode has been an established collapse mechanism, it has mostly been considered irrelevant to progressive collapse analysis because the transverse frames are assumed to be adequately proportioned so as to prevent any collapse mode other than interframe buckling. Established panel strength methodologies and test results generally focus on the interframe strength of a stiffened panel throughout the structural hierarchy: from simple plated components up to global hull girder strength assessment. Progressive collapse methodologies such as the Smith method are wholly interframe, with a stipulation that transverse frames must be adequately proportioned to ensure interframe collapse. This assumption of interframe behaviour has been challenged throughout the present work. Numerical analyses have shown that overall collapse can occur in typically proportioned panels, both steel and aluminium. This opens questions about how to account for overall buckling in simplified analytical methods to predict hull girder strength.

Furthermore, because of the dominance of steel in the shipbuilding industry, established progressive collapse methods and the associated techniques used to generate the load shortening curve data for stiffened panels are predominantly focused on steel. The review of existing research studies has shown that there are numerous studies investigating the specific properties of aluminium structures, including the effects of the heat affected zone and the nonlinear material stress-strain relationship, which show how aluminium panels can exhibit significantly different characteristics under compressive load as compared to steel. Most of these studies continue to focus on interframe panel strength. This thesis demonstrates that there is a clear requirement for the well documented differences between steel and aluminium panels to be integrated into progressive collapse theories so as to enable the specific properties of aluminium hull girders to be adequately accounted for.

In response to the questions raised by the literature review and summarised above, this study has utilised the nonlinear finite element method to provide case study data pertaining to the collapse

behaviour of stiffened structures. To ensure that the numerical analysis is reliable and robust, a rigorous modelling approach has been presented which has capabilities to account for the imperfections, residual stresses and material properties of steel and aluminium panels. An extensive review of the finite element approach as applied to thin plated structures under compression shows the importance in adequately defining boundary conditions, imperfection characteristics and material properties. Although many research studies have summarised rigorous approaches to the analysis of plates, stiffened panels and hull girders, there is a distinct lack of detail provided to describe all the steps undertaken so as to achieve an adequately reliable finite element solution.

Therefore, this thesis summarises in detail the approach used to model a plate, stiffened panel and hull girder using nonlinear FEM. In particular, the node translation approach used to model the geometric imperfections is detailed so as to provide a foundation for future FEM work in this area. This approach is recommended as applicable for automated imperfection generation, using an appropriate code to read the perfect geometry input file from the finite element software and translate individual nodes so as to produce the desired imperfection patterns. This approach is capable of introducing imperfection into a full range of structural models, from a simple plate through to a complete hull girder compartment. The approach is proposed as superior to other techniques such as the use of Eigenmode imperfection shapes because it is capable of introducing realistic imperfection shapes and allows full control of the imperfection characteristics.

The FEM modelling approach has been used to generate an extensive range of data pertaining to stiffened panel elements. The results have shown several important phenomena associated with lightly stiffened aluminium panels. In particular, it has been shown that the strength of an aluminium alloy plate is significantly affected by the weakened HAZ, which is caused by the high heat input during welding. The HAZ is a known problem associated with welding aluminium and attempts to quantify its influence have been previously undertaken. This study presents rigorous FEM analyses which demonstrate the influence of HAZ on 5xxx and 6xxx series aluminium alloys. The location of the welded joint is shown to play an important part in the strength. HAZ at the plate edges causes a greater strength reduction than in the plate centre, and welds along the loaded edges of a plate can have a significant debilitating effect on the strength of thick plates, particularly in 6xxx series alloys where the percentage reduction of strength in the HAZ is large (53% of the parent metal proof stress).

Numerical analyses of stiffened panels utilising the rigorous FEM modelling approach have clearly demonstrated the detrimental effect of overall collapse modes on the ultimate strength and general load shortening behaviour of the panel. The analyses have focused on a dataset of aluminium alloy

stiffened panels, which are typical of the scantlings of lightweight ships. The analyses have shown the important influence of the transverse frame size, and how even a relatively stocky frame may not be sufficient to prevent overall collapse. The numerical results are compared to equivalent plate-stiffener combination analyses, which follow the conventions of the established progressive collapse methodology in that they are wholly interframe. The numerical results also show how aluminium alloy panels, with realistic representations of the reduction in strength at the heat affected zone, have a significantly increased susceptibility to overall collapse modes as compared to equivalently sized steel panels.

Stemming from the findings of the extensive numerical analyses of orthogonally stiffened panels, a theoretical semi analytical methodology to predict the load shortening characteristics of an orthogonally stiffened panel has been proposed, based on the large deflection orthotropic plate approach. The method has been shown to predict the influence of overall collapse on the strength behaviour of a lightly stiffened panel, whilst also predicting interframe failure strength if the transverse framing is sturdy enough to prevent gross panel buckling. The method has been used to estimate the strength behaviour for a range of stiffened panels including a large scale deck structure with several stiffener sizes within its cross section. The results have been validated adequately against equivalent nonlinear FEM analyses both in predicting the ultimate strength and the load shortening characteristics.

The semi analytical methodology has been extended from large deflection orthotropic plate theory. It has been shown that the established orthotropic equations can be enhanced by developing a more rigorous definition of the panel properties. In the established approach the orthotropic plate is defined by flexural and stiffness constants, which are a function of the elastic material properties. The extended approach defines the instantaneous stiffness and rigidity of the plate and stiffeners in the orthotropic plate as a function of the in-plane displacement. Thus the local buckling characteristics of the constituent parts of the panel directly influence the overall panel buckling capacity.

The semi analytical methodology thus relies on a representative definition of the plate and stiffener component behaviour under in-plane compression. Several methods to predict the component response have been investigated in this thesis. Nonlinear FEM, utilising appropriate software and solution techniques, is found to be a relatively efficient method to predict the strength of welded components. As already summarised above, the method can account for the geometric imperfections and welded material properties that are typical of a component within a ship structure. A comparison of steel and aluminium plates with a range of geometric and material

properties has shown that the individual properties of different metals must be accounted for in the definition of representative load shortening curve.

The rigorous FEM approach has proved a capable validation method for the simplified semi analytical methodology. The method has also shown to satisfactorily predict the onset of overall buckling modes over several frame spaces together with the associated change in the strength behaviour. The study has benchmarked both approaches with physical experiment data of interframe panels tested beyond their ultimate capacity. The results have shown reasonable correlation between the methods and the experiment results. Statistical analysis of the predicted ultimate strengths shows that the methods perform satisfactorily when considering the inherent variability due to the geometric and material imperfections. The analysis has been further validated using qualitative comparisons of the load shortening curves generated using the FEM and semi analytical methods. These show that the ultimate strength is only a single measure of panel performance. The load shortening characteristics over the entire strain range are required for a global progressive collapse analysis. The development of the post collapse load shortening prediction is therefore a critical part of the semi analytical methodology and has been developed to give an adequate representation in comparison to equivalent FEM results.

The semi analytical method produces load shortening curves suitable for direct implementation in the progressive collapse methodology. Thus an extended progressive collapse approach is developed to account for both interframe and overall collapse of structural elements within a hull girder. Because the inclusion of overall buckling is encapsulated within the semi analytical method, the general principles of the extended progressive collapse method remain fundamentally similar. The assumption of element independency is altered so that the each discrete element in the hull girder cross section can be represented as an interframe element or as part of a larger panel element should overall buckling be the critical response characteristic.

The extended progressive collapse method is tested by analysing a range of box girder and hull girder scantlings placed under primary bending moments. The results are validated using nonlinear FEM analysis of the hull structure. The discussion highlights some of the difficulties of obtaining a reliable FEM solution. In particular, it has been shown that the FEM solver can experience significant problems maintaining convergence for a complex structure experiencing mixed mode buckling characteristics. FEM modelling techniques are proposed to minimise these difficulties. The extended progressive method is found to predict compartment level buckling with good reliability. The results generally show close correlation to equivalent compartment FEM analyses. Overall buckling modes

are shown to have a significant effect in reducing the bending capacity of a lightly stiffened hull structure.

The global FEM and simplified progressive collapse analyses have shown that both approaches produce reasonable and valid solutions for the compartment level progressive collapse problem. This means that the decision of which methodology to employ in practical design and analysis situations has as much to do with the ease of analysis and the purpose of the analysis as it does with the accuracy of the solution. In terms of providing a relatively quick model definition and fast solution, the simplified methodologies remain valid and easily applied, and in terms of simplicity of use are superior to FEM. However, the FEM approach, if completed in a rigorous manner, is an acceptable and realistic alternative. The FEM approach also continues to hold significant advantages because it is employed within a general purpose analysis package. This flexibility means that it has capabilities beyond the simplified methods developed in this thesis such as modelling unusual scantling arrangements, irregular spacing of stiffeners multiple load combinations. These example scenarios are not readily dealt with by the simplified methods as developed in this thesis.

In this respect the FEM approach is an appropriate methodology for research and some practical applications. Perhaps more importantly in the context of the present research, FEM also provides a robust validation for further development and enhancement of simplified methodologies to account for new structural arrangement and loading criteria.

## **8.2. Recommendations for Future Work**

The work performed in this thesis has considered the strength of ship structures over a full range of complexity. This broad analysis of different levels in the structural hierarchy has been necessary because the information derived from the component level has a direct bearing on the analysis of more complex structures. This means that there are many areas where future work would further enhance the capabilities of the proposed methodologies.

Because of the broad scope including component and global level analyses of ship structures, this research has only focused on a few specific types of structural configurations. The study has investigated the strength of two aluminium alloys: 5083-H116 and 6082-T6. Although the properties of other marine alloys are quoted and found to be similar to these two grades, there is much need for a better quantification of how these material properties influence the strength behaviour of component and stiffened panel structures. The materials have been represented by a relatively standard Ramberg-Osgood stress strain relationship. However, the strain hardening of aluminium in the parent metal and the welded HAZ region could be better quantified, especially because the HAZ

properties can have a significant effect on the strength of a welded plate. The effect of different welding techniques is also important. For example, friction stir welding has been suggested to give better properties within the weld zone. If these material effects were better understood, the resulting influence on plate and stiffened panel strength could be assessed using the rigorous techniques developed in this thesis.

The work has also focused on specific stiffener configurations. The majority of analyses reported in the thesis are for tee bar and flat bar stiffened panels. These are very typical of lightweight steel ships; tee bars are usually used exclusively in naval designs because of their favourable characteristics under blast loading. However, the use of aluminium as a hull structural material opens up a much broader range of scantling configurations because aluminium can be formed and extruded into a limitless variety of shapes; for example corrugated or top hat stiffened panels. In the context of the present study the orthogonal plate methodology would need to be re-evaluated to determine its suitability. In particular, a more complex panel extrusion can blur the definition of distinct “plates” and “stiffeners”.

The simplified methodologies have been investigated with regard to their application on aluminium structures. However, in certain respects, the methods are more general purpose and thus further development of the methods to deal with different materials would be an interesting extension to the study. In particular, the use of composites as a lightweight structural material is gaining increasing research and practical interest. Although most composites are currently restricted to relatively small craft, their effectiveness if used in critical areas of a large hull girder would be a highly interesting area for research. The suitability of the current methodologies would be fundamentally challenged because composites are much more difficult to define in simple terms of material tangent stiffness. Furthermore, buckling is also associated with other failure modes such as de-bonding.

The research has concentrated on in-plane loads on stiffened panels arising from primary longitudinal hull girder bending. This is usually the critical load condition for a conventional large vessel. The semi analytical method has been validated exclusively with FEM analyses of panels in uniaxial compression. Furthermore, the extended progressive collapse method has been validated almost exclusively with girders in vertical bending only. In this respect the method has been proved successful, but it must be recognised that this is only one particular load condition. The thesis provides a foundation for investigating multiple load effects on the strength of a lightweight hull girder. Biaxial bending is the obvious first extension for demonstrating the capabilities of the method for a monohull or stabilised monohull. The critical load condition for a large catamaran is the prying

moment between demi-hulls. This would impart a transverse in-plane load on the main decks, thus requiring the semi analytical method to predict strength under a biaxial in-plane load. The orthotropic plate method in Chapter 6 is derived in its general form suitable for treating biaxial load cases. However, the semi analytical method would also require an adequate representation of the biaxial behaviour of components for the definition of the instantaneous panel properties.

Progressive collapse methods are useful for determining the intact strength of a hull girder. The residual strength in a damaged condition due to collision, grounding or blast loading is an excellent area in which the current research could be extended. The methods developed in this thesis could be assessed for their suitability in determining the loss in strength of compartment level panel structures. This is a very important area with regard to assessing the crashworthiness of a proposed hull girder structure but also has application when considering the recoverability of damaged ships, where a fast and robust assessment of the residual strength of the hull can impact on the way in which a damaged ship is managed. Recoverability is of particular importance for naval vessels, whereby damage may be sustained in a hostile environment. An improved assessment of the damage strength in this situation would be of invaluable use in determining the survivability of the hull and its capacity for further engagement, evacuation and emergency recoverability.

The semi analytical method should only be considered as one of many potential ways in which the strength of a multi bay stiffened panel can be assessed, which is particularly relevant when discussing the extension of methodologies to deal with damage. The method would need considerable advancement to be able to deal with a damaged panel, where the strength of the individual plates and stiffeners are significantly altered, or even removed entirely, over a portion of the stiffened panel. This would impact on the way the tangent stiffness of the elements are input into the orthotropic plate calculations because the element tangent stiffness is likely to be non-uniform over the panel width. A simple adaptation would be to use an average element stiffness including the non-damaged, partly damaged and fully ruptured zones across the panel. However, this may not be adequate for assessing the complexity of the damage problem. In any case, an adapted method would require extensive validation with equivalent numerical analyses.

With respect to dealing with both intact and damaged analyses, the extended progressive collapse methodology has the ability to accept load shortening curves from any suitable panel strength program and is thus readily adaptable to dealing with more complex scenarios. For example, the program can easily accept load shortening curves direct from a finite element analysis of a panel. There is thus potential to further develop the extended progressive collapse method so as to accept a hybrid of analytical and numerical data in the formation of the panel load shortening curves. The

negative aspect of such an approach is that the solution time is greatly increased. This would have important repercussions especially if requiring information as part of the recoverability of a vessel. There is thus a large scope for developing efficient approaches to develop efficient analytical and numerical approaches to assess panel strength in both intact and damage scenarios.

# Chapter 9

## References

1. Claremont, C.A., *Spanning Space*1939: Pitman, London.
2. Hughes, O.F. and J.K. Paik, *Ship Structural Analysis and Design*2010: The Society of Naval Architects and Marine Engineers.
3. Lewis, E.V., *Principles of Naval Architecture*1988: The Society of Naval Architects and Marine Engineers.
4. Rutherford, S.E. and J.B. Caldwell, *Ultimate Strength of Ships: A Case Study*. Transactions of the Society of Naval Architects and Marine Engineers, 1990. **98**: p. 441-471.
5. Collette, M., *The Strength and Reliability of Aluminium Stiffened Panels*, in *School of Marine Science and Technology*2005, University of Newcastle upon Tyne.
6. Mazzolani, F.M., *Aluminium Alloy Structures*. 2nd ed1995, London ; New York: E & FN Spon. xix, 693.
7. Smith, C.S., *Influence of Local Compressive Failure on Ultimate Longitudinal Strength of a Ship's Hull*, in *Practical Design of Ships and Other Floating Structures*1977: Tokyo. p. 73-79.
8. White, W.H., *A Manual of Naval Architecture*1877: John Murray, London.

9. *The Aluminium Yacht Vendenesse*, in *The New York Times* 1894.
10. Sielski, R.A., *Aluminium Marine Structure Design and Fabrication Guide*, 2007, Ship Structures Committee.
11. Muckle, W., *The Design of Aluminium Alloy Ships' Structures* 1963, London: Hutchinson. 264.
12. Nicol, G., *Ship Construction and Calculations* 1909: J. Brown and Son.
13. Sikora, J.P. and E.A. Devine, *Guidelines for the Design of Advanced Double Hull Vessels*, 2001. p. 93pp.
14. Sikora, J.P., et al., *Double Hull Tanker Research: Further Studies*. Transactions of the Society of Naval Architects and Marine Engineers, 1995. **103**: p. 295-315.
15. Okamoto, T., et al., *Strength Evaluation of Novel Unidirectional-Girder-System Product Oil Carrier by Reliability Analysis*. Transactions of the Society of Naval Architects and Marine Engineers, 1985. **93**: p. 55-77.
16. Kramer, R.K., et al., *Structural Optimization for Conversion of Aluminium Car Ferry to Support Military Vehicle Payload*, 2005, Ship Structure Committee.
17. Alcan. *Aluminium and the Sea*. 2004 16/05/2011; Available from: <http://tinyurl.com/5rk9p8>.
18. DNV, *Rules for Classification of High Speed, Light Craft and Naval Surface Craft*, 2001, Det Norske Veritas.
19. Paik, J.K. and A. Duran, *Ultimate Strength of Aluminum Plates and Stiffened Panels for Marine Applications*. Marine Technology, 2004. **41**(3): p. 108-121.
20. Clarke, J.D. and J.W. Swan, *Interframe Buckling of Aluminium Alloy Stiffened Plating*, 1987, Admiralty Research Establishment: Dunfermline.
21. Zha, Y., T. Moan, and E. Hanken, *Experimental and Numerical Study of Torsional Buckling of Stiffeners in Aluminium Panels*, in *International Offshore and Polar Engineering Conference* 2000: Seattle, USA.
22. Paik, J.K., et al., *Mechanical Collapse Testing on Aluminum Stiffened Panels for Marine Applications*, 2008, Ship Structures Committee.
23. Kissell, J.R. and R.L. Ferry, *Aluminum Structures : A Guide to their Specifications and Design*. 2nd ed 2002, New York: J. Wiley. xi, 532.
24. Ramberg, W. and W.R. Osgood, *Description of stress-strain curves by three parameters*, in *Technical Note No. 902* 1943, National Advisory Committee For Aeronautics, Washington DC.
25. Hill, H.N., J.W. Clark, and R.J. Brungraber, *Design of Welded Aluminum Structures*. Journal of the Structural Division, Proceedings of the ASCE, 1960. **86**(ST6): p. 101-124.
26. Dwight, J., *Aluminium Design and Construction* 1999: E & FN SPON.
27. Zha, Y. and T. Moan, *Ultimate Strength of Stiffened Aluminium Panels with Predominantly Torsional Failure Modes*. Thin Walled Structures, 2001. **39**: p. 631-648.
28. British Standards, *Structural Use of Aluminium*, B. Standards, Editor 1991, British Standards.
29. British Standards, *Eurocode 9: Design of aluminium structures*, 2007, British Standards.
30. Kristensen, O. and T. Moan, *Ultimate Strength of Aluminium Plates under Biaxial Loading*, in *Proceedings of 5th International Conference on Fast Sea Transportation* 1999.

31. Zunaidi, A.N., *The Strength Characteristics of Aluminium Panels in Ships*, in *School of Marine Science and Technology* 2007, Newcastle University.
32. ABS, *Guide for Building and Classing High Speed Naval Craft*, 2007, American Bureau of Shipping.
33. Stephens, R., et al., *Metal Fatigue in Engineering*. 2nd Edition ed2001: Wiley-Interscience.
34. Peel, M., et al., *Microstructure, Mechanical Properties and Residual Stresses as a Function of Welding Speed in Aluminium AA5083 Friction Stir Welds*. *Acta Materialia*, 2003. **51**: p. 4791-4801.
35. Withers, P.J., *Residual Stress and its Role in Failure*. *Reports on Progress in Physics*, 2007. **70**: p. 2211-2264.
36. Paik, J.K., *Mechanical Collapse Testing on Aluminum Stiffened Panels for Marine Applications*, 2006, Ship Structure Committee.
37. Paik, J.K. and A.K. Thayamballi, *Ultimate Limit State Design of Steel-Plated Structures* 2003: Wiley, 2003.
38. Smith, C.S., et al., *Strength and Stiffness of Ships' Plating under In-plane Compression and Tension*. *Transactions of the Royal Institution of Naval Architects*, 1988. **130**: p. 277-296.
39. Smith, C.S., et al., *Strength of Stiffened Plating under Combined Compression and Lateral Pressure*. *Transactions of the Royal Institution of Naval Architects*, 1991: p. 131-147.
40. Caldwell, J.B., *Ultimate Longitudinal Strength*. *Transactions of the Royal Institution of Naval Architects*, 1965. **107**: p. 411-430.
41. Paik, J.K. and A. Mansour, *A Simple Formulation for Predicting the Ultimate Strength of Ships*. *Journal of Marine Science and Technology*, 1995. **1**(1): p. 52-62.
42. Bruhn, E.F., *Analysis and Design of Flight Vehicle Structures* 1973: Jacobs.
43. Gordo, J.M. and C. Guedes Soares, *Approximate Method to Evaluate the Hull Girder Collapse Strength*. *Marine Structures*, 1996. **9**: p. 449-470.
44. Ueda, Y. and S.M.H. Rashed, *Advances in the Application of ISUM to Marine Structures*, in *Advances in Marine Structures 2*, C.S. Smith and R.S. Dow, Editors. 1991, Elsevier: Dunfermline, Scotland. p. 628-649.
45. Dow, R.S., *Structural Redundancy and damage tolerance in relation to ultimate ship hull strength*, in *Advances in Marine Structures 3* 1997, DERA: Dunfermline, Scotland.
46. Bryan, G.H., *On the Stability of a Plane Plate under Thrusts in its own Plane, with Applications to the Buckling of the Sides of a Ship*. *Proceedings of the London Mathematical Society*, 1890.
47. von Karman, T., *Festigkeitsprobleme im Maschinenbau*. *Encyclopaedie der Mathematischen Wissenschaften*, 1910. **4**: p. 349.
48. Marguerre, K. *Zur Theorie der gekreummtter Platte grosser Formaenderung*. in *Proceedings of Fifth International Congress for Applied Mechanics*. 1938. Cambridge, UK.
49. Cox, H.L., *The theory of flat panels buckled in compression*, 1945.
50. Rhodes, J., *Buckling of thin plates and members -- and early work on rectangular tubes*. *Thin-Walled Structures*, 2002. **40**(2): p. 87.
51. British Standards, *Eurocode 3: Design of steel structures — Part 1-9: Fatigue*, 2005.
52. Timoshenko, S., *Theory of elastic stability*. 2d ed1961, New York,: McGraw-Hill. 541.

53. Hughes, O.F., *Ship Structural Design : A Rationally-Based, Computer-Aided Optimization Approach* 1988, Jersey City, N.J: Society of Naval Architects and Marine Engineers. 566 p.
54. Dwight, J.B. and A.T. Ratcliffe, *The Strength of Thin Plates in Compression*, in *Symposium on Thin Walled Steel Structures* 1967: University College Swansea.
55. Moxham, K.E., *Buckling Tests on Individual Welded Steel Plates in Compression*, 1971, Cambridge University.
56. Bradfield, C.D., *Tests on Plates Loaded in In-Plane Compression*. Journal of Constructional Steel Research, 1980. **1**(1): p. 27.
57. Bradfield, C.D., R.W.P. Stonor, and K.E. Moxham, *Tests of Long Plates Under Biaxial Compression*. Journal of Constructional Steel Research, 1993. **24**(1): p. 25-56.
58. Moxham, K.E., *Theoretical Prediction of the Strength of Welded Steel Plates in Compression*, 1971, Cambridge University.
59. Frieze, P.A., P.J. Dowling, and R.E. Hobbs, *Ultimate Load Behaviour of Plates in Compression*. Steel Plated Structures, 1978: p. 24-50.
60. Guedes Soares, C. and J.M. Gordo, *Compressive Strength of Rectangular Plates under Biaxial Load and Lateral Pressure Thin Walled Structures*, 1996. **24**(3).
61. Dow, R.S. and C.S. Smith, *Effects of Localized Imperfections on Compressive Strength of Long Rectangular Plates*. Journal of Constructional Steel Research, 1984. **4**: p. 51-76.
62. Valsgård, S., *Numerical Design Prediction of the Capacity of Plates in Biaxial In-Plane Compression*. Computers and Structures, 1980. **12**(5): p. 729.
63. Dier, A.F. and P.J. Dowling, *The Strength of Plates subjected to Biaxial Forces*, in *Proceedings of Conference on Behaviour of Thin-Walled Structures* 1983: University of Strathclyde, Glasgow.
64. Paik, J.K., A.K. Thayamball, and B.J. Kim, *Advanced Ultimate Strength Formulations for Ship Plating Under Combined Biaxial Compression/Tension, Edge Shear, and Lateral Pressure Loads*. Marine Technology, 2001. **38**: p. 9-25.
65. Faulkner, D., *A Review of Effective Plating for use in the Analysis of Stiffened Plating in Bending and Compression*. Journal of Ship Research, 1975. **19**(1): p. 1-17.
66. Benson, S., R.S. Dow, and J. Downes, *Ultimate strength characteristics of aluminium plates for high-speed vessels*. Ships and Offshore Structures, 2011. **6**: p. 67-80.
67. Kristensen, O.H.H., *Ultimate Capacity of Aluminium Plates under Multiple Loads, Considering HAZ Properties*, in *Department of Marine Structures* 2001, Norwegian University of Science and Technology: Trondheim.
68. Snaith, G.R., *A Note on the Comparative Buckling Properties of Mild-Steel and Aluminium-Alloy Plating*. The Shipbuilder and Marine Engine Builder, 1958.
69. Little, G.H., *Collapse Behaviour of Aluminium Plates*. International Journal of Mechanical Sciences, 1982. **24**(1): p. 37-45.
70. Mofflin, D., *Plate Buckling in Steel and Aluminium*, 1983, University of Cambridge.
71. Hopperstad, O.S., M. Langseth, and L. Hanssen, *Ultimate compressive strength of plate elements in aluminium: Correlation of finite element analyses and tests*. Thin-Walled Structures, 1997. **29**(1-4): p. 31-46.
72. Hopperstad, O.S., M. Langseth, and T. Tryland, *Ultimate strength of aluminium alloy outstands in compression: experiments and simplified analysis*. Thin Walled Structures, 1999. **34**: p. 279-294.

73. BritishStandards, *Eurocode 9: Design of aluminium structures*, 2007, British Standards.
74. Guedes Soares, C., *Design Equation for the Compressive Strength of Unstiffened Plate Elements with Initial Imperfections*. Journal of Constructional Steel Research, 1988. **9**: p. 287-310.
75. ABS, *Guide for Building and Classing High Speed Craft*, 2001, American Bureau of Shipping.
76. Chalmers, D.W., *Design of Ships' Structures*1993, London: HMSO. xiv, 484.
77. Gordo, J.M. and C. Guedes Soares, *Approximate Load Shortening Curves for Stiffened Plates Under Uniaxial Compression*, in *Integrity of Offshore Structures 5*1993, EMAS Publishers: Glasgow, Scotland.
78. Collette, M., *Rapid analysis techniques for ultimate strength predictions of aluminum structures*, in *Advances in Marine Structures*2011, Taylor & Francis: Hamburg, Germany.
79. Stowell, E.Z., *A Unified Theory of Plastic Buckling of Columns and Plates*, 1948, NACA Technical Note 1556, Washington DC.
80. Paik, J.K., A.K. Thayamballi, and B.J. Kim, *Advanced Ultimate Strength Formulations for Ship Plating Under Combined Biaxial Compression/Tension, Edge Shear, and Lateral Pressure Loads* Marine Technology, 2001. **38**(1).
81. Dow, R.S., *Effect of damage on the collapse and post-collapse behaviour of rectangular steel plates*, in *3rd International Symposium on Practical Design of Ships and Other Floating Structures*1987: Trondheim, Norway. p. 1213-1223.
82. Mansour, A., *Gross Panel Strength Under Combined Loading*, 1977, Ship Structure Committee.
83. Chen, Y., *Ultimate Strength Analysis of Stiffened Panels using a Beam-Column Method*, 2003, Virginia Polytechnic Institute.
84. Rigo, P., et al., *Sensitivity analysis on ultimate strength of aluminium stiffened panels*. Marine Structures, 2003. **16**: p. 437-468.
85. Khedmati, M.R., A. Bayatfar, and P. Rigo, *Post-buckling behaviour and strength of multi-stiffened aluminium panels under combined axial compression and lateral pressure* Marine Structures, 2010. **23**(1): p. 39-66.
86. Zha, Y. and T. Moan, *Experimental and Numerical Prediction of Collapse of Flatbar Stiffeners in Aluminum Panels*. Journal of Structural Engineering, 2003. **129**(2): p. 160-168.
87. Aalberg, A., M. Langseth, and P.K. Larsen, *Stiffened aluminium panels subjected to axial compression*. Thin-Walled Structures, 2001. **39**: p. 861-885.
88. Benson, S., J. Downes, and R. Dow, *Ultimate strength characteristics of aluminium plates for high speed vessels*, in *Analysis and Design of Marine Structures*, C. Guedes Soares and P.K. Das, Editors. 2009, Taylor & Francis: Lisbon, Portugal. p. 121-131.
89. Zhang, S. and I. Khan, *Buckling and ultimate capability of plates and stiffened panels in axial compression*. Marine Structures, 2009. **22**(4): p. 791-808.
90. Sun, H. and X. Wang, *Buckling and Ultimate Strength Assessment of FPSO Structures*, in *SNAME Marine Technology Conference & Expo*2005.
91. Dorman, A.P. and J.B. Dwight. *Tests on Stiffened Compression Panels and Plate Panels*. in *Proceedings of the International Conference on Steel Box Girder Bridges*. 1973. London.

- 
92. Chen, W.F. and E.M. Lui, *Structural Stability. Theory and Implementation*. 1987: Elsevier.
  93. Cook, R.D., *Concepts and applications of finite element analysis*. 4th ed ed2002, New York, NY: Wiley. xvi, 719 p.
  94. Newmark, N.M., *Numerical Procedure for Computing Deflections, Moments and Buckling Loads*. Transactions ASCE, 1943. **108**.
  95. Bleich, F., *Buckling Strength of Metal Structures* 1952: McGraw Hill.
  96. Paik, J.K., A.K. Thayamballi, and B. Ju Kim, *Large deflection orthotropic plate approach to develop ultimate strength formulations for stiffened panels under combined biaxial compression/tension and lateral pressure*. Thin-Walled Structures, 2001. **39**(3): p. 215-246.
  97. Steen, E., E. Byklum, and K.G. Vilming, *Computer Efficient Non-Linear Buckling Models for Capacity Assessments of Stiffened Panels Subjected to Combined Loads*, in *Fourth International Conference on Thin Walled Structures* 2004: Loughborough, UK.
  98. Smith, C.S., *Elastic Buckling and Beam Column Behaviour of Ship Grillages*. Transactions of the Royal Institution of Naval Architects, 1968. **110**: p. 127-147.
  99. Rostovtsev, G.G., *Calculation of a thin plane sheeting supported by ribs*. Trudy Leningrad Institute, Inzhenerov Grazhdanskogo Vosdushnogo Flota, No. 20, 1940(in Russian).
  100. *Ambuja Knowledge Initiative*. 17/05/11; Available from: <http://www.foundationsakc.com/people/legends/sir-ove-arup>.
  101. Hibbitt, Karlsson, and Sorensen, *ABAQUS 6.9 User Manual*, Dassault Systemes Simulia Corp.
  102. Conrardy, C. and R. Dull, *Control of Distortion in Thin Ship Panels*. Journal of Ship Production, 1997. **13**(2): p. 83-92.
  103. Paik, J.K., A.K. Thayamballi, and J.M. Lee, *Effect of Initial Deflection Shape on the Ultimate Strength Behavior of Welded Steel Plates Under Biaxial Compressive Loads* Journal of Ship Research, 2004. **48**(1): p. 45-60.
  104. Ueda, Y. and T. Yao, *Ultimate Strength of a Rectangular Plate under Thrust : with Consideration of the Effects of Initial Imperfections due to Welding*. Transactions of Japanese Welding Research Institute, 1979. **8**(2): p. 257-264.
  105. Ueda, Y. and T. Yao, *The influence of complex initial deflection modes on the behaviour and ultimate strength of rectangular plates in compression*. Journal of Constructional Steel Research, 1985. **5**: p. 265-302.
  106. Featherston, C.A., *Imperfection sensitivity of flat plates under combined compression and shear*. International Journal of Non-Linear Mechanics, 2001. **36**(2): p. 249-259.
  107. Gannon, L.G., et al., *Shakedown of welding induced residual stress and effect on stiffened plate strength and behaviour*, in *Advances in Marine Structures* 2011, Taylor & Francis: Hamburg, Germany.
  108. Dykes, A.R., *Chairmans Address to IStructE*. The Structural Engineer: p. 150-151.
  109. Mansour, A.E. and R.C. Ertekin, *Committee III.1 Ultimate Strength*, in *15th International Ship and Offshore Structures Congress* 2003, Elsevier Science: Oxford. p. 265-328.
  110. Paik, J.K., et al., *Committe III.1 Ultimate Strength*, in *17th International Ship and Offshore Structures Congress* 2009: Seoul, Korea.

111. Amlashi, H.K.K. and T. Moan, *Ultimate strength analysis of a bulk carrier hull girder under alternate hold loading condition – A case study Part 1: Nonlinear finite element modelling and ultimate hull girder capacity*. Marine Structures, 2008. **21**: p. 327-352.
112. Amlashi, H.K.K. and T. Moan, *Ultimate strength analysis of a bulk carrier hull girder under alternate hold loading condition, Part 2: Stress distribution in the double bottom and simplified approaches*. Marine Structures, 2009. **22**(3): p. 522-544.
113. Kippenes, J., et al., *Ultimate Strength of Cape Size Bulk Carrier under Alternate Hold Loading*, in *Practical Design of Ships and other Floating Structures (PRADS)2010*, COPPE UFRJ: Rio de Janeiro, Brazil. p. 1114-1122.
114. Khedmati, M.R., M.R. Zareei, and P. Rigo, *Sensitivity analysis on the elastic buckling and ultimate strength of continuous stiffened aluminium plates under combined in-plane compression and lateral pressure*. Thin Walled Structures, 2009. **47**(11): p. 1232-1245.
115. Smith, C.S., *Compressive Strength of Welded Steel Ship Grillages*. Transactions of the Royal Institution of Naval Architects, 1976. **118**: p. 325-359.
116. Wang, X., et al., *Buckling and Ultimate Strength of Aluminium Plates and Stiffened Panels in Marine Structures*, in *Fifth International Forum on Aluminium Ships2005*: Tokyo, Japan.
117. Hughes, O.F., B. Ghosh, and Y. Chen, *Improved prediction of simultaneous local and overall buckling of stiffened panels*. Thin-Walled Structures, 2004. **42**(6): p. 827-856.
118. Collette, M., et al., *Ultimate Strength and Optimisation of Aluminium Extrusions*, 2008, Ship Structure Committee.
119. Girard, P.S., *Traité analytique de la résistance des solides*1798.
120. Dow, R.S., *Testing and Analysis of a 1/3 Scale Frigate Model*, in *Advances in Marine Structures 21991*, Elsevier: Dunfermline, Scotland. p. 749-773.
121. Gordo, J.M. and C. Guedes Soares, *Tests on ultimate strength of hull box girders made of high tensile steel*. Marine Structures, 2009. **22**(4): p. 770-790.
122. Gordo, J.M., C. Guedes Soares, and D. Faulkner, *Approximate assessment of the ultimate longitudinal strength of the hull girder*. Journal of Ship Research, 1996. **40**(1).
123. Hughes, O.F. and M. Ma, *Elastic tripping analysis of asymmetrical stiffeners*. Computers and Structures, 1995. **60**(3): p. 369-389.
124. Paik, J.K., et al., *Modified Paik-Mansour Formula for Ultimate Strength Calculations of Ship Hulls*, in *Advances in Marine Structures*, C. Guedes Soares and W. Fricke, Editors. 2011, Taylor & Francis: Hamburg, Germany.
125. Reckling, K.A., *Behaviour of Box Girders under Bending and Shear*, in *Proceedings of 7th International Ship Structures Committee*1979.
126. Dow, R.S., et al., *Evaluation of Ultimate Ship Hull Strength*, in *Extreme Loads Response Symposium*1981, Society of Naval Architects and Marine Engineers: Arlington, VA.
127. Dowling, P.J., P. Moolani, and P.A. Frieze, *The Effect of Shear Lag on the Ultimate Strength of Box Girders*, in *Steel Plated Structures: An International Symposium*, P.J. Dowling, J.E. Harding, and P.A. Frieze, Editors. 1976, CLS: Imperial College, London.
128. Ostapenko, A., *Strength of Ship Hull Girders under Moment, Shear and Torsion*, in *Extreme Loads Response Symposium*1981, Society of Naval Architects and Marine Engineers: Arlington, VA.

129. Nishihara, S., *Ultimate Longitudinal Strength of Midship Cross Sections*. Naval Architecture and Ocean Engineering, 1984. **22**: p. 200-214.
130. Zipfel, B. and E. Lehmann, *Ultimate load calculation during stranding*, in *Advances in Marine Structures* 2011, Taylor & Francis: Hamburg, Germany.
131. Adams, D., *Mostly Harmless* 1992: Pan Books.

# Chapter **10**

**Appendix: ProColl User Manual**

# **ProColl**

**Compartment Level Progressive Collapse Program**

**Version 1.0**

**USER MANUAL**

## **Introduction**

The ProColl progressive collapse program will calculate the moment-curvature response of an orthogonally stiffened box girder placed under a specified combination of vertical and horizontal bending. ProColl is specifically developed to calculate the progressive collapse behaviour of lightweight aluminium ship structures such as high speed ferries, Naval vessels and other large craft, although the program is equally applicable to conventional steel vessels. ProColl has options to use a compartment level progressive collapse methodology, which takes into account the response of stiffened panels over multiple frame spaces, typically between adjacent bulkheads. Alternatively, the program can be set to calculate interframe progressive collapse only.

The incremental progressive collapse methodology used by ProColl follows the general principles laid down by Smith (1977) and extended to deal with biaxial bending by Dow (1997). The girder cross section is subdivided into elements, each element is assigned a load shortening curve (LScurve) and the response of each element to bending moment or curvature increments about the instantaneous neutral axis of the cross section are calculated. The response is summed over the entire cross section to calculate either the bending moment for a specified increment of curvature or the curvature for a specified incremental increase in bending moment. The calculations are repeated incrementally to calculate the moment-curvature relationship of the cross section up to and beyond its ultimate capacity.

## **Concepts**

The program has various options to specify the extents of each stiffened panel element and the method used to derive its load-shortening behaviour. For the purposes of compartment level progressive collapse analysis, LScurves can be derived using the semi analytical methodology described in Chapter 6. This calculates the response of an orthogonally stiffened panel and can predict the onset of gross panel buckling and its effect on the panel strength. Alternatively, LScurves can be derived from finite element analysis, using an interface to ABAQUS software, or defined using a separate curve datafile written independently from ProColl.

The program follows a simple procedure to generate a bending moment-curvature plot for a hull girder:

1. The user writes an input file with information on the cross section geometry. A Microsoft Excel macro enabled template is available to aid this process.
2. The input file is processed by the ProColl solver, choosing options such as the increment method and solution type (vertical only or full interaction curve).
3. Results can be analysed using the built in post processor or opening the output files in Microsoft Excel or equivalent.

## **Installation and System Requirements**

Required:

- A PC running Windows XP/Vista/7

Optional:

- Microsoft Excel 2007 or equivalent to open the template file
- A dxf viewer for opening the graphical output (e.g. edrawings – [www.edrawingsviewer.com](http://www.edrawingsviewer.com))
- Abaqus 6.9 - if using the Abaqus features of the program. [www.simulia.com](http://www.simulia.com)
- IrfanView - if using the IrfanView features of the program ([www.irfanview.com](http://www.irfanview.com))<sup>1</sup>

The program is supplied as a zipped folder. Unzip the entire contents to a separate hard drive folder. The main program executable is in the root folder. Additional libraries required by the program are in the folder "lib". Scripts for the optional Abaqus interface are contained in the folder "lsp". The plate and stiffener component load shortening curve data is contained in the folder "lsp/database".

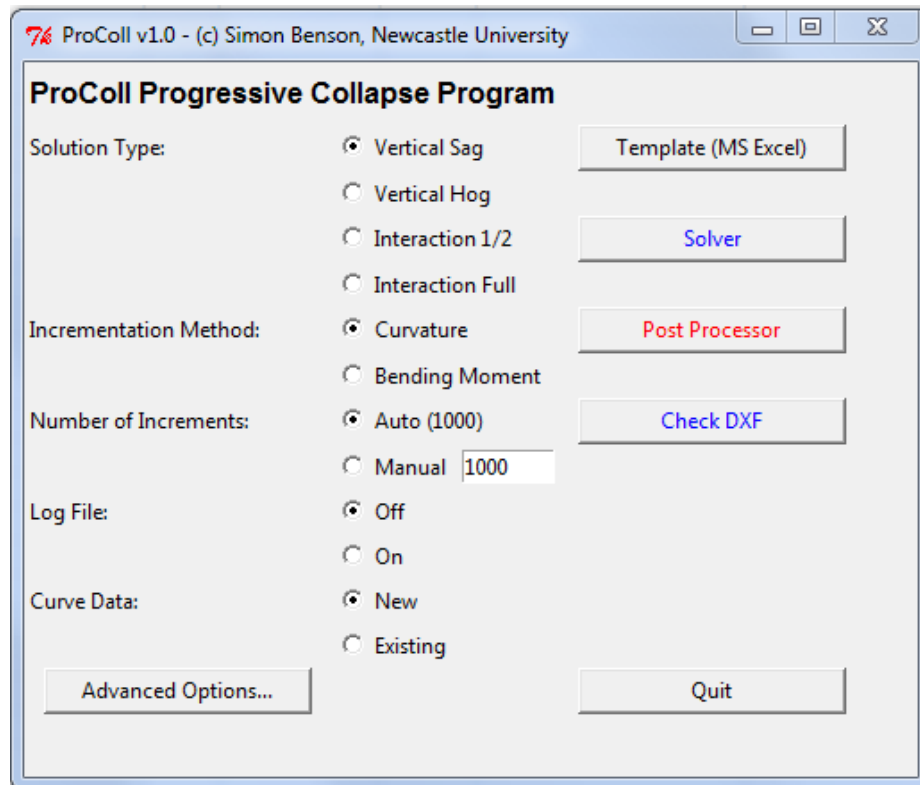
---

<sup>1</sup> Plugins for irfan view are included in the irfanplugin folder. These enable irfan view to open dxf files and convert to png format. The plugins should be copied to the appropriate subfolder in the irfan view program folder.

## Tutorial

### Opening the Program

Start the program by running the executable “ProCollv4\_4.exe”. The program homescreen will appear:



### Solver Options

The solver options are:

- Solution Type: Either a vertical bending moment analysis only or an interaction analysis consisting of 13/24 combinations of horizontal and vertical bending moments
- Increment Method: The program can run analyses using incremental curvature or bending moment. It is suggested to use incremental curvature for vertical analyses and incremental bending moment for generating a full interaction diagram

- Number of Increments: The program automatically calculates the bending moment or curvature range required to calculate the girder response beyond the ultimate capacity. The increment size is thus determined by the total number of increments used.
- Log File: Specifies whether the program writes a log file containing additional calculation information for each element at each increment. The log file size can become large and may significantly slow the calculation time for larger models.
- Curve Data: The program can either calculate new load shortening curves or use the existing curves generated from a previous analysis. This option can be used to speed up repeat analyses where regenerating LScurves is unnecessary.
- Advanced Options are available in the ProColl.env file, which can be accessed through the advanced options tab.

## Input File

The input file is written in .csv format, which enables the use of Microsoft Excel or an equivalent spreadsheet program to help produce the file. A template input file can be opened using the template tab on the homescreen. The template includes a macro which writes out the input file in the same directory as the template, with the name specified in cell A5. Do not insert additional rows above the overall header as this will make the macro inoperable.

The first lines of the input file are the main header, which must include “Filename”, “Length” and “Units”. The length defines the spacing between frames (not the total length of the section). Supported units are mm and m.

The main body of the data file consists of data rows, each containing information for a single element element in the cross section. The data rows are preceded by a header row. It is important that the header row is included as the program reads the data corresponding to the header titles.

### Overall Header

	A	B	C	D	E
1	##				
2	##	ProColl Template			
3	##				
4	Filename	Length	Units	Export to csv	
5	Template	1200	mm		

- **Filename: string**
- **Length: float**
- **Units: "mm", "m"**

## is used in the first column to comment out the row

The overall header must be written in Excel as shown above or in the .csv text file as follows:

```
##
Filename, Length, Units
Template, 1200, mm
##
```

The input and output files will be named using the "Filename" entry. "Length" refers to the length between frame spaces, NOT the overall compartment length. "Units" are in millimetres (mm) or metres (m).

**Element Descriptors**

##	ELEMENT DESCRIPTORS		
ID	Type	Description	Mirror
1	LSC	LSC 1	N
2	LSC	LSC 2	N
3	E	Element	Y

- **ID: integer (sequential numbering of lines)**
- **Type: "LSC", "E"**
- **Description: string (Optional)**
- **Mirror: "Y", "N"**

The first column must contain the title "ID". Each line is then numbered sequentially in the first column. **Lines must be numbered sequentially!**

The “Type” column defines whether each element is to be included in the cross section (E) or is used to define a load shortening curve only (LSC). This means a large panel can be described as a single element for the purposes of deriving the load shortening curve, and can then be split into numerous small elements in the progressive collapse analysis; each assigned the large panel load shortening curve. The options for assigning the load shortening curve are in the load shortening curve section.

The “Description” column is optional

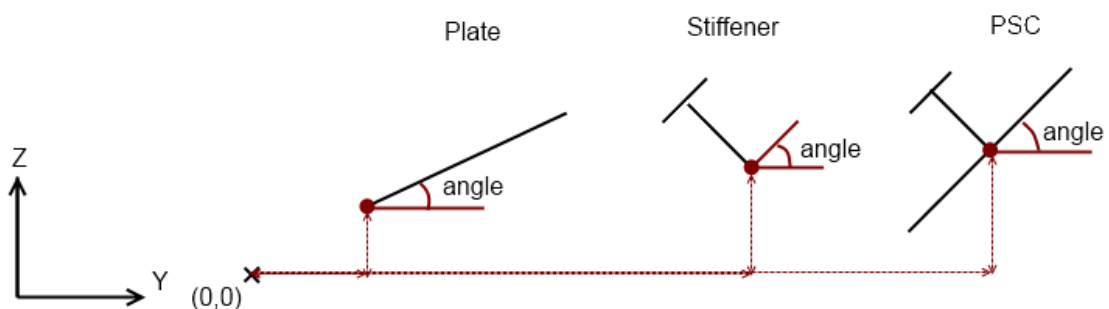
The “Mirror” column allows a symmetrical section (about the Z axis) to be developed without the need to specify elements on both sides of the symmetrical (Z) axis.

**Coordinates**

COORDINATES:		
angle	ycoord	zcoord
0	0	0
0	0	0
30	1000	2000.54

- **angle: float (between 0 and 360)**
- **ycoord: float**
- **zcoord: float**

The coordinates define the position of the element whilst the angle describes its orientation using the system below:



Note that plates are positioned differently if defined separately or as part of a PSC.

**Plate Dimensions**

PLATE DIM	
b	tp
200	10
300	5
300	5

- ***b: positive float (spacing between primary longitudinal members)***
- ***tp: positive float (plate thickness)***

**Primary Longitudinal Dimensions**

PRIMARY LONGITUDINAL DIMENSIONS:				
hwx	twx	bfx	tfx	nsx
120	5	40	7	10
80	3	70	5	20
80	3	70	5	1

- ***hwx: positive float (stiffener web height)***
- ***twx: positive float (stiffener web thickness)***
- ***bfx: positive float (stiffener flange width)***
- ***tfx: positive float (stiffener flange thickness)***
- ***nsx: integer (number of stiffeners over panel extents OR between deep longitudinals (if specified))***

If the element is a plate then all values should be zero. hwx, twx and nsx must be positive if the element is an LSC or is assigned to calculate a load shortening curve.

**Deep Longitudinal Dimensions**

DEEP LONGITUDINAL DIMENSIONS				
hwx2	twx2	bfx2	tfx2	nsx2
200	10	0	0	5

- ***hwx2: positive float (stiffener web height)***
- ***twx2: positive float (stiffener web thickness)***
- ***bfx2: positive float (stiffener flange width)***
- ***tfx2: positive float (stiffener flange thickness)***
- ***nsx2: integer (number of stiffeners over panel extents OR between deep longitudinals (if specified))***

If there are no deep longitudinals then these can be left blank or as zero.

**Frame Dimensions**

FRAME DIMENSIONS:				
hwy	twy	bfy	tfy	nsy
200	10	0	0	10
200	10	0	0	10
0	0	0	0	0

- ***hwy: positive float (frame web height)***
- ***twy: positive float (frame web thickness)***
- ***bfy: positive float (frame flange width)***
- ***tfy: positive float (frame flange thickness)***
- ***nsy: integer (number of frames in the compartment)***

**Material Definition**

<b>MATERIAL DEFINITIONS:</b>						
HAZ	Pmat	Smat	str0eq	E	v	Imp
25	5083	5083	215	70000	0.33	A
25	6082	5083	260	70000	0.33	S
25	Steel	5083	245	210000	0.3	L

- **HAZ: positive float (used for defining residual stress field for all materials and softened zone for aluminium)**
- **Pmat: "5083", "6082", "Steel" (plate material)**
- **Smat: "5083", "6082", "Steel" (stiffener material)**
- **str0eq: positive float (average yield/proof strength of element)**
- **E: positive float (Young's Modulus)**
- **v: positive float (Poisson Ratio)**
- **Imp: S, A, L (slight, average, severe imperfections)**

**Load Shortening Curve**

<b>LOAD SHORTENING CURVE:</b>		
LSCurve	Clone	Sname
1		gamma
1		T80
2	1	

- **LSCurve: 1, 2, EP (see below)**
- **Clone: blank or integer (element used for load shortening curve definition)**
- **Sname: gamma, T60, T80, T100, T120, T140, T170, ALS1, ALS2, ALS3, ALS7**

The LSCurve code determines the method used to calculate the element load shortening curve.

**1 – Use the semi analytical method (LSP).**

Runs the orthotropic plate program to calculate the load shortening curve. The curve data is stored in the Data folder as IDxx\_LSCurve.csv.

**2 – Clone a previously defined curve**

Uses a curve defined for another element (which must be defined on a previous line in the input file). If this option is selected the element number of the parent should be entered into the “Clone” column.

**abq – Use the Abaqus AutoPSC program**

This option runs AutoPSC, which automatically builds a PSC model in Abaqus 6.9 and solves it for uniaxial compression.

**EP – Hard Corner**

This option uses an elastic-perfectly-plastic curve definition using str0eq as the yield stress

**“CurveName” – Use a predefined curve file**

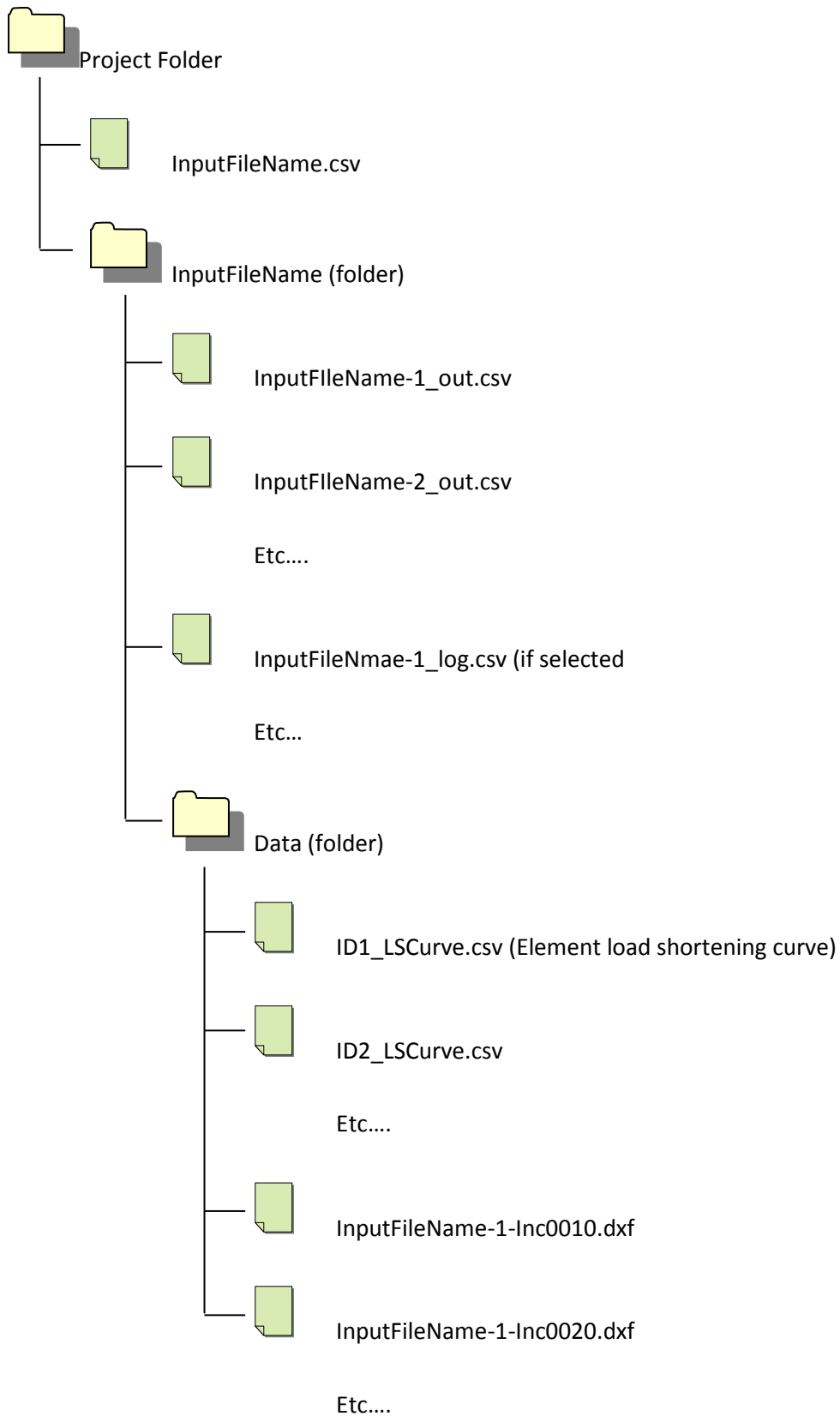
This option uses a predefined curve file (in.csv format) which must be placed in the Data directory

## **Solver**

The input file should be written to a project directory on your hard drive.

Launch the solver and select the input file in the file browser.

The solver will run with information displayed in the DOS window. The solver creates a number of output files in the project folder under a subdirectory with the same name as the input file. The files are arranged as follows:



The results are displayed in the InputFileName-x\_out.csv file where x denotes the interaction ratio between vertical and horizontal curvature:

<b>x</b>	<b>MV / Cy</b>	<b>MH / Cz</b>
1	1	0
2	1	0.33
3	1	0.66
4	1	1
5	0.66	1
6	0.33	1
7	0	1
8	-0.33	1
9	-0.66	1
10	-1	1
11	-1	0.66
12	-1	0.33
13	-1	0

The results file can be opened directly into MSExcel and is displayed as follows:

	A	B	C	D	E	F	G	H
1	Initial yNA =	7.36472233	Initial zNA =	8.09971083	X-Section Area =	0.99367		
2	Initial lyNA =	18.7558042	Initial lzNA =	16.0090083				
3	PBMy =	823939775	PBMz =	732655603				
4	Cy =	1.26E-06	Cz =	0				
5	Catamaran							
6								
7	Section Length	1.2						
8	Increment	yNA	zNA	Cy	MV	Cz	MH	
9	10	7.37143253	8.200322215	1.26E-05	16845167.24	0	-2399638	
10	20	7.37146243	8.199887457	2.51E-05	33687877.52	0	-4799222	
11	30	7.37146048	8.199357385	3.77E-05	50527862.06	0	-7198640	
12	40	7.37151189	8.198483087	5.02E-05	67363454.63	0	-9597701	
13	50	7.37157633	8.197337366	6.28E-05	84193479.07	0	-1.2E+07	
14	60	7.37172134	8.195156411	7.53E-05	101016008.8	0	-1.4E+07	
15	70	7.37183562	8.193415393	8.79E-05	117829659.2	0	-1.7E+07	
16	80	7.37196402	8.191399424	0.00010041	134634275.5	0	-1.9E+07	
17	90	7.37194477	8.189616744	0.00011296	151427838.1	0	-2.2E+07	
18	100	7.37226847	8.185945283	0.00012551	168207188	0	-2.4E+07	
19	110	7.37254075	8.182535303	0.00013807	184973303.4	0	-2.6E+07	

The log file contains information about each element at each recording increment (default is every 10 increments). The log file looks as follows:

	A	B	C	D	E	F	G	H	I	J	K	L	M	N	O	P	Q
1																	
2	INCREMENT 10																
3																	
4	Iteration	1	yNA =	0.066269	zNA =	7.936387											
5	Element	Strain	yv	zv	dy	dz	Stress	Area	dy	dz	Force	Et	DH	DV	DHV	Force	
6	ID14	2.38E-05	0.125	5.7	0.058731	-2.23639	1788490	0.0025	0.058731	-2.23639	4471.224	7.51E+10	647914.2	9.39E+08	-2.5E+07	4471.224	
7	ID15	2.45E-05	0.375	5.7	0.308731	-2.23639	1841000	0.0025	0.308731	-2.23639	4602.5	7.51E+10	17903715	9.39E+08	-1.3E+08	4602.5	
8	ID16	2.52E-05	0.625	5.7	0.558731	-2.23639	1893510	0.0025	0.558731	-2.23639	4733.776	7.51E+10	58639222	9.39E+08	-2.3E+08	4733.776	
9	ID17	2.59E-05	0.875	5.7	0.808731	-2.23639	1946021	0.0025	0.808731	-2.23639	4865.052	7.51E+10	1.23E+08	9.39E+08	-3.4E+08	4865.052	
10	ID18	2.66E-05	1.125	5.7	1.058731	-2.23639	1998531	0.0025	1.058731	-2.23639	4996.328	7.51E+10	2.11E+08	9.39E+08	-4.4E+08	4996.328	
11	ID19	2.73E-05	1.375	5.7	1.308731	-2.23639	2051042	0.0025	1.308731	-2.23639	5127.604	7.51E+10	3.22E+08	9.39E+08	-5.5E+08	5127.604	
12	ID20	2.80E-05	1.625	5.7	1.558731	-2.23639	2103552	0.0025	1.558731	-2.23639	5258.88	7.51E+10	4.56E+08	9.39E+08	-6.5E+08	5258.88	
13	ID21	2.87E-05	1.875	5.7	1.808731	-2.23639	2156062	0.0025	1.808731	-2.23639	5390.156	7.51E+10	6.15E+08	9.39E+08	-7.6E+08	5390.156	
14	ID22	2.94E-05	2.125	5.7	2.058731	-2.23639	2208573	0.0025	2.058731	-2.23639	5521.432	7.51E+10	7.96E+08	9.39E+08	-8.6E+08	5521.432	
15	ID23	3.01E-05	2.375	5.7	2.308731	-2.23639	2261083	0.0025	2.308731	-2.23639	5652.708	7.51E+10	1E+09	9.39E+08	-9.7E+08	5652.708	
16	ID24	3.08E-05	2.625	5.7	2.558731	-2.23639	2313593	0.0025	2.558731	-2.23639	5783.984	7.51E+10	1.23E+09	9.39E+08	-1.1E+09	5783.984	
17	ID25	3.15E-05	2.875	5.7	2.808731	-2.23639	2366104	0.0025	2.808731	-2.23639	5915.26	7.51E+10	1.48E+09	9.39E+08	-1.2E+09	5915.26	

The program stores the load shortening curves for each element in the Data subfolder as IDx\_LSCurve.csv files. These can be opened directly in MSExcel if required.

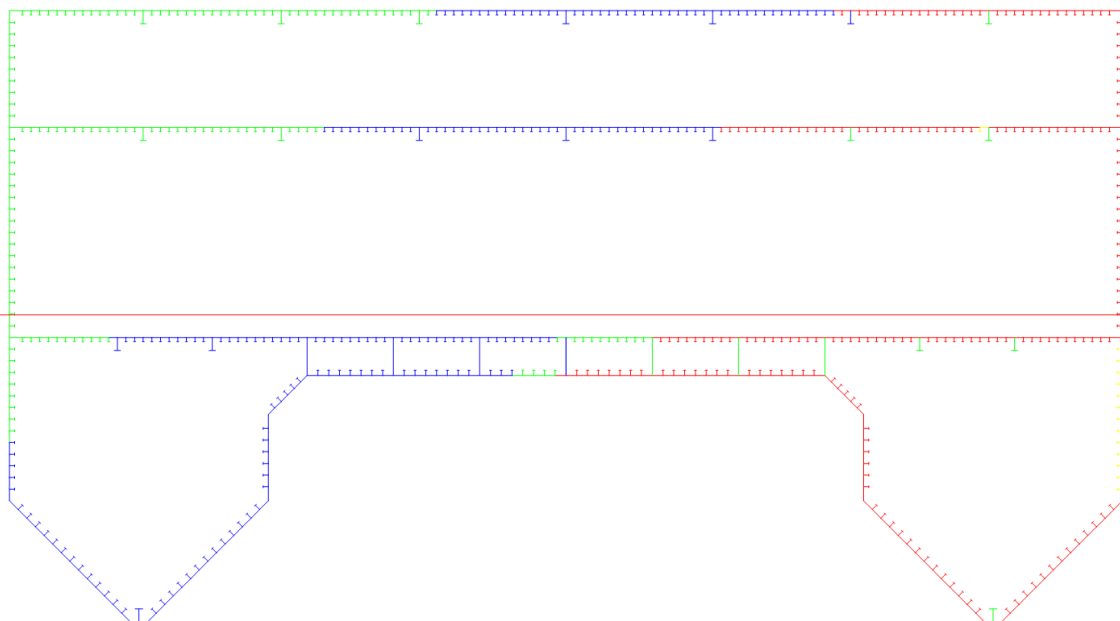
The program also outputs a dxf file for each recorded increment which shows the instantaneous stiffness of the cross section elements at that increment. The dxf files can be opened using any standard CAD viewer such as eDrawings ([www.edrawings.com](http://www.edrawings.com)). A typical output is shown below. Each element is coloured to reflect its current tangent stiffness:

**Blue:**  $E_t > E/2$

**Green:**  $0 < E_t < E/2$

**Yellow:**  $E_t = 0$

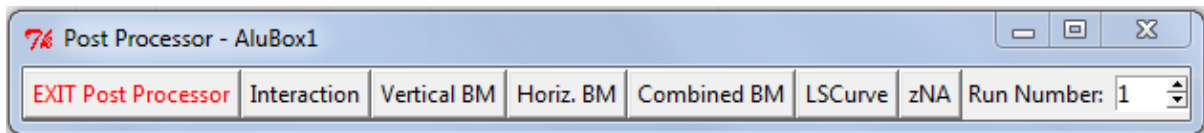
**Red:**  $E_t < 0$



## Post Processor

The solver produces all output files in .csv format for use with Microsoft Excel or equivalent spreadsheet/graph software. Alternatively, the ProColl program has some limited post processing capabilities.

To access the ProColl post processor click on the tab in the homescreen. Point the file browser to the InputFileName.csv file previously solved using ProColl. The post processor opens in a new window, allowing plots of the vertical and horizontal bending moment-curvature and the position of the instantaneous vertical neutral axis as a function of the applied curvature. An interaction curve can also be plotted if ProColl has been run in interaction mode.



Comparative plots between different models can be plotted by opening multiple post processor windows.